Controllability, Visual Illusions and Perception

Cyprien Tamekue

université PARIS-SACLAY

Controllability, Visual Illusions and Perception

Contrôlabilité, illusions visuelles et perception

Thèse de doctorat de l'université Paris-Saclay

École doctorale n°580, sciences et technologies de l'information et de la communication (STIC)
Spécialité de doctorat: Automatique
Graduate School: Sciences de l'ingénierie et des systèmes, Réferent: Faculté des sciences d'Orsay

Thèse préparée dans l'unité de recherche **Laboratoire des Signaux et Systèmes** (Université Paris-Saclay, CNRS, CentraleSupélec), sous la direction de **Yacine CHITOUR**, Professeur, Université Paris-Saclay et sous la co-direction de **Dario PRANDI**, chargé de recherche CNRS, Université Paris-Saclay.

Thèse soutenue à Paris-Saclay, le 02 Octobre 2023, par

Cyprien TAMEKUE

Composition du jury

Membres du jury avec voix déliberative

Lucie BAUDOUIN Directrice de Recherche CNRS, LAAS, CNRS	Présidente
Stephen COOMBES Professeur, University of Nottingham	Rapporteur & Examinateur
Sylvain ERVEDOZA Directeur de Recherche CNRS, Université de Bordeaux	Rapporteur & Examinateur
Nina AMINI Chargé de Recherche CNRS, Université Paris Saclay	Examinatrice
Daniele AVITABILE Associate Professor, Vrije Universiteit Amsterdam	Examinateur

THESE DE DOCTORAT
NNT : 2023UPAST105

université PARIS-SACLAY

ÉCOLE DOCTORALE
Sciences et technologies de l'information et de la communication (STIC)

Titre: Contrôlabilité, illusions visuelles et perception.

Mots clés: Géométrie presque riemannienne, contrôlabilité à zéro, équations paraboliques dégénérées, inégalités de Carleman, opérateur de Baouendi-Grushin, contrôle en neurosciences, modélisation des systèmes biologiques, équations des champs neuronaux, système visuel humain, illusions visuelles et perception, l'effet MacKay, experiences psychophysics de Billock et Tsou.

Résumé: Cette thèse explore deux applications distinctes de la théorie du contrôle dans différents domaines scientifiques : la physique et les neurosciences. La première application se concentre sur la contrôlabilité à zéro de l'équation parabolique associée à l'opérateur de Baouendi-Grushin sur la sphère de dimension 2. En revanche, la deuxième application concerne la description mathématique des illusions visuelles du type MacKay, et se focalise sur l'effet MacKay et les expériences psychophysiques de Billock et Tsou, via le contrôle de l'équation des champs neuronaux à une seule couche du type Amari. De plus, la thèse examine l'existence d'un équilibre dans un modèle de population de champs neuronaux à plusieurs couches de Wilson-Cowan, plus précisément lorsque l'entrée sensorielle est un retour d'état proportionnelle agissant uniquement sur l'état des populations de neurones excitateurs.

Dans la première partie, nous étudions les propriétés de contrôlabilité à zéro de l'équation parabolique associée à l'opérateur de Baouendi-Grushin défini par la structure presque-riemannienne canonique sur la sphère bidimensionnelle. Cet opérateur présente une dégénérescence à l'équateur de la sphère. Nous fournissons certaines propriétés de contrôlabilité à zéro de cette équation dans ce cadre courbé, ce qui généralise celles de l'équation parabolique de Baouendi-Grushin définie sur le plan.

Concernant les neurosciences, dans un premier temps, on s'intéresse à la description des illusions visuelles pour lesquelles les outils de la théorie de bifurcation et même de l'analyse multiéchelle semblent inappropriés. Dans notre discussion, nous utilisons l'équation des champs neuronaux de type Amari, dans laquelle l'entrée sensorielle est interprétée comme une représentation corticale du stimulus visuel utilisé dans chaque expérience. Elle contient une fonction de contrôle distribuée localisée qui modélise la spécificité du stimulus, par exemple, l'information redondante au centre du motif en entonnoir de MacKay ("rayons de MacKay") ou le fait que les stimuli visuels dans les expériences de Billock et Tsou sont localisés dans le champ visuel.

Toujours dans le cadre des neurosciences, nous étudions l'existence d'un équilibre dans un modèle de population de champs neuronaux à plusieurs couches de Wilson-Cowan lorsque l'entrée sensorielle est un retour d'état proportionnelle agissant uniquement sur l'état du système des populations de neurones excitateurs. Nous proposons une condition suffisante modérée sur les fonctions de réponse garantissant l'existence d'un tel point d'équilibre. L'objectif de cette étude réside dans son application lors de l'étude de la pertubation des oscillations cérébrales pathologiques associées à la maladie de Parkinson lorsqu'on stimule et mesure uniquement la population de neurones excitateurs.

université PARIS-SACLAY

ÉCOLE DOCTORALE
Sciences et technologies de l'information et de la communication (STIC)

Title: Controllability, Visual Illusions and Perception.

Keywords: Almost-Riemannian geometry, null controllability, degenerate parabolic equations, Baouendi-Grushin operator, Carleman estimates, Control in neurosciences, modelling of biological systems, Neural field equations, non-linear systems, human visual system, visual perception and psychophysics, the MacKay effect, Billock and Tsou's experiments

Abstract: This thesis explores two distinct control theory applications in different scientific domains: physics and neuroscience. The first application focuses on the null controllability of the parabolic, spherical Baouendi-Grushin equation. In contrast, the second application involves the mathematical description of the MacKay-type visual illusions, focusing on the MacKay effect and Billock and Tsou's psychophysical experiments by controlling the one-layer Amari-type neural fields equation. Additionally, the thesis investigates the existence of equilibrium in a multi-layer neural fields population model of Wilson-Cowan, specifically when the sensory input is a proportional feedback acting only on the system's state of the populations of excitatory neurons.

In the first part, we investigate the null controllability properties of the parabolic equation associated with the Baouendi-Grushin operator defined by the canonical almost-Riemannian structure on the 2-dimensional sphere. It presents a degeneracy at the equator of the sphere. We provide some null controllability properties of this equation to this curved setting, which generalize that of the parabolic Baouendi-Grushin equation defined on the plane.

Regarding neuroscience, initially, the focus lies on the description of visual illusions for which the tools of bifurcation theory and even multiscale analysis appear unsuitable. In our study, we use the neural fields equation of Amari-type in which the sensory input is interpreted as a cortical representation of the visual stimulus used in each experiment. It contains a localised distributed control function that models the stimulus's specificity, e.g., the redundant information in the centre of MacKay's funnel pattern ("MacKay rays") or the fact that visual stimuli in Billock and Tsou's experiments are localized in the visual field.

Always within the framework of neurosciences, we investigate the existence of equilibrium in a multi-layers neural fields population model of Wilson-Cowan when the sensory input is a proportional feedback that acts only on the system's state of the population of excitatory neurons. There, we provide a mild condition on the response functions under which such an equilibrium exists. The purpose of this study lies in its application when studying the disruption of pathological brain oscillations associated with Parkinson's disease when stimulating and measuring only the population of excitatory neurons.

Contents

To my Grandparents,
To my Parents,
To Family,...

How do we control the complexities around us,
whether they are mathematical equations or
even our own perceptions of reality?

Acknowledgments

First, thank you to my thesis advisors, Yacine Chitour and Dario Prandi. We've been working together for five years. You gave me the opportunity to work with you, even though we had never met in person. This started when I studied in Benin at the Institut de Mathématiques et des Sciences Physiques. A special mention to Jean-Michel Coron: he was the one who first taught me about control theory. It was he who recommended me to Yacine and Dario. I'm very grateful for that. Later, when I moved to Paris Dauphine University for my second Master's, Yacine and Dario introduced me to a new and exciting area: understanding visual patterns in our brain. This eventually led to my PhD work on the theoretical replication and understanding of intriguing visual phenomena of MacKay-type. Throughout all this time, Yacine and Dario were not just my advisors. You were patient and kind and always treated me like a friend. I have learned so much from you about my studies and life. I also want to thank Jean-Michel again. Every time we meet, he asks about my research and how it's going. This means a lot to me.

I want to give a big thank you to all the jury members who helped with my thesis. Firstly, thank you to Lucie Baudouin, the president of the jury and who examined my thesis. I truly value the time and effort you put into examining my work. Next, I want to thank Nina Amini, another examiner of my thesis. We work in the same place, and she often asked me how my thesis was coming along. This was really kind of her, and I always appreciated our chats. Sylvain Ervedoza deserves a special mention too. He was a reviewer for my thesis and taught me a lot about my subject when I was studying in Benin. His classes set the foundation for much of my current work, and his feedback greatly improved the first part of my thesis. Steve Coombes, another reviewer of my work, also gave me valuable feedback. We first talked about my thesis at a workshop in 2022 at Vu Amasterdam. His input, especially on the second part of my thesis, was very helpful. Last, but certainly not least, thank you to Daniele Avitabile, who also examines my thesis. He consistently showed interest in my work. His comments and questions helped me dive deeper into the topic of visual illusions and perceptions.

I also want to give thanks to some special people at my laboratory. Big thanks to Riccardo Bonalli, Islam Boussaada, Antoine Chaillet, Luca Greco, Paolo Mason, Guilherme Mazanti, Laurent Pfeiffer, and Sami Tliba. Every time we met, they would ask about how my thesis was going, showing genuine interest in my work. I'm also very grateful to Fréderic Jean at ENSTA. He gave me a great chance by letting me tutoring his course on dynamical systems and control theory for the past three years. Every time we talked, he was keen to know how my thesis was progressing.

I'd like to express my warm thanks to all my colleagues in the laboratory and to my dear friends who, like me, are immersed in the realm of research. To Kenneth Assogba, Christelle Agonkoui, Ismaila Balogoun, Mael Bompais, Baparou Danhane, Michaelis Dotse, Jean-Jacques Godeme, Émile Kouandé, Florent Koudohode, Moria Mayala, Pierre-Jean Ménabe, Hilaire Segning, Suney Tosté, and Emmanuel Zongo: your unwavering support and friendship have been invaluable to me throughout this journey.

To my longstanding friends who've been there every day, offering unwavering support throughout these three years of my thesis journey: Dexter, Elvire, Evrard-Valery, Gilles-Arnaud, Guy-Roland, Hervé-Patrick, Hugues-Roland, Joël, Laura, Lethitia, Mathurin, Mireille, Packil, Patrick, Pamela Pawua, Pamela Tchuem, Romaric, Steve, Tony, Valere, Vanessa, and Yannick - your encouragement and camaraderie have been pillars of strength. Your presence, advice, and encouragement have been the soothing balm during the most challenging times.

I want to say a big thank you to my grandparents, Josephine and Michel Kengne. You educated me with my lovely mother and your love and support have always meant so much to me. I'm also really grateful to my lovely mom, Florence, and my dad, Jean-Claude. You've always been there for me. To all my family members, your encouragement and belief in me helped me a lot in finishing this thesis. Without all of you by my side, this journey would have been much harder. I also want to give special thanks to Oun and Noé, the wonderful owners of the home I've lived in since the beginning of my thesis journey. Their kindness is beyond words, and over time, they've become like family to me. I deeply appreciate their warmth, support, and the safe haven they've provided.

A big thank you to Pam's. Her constant love, support, and daily encouragement played a huge role in helping me complete this thesis. Your belief in me pushed me forward, even on the most challenging days. I'm grateful to have had you by my side throughout this journey.

Last but by no means least, I extend my sincere gratitude to the "Fondation Jean-Pierre Aguilar". Their generous funding for the past three years made my PhD journey possible. I sincerely appreciate their belief in my research and commitment to supporting academic endeavours.

Cyprien Tamekue
Paris-Saclay, Octobre 2023.

General Introduction

Control theory, a fundamental branch of mathematics and engineering, plays a crucial role in understanding and influencing the behaviour of dynamic systems across a wide range of scientific disciplines, see, for instance, [Cor07]. By providing tools and methodologies to manipulate system dynamics, control theory has found applications in fields as diverse as physics, biology, and neuroscience.

The study of partial differential equations and their associated control problems significantly contributes to many areas of science and engineering. In particular, understanding the controllability properties of these equations is essential for designing efficient control strategies. In this context, the null controllability of parabolic equations associated with the Baouendi-Grushin type operators has gained considerable attention in the fields of differential geometry and control theory in recent decades [BCG14; BMM15; BDE20; Koe17; DK20; Mor15; CG14; Tam22].

With its intricate network of neurons, the brain is a prime example of a complex system that can be understood through the lens of control theory. Neuroscientists have long been intrigued by the mechanisms underlying brain function and how neuronal activity gives rise to perception, cognition, and behaviour. Control theory provides a powerful framework for investigating these phenomena, enabling researchers to study the controllability and stability of neuronal networks [Cha+17; Bri+23; ZME19; Det+15]. Moreover, control theory has been instrumental in developing brain-computer interfaces, allowing individuals with motor disabilities to regain control over their movements and interact with the external world.

By utilizing control theory principles, researchers aim to uncover the mysteries of brain function and develop novel therapeutic interventions for neurological disorders. In this regard, control theory can be used to study how to disrupt pathological brain oscillations associated with Parkinson's disease by focusing on stimulation and measurements of the excitatory neuronal population [Cha+17; Det+15].

An excellent network of neurons called the human visual system makes our ability to see and understand the world possible. Neuroscientists and psychophysics researchers have been fascinated by intriguing phenomena like the MacKay effect, which have helped us learn more about our visual system's workings. The MacKay-type effect is an interesting discovery in our visual system that challenges what we thought we knew about perception [Mac57; Mac61; BT07; BT10; BT12; Nic+21]. It reveals that sometimes, a distracting object that stands out can help us see and distinguish what we are focusing on. By studying the underlying patterns

of how neurons interact in the MacKay effect, we can gain valuable insights into how our visual system combines information from our senses to shape what we perceive in our daily experiences.

In this thesis, we address two specific applications of control theory in distinct scientific domains. First, we investigate the null controllability of the parabolic spherical Baouendi-Grushin equation, which has implications in understanding the controllability properties of partial differential equations that are degenerate, singular or with non-standard structures. Second, we explore the mathematical description of the MacKay effect and Billock and Tsou's experiments using the Amari-type neuronal field equation, aiming to uncover the underlying mechanisms of sensory hallucinations and visual illusions.

By delving into these topics, we aim to contribute to the growing body of knowledge in control theory and its applications, bridging the gap between theoretical frameworks and real-world phenomena. Through our research, we hope to shed light on fundamental questions, uncover novel insights, and pave the way for practical applications in physics and neuroscience.

3.1 . Publications

The following publications have arisen from some of the research carried out during my doctoral studies.

Peer-review journal articles

1. *C., Tamekue, (2022). Null controllability of the parabolic spherical Grushin equation. ESAIM: Control, Optimisation and Calculus of Variations, 28, 70.(see online link).*

2. *L., Brivadis, C., Tamekue, A., Chaillet, & J., Auriol (2023). Existence of an equilibrium for delayed neural fields under output proportional feedback. Automatica, 151, 110909. (see online link).*

Conference papers

3. *C., Tamekue, D., Prandi, & Y., Chitour, (2022). Cortical origins of MacKay-type visual illusions: A case for the non-linearity. to appear in IFAC world congress, July 2023. (see online link).*

4. *C., Tamekue, D., Prandi, & Y., Chitour, (2022, October). Reproducing sensory induced hallucinations via neural fields. In 2022 IEEE International Conference on Image Processing (ICIP) (pp. 3326-3330). IEEE. (see online link).*

Book Chapters

5. *C., Tamekue, D., Prandi, & Y., Chitour, (2023). MacKay-Type Visual Illusions via Neural Fields. In: Nielsen, F., Barbaresco, F. (eds) Geometric Science of Information. GSI 2023. Lecture Notes in Computer Science, vol 14072. Springer, Cham. (see online link).*

The complementary GitHub repository containing the relevant code can be found at https://github.com/dprn/MacKay-Billock_Tsou-2022/.

3.2 . Publications in Preparation

The first publication-in-preparation in the following represents a significant portion of this thesis's research conducted in Chapter 3. Additionally, the second publication-in-preparation will serve as a complementary contribution to the initial work presented in the first part of this thesis, which focuses on the null controllability of the parabolic, spherical Baouendi-Grushin equation discussed in Chapters 1 and 2. Both publications are intended to be submitted as peer-reviewed journal papers, showcasing the academic rigour and quality of the research conducted.

6. *Y. Chitour, D. Prandi, & C. Tamekue. A mathematical replication of MacKay-type visual illusions. In preparation, expected soon.*

7. *C. Tamekue. Parabolic spherical Baouendi-Grushin equation: Minimal time for null controllability. In progress.*

Part I

Controllability of degenerate parabolic equations

Contents

Introduction

1.1 . Purpose and motivation

This part of the thesis focuses on investigating the null controllability properties of the degenerate parabolic equation associated with the sub-Laplacian operator defined on a two-dimensional (2D) sphere equipped with its canonical almost-Riemannian structure known as the Grushin sphere. When expressed in terms of latitude and longitude coordinates on the sphere, this sub-Laplacian operator is represented as

$$\Delta_{\mathrm{BG}} := \frac{1}{\cos x}\partial_x(\cos x \partial_x) + \tan^2 x \partial_y^2, \qquad (x, y) \in (-\pi/2, \pi/2) \times [0, 2\pi).$$

Interestingly, near $x = 0$, the operator Δ_{BG} exhibits behaviour akin to the Baouendi-Grushin operator $\mathcal{G} = \partial_x^2 + x^2\partial_y^2$, which is defined in the Grushin plane, the free almost-Riemannian structure defined in $\mathbb{R}^2$.

In last decades, the operator $\mathcal{G}$ appeared as the prototypical example of degenerate elliptic operators whose associated parabolic equation has interesting null controllability properties. In this thesis, we aim to investigate whether the degenerate parabolic equation associated with the sub-Laplacian operator on the Grushin sphere shares similar properties. By understanding the controllability of this equation, we hope to contribute to the knowledge and understanding of this mathematical concept, which can help in studying the null controllability on other 2D compact almost-Riemannian manifolds.

Motivation for being interested in these operators can be related to the connection between the heat kernel of the sub-Laplacian operator on the three-dimensional Heisenberg group with that of the operator $\mathcal{G}$ as obtained in [FIK12, Section 5]. In representation theory, the three-dimensional Heisenberg group arises in the description of a one-dimensional quantum mechanical system generated by the position and momentum of a single particle in motion on a straight line [Wey50]. In particular, studying the parabolic equation associated with the operator Δ_{BG} should be physically relevant.

The interest in studying the null controllability properties of parabolic equations can also be associated with studying thermal diffusion in a homogeneous medium. Since the work by Joseph Fourier [Fou22], it is well-known that the diffusion of heat and that of chemical species in solids

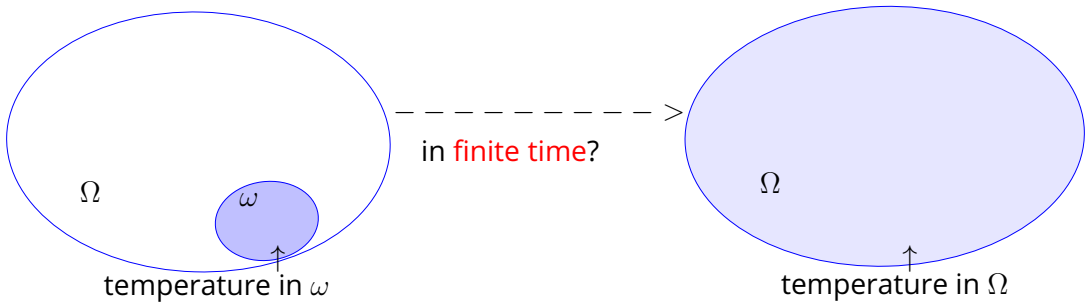

Figure 1.1: Thermal diffusion in a homogenous medium.

or gels evolves according to the same partial differential equation called the heat equation,

$$\frac{\partial f}{\partial t}(t,x) - D\Delta f(t,x) = 0. \tag{1.1}$$

For $d \in \mathbb{N}^*$, $x = (x_1, \cdots, x_d) \in \Omega$ models a location in $\Omega \subset \mathbb{R}^d$, the domain modelling, e.g., the medium in which the heat is diffusing, $t > 0$ is the time elapsed from the initial state, the state $f(t,x)$ represents the temperature in the medium at x at the time t, $D > 0$ is the thermal diffusivity of the medium usually equal to 1 and Δ is the Laplace operator defined by

$$\Delta = \partial_{x_1}^2 + \partial_{x_2}^2 + \cdots + \partial_{x_d}^2. \tag{1.2}$$

In general, the behaviour of the temperature inside a medium for a large time will depend on several factors, such as the thermal properties of the medium, the boundary conditions, and the initial temperature distribution.The heat equation's regularizing effect implies that the temperature distribution inside the medium becomes increasingly smooth and uniform, with smaller and smaller temperature gradients that become negligible. Therefore, the temperature distribution becomes constant throughout the medium. It is worth emphasizing that this thermal equilibrium, where the temperature is uniformly constant throughout the medium happens in the particular case of Neumann boundary conditions. In the case of Dirichlet boundary conditions, it happens if all the boundary surfaces are set to that same constant temperature. It follows whatever that considering a medium Ω in which the initial temperature is homogeneous (almost) everywhere will behave in large time as the temperature of the boundary, which is, in turn, equal to the temperature of the external environment to Ω.

Given now a medium modelled by Ω, a natural question which arises is how can we suitably choose a subdomain ω of Ω and what is the minimal time of diffusing in whole Ω a given temperature homogeneously distributed in ω? See, Fig. 1.1. The first answer to this question was given in dimension one, i.e., when $d = 1$ by Fattorini and Russell [FR71, Theorem 3.3].

Consider the following control system

$$\begin{cases} \partial_t f - \Delta f = u(t,x)\mathbb{1}_\omega(x), & (t,x) \in (0,T) \times \Omega, \\ f(t,x) = 0, & (t,x) \in (0,T) \times \partial\Omega, \\ f(0,x) = f_0(x), & x \in \Omega, \end{cases} \tag{1.3}$$

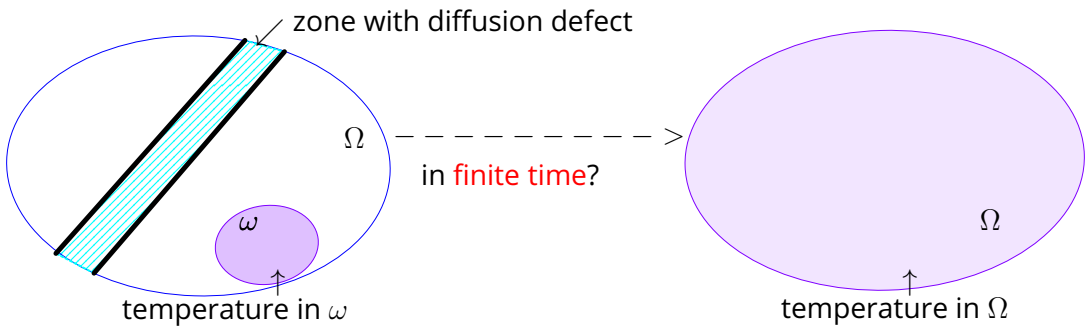

Figure 1.2: Thermal diffusion in a medium with a zone of diffusion defect.

where Ω is an open subset of $\mathbb{R}^d$ and f_0 is the initial temperature in Ω. The source term $u\mathbb{1}_\omega$ is localized in the non-empty open subset $\omega \subset \Omega$ through the characteristic function $\mathbb{1}_\omega$ of ω, and the function u is the control function.

Providing a positive answer to the above question is somehow equivalent to proving that Equation (1.3) posed in Ω is *null controllable* from $\omega \subset \Omega$ in time $T \geq T_{\min}(\omega)$, where the minimal time $T_{\min}(\omega) \geq 0$ is to determine. Note that equation (1.3) is said to be *null controllable* from $\omega \subset \Omega$ in time $T > 0$ if, for every $f_0 \in L^2(\Omega)$, there exists a control $u \in L^2(0,T;L^2(\Omega))$ supported in $(0,T) \times \omega$ such that the solution f of (1.3) satisfies $f(T,\cdot) = 0$.

Using the moment's method respectively, Carleman estimates and spectral inequalities, the null controllability properties for heat control system (1.3) was proved in dimension $d = 1$ by Fattorini and Russell [FR71] and in any finite dimension, $d \geq 1$ by Imanuvilov [Ima95], Lebeau and Robbiano [LR95] and Fursikov and Imanuvilov [FI96]. In particular, their results show that the minimal time $T_{\min}(\omega)$ of null controllability of the heat equation on a smooth bounded domain Ω equals zero and that the control domain $\omega \subset \Omega$ can be chosen arbitrarily. For a pedagogical proof of this result using Carleman inequalities, we refer the reader to the amazing book [Cor07, p. 80].

Given that null controllability of parabolic equations associated with the Laplace operator (1.2) can be used to answer the question on the thermal diffusion in a homogenous medium, which parabolic equations could be used to describe heat diffusion in a medium with a diffusion defect somewhere? See Fig. 1.2. Do these equations have similar null controllability properties to that of heat control system (1.3)?

The diffusion defect of heat somewhere in a medium Ω, e.g., in a zone $\mathcal{Z} \subset \Omega$ can be modelled by a parabolic equation associated with an elliptic operator whose coefficients of the principal symbol vanish inside $\mathcal{Z}$. Such an operator is called a *degenerate elliptic operator*. Among operators having this property, the one receiving considerable attention in the field of differential geometry and control theory is undoubtedly the 2D Baoeundi-Grushin operator $\mathcal{G}$ probably due to its connection with the sub-Riemannian geometry.

1.2 . Presentation of the main result

As announced in the first paragraph of the previous section, we will investigate the null controllability properties of the parabolic equation associated with the degenerate elliptic operator defined on the Grushin sphere. For clarity in the exposition, let us recall some important notions about differential geometry that will be used throughout the following. These are widely taken from [ABB19, Chapter 1] and [BG88, Chapter 2].

1.2.1 . Two-dimensional almost-Riemannian (AR) manifolds

We present a definition of 2D manifold as embedded surfaces in $\mathbb{R}^3$, that will be enough for our purposes. We stress that almost Riemannian structures can be defined on abstract manifolds (not necessarily embeddable in $\mathbb{R}^3$), and we refer to [ABB19] for a general definition.

Definition 1.2.1 *A (smooth) surface of $\mathbb{R}^3$ is a non-empty subset $M \subset \mathbb{R}^3$ such that for every $p \in M$, there exists an open neighbourhood $U \subset \mathbb{R}^3$ of p and a smooth map $\varphi : U \to \mathbb{R}$ such that $U \cap M = \varphi^{-1}(0)$ and the differential of φ is surjective on $U \cap M$.*

Unless explicitly stated, throughout the following, $M \subset \mathbb{R}^3$ denotes a 2D smooth manifold and φ a smooth map having the properties given by Definition 1.2.1. For every $p \in M$, the tangent space T_pM to M at p is defined as the kernel of the differential of φ at p, viz.

$$T_pM = \ker(d\varphi(p)). \tag{1.4}$$

An element $v \in T_pM$ is called a *tangent vector* to M at p. In particular, for every smooth curve $\gamma : [0,1] \to M$ in M such that $\gamma(0) = p$, one has

$$\dot{\gamma}(0) = \frac{d}{dt}\Big|_{t=0} \gamma(t) = v. \tag{1.5}$$

A smooth *vector field* on M is a smooth map

$$X : p \in M \longmapsto X(p) \in T_pM, \tag{1.6}$$

that associate with every point p in M a tangent vector to M at p. In particular, a smooth curve $\gamma : [0,1] \to M$ satisfying

$$\dot{\gamma}(t) = X(\gamma(t)), \qquad \forall t \in [0,1], \tag{1.7}$$

is called an *integral curve* of the vector field X. We denote by $\mathrm{Vec}(M)$ the set of smooth vector fields on M. Let $X \in \mathrm{Vec}(M)$ be such that every integral curve of X is defined on $\mathbb{R}$. The *flow* of the vector field X is the map $\phi_t : p \in M \mapsto \phi_t(p) \in M$, $t \in \mathbb{R}$ satisfying

$$\frac{\partial \phi_t}{\partial t}(p) = X(\phi_t(p)), \qquad \phi_0(p) = p, \qquad \frac{\partial \phi_t}{\partial t}\Big|_{t=0}(p) = X(p), \qquad \forall p \in M. \tag{1.8}$$

Given $X, Y \in \mathrm{Vec}(M)$, we denote by $[X, Y]$ their Lie bracket. Since we are only using vector fields as derivations on functions, the following identity will be used as a definition

$$[X, Y] = XY - YX. \tag{1.9}$$

We say that the pair of smooth vector fields X, $Y \in \mathrm{Vec}(M)$ is *Lie bracket generating* (or satisfy the Hörmander condition), if the following holds for every $p \in M$

$$\mathrm{span}\{X(p), Y(p), [X, Y](p), [X, [X, Y]](p), \cdots\} = T_pM. \tag{1.10}$$

We can now define a 2D almost-Riemannian manifold, see also [ABS08; BL13; BPS16].

Definition 1.2.2 *A 2D trivializable almost-Riemannian manifold is a couple $(M, \{X_1, X_2\})$ where M is a 2D manifold and $\{X_1, X_2\} \subset \mathrm{Vec}(M)$ is a Lie bracket generating family.*

Due to Hörmander condition satisfying by the generating frame $\{X_1, X_2\}$, we have that $\mathcal{D}(p) = \mathrm{span}\{X_1(p), X_2(p)\}$ is one or two-dimensional for every $p \in M$. We denote by $\mathcal{Z}$ the set of points p where $\mathcal{D}(p)$ is one-dimensional.

We recall that to every 2D trivializable ARS is naturally associated a metric g on the distribution $\mathcal{D}$, obtained by declaring $\{X_1, X_2\}$ to be g-orthonormal.

1.2.2 . The Grushin sphere and associated sub-Laplacian operator

We consider the sphere $\mathbb{S}^2 = \{p = (x_1, x_2, x_3) \in \mathbb{R}^3 \mid x_1^2 + x_2^2 + x_3^2 = 1\}$ which is a (compact) 2D manifold by Definition 1.2.1. We recall that we are using vector fields as derivations on functions.

Introduce for fixed $t \in \mathbb{R}$, the map $\phi_t : \mathbb{S}^2 \to \mathbb{S}^2$ defined for every $p \in \mathbb{S}^2$ by $\phi_t(p) = (x_1, x_2 \cos t - x_3 \sin t, x_2 \sin t + x_3 \cos t)$. Indeed, $\phi_t(p)$ is the counterclockwise rotation of angle t of $p \in \mathbb{S}^2$ around the x_1-axis.

Since ϕ_t is linear with respect to p, one has for every tangent vector $u = (u_1, u_2, u_3) \in T_p\mathbb{S}^2$, $d\phi_t(p)u = (u_1, u_2 \cos t - u_3 \sin t, u_2 \sin t + u_3 \cos t)$. Let $\langle \cdot, \cdot \rangle$ denotes the scalar product on $\mathbb{R}^3$, then it holds for all $v = (v_1, v_2, v_3) \in T_p\mathbb{S}^2$, $\langle d\phi_t(p)u, d\phi_t(p)v \rangle = \langle u, v \rangle$. It follows that $d\phi_t : T_pM \to T_pM$ is a smooth isometry and

$$X_1(p) = \left.\frac{d}{dt}\right|_{t=0} \phi_t(p) = -x_3\partial_{x_2} + x_2\partial_{x_3}, \qquad p = (x_1, x_2, x_3) \in \mathbb{S}^2, \tag{1.11}$$

defines the Killing[1] vector field on $\mathbb{S}^2$ generating the counterclockwise rotations around the x_1-axis. Arguing similarly, we can construct the Killing vector fields X_2 and X_3 generating the counterclockwise rotations around the x_2 and x_3 axes respectively, viz.

$$X_2 = -x_3\partial_{x_1} + x_1\partial_{x_3}, \qquad X_3 = -x_2\partial_{x_1} + x_1\partial_{x_2}. \tag{1.12}$$

[1] Let X be a vector field on a manifold M and $(\phi_t)_{t\in\mathbb{R}}$ denotes the flow of X. We say that X is a Killing vector field on M, if for all $t \in \mathbb{R}$ and for every $p \in M$, the differential $d\phi_t(p) : T_pM \to T_pM$ is a smooth isometry.

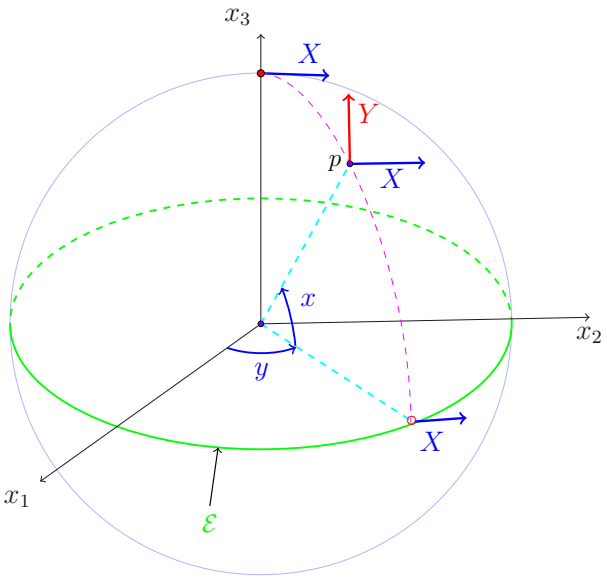

Figure 1.3: The Grushin sphere: The vector fields X (in *blue*) and Y (in *red*) are generator of this structure in latitude-longitude coordinates (x, y). The degeneracy set coincides with the equator $\mathcal{E}$ (in *green*). The *red circle* (resp. *red dot*) on the equator (resp. at north pole) means that the vector field Y *vanishes* (resp. is *singular*) there.

These three Killing vector fields have the good properties to generate the tangent space $T_p\mathbb{S}^2$ at each $p \in \mathbb{S}^2$. Observe also that $\{X_1, X_2\}$ are linearly independent outside of the equator $\mathcal{E} := \{x_3 = 0\}$. Nevertheless, since the Lie bracket $[X_1, X_2] = X_3$, the system of vector fields $\{X_2, X_2\}$ is Lie bracket-generating and determines a 2D almost-Riemannian structure on $\mathbb{S}^2$ (Definition 1.2.2), and $\mathbb{S}^2$ endowed with this structure is called the *Grushin sphere*, see Figure 1.3. In Section 2.3 of the next chapter, we will see how do this structure look-like when describing it in spherical coordinates, namely the latitude-longitude coordinates.

Let μ be the standard Riemannian volume form on $\mathbb{S}^2$, as induced by the Euclidean Lebesgue measure. We are interested in the sub-Laplacian operator defined by

$$\mathcal{L} := \mathrm{div}_\mu \circ \nabla_{\mathsf{sR}} = -X_1^+ X_1 - X_2^+ X_2. \tag{1.13}$$

Here, ∇_{sR} is the sub-Riemannian gradient defined by $\nabla_{\mathsf{sR}}\phi = (X_1\phi)X_1 + (X_2\phi)X_2$ for any[2] $\phi \in C^\infty(\mathbb{S}^2)$, while div_μ denotes the divergence w.r.t. μ. More precisely, given a vector field $W \in \mathrm{span}\{X_1, X_2\}$, say, $W = \alpha X_1 + \beta X_2$, $\alpha,\ \beta \in C^\infty(\mathbb{S}^2)$, $\mathrm{div}_\mu(W)$ is the unique $C^\infty(\mathbb{S}^2)$ function satisfying

$$\int_{\mathbb{S}^2} \mathrm{div}_\mu(W)\phi d\mu = -\int_{\mathbb{S}^2} d\phi(W) d\mu, \qquad \forall \phi \in \mathcal{C}^\infty(\mathbb{S}^2), \tag{1.14}$$

where $d\phi(W)$ is the differential of ϕ in the direction of W, viz. $d\phi(W) = W(\phi) = \alpha X_1(\phi) +$

[2]Note that, $C^\infty(\mathbb{S}^2)$ is canonically defined as the space of the restrictions to $\mathbb{S}^2$ of functions (with compact support) that are C^∞ on an open neighbourhood of $\mathbb{S}^2$.

$\beta X_2(\phi)$, and[3]

$$d\mu = x_1 dx_2 \wedge dx_3 + x_2 dx_3 \wedge dx_1 + x_3 dx_1 \wedge dx_2. \tag{1.15}$$

Moreover, $X_1^+ := -X_1 - \mathrm{div}_\mu(X_1)$ and $X_2^+ := -X_2 - \mathrm{div}_\mu(X_2)$ denote respectively the formal adjoints of X_1 and X_2 taken in the space $L^2(\mathbb{S}^2;\mu)$, the Hilbert space of measurable and square-integrable functions over $\mathbb{S}^2$ with respect to μ.

As evident from the latitude-longitude coordinate expression we will present in Section 2.3 of the next chapter, $\mathcal{L}$ is a degenerate operator on $\mathbb{S}^2$ that generalizes the Baouendi-Grushin operator (BG) on $\mathbb{R}^2$. We will refer to $\mathcal{L}$ as the *intrinsic spherical Baouendi-Grushin* operator.

1.2.3 . Parabolic Baouendi-Grushin equation on Grushin sphere and main result

Let $\widetilde{\omega}$ be a non-empty open subset on $\mathbb{S}^2$ and consider the intrinsic parabolic spherical Baouendi-Grushin (PSBG) equation degenerating on the equator, viz.

$$\begin{cases} \partial_t f - \mathcal{L} f = u \mathbb{1}_{\widetilde{\omega}}, & \text{in } (0,T)\times\mathbb{S}^2, \\ f|_{t=0} = f_0, & \text{in } \mathbb{S}^2. \end{cases} \tag{1.16}$$

Here, $f = f(t,p)$ is the state describing, e.g. the temperature at $p = (x_1,x_2,x_3) \in \mathbb{S}^2$ at the time $t > 0$, the time horizon $T > 0$, $f_0 = f_0(p)$ is the initial datum and $u = u(t,p)$ is the control function.

We are interested in the null controllability properties of the control system (1.16).

Definition 1.2.3 (Null controllability of the PSBG equation) *We say that control system (1.16) is null controllable from $\widetilde{\omega} \subset \mathbb{S}^2$ in time $T > 0$ if, for every $f_0 \in L^2(\mathbb{S}^2;\mu)$, there exists a control $u \in L^2(0,T;L^2(\mathbb{S}^2;\mu))$ supported in $(0,T)\times\widetilde{\omega}$ such that the solution f of (1.16) satisfies $f(T,\cdot) = 0$.*

The main result is then the following.

Theorem 1.2.1 ([Tam22]) *Let $\widetilde{\omega} = \{(x_1,x_2,x_3) \in \mathbb{S}^2 \mid \alpha < |x_3| < \beta\}$ with $0 < \alpha < \beta \leq 1$. Then a positive minimal time is required for null controllability of (1.16) from $\widetilde{\omega}$, namely*

$$T_{\min}(\widetilde{\omega}) := \inf\{T > 0 : \textit{system (1.16) is null controllable from } \widetilde{\omega} \textit{ in time } T\}$$

satisfies $T_{\min}(\widetilde{\omega}) \geq \log(1/\sqrt{1-\alpha^2})$. Moreover, there exists $T^* > 0$ such that, for every $T \geq T^*$, system (1.16) is null controllable from $\widetilde{\omega}$ in time T.

The proof of Theorem 1.2.1 will be expounded in the next chapter. We stress that Theorem 1.2.1 only concerns the case when the control region $\widetilde{\omega}$ does not touch the degeneracy $\mathcal{E} = \{x_3 = 0\}$ due to the hypothesis $\alpha > 0$. Moreover, the result given in Theorem 1.2.1 is the extension of Beauchard *et al.* [BMM15, Theorem 1.3] in the curved setting of the 2D sphere. Indeed, the control function u in Theorem 1.2.1 acts on $\widetilde{\omega}$ which is two spherical crowns

[3] Actually, $d\mu = i^*(\imath_\nu dV)$, where i^* is the pull-back of the inclusion $i : \mathbb{S}^2 \to \mathbb{R}^3$, and $\imath_\nu$ is the interior product (contraction) of the 3-form $dV = dx_1 \wedge dx_2 \wedge dx_3$ with a smooth unit normal vector field $\nu = (x_1,x_2,x_3)$ to the sphere $\mathbb{S}^2$.

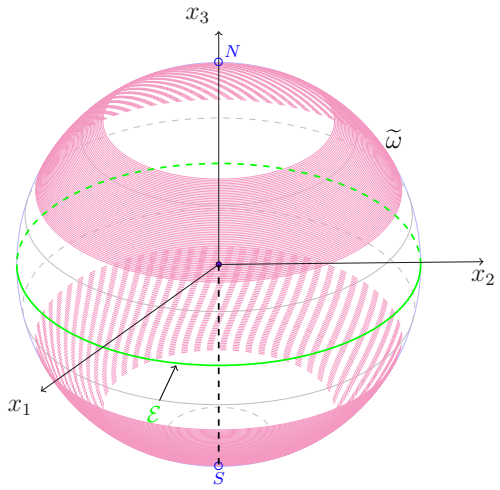

Figure 1.4: The equator $\mathcal{E}$ (in *green*), a control region $\widetilde{\omega}$ (in *magenta*), north and south pole (in *blue*).

symmetric and non-intersecting the equator $\mathcal{E} = \{x_3 = 0\}$, see Figure 1.4. This is the case for the control set in [BMM15, Theorem 1.3] giving the result on the null controllability of the parabolic equation associated with the Baouendi-Grushin operator $\mathcal{G} = \partial_x^2 + x^2\partial_y^2$ when the control set is two vertical stripes symmetric and non-intersecting the y-axis $\mathcal{Z} = \{x = 0\}$.

The system of coordinates that we will use to prove Theorem 1.2.1 have the particularity to generate singularities at the north and south pole. Therefore, considering the union of two spherical crowns instead of one spherical crown non-intersecting with the equator is a technical assumption to deal with these singularities when proving the Carleman estimate in Section 2.7 of the next chapter.

Remark 1.2.1 *It is worth emphasizing that the proof we will present in Section 2.5 of the next chapter shows that Equation (1.16) is not null controllable from $\widetilde{\omega}$ in time $T = \log(1/\sqrt{1-\alpha^2})$. Moreover, this proof also shows that even with a control set $\overline{\omega} := \{(x_1, x_2, x_3) \in \mathbb{S}^2 \mid 0 < x_3 < \alpha \leq 1\}$, a spherical crown non-intersecting the equator, Equation (1.16) is not null controllable from $\overline{\omega}$ in time $T \leq \log(1/\sqrt{1-\alpha^2})$ showing that $T_{\min}(\overline{\omega}) \geq \log(1/\sqrt{1-\alpha^2})$.*

1.3 . Ongoing and further works

1.3.1 . Ongoing works

The result in Theorem 1.2.1 is somewhat restrictive compared to known results on null controllability for 2D parabolic equations of Baouendi-Grushin (PEBG) type. For example, null controllability for PEBG is known to hold when controlling from one side of the degeneracy with the precise value of the minimal time [BCG14; Bea+15; BDE20; Koe17; DK20]. It is also known that PEBG is null controllable in an arbitrarily small time when the control set intersects the degeneracy, see for instance, [BCG14, Appendix], [Bea+15, Section 3] and [All18, Section 4.2].

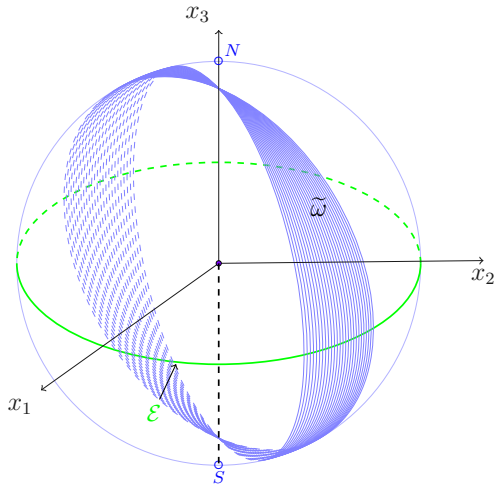

Figure 1.5: The control region $\widetilde{\omega}$ (in *blue*), the equator $\mathcal{E}$ (in *green*), and the north and south poles (in *blue*).

Therefore, the result in Theorem 1.2.1 is part of ongoing work. We are currently engaged in [Tam23] on studying the null controllability of Equation (1.16) from $\overline{\omega} := \{(x_1, x_2, x_3) \in \mathbb{S}^2 \mid 0 < \alpha < x_3 < \beta \leq 1\}$, a spherical crown non-intersecting the equator and by the way determine the exact minimal time of null controllability from $\overline{\omega}$, and therefore from $\widetilde{\omega} = \{(x_1, x_2, x_3) \in \mathbb{S}^2 \mid 0 < \alpha < |x_3| < \beta \leq 1\}$, which is a union of two spherical crowns symmetric and non-intersecting the equator.

We are tackling this question by studying the uniform null controllability of the associated family of one-dimensional non-degenerate and singular parabolic equations using moment methods. More precisely, we are proving that Equation (1.16) is null controllable from $\overline{\omega}$ and $\widetilde{\omega}$ in any time $T > \log(1/\sqrt{1-\alpha^2})$, showing that $T_{\min}(\overline{\omega}) = \log(1/\sqrt{1-\alpha^2}) = T_{\min}(\widetilde{\omega})$. Moreover, the same method will allow us to show that Equation (1.16) is null controllable in arbitrarily small time $T > 0$ when the control set is a spherical crown having the equator on its boundary.

By establishing suitable Carleman estimates, we are also proving that with a control acting on a spherical crown with the equator in its interior, Equation (1.16) is null controllable in arbitrarily small time $T > 0$.

1.3.2 . Further works

More general geometrical shapes of the control set have been considered in studying the null controllability for the 2D parabolic Baouendi-Grushin equation; see, for instance, [DK20; Koe17]. In particular, when the control set ω is a complement of a horizontal strip intersecting the degeneracy set, it has been proved in [Koe17, Theorem 2] that the 2D parabolic Baouendi-Grushin equation is never null controllable from ω.

Natural interesting open questions related to this thesis's part is to study the null controllability properties of control system (1.16) when the control set $\widetilde{\omega}$ is a subset of the sphere $\mathbb{S}^2$ having a more general geometrical shape, see, for instance, Figure 1.5. A starting point for these questions could be to verify if the control system (1.16) is null controllable from the control

set $\widetilde{\omega}$ defined by two distinct meridians.

The techniques we will use to prove Theorem 1.2.1 in the next chapter may be of interest to further works studying the null controllability properties of similar equations on other general 2D compact, almost-Riemannian manifolds.

Indeed, although the parabolic equation associated with the standard sub-Laplacian on 2D compact almost-Riemannian manifolds M is never null controllable when the control function acts on ω, subset of a connected component of $M\backslash\mathcal{Z}$ (here $\mathcal{Z}\subset M$ is the set where the associated almost-Riemannian metric on the manifold M explodes), see [BL13], it could be interesting to analyse the null controllability properties for the parabolic equation associated with Baouendi-Grushin operator on the manifold M. Indeed, if μ is a smooth volume form everywhere on M (a Riemannian volume form, for instance), we mean by the Baouendi-Grushin operator on M the operator defined intrinsically by $\mathcal{L}:=\operatorname{div}_\mu\circ\nabla_{\mathrm{sR}}$, where ∇_{sR} is the sub-Riemannian gradient on M and div_μ denotes the divergence with respect to μ. Note that the operator $\mathcal{L}$ differs from that studied in [BL13]. Indeed in the latter, the divergence is taken with respect to ν, the sub-Riemannian area associated with the sub-Riemannian metric g on M, which explodes on $\mathcal{Z}$.

CHAPTER 2

Null controllability of the parabolic spherical Baouendi-Grushin equation

2.1 . Introduction

This chapter essentially contains the results published in the article [Tam22]. As announced in the introductory chapter 1, the goal is to expound the proof of Theorem 1.2.1 related to the null controllability properties of the parabolic equation associated with the Baouendi-Grushin operator defined by the canonical almost-Riemannian structure on the 2D sphere $\mathbb{S}^2$, the Grushin sphere. The chapter is organised as follows:

The first part contained in Section 2.2, recalls some known null controllability results for 2D parabolic equations of Baouendi-Grushin type.

In Section 2.3, we expound the strategy to prove Theorem 1.2.1 . Here we express in spherical coordinates the Grushin sphere and Theorem 1.2.1, and we relate the proof of the null controllability with that of observability inequality of the adjoint system. The strategy to prove the observability inequality is also provided.

Section 2.4 is dedicated to proving that all equations that we will study are well-posed in convenient Banach spaces.

Section 2.5 starts with the proof of the main result. Here we turn out an argument showing why the adjoint system to the parabolic, spherical Baoeundi-Grushin equation is not observable in a small time when the observation set is a spherical crown (or a union of two spherical crowns) non-intersecting the equator.

Section 2.6 is dedicated to proving the observability result in large time when the observation set is a union of two spherical crowns non-intersecting the equator. Here we start with the Hardy-Poincaré inequality necessary to prove Carleman estimates. Section 2.6.1 focuses on studying the properties of Fourier components of the solution of the adjoint system and their dissipation rate. In Section 2.6.2, we show how the uniform observability estimate of Fourier components yields the observability estimate of the solution of the adjoint system. Respectively in Section 2.6.3 and Section 2.6.4, we recast the equation satisfied by the Fourier component

for the zero frequency and the Fourier components for non-zero frequencies in spaces L^2 without weight (on the Lebesgue measure) using unitary transformations. We provide a uniform observability inequality for each case's 1D parabolic equation.

2.2 . Preliminaries results

We begin this chapter by recalling some known results about the null controllability properties for equations of Baouendi-Grushin type in 2D. Section 2.2.1 focuses on defining the Grushin plane, the free almost-Riemannian structure defined in $\mathbb{R}^2$. In Section 2.2.2, we recall the null controllability properties of parabolic equations associated with the Baouendi-Grushin operator (BG) in the Grushin plane.

2.2.1 . The Grushin plane

In recent decades, the following operator appeared as the prototypical example of degenerate and hypoelliptic operators,

$$\mathcal{G} = \partial_x^2 + x^2\partial_y^2, \qquad (x,y) \in \mathbb{R}^2. \tag{BG}$$

It was first evoked by Baoeundi [Bao67] in studying inhomogeneous boundary problems associated with elliptic operators degenerating inside a domain and by Grushin [Gru70] where he proved that this operator is hypoelliptic. This operator also falls into the class of second-order operators intensively studied by Hörmander [Hör67] known as operators "sum of squares".

In connection with sub-Riemannian geometry, the operator $\mathcal{G}$ can be defined by a global orthonormal frame $\{X_1, X_2\}$ on $\mathbb{R}^2$, where $X_1(x,y) = \partial_x$ and $X_2(x,y) = x\partial_y$ (here, we are using the identification of vector fields with derivations). Indeed, one has

$$\mathcal{G} = -X_1^+X_1 - X_2^+X_2 = X_1^2 + X_2^2 = \partial_x^2 + x^2\partial_y^2, \tag{2.1}$$

where X_1^+ and X_2^+ are respectively formal adjoints of X_1 and X_2 taken in the space $L^2(\mathbb{R}^2)$. Since the Lie-bracket $[X_1, X_2](x,y) = \partial_y$, it follows that $\{X_1, [X_1, X_2]\}_{|_{(x,y)}}$ generates the tangent space at each point $(x,y) \in \mathbb{R}^2$. Therefore the system of vector fields $\{X_1, X_2\}$ is bracket-generating and defines a step 2 free almost-Riemannian structure, and $\mathbb{R}^2$ endowed with this frame is called the *Grushin plane* [ABB19, p. 478], see, Fig. 2.1 for visual illustration.

Finally, observe that operator (BG) is a degenerate elliptic operator on $\mathbb{R}^2$ and the degeneracy set is the y-axis,

$$\mathcal{Z} = \{(x,y) \in \mathbb{R}^2 : x = 0\} = \{0\} \times \mathbb{R}.$$

2.2.2 . Null controllability of the parabolic Baouendi-Grushin (PBG) equation in the Grushin plane

In contrast with what happens for the heat control system (1.3), which is null controllable in an arbitrarily small time, in [BCG14], it has been shown that the minimal time of null controllability for the parabolic equation associated with Baouendi-Grushin operator (BG) from a control set

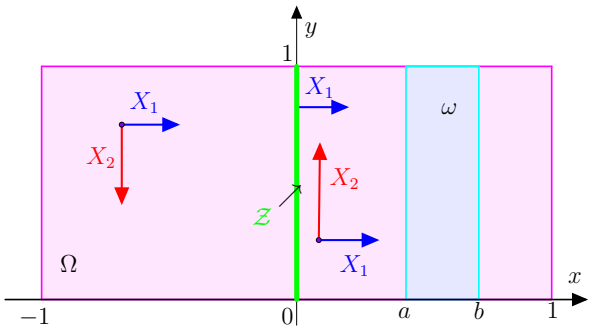

Figure 2.1: The Grushin plane depicted in upper-half plane $y \geq 0$: The generating vector fields X_1 and X_2 and the degeneracy set $\mathcal{Z}$. The medium Ω and the control set ω, a vertical strip non-intersecting $\mathcal{Z}$.

ω satisfies $T_{\min}(\omega) > 0$. More precisely, null controllability may hold true or not depending on the geometry of the control domain ω and the time horizon T. The authors considered the following parabolic control system, which presents a degeneracy at $x = 0$

$$\begin{cases} \partial_t f - \mathcal{G} f = u(t,x,y)\mathbb{1}_\omega(x,y), & (t,x,y) \in (0,T) \times \Omega, \\ f(t,x,y) = 0, & (t,x,y) \in (0,T) \times \partial\Omega, \\ f(0,x,y) = f_0(x,y), & (x,y) \in \Omega, \end{cases} \tag{2.2}$$

where $T > 0$, $\Omega = (-1,1) \times (0,1)$, $\omega \subset \Omega$ is an open subset, f is the state, u is the control function, f_0 is the initial datum. We refer to Fig. 2.1 for the visual illustration of Ω and ω.

Definition 2.2.1 (Null controllability of the PBG equation) *We say that equation* (2.2) *is null controllable from $\omega \subset \Omega$ in time $T > 0$ if, for every $f_0 \in L^2(\Omega)$, there exists a control $u \in L^2(0,T; L^2(\Omega))$ supported in $(0,T) \times \omega$ such that the solution f of* (2.2) *satisfies $f(T,\cdot) = 0$.*

Then, we have the following, see [BCG14, Theorem 1].

Theorem 2.2.1 ([BCG14]) *Let $\omega = (a,b) \times (0,1)$, where $0 < a < b \leq 1$. Then a positive minimal time is required for null controllability of* (2.2) *from ω, namely*

$$T_{\min}(\omega) := \inf\{T > 0 : \textit{system } (2.2) \textit{ is null controllable from } \omega \textit{ in time } T\}$$

satisfies $T_{\min}(\omega) \geq \frac{a^2}{2}$. Moreover, there exists $T^* > 0$ such that, for every $T \geq T^*$, system (2.2) *is null controllable from ω in time T.*

Remark 2.2.1 *In Theorem 2.2.1, if the control set ω intersect the degeneracy set $\mathcal{Z}$, viz. $a = 0$, then the control system* (2.2) *is null controllable in arbitrarily small time $T > 0$, see [BMM15, Theorem 1.2]. More precisely, if $\omega = (0,a) \times (0,1)$, $0 < a < 1$, then the minimal time of null controllability of PBG Equation* (2.2) *from ω is $T_{\min}(\omega) = 0$.*

Remark 2.2.2 *When the control set ω is the union of two symmetric vertical stripes located on both sides of the degeneracy set $\mathcal{Z}$, namely $\omega = [(-b,-a)\cup(a,b)]\times(0,1)$, it is shown in [BMM15, Theorem 1.3] that $T_{\min}(\omega) = \frac{a^2}{2}$ and that the PBG Equation (2.2) is not null controllable in time $T = \frac{a^2}{2}$. This minimal time corresponds to the Agmon "distance" associated with potential $q(x) = x^2$, between 0 (related to the degeneracy set ω) and a (related to control set ω). Recall from [BMM15] that, for a given potential $q \in C^1(\mathbb{R},\mathbb{R}^+)$, the associated Agmon "distance" between two points $z_1 < z_2$ is defined as*

$$d_{\mathrm{Ag}}(z_1,z_2) = \int_{z_1}^{z_2} \sqrt{q(s)}ds. \tag{2.3}$$

The above two remarks highlight that null controllability properties of PBG Equation (2.2) strongly depend on the geometrical shape of the control set ω and the time horizon T. When the control set ω is a complement of a horizontal strip intersecting the degeneracy set $\mathcal{Z}$, we have the following non-null controllability result obtained by Koenig in [Koe17, Theorem 2].

Theorem 2.2.2 ([Koe17]) *Let $[a,b]$ be a non-trivial segment of $(0,1)$, $\omega_y = (0,1)\backslash[a,b]$ and $\omega = (-1,1)\times\omega_y$. The control system (2.2) is non-null controllable from ω in any time $T > 0$.*

More general results have been obtained in the literature for the Baouendi-Grushin operator of the form $\mathcal{G}_q = \partial_x^2 + q(x)^2\partial_y^2$ in two-dimension. In [BDE20, Theorem 1.4], Beauchard, Dardé, and Ervedoza consider a potential q satisfying for some $L_\pm > 0$ the following

$$q(0) = 0, \qquad q \in \mathcal{C}^3([-L_-,L_+]), \qquad \inf_{(-L_-,L_+)} q' > 0. \tag{2.4}$$

For the associated parabolic equation on $\Omega = (-L_-,L_+)\times(0,\pi)$ degenerating at $x = 0$, with boundary control at the vertical side $\omega = \{L_+\}\times(0,\pi)$, and with initial datum $f_0 \in H_0^1(\Omega)$ the authors were able to obtain the sharp value of the minimal time for null controllability from ω, namely

$$T_{\min}(\omega) = \frac{d_{\mathrm{Ag}}(0,L_+)}{q'(0)}. \tag{2.5}$$

This minimal time result for null controllability from the boundary can be successfully used via a cut-off argument to prove that the lower bound $a^2/2$ on the minimal time in Theorem 2.2.1 is actually the exact minimal time [DK20, Theorem 5.1]. Moreover, the PBG Equation (2.2) is not null controllable from $\omega = (a,b)\times(0,1)$, $0 < a < b \leq 1$, in time $a^2/2$.

We also refer to [DK20] where general assumptions are made on the geometrical shape of the control set ω for null controllability of the PBG Equation (2.2) to holds true or not. Finally, for a comprehensive review of the minimal time issue to control the Baouendi-Grushin type operator, the reader could refer to [All18, Chapter 4].

2.3 . Parabolic Baouendi-Grushin equation in spherical coordinates

This section provides the trick to prove Theorem 1.2.1. To this aim and, by the way, understand how the operator $\mathcal{L}$ is connected with the Baouendi-Grushin operator (BG), we use spherical

coordinates. It is slightly easier to consider the vector fields X_1 and X_2 defined respectively in (1.11) and (1.12) as the restriction on $\mathbb{S}^2$ of the vector fields in $\mathbb{R}^3$ given by the same formulae.

Let

$$\Omega := (-\pi/2, \pi/2) \times [0, 2\pi), \qquad \text{and} \qquad U := \mathbb{R}_+^* \times \Omega, \tag{2.6}$$

and consider the latitude x and longitude y coordinates, viz.

$$\begin{aligned} \mathrm{F}: \quad U \quad &\longrightarrow \mathbb{R}^3 \\ (r, x, y) \quad &\longmapsto \mathrm{F}(r, x, y) = (r\cos x \cos y, r \cos x \sin y, r \sin x). \end{aligned} \tag{2.7}$$

Then $\mathrm{F}^{-1}(\mathbb{S}^2 \backslash \{N, S\}) = \{1\} \times \Omega \cong \Omega$. We let $\Phi := \mathrm{F}\,|_\Omega$, then the pullback by Φ of the vector fields X_1 and X_2 are given for every $(x, y) \in \Omega$, by

$$\Phi^* X_1 = (d\,\mathrm{F}^{-1} \cdot X_1)|_{\Phi(r,x,y)} = \cos\left(\frac{\pi}{2} - y\right) \partial_x - \sin\left(\frac{\pi}{2} - y\right) \tan x \partial_y, \tag{2.8}$$

$$\Phi^* X_2 = (d\,\mathrm{F}^{-1} \cdot X_2)|_{\Phi(r,x,y)} = \sin\left(\frac{\pi}{2} - y\right) \partial_x + \cos\left(\frac{\pi}{2} - y\right) \tan x \partial_y, \tag{2.9}$$

where $d\,\mathrm{F}^{-1}$ denotes the inverse of the Jacobian matrix of F. Let $\mathcal{R}_{y-\frac{\pi}{2}}$ be the rotation of angle $y - \pi/2$ centred at the origin and set

$$\{X, Y\} := \mathcal{R}_{y-\frac{\pi}{2}} \{\Phi^* X_1, \Phi^* X_2\} = \{\partial_x, \tan x \partial_y\}. \tag{2.10}$$

Therefore, the pair of vector fields $\{X, Y\}$ defines the same AR structure on $\mathbb{S}^2$ than $\{\Phi^* X_1, \Phi^* X_2\}$ which is the Grushin sphere in these coordinates setting, see Figure 2.2. We may also observe that, due to the system of coordinates, the vector field Y is singular at $\pm\pi/2$. Moreover, the coordinates representation on Ω of the Riemannian area $d\mu$ on $\mathbb{S}^2$ is given by

$$d\sigma(x, y) = \cos x dx dy, \qquad (x, y) \in \Omega. \tag{2.11}$$

Observe finally that the diffeomorphism $\Phi : \Omega \to \mathbb{S}^2 \backslash \{N, S\}$ induces a unitary transformation[1]

$$\begin{aligned} \mathrm{T}_\Phi: \quad L^2(\mathbb{S}^2 \backslash \{N, S\}; \mu) \quad &\longrightarrow L^2(\Omega; \sigma) \\ v \quad &\longmapsto \mathrm{T}_\Phi\, v = v \circ \Phi, \end{aligned} \tag{2.12}$$

and that $\Phi^* X_1 = \mathrm{T}_\Phi\, X_1\, \mathrm{T}_\Phi^+$ and $\Phi^* X_2 = \mathrm{T}_\Phi\, X_2\, \mathrm{T}_\Phi^+$. Here T_Φ^+ is the adjoint (which is also its inverse) of T_Φ. From now on we let the *spherical Baouendi-Grushin* operator be the coordinate representation under Φ of $\mathcal{L}$. That is, the operator defined by

$$\Delta_{\mathrm{BG}} := \Phi^* \mathcal{L} = \mathrm{T}_\Phi\, \mathcal{L}\, \mathrm{T}_\Phi^+ . \tag{2.13}$$

In terms of the local generating family of vector fields $\{X, Y\}$ we have

$$\Delta_{\mathrm{BG}} = -X^+ X - Y^+ Y = \frac{1}{\cos x} \partial_x (\cos x \partial_x) + \tan^2 x \partial_y^2, \tag{2.14}$$

with X^+ and Y^+ being the formal adjoints of X and Y respectively, taken in the space $L^2(\Omega; \sigma)$.

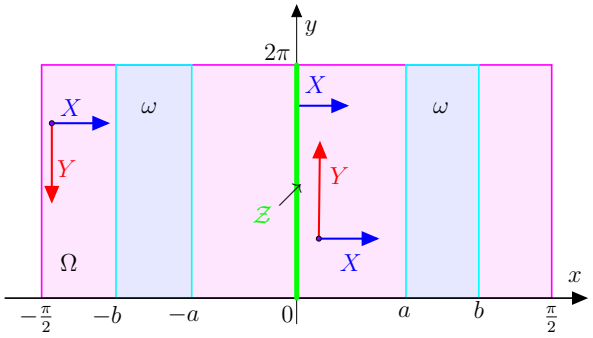

Figure 2.2: The Grushin sphere in latitude-longitude coordinates (x, y): The generating vector fields X and Y and the degeneracy set $\mathcal{Z} = \Phi^{-1}(\mathcal{E})$. The medium $\Omega = \Phi^{-1}(\mathbb{S}^2 \backslash \{N, S\})$ and a control set ω, union of two symmetric vertical stripes non-intersecting $\mathcal{Z}$.

Remark 2.3.1 *The intrinsic operator $\mathcal{L}$ defined in (2.14) and the spherical Baouendi-Grushin operator Δ_{BG} defined in (2.13)-(2.14) are formally self adjoint respectively in Hilbert spaces $L^2(\mathbb{S}^2; \mu)$ and $L^2(\Omega; \sigma)$.*

Remark 2.3.2 *The singularity of Δ_{BG} at the north and south poles is due to the latitude-longitude chart Φ. We stress that whatever chart is chosen, this phenomenon of singularity will always occur since global coordinates do not exist[2] on $\mathbb{S}^2$.*

The following remark illustrates the connection between the spherical Baouendi-Grushin operator Δ_{BG} and the Baouendi-Grushin operator (BG).

Remark 2.3.3 *Consider (2.14) and take the first order Taylor expansion of $\cos x$ and $\tan x$ at $x = 0$. We observe that $d\sigma = dxdy$ and $\Delta_{\mathrm{BG}} = \partial_x^2 + x^2\partial_y^2$, so that Δ_{BG} behaves like the Baouendi-Grushin operator (BG) in a neighbourhood of the degeneracy set. In other words, the $2D$ Baouendi-Grushin operator $\mathcal{G}$ can be thought of as a "local model" of the spherical Baouendi-Grushin operator Δ_{BG} at each point of the equator. As a consequence, we should expect the same null controllability properties for the parabolic equation associated with Δ_{BG} as that of parabolic Baouendi-Grushin Equation (2.2).*

In these coordinates settings, the intrinsic control system (1.16) is equivalent to

$$\begin{cases} \partial_t f - \Delta_{\mathrm{BG}} f = u \mathbb{1}_\omega, & \text{in } (0,T) \times \Omega, \\ f|_{t=0} = f_0, & \text{in } \Omega, \end{cases} \tag{2.15}$$

with corresponding underlying boundary conditions satisfying by f, see Lemma 2.4.1. Here $\omega \subset \Omega$, $f = f(t, x, y)$ is the state describing, e.g., the temperature at $(x, y) \in \Omega$ at the time

[1]Here $L^2(\Omega; \sigma)$ is the Hilbert space of measurable and square-integrable functions over Ω with respect to σ.

[2]In fact, $\mathbb{S}^2$ is not a *local* surface of $\mathbb{R}^3$ in the sense that it can not be defined by a single chart [BG88, p. 348]. That is, there is no open set $U \subset \mathbb{R}^2$ and an immersion $\phi \in C^\infty(U; \mathbb{R}^3)$ such that ϕ is a homeomorphism between U and its image $\mathbb{S}^2 = \phi(U)$.

$t > 0$, the time horizon $T > 0$, $f_0 = f_0(x, y)$ is the initial datum and $u = u(t, x, y)$ is the control function.

Recall that the control system (2.15) is null controllable from $\omega \subset \Omega$ in time $T > 0$ if, for every $f_0 \in L^2(\Omega; \sigma)$, there exists a control $u \in L^2(0, T; L^2(\Omega; \sigma))$ supported in $(0, T) \times \omega$ such that the solution f of (2.15) satisfies $f(T, \cdot, \cdot) = 0$.

Throughout the following, we let the real numbers $0 < a < b \leq \pi/2$ be such that $\alpha = \sin a$ and $\beta = \sin b$ with α and β being defined as in Theorem 1.2.1. We therefore set

$$\omega := \omega_{a,b} \times [0, 2\pi), \qquad \text{with} \qquad \omega_{a,b} = (-b, -a) \cup (a, b). \tag{2.16}$$

Then, Theorem 1.2.1 is equivalent to the following [Tam22, Theorem 1.4].

Theorem 2.3.1 *Let ω be defined as in (2.16). Then a positive minimal time is required for null controllability of (2.15) from ω, namely*

$$T_{\min}(\omega) := \inf\{T > 0 : \textit{system (2.15) is null controllable from } \omega \textit{ in time } T\}$$

satisfies $T_{\min}(\omega) \geq \log(1/\cos a)$. Moreover, there exists $T^* > 0$ such that, for every $T \geq T^*$, system (2.15) is null controllable from ω in time T.

Remark 2.3.4 *If the elevation angle (latitude) a of the control region ω with respect to the equator is equal to zero, i.e., if ω contains the equator, then the strategy used in Section 2.5 to obtain the lower bound of the minimal time $T_{\min}(\omega)$ can not be applied. On the other hand, if the control acts only on one spherical crown (i.e., $\omega = (a, b) \times [0, 2\pi)$ with $0 < a < b < \pi/2$), the proof presented here still applies and shows that the lower bound of minimal time is still $\log(1/\cos a)$.*

Constructing a direct control function u, which allows solving a null controllability question as that of Theorem 2.3.1 is a difficult task in general, mainly when $\omega \subset \Omega$ is a subset of an Euclidean space of dimension greater than one. As it is now well-used in the literature, a strategy to deal with this difficulty relies on the link (see, for instance, [DR77; Lio88]) between null controllability and *observability inequality* of the same control system with a zero control in the right-hand side (called the adjoint system), namely,

$$\begin{cases} \partial_t g - \Delta_{\mathrm{BG}} g = 0, & \text{in } (0, T) \times \Omega, \\ g|_{t=0} = g_0, & \text{in } \Omega, \end{cases} \tag{2.17}$$

with corresponding underlying boundary conditions satisfying by g, see Lemma 2.4.1.

Definition 2.3.1 *The system (2.17) is observable in $\omega \subset \Omega$ in time $T > 0$ if, there exists $C := C(T, \omega) > 0$ such that, for every $g_0 \in L^2(\Omega; \sigma)$, the solution g of (2.17) satisfies*

$$\int_\Omega |g(T, x, y)|^2 d\sigma \leq C \int_0^T \int_\omega |g(t, x, y)|^2 d\sigma dt. \tag{2.18}$$

The observability inequality (2.18) means that the energy of the solution of (2.17) concentrated in ω yields an upper bound of the energy in time T everywhere in Ω.

Theorem 2.3.1 is then equivalent to the following [Tam22, Theorem 1.6].

Theorem 2.3.2 *Let ω be defined as in (2.16). Then a positive minimal time is required for observability of (2.17) in ω, namely*

$$T_{\min}(\omega) := \inf\{T > 0 : \textit{system (2.17) is observable in } \omega \textit{ in time } T\}$$

satisfies $T_{\min}(\omega) \geq \log(1/\cos a)$. Moreover, there exists $T^* > 0$ such that, for every $T \geq T^*$, system (2.17) is observable in ω in time T.

The proof of Theorem 2.3.2 is divided into two distinct steps:

1. Prove that for any time $T \leq \log(1/\cos a)$, the equation is not observable in ω in time T. We achieve this by exploiting an appropriate family of spherical harmonics, concentrating at the equator, to falsify the observability inequality (2.18);

2. Prove that there exists $T^* > 0$ such that, for every $T \geq T^*$, the equation is observable in ω in time T. It is done by following the strategy used by [BCG14], which consists of three distinct steps:

   (a) Expansion of solution $g(t, x, y)$ of system (2.17) into the Fourier basis of $L^2(0, 2\pi; dy)$ to deal with the degeneracy in front of ∂_y^2 in the definition of the operator Δ_{BG}. So, we let
   $$g(t, x, y) = \sum_{n\in\mathbb{Z}} g_n(t, x)e^{iny}, \tag{2.19}$$
   where each Fourier coefficient $g_n(t, x)$ solves a uniform parabolic equation which is *singular* at $\pm\pi/2$;

   (b) Prove a suitable Carleman estimate[3] for each parabolic equation solving by $g_n(t, x)$. In contrast to the work done in [BCG14], here we need to deal with the singularity at $\pm\pi/2$. To this end, we prove a suitable Hardy-Poincaré inequality and then take advantage of suitable unitary transformations to obtain these estimates;

   (c) With the help of these Carleman estimates, prove a uniform observability inequality for the family of one-dimensional parabolic equations satisfying $g_n(t, x)$ and use Bessel-Parseval's equality to recover the observability inequality (2.18).

Before doing these, let us first prove that systems (1.16), (2.15) and (2.17) are well-posed in appropriate Banach spaces.

2.4 . Well-posedness of Cauchy problems

It is interesting and useful to start with the well-posedness of the parabolic Equation (1.16) associated with the intrinsic Baouendi-Grushin operator $\mathcal{L}$ as defined in (1.13). Since $\{X_1, X_2, [X_1, X_2]\}_p$

[3] Carleman estimates are exponentially weighted energy estimates named after Torsten Carleman [Car39], where he introduced them in studying the unicity of solutions for elliptic equations with smooth coefficients in two-dimension.

generates the tangent space $T_p\mathbb{S}^2$ for any $p \in \mathbb{S}^2$, it follows from Strichartz [Str86, p.260-261] that $-\mathcal{L}$ with domain

$$D(\mathcal{L}) = \{u \in L^2(\mathbb{S}^2;\mu) : \mathcal{L}u := -X_1^+X_1u - X_2^+X_2u \in L^2(\mathbb{S}^2;\mu)\}, \tag{2.20}$$

is a nonnegative, densely-defined, self-adjoint operator on $L^2(\mathbb{S}^2;\mu)$, hypoelliptic [Hör67, Theorem 1.1] and has a compact resolvent. Therefore, its spectrum is real, discrete and consists of eigenvalues with finite multiplicity, labelled in increasing order, that is, $(\lambda_m)_{m\in\mathbb{N}^*}$, with $0 = \lambda_1 < \lambda_2 \leq \cdots \leq \cdots$, with $\lambda_m \to \infty$ as $m \to \infty$. Moreover, there exists an orthonormal Hilbert basis $(\varphi_m)_{m\in\mathbb{N}^*}$ of $L^2(\mathbb{S}^2;\mu)$ consisting of eigenfunctions of $\mathcal{L}$ associated with the eigenvalues $(\lambda_m)_{m\in\mathbb{N}^*}$.

Remark 2.4.1 *It should be noted that the Grushin sphere described in Section 1.2.2 is obtained as a restriction of complete Riemannian structure on the sphere $\mathbb{S}^2$. So, it is complete as metric space. It follows that, the operator $\mathcal{L}$ (a sub-Riemannian Laplacian in fact) defined on $C^\infty(\mathbb{S}^2)$ is essentially self-adjoint in $L^2(\mathbb{S}^2;\mu)$ and the domain of its unique self-adjoint extension coincides with (2.20) (see, Strichartz [Str86, p.261], [Str83, p.50 and Theorem 2.4]).*

We define the intrinsic semigroup on $L^2(\mathbb{S}^2;\mu)$ denoted $(e^{t\mathcal{L}})_{t\geq 0}$, as the family of operator $L^2(\mathbb{S}^2;\mu) \to L^2(\mathbb{S}^2;\mu)$ defined as follows for every $t \geq 0$: given $f_0 \in L^2(\mathbb{S}^2;\mu)$, $e^{t\mathcal{L}}f_0$ is the unique solution at time t of the homogeneous equation of (1.16), which is C^∞ on $]0,+\infty[\times\mathbb{S}^2$ (by the hypoellipticity[4] of operator $\mathcal{L}$) and given by

$$e^{t\mathcal{L}}f_0 = \sum_{m\in\mathbb{N}^*} e^{-t\lambda_m}\langle f_0, \varphi_m\rangle_{L^2(\mathbb{S}^2;\mu)}\varphi_m. \tag{2.21}$$

Let us state the following well-posedness result of the intrinsic parabolic Equation (1.16) whose proof is classical (see, e.g., [Paz12, Chapter 4]).

Proposition 2.4.1 *Given $T > 0$, $f_0 \in L^2(\mathbb{S}^2;\mu)$ and $v := \mathbb{1}_\omega u \in L^2(0,T;L^2(\mathbb{S}^2;\mu))$, there exists a unique solution $f \in C([0,T];L^2(\mathbb{S}^2;\mu))$ of Equation (1.16), given by Duhamel's formula*

$$f(t) = e^{t\mathcal{L}}f_0 + \int_0^t e^{(t-s)\mathcal{L}}v(s)ds, \qquad t \in [0,T]. \tag{2.22}$$

We now can provide an argument about the well-posedness of the parabolic Equation (2.15) associated with the spherical Baouendi-Grushin operator Δ_{BG} defined in (2.13) (or equivalently in (2.14)).

Let $\mathrm{H}_\sigma := L^2(\Omega;\sigma)$, and denote by $\langle\cdot,\cdot\rangle_{\mathrm{H}_\sigma}$ and $\|\cdot\|_{\mathrm{H}_\sigma}$, respectively, the scalar product and norm in H_σ.We have that $(\mathcal{L},\mathrm{D}(\mathcal{L}))$ and $(\Delta_{\mathrm{BG}},D(\Delta_{\mathrm{BG}}))$ are unitarily equivalent, where we let

$$\Delta_{\mathrm{BG}} = \mathrm{T}_\Phi\,\mathcal{L}\,\mathrm{T}_\Phi^+ \qquad \text{on} \qquad D(\Delta_{\mathrm{BG}}) = \mathrm{T}_\Phi(D(\mathcal{L})). \tag{2.23}$$

[4] A partial differential operator E defined on a smooth manifold M is called hypoelliptic if for every distribution u defined on an open subset $\Omega \subset M$ such that $Eu \in C^\infty(\Omega)$, u must also be $C^\infty(\Omega)$.

Here, T_Φ is the unitary transformation defined in (2.12), T_Φ^+ being is adjoint. Therefore, $-\Delta_{\mathrm{BG}}$ with domain $D(\Delta_{\mathrm{BG}})$ is a nonnegative, densely-defined, self-adjoint operator on H_σ and has compact resolvent. We also remark that $v \in D(\Delta_{\mathrm{BG}})$ means $v = u \circ \Phi$ for some $u \in D(\mathcal{L})$. So, we have the following.

Lemma 2.4.1 *Let $v \in D(\Delta_{\mathrm{BG}})$. Then, we have that $v,\ \Delta_{\mathrm{BG}} v \in \mathrm{H}_\sigma$, the function $y \mapsto v(\pi/2, y)$ (resp. $y \mapsto v(-\pi/2, y)$) is constant, and $y \mapsto v(x, y)$ is 2π-periodic for any $x \in [-\pi/2, \pi/2]$. Moreover, the following functions are well-defined and real-valued:*

$$y \in [0, 2\pi) \mapsto \partial_x v(\pi/2, y), \quad y \in [0, 2\pi) \mapsto \partial_x v(-\pi/2, y), \quad (x, y) \in \Omega \mapsto \tan x\, \partial_y v(x, y). \tag{2.24}$$

Remark 2.4.2 *We stress that boundary conditions of Lemma 2.4.1 are naturally associated with Cauchy problems (2.15) and (2.17).*

Let $\{W_{\ell,n}\}_{\ell\in\mathbb{N}, -\ell\le n\le\ell}$ denotes the family of spherical harmonics, defined by

$$W_{\ell,n}(x, y) = \sqrt{\frac{2\ell+1}{4\pi}\frac{(\ell-n)!}{(\ell+n)!}} P_\ell^n(\sin x) e^{iny}, \qquad \forall x \in [-\pi/2, \pi/2] \times [0, 2\pi), \tag{2.25}$$

with P_ℓ^n being associated Legendre functions of the first kind. Then we can check that each $W_{\ell,n}$ lies in $D(\Delta_{\mathrm{BG}})$ and the operator Δ_{BG} satisfies (see, [CCM19, p.9] and references within)

$$-\Delta_{\mathrm{BG}} W_{\ell,n} = \lambda_{n,\ell} W_{\ell,n}, \qquad \lambda_{n,\ell} := \ell(\ell+1) - n^2, \qquad \forall\ |n| \le \ell \in \mathbb{N}. \tag{2.26}$$

Moreover, by using the identification $\mathrm{H}_\sigma \cong L^2((-\pi/2, \pi/2); \cos x dx) \otimes L^2([0, 2\pi), dy)$, we have that $\{W_{\ell,n}\}_{\ell\in\mathbb{N}, -\ell\le n\le\ell}$ form an orthonormal Hilbert basis of the space H_σ [CH53, p. 512]. In particular, $D(\Delta_{\mathrm{BG}})$ is a non-empty and dense subspace of H_σ.

The spherical Baouendi-Grushin semigroup on H_σ denoted $(e^{t\Delta_{\mathrm{BG}}})_{t\ge0}$ is then the family of operators $\mathrm{H}_\sigma \to \mathrm{H}_\sigma$ defined as follows for every $t \ge 0$: given $f_0 \in \mathrm{H}_\sigma$, $e^{t\Delta_{\mathrm{BG}}} f_0$ is the unique solution at time t of the homogeneous Equation (2.17), which is C^∞ on $]0, +\infty[\times\Omega$ and given by

$$e^{t\Delta_{\mathrm{BG}}} f_0 = \sum_{|n|\le\ell\in\mathbb{N}} e^{-t\lambda_{n,\ell}} \langle f_0, W_{\ell,n}\rangle_{\mathrm{H}_\sigma} W_{\ell,n}. \tag{2.27}$$

We now can state the following well-posedness result of the parabolic Equation (2.15) associated with the spherical Baouendi-Grushin operator Δ_{BG} (see, e.g., [Paz12, Chapter 4]).

Proposition 2.4.2 *Given $T > 0$, $f_0 \in \mathrm{H}_\sigma$ and $v := \mathbb{1}_\omega u \in L^2(0, T; \mathrm{H}_\sigma)$, there exists a unique solution $f \in C([0, T]; \mathrm{H}_\sigma)$ of Equation (2.15), and Duhamel's formula gives*

$$f(t) = e^{t\Delta_{\mathrm{BG}}} f_0 + \int_0^t e^{(t-s)\Delta_{\mathrm{BG}}} v(s) ds, \quad t \in [0, T]. \tag{2.28}$$

2.5 . Non observability result in small time

As announced at the end of Section 2.3, this section is dedicated to proving that there exist initial data in $L^2(\Omega;\sigma)$ for which the corresponding solutions for Equation (2.17) do not satisfy observability inequality (2.18) in ω in time $T \leq \log(1/\cos a)$, where ω and a are defined as in (2.16). We have the following.

Proposition 2.5.1 *Let $a, b \in \mathbb{R}$ be such that $0 < a < b \leq \pi/2$ and $T \leq \log(1/\cos a)$. Then system (2.17) is not observable in $(a,b)\times[0,2\pi)$ in time T.*

Proof . We recall that the highest weight spherical harmonics of degree n present extreme concentration around the equator. These are defined by

$$W_{n,n}(x,y) = \frac{(-1)^n}{2^n n!}\sqrt{\frac{(2n+1)!}{4\pi}}e^{iny}\cos^n x, \tag{2.29}$$

where $n \in \mathbb{N}^*$, $(x,y) \in [-\pi/2, \pi/2]\times[0,2\pi)$. Fix $n \in \mathbb{N}^*$ and let g be the solution of (2.17) corresponding to the initial datum $g_0(x,y) = W_{n,n}(x,y)$. Then one has by (2.27),

$$g(t,x,y) = e^{-t\lambda_{n,n}}\|W_{n,n}\|^2_{\mathrm{H}_\sigma}W_{n,n}(x,y) = e^{-tn}W_{n,n}(x,y), \tag{2.30}$$

for every $t \geq 0$. Indeed, by Wallis' formula, we have for every $n \in \mathbb{N}^*$,

$$\int_0^{\frac{\pi}{2}}\cos^{2n+1}x dx = \frac{2^{2n}(n!)^2}{(2n+1)!}.$$

It follows that for every $n \in \mathbb{N}^*$,

$$\|W_{n,n}\|^2_{\mathrm{H}_\sigma} = \frac{(2n+1)!}{2^{2n}(n!)^2}\int_0^{\frac{\pi}{2}}\cos^{2n+1}x dx = 1, \qquad \int_{-\frac{\pi}{2}}^{\frac{\pi}{2}}\int_0^{2\pi}|g(T,x,y)|^2\cos x dx dy = e^{-2nT}.$$

Observe also that

$$\int_0^T\int_a^b\int_0^{2\pi}|g(t,x,y)|^2\cos x dx dy dt = \frac{(2n+1)!}{\pi n 2^{2n+2}(n!)^2}\left[1-e^{-2nT}\right]\int_a^b\cos^{2n+1}x dx.$$

On the other hand, by Stirling's formula, one has $n! \sim \sqrt{2\pi n}n^n e^{-n}$ as $n \to +\infty$. It follows that If g satisfied observability inequality (2.18) in $\omega = (a,b)\times[0,2\pi)$ in time $T \leq \log(1/\cos a)$, then there will exists a positive constant $C := C(T,a,b) > 0$ such that the following holds

$$1 \leq C\frac{\cos a}{2\pi^{3/2}}\frac{(2n+1)}{n^{3/2}}e^{2n(T+\log(\cos a))}(b-a) \longrightarrow 0 \quad \text{as} \quad n \longrightarrow +\infty, \tag{2.31}$$

which is untrue. This completes the proof of the proposition. □

Remark 2.5.1 *Notice that the not null observability result provided here remains true in the observation set $[(-b,-a)\cup(a,b)]\times[0,2\pi)$ by symmetry of this domain and parity of $W_{n,n}$ with respect to x.*

2.6 . Observability result in large time

In this section, following the strategy explained at the end of Section 2.3, we will split the proof of the following result for clarity in the presentation. There exists $T^* > 0$ such that, for every $T \geq T^*$, the adjoint system (2.17) is observable in ω in time T. Here ω is the control set defined in (2.16).

We recall that $H^1(-\pi/2, \pi/2)$ is the classical Sobolev space of functions in $L^2(-\pi/2, \pi/2)$ whose derivative in the sense of distribution also belongs to $L^2(-\pi/2, \pi/2)$, and $H_0^1(-\pi/2, \pi/2)$ stands to be the subspace of functions $u \in H^1(-\pi/2, \pi/2)$ such that $u(\pm\pi/2) = 0$. These Hilbert spaces are endowed with their standard norm.

We admit the following lemma where the detailed proof could be found in [Tam22, Lemma 2.6]. It is a key ingredient for the proof of Carleman estimates in Appendix 2.7.

Lemma 2.6.1 (Hardy-Poincaré inequality) *Let $w \in H_0^1(-\pi/2, \pi/2)$ and w' its derivative in the sense of distribution. Then, it holds*

$$\int_{-\frac{\pi}{2}}^{\frac{\pi}{2}} \frac{|w(x)|^2}{\cos^2 x} dx \leq 4 \int_{-\frac{\pi}{2}}^{\frac{\pi}{2}} |w'(x)|^2 dx. \tag{2.32}$$

2.6.1 . Fourier expansion of the solution of the adjoint system

Using the complete orthonormal eigenbasis $(e^{iny})_{n\in\mathbb{Z}}$ of $L^2([0, 2\pi); dy)$, we separate the space $\mathrm{H}_\sigma = \oplus_{n\in\mathbb{Z}}^{\perp} \mathcal{H}_n$, where $\mathcal{H}_n \cong L^2((-\pi/2, \pi/2); \cos x dx)$. Therefore, one has for every $t \geq 0$,

$$e^{t\Delta_{\mathrm{BG}}} = \bigoplus_{n\in\mathbb{Z}}^{\perp} e^{t\mathcal{L}_n}. \tag{2.33}$$

Here for any $n \in \mathbb{Z}$, the operator $\mathcal{L}_n$ is defined on $\mathcal{H}_n$ by

$$D(\mathcal{L}_n) = \left\{ v \in \mathcal{H}_n \mid \mathcal{L}_n v \in \mathcal{H}_n, v(\pm\pi/2) \in \mathbb{R}, v'(\pm\pi/2) \in \mathbb{R} \right\}, \tag{2.34}$$

$$\mathcal{L}_n v = \frac{1}{\cos x}(\cos x v')' - n^2 \tan^2 x v, \qquad v \in D(\mathcal{L}_n). \tag{2.35}$$

Remark 2.6.1 *The boundary conditions in $D(\mathcal{L}_n)$ naturally come from Lemma 2.4.1. Moreover, from (2.33), one deduces that for every $n \in \mathbb{Z}$, the operator $(\mathcal{L}_n, D(\mathcal{L}_n))$ is the generator of the one-parameter strongly continuous semigroup of contraction $(e^{t\mathcal{L}_n})_{t\geq 0}$ on $\mathcal{H}_n$.*

Since the solution g of adjoint system (2.17) belongs to $C([0, T]; \mathrm{H}_\sigma)$, the function $y \mapsto g(t, x, y)$ belongs to $L^2([0, 2\pi); dy)$ for a.e. $(t, x) \in (0, T) \times (-\pi/2, \pi/2)$. It follows that (2.17) is formally equivalent to the following family of one-dimensional parabolic equations indexed by $n \in \mathbb{Z}$,

$$\begin{cases} \partial_t g_n - \mathcal{L}_n g_n = 0, & \text{in } (0, T) \times (-\pi/2, \pi/2), \\ g_n|_{t=0} = g_{0,n}, & \text{in } (-\pi/2, \pi/2). \end{cases} \tag{2.36}$$

Here, the n-th Fourier component g_n is given by

$$g_n(t,x) = \int_0^{2\pi} g(t,x,y)e^{iny}dy, \qquad (t,x) \in (0,T)\times(-\pi/2,\pi/2), \tag{2.37}$$

and $g_{0,n}$ is the n-th Fourier coefficients of the initial datum $g_0 \in \mathrm{H}_\sigma$ in Equation (2.17).

In the following lemmas we derive some useful properties of functions belonging to $D(\mathcal{L}_n)$ as well as their behaviour at $\pm\pi/2$. We begin by the case $n = 0$.

Lemma 2.6.2 *Let $v \in D(\mathcal{L}_0)$. Then v belongs to the Sobolev space $H^1(-\pi/2,\pi/2)$ and v is locally absolutely continuous on $[-\pi/2,\pi/2]$. Moreover, it holds*

$$v'(x) = o(1) \qquad \text{as} \quad x \to \pm\frac{\pi}{2}. \tag{2.38}$$

Proof. Let $v \in D(\mathcal{L}_0)$. Then v and $\mathcal{L}_0 v$ belong to $\mathcal{H}_0 \cong L^2((-\pi/2,\pi/2);\cos x dx)$ and $v(\pm\pi/2) \in \mathbb{R}$, $v'(\pm\pi/2) \in \mathbb{R}$. It follows by integration by parts that

$$\|v'\|^2_{\mathcal{H}_0} = -\langle \mathcal{L}_0 v, v\rangle_{\mathcal{H}_0} < \infty. \tag{2.39}$$

Since $\sin x v', \cos x v, \sqrt{\cos x}v, \sqrt{\cos x}v' \in \mathcal{H}_0$, the following is finite

$$\|v\|^2_{H^1(-\pi/2,\pi/2)} = 2\left[\langle \mathcal{L}_0 v, -\cos x v + \sin x v'\rangle_{\mathcal{H}_0} + \|\sqrt{\cos x}v\|^2_{\mathcal{H}_0} + \|\sqrt{\cos x}v'\|^2_{\mathcal{H}_0}\right]. \tag{2.40}$$

It follows that v belongs to the Sobolev space $H^1(-\pi/2,\pi/2) \hookrightarrow W^{1,1}(-\pi/2,\pi/2)$, and then v is locally absolutely continuous on $[-\pi/2,\pi/2]$. On the other hand, one has

$$\begin{aligned}\int_{-\frac{\pi}{2}}^{\frac{\pi}{2}} \frac{|v'(x)|^2}{\cos x}dx &\leq \int_{-\frac{\pi}{2}}^{\frac{\pi}{2}} \left(|v''(x)|^2 + \frac{|v'(x)|^2}{\cos^2 x}\right)\cos x dx \\ &= \int_{-\frac{\pi}{2}}^{\frac{\pi}{2}} |\mathcal{L}_0 v(x)|^2 \cos x dx + \left|v'(\pi/2)\right|^2 + \left|v'(-\pi/2)\right|^2 < \infty. \end{aligned} \tag{2.41}$$

Since $\cos(\pm\pi/2) = 0$ this implies (2.38). Moreover (2.41) also shows that $v'' \in \mathcal{H}_0$. In particular, $\tan x v' \in \mathcal{H}_0$, since $\mathcal{L}_0 v \in \mathcal{H}_0$ and $v'' \in \mathcal{H}_0$. □

In the cases $n \in \mathbb{Z}\backslash\{0\}$, we have the following

Lemma 2.6.3 *Let $n \in \mathbb{Z}\backslash\{0\}$ and $v \in D(\mathcal{L}_n)$. Then v belongs to the Sobolev space $H^1(-\pi/2,\pi/2)$ and v is locally absolutely continuous on $[-\pi/2,\pi/2]$. Moreover, it holds*

$$v(x) = o(1) \qquad \text{and} \qquad \frac{v(x)}{\sqrt{\cos x}} = o(1) \qquad \text{both as} \quad x \to \pm\frac{\pi}{2}. \tag{2.42}$$

Proof. Let $n \in \mathbb{Z}\backslash\{0\}$ and $v \in D(\mathcal{L}_n)$. Since $v,\ \mathcal{L}_n v \in \mathcal{H}_n \cong L^2((-\pi/2,\pi/2);\cos x dx)$, $v(\pm\pi/2) \in \mathbb{R}$ and $v'(\pm\pi 2) \in \mathbb{R}$, one obtain using integration by parts that the following is finite

$$\|v'\|^2_{\mathcal{H}_n} \leq \int_{-\frac{\pi}{2}}^{\frac{\pi}{2}} \left(|v'(x)|^2 + |n\tan x v|^2\right)\cos x dx = -\langle v, \mathcal{L}_n v\rangle_{\mathcal{H}_n}. \tag{2.43}$$

In particular, $\tan xv \in \mathcal{H}_n$ so that

$$\|\cos^{-1} xv\|^2_{\mathcal{H}_n} = \|\tan xv\|^2_{\mathcal{H}_n} + \|v\|^2_{\mathcal{H}_n} < \infty, \tag{2.44}$$

and by Cauchy-Schwarz inequality,

$$\|v\|^2_{L^2(-\pi/2,\pi/2)} \leq \|\cos^{-1} xv\|_{\mathcal{H}_n}\|v\|_{\mathcal{H}_n} < \infty. \tag{2.45}$$

Therefore, using $\sin xv' \in \mathcal{H}_n$, (2.44) and (2.45) one deduce successively that the following are finites

$$\int_{-\frac{\pi}{2}}^{\frac{\pi}{2}} \frac{|v(x)|^2}{\cos x}dx = \|v\|^2_{L^2(-\pi/2,\pi/2)} + \frac{1}{n^2}\left[\left\langle -\mathcal{L}_n v, \frac{v}{\cos x}\right\rangle_{\mathcal{H}_n} - \int_{-\frac{\pi}{2}}^{\frac{\pi}{2}} \tan x|v(x)|^2 dx\right], \tag{2.46}$$

$$\|v'\|^2_{L^2(-\pi/2,\pi/2)} = -2\langle \mathcal{L}_n v, \sin xv'\rangle_{\mathcal{H}_n} + n^2\int_{-\frac{\pi}{2}}^{\frac{\pi}{2}} \sin^2 x(3+\tan^2 x)|v(x)|^2 dx. \tag{2.47}$$

Thus v belongs to the Sobolev space $H^1(-\pi/2,\pi/2) \hookrightarrow W^{1,1}(-\pi/2,\pi/2)$, and then v is locally absolutely continuous on $[-\pi/2,\pi/2]$. In particular, it holds

$$v(x_2) - v(x_1) = \int_{x_1}^{x_2} v'(s)ds \qquad \forall x_1, x_2 \in [-\pi/2,\pi/2]. \tag{2.48}$$

On the other hand, since $\tan xv \in \mathcal{H}_n$, the first identity in (2.42) immediately follows. Let us turn to an argument for the second identity of (2.42). Let $\varepsilon > 0$, then by the first identity of (2.42), and (2.48) one has for all $v \in D(\mathcal{L}_n)$, $n \neq 0$,

$$\left|v\left(-\frac{\pi}{2}+\varepsilon\right)\right| \leq \int_{-\frac{\pi}{2}}^{-\frac{\pi}{2}+\varepsilon} |v'(t)|dt \leq \|v'\|_\infty \varepsilon.$$

Hence,

$$\lim_{x\to-\frac{\pi}{2}^+} \frac{|v(x)|}{\sqrt{\cos x}} = \lim_{\varepsilon\to 0} \frac{|v(-\frac{\pi}{2}+\varepsilon)|}{\sqrt{\cos(-\frac{\pi}{2}+\varepsilon)}} \leq \|v'\|_\infty \lim_{\varepsilon\to 0} \frac{\varepsilon}{\sqrt{\sin\varepsilon}} = 0.$$

The proof of the limit at $\pi/2$ is similar. □

Remark 2.6.2 *Lemmas 2.6.2 and 2.6.3 show in particular that, for all $v \in D(\mathcal{L}_n)$, $\mathcal{L}_n v$ has a meaning* a. e. *in $(-\pi/2,\pi/2)$. Moreover, Lemma 2.6.3 also shows that the domain $\mathrm{D}(\mathcal{L}_\mathrm{n})$ is a subspace of the Sobolev space $H^1_0(-\pi/2,\pi/2)$ in the case $n \in \mathbb{Z}\backslash\{0\}$, hence Lemma 2.6.1 holds true in $D(\mathcal{L}_n)$.*

The following proposition is the direct consequence of Section 2.4. We also refer to [Nai68, p. 68] in which the theory of the singular Sturm-Liouville equation is well-elaborated.

Proposition 2.6.1 *Let $n \in \mathbb{Z}$. Then, $-\mathcal{L}_n : D(\mathcal{L}_n) \subset \mathcal{H}_n \to \mathcal{H}_n$ is a densely defined, self-adjoint, positive operator and has compact resolvent.*

One can check that the functions $v_{n,\ell}$ defined for $\ell \in \mathbb{N}$, $n \in \mathbb{Z}$ and $|n| \leq \ell$ by

$$v_{n,\ell}(x) = \sqrt{\frac{2\ell+1}{2}\frac{(\ell-n)!}{(\ell+n)!}} P_\ell^n(\sin x), \qquad \forall x \in [-\pi/2, \pi/2], \tag{2.49}$$

form a complete orthonormal set of the Hilbert space $\mathcal{H}_n$ [CH53, p. 512], with P_ℓ^n being the associated Legendre function of the first kind. Moreover, each $v_{n,\ell}$ lies in $D(\mathcal{L}_n)$ and we have

$$-\mathcal{L}_n v_{n,\ell} = \lambda_{n,\ell} v_{n,\ell}, \qquad \lambda_{n,\ell} = \ell(\ell+1) - n^2.$$

Therefore, the functions $v_{n,\ell}$ are the eigenfunctions of operators $-\mathcal{L}_n$ with eigenvalues $\lambda_{n,\ell}$.

The following result is then an immediate consequence of Proposition 2.6.1.

Proposition 2.6.2 *Let $T > 0$ and g be the solution of the adjoint system (2.17). For every $n \in \mathbb{Z}$, the n-th Fourier component g_n of g as given by (2.37), is the unique solution of (2.36) belonging to the class*

$$C([0,T]; \mathcal{H}_n) \cap C^\infty((0,T); \mathcal{H}_n). \tag{2.50}$$

Moreover, it can be represented for every $t \geq 0$ as

$$g_n(t) = e^{t\mathcal{L}_n} g_{0,n} = \sum_{\ell \in \mathbb{N}} e^{-\lambda_{n,\ell} t} \langle g_{0,n}, v_{n,\ell} \rangle_{\mathcal{H}_n} v_{n,\ell}, \tag{2.51}$$

where $g_{0,n} \in \mathcal{H}_n$ is given by $g_{0,n}(x) = \displaystyle\int_0^{2\pi} g_0(x,y) e^{iny} dy$, with g_0 being the initial condition in Equation (2.17).

Remark 2.6.3 *We may show by an inductive argument that for all $n \in \mathbb{Z}$, $g_n \in C^\infty((0,T); D(\mathcal{L}_n))$.. Moreover, g_n is C^∞ on $]0, +\infty[\times(-\pi/2, \pi/2)$.*

Remark 2.6.4 (Decay rate) *Using Proposition 2.6.2, we immediately obtain that the Fourier component g_n satisfies the following dissipation rate*

$$\|g_n(T,\cdot)\|_{\mathcal{H}_n} \leq e^{-|n|(T-t)} \|g_n(t,\cdot)\|_{\mathcal{H}_n}, \qquad \forall t \in (0,T). \tag{2.52}$$

Notation 1 *In what follows, to simplify the notation, we shall assume $n \in \mathbb{N}$. The same considerations hold for $n \in \mathbb{Z}_-$ by replacing n with $|n|$.*

2.6.2 . Strategy for proving observability inequality in large time

We illustrate in this section how the proof of observability inequality for the adjoint system (2.17) in large time reduces to the proof of an observability inequality in large time for the $1D$ parabolic equations (2.36) that is uniform with respect to $n \in \mathbb{N}$. Recall that if g is the solution of (2.17), then it can be represented by

$$g(t,x,y) = \sum_{n \in \mathbb{Z}} g_n(t,x) e^{iny}, \qquad \text{for a.e. } (t,x,y) \in (0,T) \times \Omega. \tag{2.53}$$

We also emphasize that, by Bessel-Parseval's equality, one has, for a.e. $t \in (0,T)$ and every $-\pi/2 \leq a_1 \leq b_1 \leq \pi/2$, that

$$\int_{a_1}^{b_1}\int_0^{2\pi} |g(t,x,y)|^2 d\sigma = \sum_{n\in\mathbb{Z}} \int_{a_1}^{b_1} |g_n(t,x)|^2 \cos x dx. \tag{2.54}$$

Thus, if there exists a positive constant $C>0$, independent of $n \in \mathbb{N}$, and such that the following uniform observability holds for system (2.36)

$$\int_{-\frac{\pi}{2}}^{\frac{\pi}{2}} |g_n(T,x)|^2 dx \leq C \int_0^T \int_{\omega_{a,b}} |g_n(t,x)|^2 \cos x dx dt, \tag{2.55}$$

then, we can easily show that the observability inequality (2.18) is verified. Indeed, thanks to (2.53), (2.54) and (2.55), we find

$$\begin{aligned}\int_\Omega |g(T,x,y)|^2 d\sigma &= \sum_{|n|\leq \ell\in\mathbb{N}} \int_{-\frac{\pi}{2}}^{\frac{\pi}{2}} |g_n(T,x)|^2 \cos x dx \\ &\leq C \sum_{|n|\leq \ell\in\mathbb{N}} \int_0^T \int_{\omega_{a,b}} |g_n(t,x)|^2 \cos x dx dt = C \int_0^T \int_{\omega_{a,b}} \int_0^{2\pi} |g(t,x,y)|^2 d\sigma dt. \end{aligned} \tag{2.56}$$

This immediately yields (2.18). We recall the following.

Definition 2.6.1 *(Uniform observability) Let $\omega_{a,b}$ be defined as in (2.16). System (2.36) is observable in $\omega_{a,b}$ in time $T>0$ uniformly with respect to $n \in \mathbb{N}$, if there exists $C>0$ such that, for every $n \in \mathbb{N}$, and $g_{0,n} \in \mathcal{H}_n$, the solution of (2.36) satisfies (2.55).*

We recall that we cannot directly apply existing results in [BCG14; BMM15; BDE20] to obtain a uniform observability inequality for systems (2.36) due to the singularity at $\pm\pi/2$. In particular, in contrast to the classical singularity (at 0) of the form $1/x^2$, which is frequently studied in the literature (see, for instance, [CG14; Erv08; Mor15]) using the classical Hardi-Poincaré inequality [BM97, eq. (0.1)], we have here the singular term $1/\cos^2 x$ at $\pm\pi/2$ that we deal with by using the Hardy-Poincaré inequality provided by Lemma 2.6.1.

We shown in Lemmas 2.6.2 and 2.6.3 that function belonging respectively to $D(\mathcal{L}_0)$ and $D(\mathcal{L}_n)$ $(n \neq 0)$ have different behaviours at $\pm\pi/2$. Therefore we will distinguish these two cases by using a suitable unitary transformation in each case.

2.6.3 . Uniform observability for the one-dimensional parabolic equation for the zero frequency

We start by recasting when $n=0$ the one-dimensional system (2.36) in the space $L^2(-1,1)$ with the standard Lebesgue measure.

Let us consider the unitary transformation

$$\begin{aligned} \mathrm{V}: \quad L^2((-\pi/2,\pi/2);\cos x dx) &\longrightarrow L^2(-1,1) \\ v &\longmapsto (\mathrm{V}\, v)(x) = v(\arcsin x). \end{aligned}$$

We define the unbounded operator M_0 on the space $L^2(-1,1)$ by

$$\mathrm{M}_0 = \mathrm{V}\,\mathcal{L}_0\,\mathrm{V}^+, \qquad D(\mathrm{M}_0) = \mathrm{V}(D(\mathcal{L}_0)). \tag{2.57}$$

Here, V^+ is the adjoint of the unitary operator V, that is,

$$\begin{aligned} \mathrm{V}^+ : \quad L^2(-1,1) &\longrightarrow L^2((-\pi/2,\pi/2);\cos x dx) \\ w &\longmapsto (\mathrm{V}^+ w)(x) = w(\sin x). \end{aligned}$$

We then have the following expression for M_0,

$$\mathrm{M}_0\, w = ((1-x^2)w')', \qquad \forall w \in D(\mathrm{M}_0). \tag{2.58}$$

Since the differential operator ∂_t commutes with the unitary transformation V, one deduces easily that, when $n=0$, system (2.36) is equivalent to the following

$$\begin{cases} \partial_t \tilde{g}_0 - \mathrm{M}_0\,\tilde{g}_0 = 0, & \text{in } (0,T)\times(-1,1), \\ \tilde{g}_0|_{t=0} = \tilde{g}_{0,0}, & \text{in } (-1,1). \end{cases} \tag{2.59}$$

In particular, the solution $\tilde{g}_0 = \mathrm{V}\,g_0$ belongs to the class (see Proposition 2.6.2 and Remark 2.6.3)

$$C([0,T];L^2(-1,1)) \cap C^\infty((0,T);D(M_0)). \tag{2.60}$$

We characterise in the following some useful properties of functions belonging to the domain $D(\mathrm{M}_0)$, that is obtained by Lemma 2.6.2.

Lemma 2.6.4 *Let $w \in D(\mathrm{M}_0)$. Then w belongs to the Sobolev space $H^1(-1,1)$ and w is locally absolutely continuous on $[-1,1]$. Moreover, it holds*

$$w(\pm 1) \in \mathbb{R} \qquad \textit{and} \qquad w'(x)\sqrt{1-x^2} = o(1) \qquad \textit{as} \quad x \to \pm 1. \tag{2.61}$$

Proof. Let $w \in D(\mathrm{M}_0)$. Then $w(x) = v(\arcsin x)$ for some $v \in D(\mathcal{L}_0)$ and $x \in (-1,1)$. Since $v(\pm\pi/2) \in \mathbb{R}$, the first property in (2.61) immediately follows. Similarly, using the fact that $v \in \mathcal{H}_0 \cong L^2((-\pi/2,\pi/2);\cos x dx)$, and using (2.41), we obtain that the following are finites

$$\int_{-1}^{1} |w(x)|^2 dx = \int_{-\frac{\pi}{2}}^{\frac{\pi}{2}} |v(x)|^2 \cos x dx \qquad \text{and} \qquad \int_{-1}^{1} |w'(x)|^2 dx = \int_{-\frac{\pi}{2}}^{\frac{\pi}{2}} \frac{|v'(x)|^2}{\cos x} dx.$$

It follows that, $w, w' \in L^2(-1,1)$. Finally, $w'(x)\sqrt{1-x^2}|_{x=\pm 1} = v'(\pm\pi/2) = 0$, by (2.38). □

Remark 2.6.5 *We notice that an observability inequality for Equation (2.59) was established by Martinez and Vancostenoble in [MV06]. Indeed, thanks to Lemma 2.6.4, we aim to prove an observability inequality for the following equation*

$$\begin{cases} \partial_t w - \partial_x(a(x)\partial_x w) = 0, & \textit{a.e. in } (0,T)\times(-1,1), \\ (a(x)\partial_x w)(t,\pm 1) = 0, & t \in (0,T), \\ w(0,x) = w_0(x), & x \in (-1,1), \end{cases} \tag{2.62}$$

where $a(x) := 1 - x^2$, $w_0 \in L^2(-1,1)$ *and the solution* w *belongs to the class* (2.60). *We observe that the weight function* a *satisfies* $0 \leq a \in C^2([-1,1])$, $a(\pm 1) = 0$, $a > 0$ *on* $(-1,1)$, $\frac{1}{\sqrt{a}} \in L^1(-1,1)$ *and*

$$\frac{(1+x)a'(x)}{a(x)} \xrightarrow[x\to -1^+]{} 1 \qquad \text{and} \qquad \frac{(1-x)a'(x)}{a(x)} \xrightarrow[x\to 1^-]{} -1.$$

The above remark highlight that we are in the framework of [MV06, Theorem 3.4]. We then deduce the following.

Lemma 2.6.5 *Let* $T > 0$ *and* $a, b \in \mathbb{R}$ *defined as in* (2.16). *Let* $\widetilde{\omega}_{a,b} := (-\sin b, -\sin a) \cup (\sin a, \sin b)$. *Then, there exists a positive constant* $C_0 > 0$ *such that every solution* w *of system* (2.62) *satisfies*

$$\int_{-1}^{1} |w(T,x)|^2 dx \leq C_0 \int_0^T \int_{\widetilde{\omega}_{a,b}} |w(t,x)|^2 dx dt. \tag{2.63}$$

Finally, thanks to the Lemma 2.6.5 and the fact that $w := \mathrm{V}\, g_0$ is the solution of system (2.59), we deduce the following observability inequality for Equation (2.36) when $n = 0$.

Proposition 2.6.3 *Let* $T > 0$ *and* $\omega_{a,b}$ *be defined as in* (2.16). *Then, there exists a positive constant* $C_0 > 0$ *such that the first Fourier component* g_0, *which is the solution of Equation* (2.36) *when* $n = 0$ *satisfies*

$$\int_{-\frac{\pi}{2}}^{\frac{\pi}{2}} |g_0(T,x)|^2 \cos x dx \leq C_0 \int_0^T \int_{\omega_{a,b}} |g_0(t,x)|^2 \cos x dx dt. \tag{2.64}$$

Remark 2.6.6 *We highlight that the result of [MV06, Theorem 3.4] ensures that when* $n = 0$, *system* (2.36) *is observable in any subset* $\omega \subset\subset (-\pi/2, \pi/2)$ *and in arbitrary small time* $T > 0$.

2.6.4 . Uniform observability for one-dimensional parabolic equations corresponding to non-zero frequencies

In the case of a non-zero frequency $n \neq 0$, we recast the one-dimensional system (2.36) in the space $L^2(-\pi/2, \pi/2)$ with the standard Lebesgue measure.

We consider the unitary transformation

$$\begin{aligned} \mathrm{U}: \quad L^2((-\pi/2,\pi/2); \cos x dx) &\longrightarrow L^2(-\pi/2,\pi/2) && (2.65)\\ v &\longmapsto (\mathrm{U}\, v)(x) = \sqrt{\cos x} v(x). && (2.66) \end{aligned}$$

We define for all $n \in \mathbb{N}^*$ the unbounded operator $\mathrm{M_n}$ on the space $L^2(-\pi/2, \pi/2)$ by

$$\mathrm{M_n} = \mathrm{U}\, \mathcal{L}_n\, \mathrm{U}^+, \qquad D(\mathrm{M_n}) = \mathrm{U}(D(\mathcal{L}_n)), \tag{2.67}$$

where U^+ is the adjoint of the unitary operator U, that is,

$$\begin{aligned} \mathrm{U}^+: \quad L^2(-\pi/2,\pi/2) &\longrightarrow L^2((-\pi/2,\pi/2); \cos x dx)\\ w &\longmapsto (\mathrm{U}^+ w)(x) = w(x)/\sqrt{\cos x}. \end{aligned}$$

So, we deduce the following expression for $\mathrm{M_n}$,

$$\mathrm{M_n}\, w = w'' - q_n(x)w, \qquad \forall w \in D(\mathrm{M_n}), \tag{2.68}$$

where, for all $n \in \mathbb{N}^*$, the potential q_n is given by

$$q_n(x) = (n^2 - 1/4)\tan^2 x - 1/2, \qquad \forall x \in (-\pi/2, \pi/2). \tag{2.69}$$

Remark 2.6.7 *Let us emphasis that, since* U *is an unitary transformation, the unbounded operator* $(\mathrm{M_n}, D(\mathrm{M_n}))$ *defined on the space* $L^2(-\pi/2, \pi/2)$ *inherits properties of the operator* $(\mathcal{L}_n, D(\mathcal{L}_n))$. *That is, the operator* $(-\mathrm{M_n}, D(\mathrm{M_n}))$ *is a densely defined, self-adjoint, and positive operator with compact resolvent in* $L^2(-\pi/2, \pi/2)$ *for all* $n \in \mathbb{N}^*$.

Since the differential operator ∂_t commutes with the unitary transformation U, one deduces easily that system (2.36) is equivalent to the following

$$\begin{cases} \partial_t \tilde{g}_n - \mathrm{M_n}\, \tilde{g}_n = 0, & \text{in } (0,T)\times(-\pi/2,\pi/2), \\ \tilde{g}_n|_{t=0} = \tilde{g}_{0,n}, & \text{in } (-\pi/2,\pi/2). \end{cases} \tag{2.70}$$

In particular, the solution $\tilde{g}_n = \mathrm{U}\, g_n$ belongs to the class (see Proposition 2.6.2 and Remark 2.6.3)

$$C([0,T]; L^2(-\pi/2,\pi/2)) \cap C^\infty((0,T); D(\mathrm{M_n})). \tag{2.71}$$

In the following, we collect some properties of the functions belonging to the domain $D(\mathrm{M_n})$ ($n \in \mathbb{N}^*$), which will be helpful in the proof of a global Carleman estimate for system (2.70) in Appendix 2.7.

Lemma 2.6.6 *Let* $n \in \mathbb{N}^*$ *and* $w \in D(\mathrm{M_n})$. *Then* w' *belongs to* $L^2(-\pi/2,\pi/2)$ *and* w *is locally absolutely continuous on* $[-\pi/2,\pi/2]$. *Moreover,*

$$w(x) = o(1) \qquad \textit{and} \qquad w'(x) = o(1) \qquad \textit{both as} \quad x \to \pm\frac{\pi}{2}. \tag{2.72}$$

Proof. Let $n \in \mathbb{N}^*$ and $w \in D(\mathrm{M_n})$. Then $w = \sqrt{\cos x}\, v$ for some $v \in D(\mathcal{L}_n)$ and a. e., $x \in (-\pi/2, \pi/2)$. Since $v(\pm\pi/2) \in \mathbb{R}$, the first identity in (2.72) immediately follows. Similarly, since $\tan x v \in \mathcal{H}_n$ (see, (2.43)), the following is finite

$$\|\tan x w\|^2_{L^2(-\pi/2,\pi/2)} = \|\tan x v\|^2_{\mathcal{H}_n}.$$

By deriving w, we find that $w' + \tan x w/2 = \sqrt{\cos x}\, v'$ belongs to $L^2(-\pi/2,\pi/2)$, due to (2.43). Therefore, $w' \in L^2(-\pi/2,\pi/2)$. Since $v'(\pm\pi/2) \in \mathbb{R}$, it holds

$$\lim_{x\to-\frac{\pi}{2}+} w'(x) = \lim_{x\to-\frac{\pi}{2}+} -\frac{1}{2}\frac{\sin x}{\sqrt{\cos x}} v(x) + \sqrt{\cos x}\, v'(x) = 0,$$

by the second identity in (2.42). The proof of the limit at $\pi/2$ is similar. It then follows that w is locally absolutely continuous on $[-\pi/2,\pi/2]$. □

Remark 2.6.8 *Lemma 2.6.6 also shows that for all $n \in \mathbb{N}^*$, the domain $D(\mathrm{M_n})$ is a subspace of the Sobolev space $H_0^1(-\pi/2, \pi/2)$. In particular, Lemma 2.6.1 holds true in $D(\mathrm{M_n})$.*

We now have all ingredients to state the result on a Carleman estimate for system (2.70), which will allow us, using dissipation rate (2.52) to prove the uniform observability inequality (2.55) for system (2.36) for non-zero frequencies. We drop the tilde and the index n to simplify the notations. We will sketch the proof of the following proposition in Appendix 2.7. The complete explanation can be found in [Tam22, Section 4].

We introduce for every $n \in \mathbb{N}^*$ the following parabolic operator, which is singular at $x = \pm\pi/2$,

$$\mathcal{P}_n := \partial_t - \partial_x^2 + q_n(x) \qquad \text{with} \qquad q_n(x) = \left(n^2 - \frac{1}{2}\right)\tan^2 x - 1/2. \tag{2.73}$$

Proposition 2.6.4 (Carleman estimate) *Let $\omega_{a,b}$ be defined as in (2.16). Then there exist a weight function $\beta \in C^4([-\pi/2, \pi/2])$ and positive constants $R_0, R_1 > 0$ such that for every $T > 0$, $n \in \mathbb{N}^*$ and $s \geq R_0 \max(T + T^2, T^2 n)$, every $g \in C([0,T]; L^2(-\pi/2, \pi/2)) \cap C^2((0,T); D(\mathrm{M_n}))$ satisfies*

$$\begin{aligned} &R_1 \int_0^T \int_{-\frac{\pi}{2}}^{\frac{\pi}{2}} \left(\frac{s}{t(T-t)} |\partial_x g(t,x)|^2 + \frac{s^3}{(t(T-t))^3} |g(t,x)|^2 \right) e^{-\frac{2s\beta(x)}{t(T-t)}} dx dt \\ &\leq \int_0^T \int_{\omega_{a,b}} \frac{s^3}{(t(T-t))^3} |g(t,x)|^2 e^{-\frac{2s\beta(x)}{t(T-t)}} dx dt + \int_0^T \int_{-\frac{\pi}{2}}^{\frac{\pi}{2}} |\mathcal{P}_n g(t,x)|^2 e^{-\frac{2s\beta(x)}{t(T-t)}} dx dt, \end{aligned} \tag{2.74}$$

where, $R_i := R_i(\beta, a, b)$, $i = 0, 1$ and $\mathcal{P}_n$ is defined in (2.73).

The following proposition shows that the one-dimensional parabolic system (2.36) for non-zero frequencies $n \neq 0$ is uniformly observable from $\omega_{a,b}$ in large time.

Proposition 2.6.5 *Let $a, b \in \mathbb{R}$ be such that $0 < a < b \leq \pi/2$. Then there exists a positive time $T^* > 0$ such that, for every $T \geq T^*$, system (2.36) is observable in $\omega_{a,b} = (-b, -a) \cup (a, b)$ in time T uniformly with respect to $n \in \mathbb{N}^*$.*

Proof. We obtain the uniform observability inequality (2.55) in large time for system (2.36) when $n \in \mathbb{N}^*$. Let $\tilde{g}_n = \mathrm{U}\, g_n \in C([0,T]; L^2(-\pi/2, \pi/2)) \cap C^2((0,T); D(\mathrm{M_n}))$ be the solution of system (2.70), where g_n is the Fourier component (2.37) and U, the unitary transformation defined in (2.65). Then by Carleman estimate (2.74), one deduces

$$R_1 \int_Q \theta(t)^3 |\tilde{g}_n(t,x)|^2 e^{-2\varphi} dQ \quad \leq \quad \int_0^T \int_{\omega_{a,b}} \theta(t)^3 |\tilde{g}_n(t,x)|^2 e^{-2\varphi} dQ, \tag{2.75}$$

for all $s \geq R_0 \max(T + T^2, T^2 n)$, and for some constants $R_0, R_1 > 0$ independent of n, T and $\tilde{g}_n$. Here we let $\theta(t) = 1/t(T-t)$, $t \in (0,T)$ and $\varphi(t,x) = s\theta(t)\beta(x)$, with β being as in Proposition 2.6.4.

From now on, we set

$$s := R_0 \max(T + T^2, T^2 n).$$

For $t \in (T/3, 2T/3)$, we have due to dissipation rate (2.52),

$$\frac{4}{T^2} \leq \theta(t) \leq \frac{9}{2T^2} \quad \text{and} \quad \int_{-\frac{\pi}{2}}^{\frac{\pi}{2}} |\tilde{g}_n(T,x)|^2 dx \leq e^{-\frac{2}{3}nT} \int_{-\frac{\pi}{2}}^{\frac{\pi}{2}} |\tilde{g}_n(t,x)|^2 dx.$$

Integrating over $(T/3, 2T/3)$, we find, using (2.75)

$$\frac{T}{3} \int_{-\frac{\pi}{2}}^{\frac{\pi}{2}} |\tilde{g}_n(T,x)|^2 dx \leq \frac{1}{R_1} \frac{T^6}{64} \frac{6}{8s^3\beta_*^3} e^{-\frac{2}{3}nT} e^{\frac{9}{T^2}s\beta^*} \int_0^T \int_{\omega_{a,b}} |\tilde{g}_n(t,x)|^2 dx dt, \tag{2.76}$$

where $\beta_* := \min\{\beta(x) : x \in [-\pi/2, \pi/2]\}$ and $\beta^* := \max\{\beta(x) : x \in [-\pi/2, \pi/2]\}$. Then, the following two cases may occur.

First case: $n < 1 + 1/T$. Then $s = R_0(T + T^2)$, and thus (2.76) yields

$$\int_{-\frac{\pi}{2}}^{\frac{\pi}{2}} |\tilde{g}_n(T,x)|^2 dx \leq \frac{1}{R_1} \frac{T^5}{64} \frac{18}{8R_0^3(T+T^2)^3\beta_*^3} e^{\frac{9}{T^2}R_0(T+T^2)\beta^*} \int_0^T \int_{\omega_{a,b}} |\tilde{g}_n(t,x)|^2 dx dt. \tag{2.77}$$

Second case: $n \geq 1 + 1/T$. Then $s = R_0 T^2 n$, and thus (2.76) yields

$$\int_{-\frac{\pi}{2}}^{\frac{\pi}{2}} |\tilde{g}_n(T,x)|^2 dx \leq \frac{1}{R_1} \frac{1}{64} \frac{18}{8R_0^3 T(1+1/T)^3\beta_*^3} e^{-\frac{2}{3}nT} e^{9nR_0\beta^*} \int_0^T \int_{\omega_{a,b}} |\tilde{g}_n(t,x)|^2 dx dt.$$

It then suffices to observe that $-2nT/3 + 9nR_0\beta^* \leq 0$ as soon as $T \geq T^* := 27R_0\beta_*/2$.

So, in both cases, there exists a positive constant $C_0' > 0$, which is independent of $n \in \mathbb{N}^*$, such that

$$\int_{-\frac{\pi}{2}}^{\frac{\pi}{2}} |g_n(T,x)|^2 \cos x dx \leq C_0' \int_0^T \int_{\omega_{a,b}} |g_n(t,x)|^2 \cos x dx dt, \tag{2.78}$$

provided $T \geq T^*$. □

Remark 2.6.9 *To achieve the proof of observability inequality* (2.55) *in large time for one-dimensional parabolic equations* (2.36) *uniformly with respect to* $n \in \mathbb{N}$*, it suffices to consider inequalities* (2.64) *and* (2.78) *and let* $C := \max(C_0, C_0') > 0$.

2.7 . Appendix: Carleman estimates for one-dimensional parabolic equation for non-zero frequencies

This section aims to give a sketch of the proof of Proposition 2.6.4 about Carleman estimate (2.74). The main difficulty in proving inequality as (2.74) is identifying a suitable weight function β which can deal with the specificity of the parabolic operator under consideration. For example, for the standard parabolic operator, see the pioneering work by Imanuvilov [Ima95] or Fursikov and Imanuvilov [FI96]; for the standard parabolic operator with interior quadratic singularities (resp. boundary singularity) see the work by Ervedoza [Erv08] (resp. Cazacu [Caz14] or Biccari

and Zuazua [BZ16]); for the $2D$ parabolic Grushin operator, see the work by Beauchard *et al.*[BCG14; Bea+15; BDE20] and Koenig [Koe17]; for $2D$ parabolic Grushin operator with internal (resp. boundary) singular potential see the work by Morancey [Mor15] (resp. Cannarsa and Guglielmi [CG14]). We remark that, in general, the function β is chosen to be strictly monotone outside of the control region and concave so that the term in s^3 is the leading one. Particularly in the singular cases, this choice allows getting rid of the singular terms which can not be bounded at the singularity, usually by taking advantage of Hardy-Poincaré type inequalities.

In the case at hand, the potential q_n is singular in $\pm\pi/2$. Thus, we shall apply the Hardy-Poincaré inequality of Lemma 2.6.1 (see, Remark 2.6.8) to get rid of the singular terms which can not be bounded at $\pm\pi/2$.

Notation 2 *We introduce notations that will be used in what follows. We let a' and b' are real numbers such that*

$$0 < a < a' < b' < b \leq \pi/2 \qquad \text{and} \qquad [a', b'] \subset (a, b). \tag{2.79}$$

We consider the subdomains

$$\omega_{con} := (-b', -a') \cup (a', b'), \quad \omega_{deg} := (-a', a'), \quad \omega_{bdy} := \left(-\pi/2, -b'\right) \cup \left(b', \pi/2\right), \tag{2.80}$$

so that

$$(-\pi/2, \pi/2) = \omega_{bdy} \cup \omega_{deg} \cup \omega_{con} \qquad \text{and} \qquad \omega_{con} \subset\subset \omega_{a,b}.$$

We also introduce the weight function

$$\varphi(t, x) = s\theta(t)\beta(x), \qquad (t, x) \in Q := (0, T) \times I, \qquad I := (-\pi/2, \pi/2), \tag{2.81}$$

where the positive constant $s = s(T, n, \beta) > 0$ will be chosen later on and the temporal weight θ is given by

$$\theta(t) = \frac{1}{t(T - t)}, \qquad t \in (0, T). \tag{2.82}$$

Finally, we introduce for all $n \in \mathbb{N}^*$ and every $g \in C([0, T]; L^2(-\pi/2, \pi/2)) \cap C^2((0, T); D(\mathrm{M_n}))$, the change of function

$$z(t, x) = g(t, x)e^{-\varphi(t,x)}, \qquad (t, x) \in Q. \tag{2.83}$$

We can now present the main steps that are necessary to complete the proof of (2.74). As announced above, we will omit details and refer the reader to [Tam22, Section 4], where detailed proof is given.

Remark 2.7.1 *We stress that these steps follow the classical strategy [FI96] by Fursikov and Imanuvilov (we also refer to [Cor07, p.79] for a pedagogical presentation of a Carleman estimate for the heat equation in Euclidean spaces). Let us emphasize that functions in $D(\mathrm{M_n})$ have the regularity in the space variable that we need to apply integrations by parts (see, e. g. Lemma 2.6.6).*

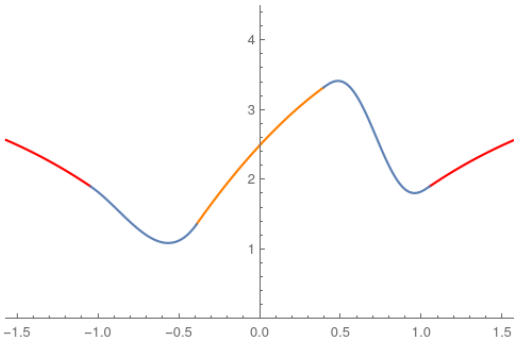

Figure 2.3: The spatial weight function β depicted in $[-\pi/2, \pi/2]$. The curves parts in *blue*, *red* and *orange* correspond respectively to the subcontrol region ω_{con}, the boundary domain ω_{bdy} containing the singular points $\pm\pi/2$ and the region ω_{deg} intersecting the degeneracy set $\{x = 0\}$.

Step 1: design of the spatial weight function $\beta(x)$, key properties satisfying the temporal weight $\theta(t)$ and the function $z(t, x)$

In the following lemma, we design the weight function β as depicted in Figure 2.3.

Lemma 2.7.1 *The function $\beta \in C^4([-\pi/2, \pi/2])$ satisfies*

$$\beta \geq 1, \qquad \text{on} \qquad (-\pi/2, \pi/2), \tag{2.84}$$

$$\beta(x) = \begin{cases} \log|\sin x| + A_1|x| + A_2 & \text{if} \quad x \in \overline{\omega_{bdy}}, \\ \log\cos x - \dfrac{x^2}{2} + A_3(x+1) & \text{if} \quad x \in \overline{\omega_{deg}}, \end{cases} \tag{2.85}$$

where the positive constants A_i, $1 \leq i \leq 3$ are such that (2.84) is verified and

$$\begin{cases} |\beta'(x)| \geq \eta_1, & x \in \overline{\omega_{bdy}}, \\ \beta'(x) \geq \eta_2, & x \in \overline{\omega_{deg}}, \end{cases} \tag{2.86}$$

for some positive constants $\eta_1, \eta_2 > 0$.

Remark 2.7.2 *We stress that the explicit expression of the weight β is only needed near $\pm\pi/2$ to eliminate the singular terms that can not be bounded at $\pm\pi/2$. Apart from this, assuming that β is strictly monotonous and concave outside the subcontrol region ω_{con} suffices.*

The following lemma gives some useful properties of the temporal weight θ obtained by direct computations.

Lemma 2.7.2 *Let the temporal weight θ be given by (2.82). Then we have for all $t \in (0, T)$,*

$$\theta'(t) = (2t - T)\theta^2(t), \qquad \theta''(t) = 2\theta^2(t)(1 + (2t - T)^2\theta(t)),$$

and the following inequalities hold

$$\theta(t) \leq 2^{-4}T^4\theta^3(t), \quad |\theta'(t)| \leq 2^{-2}T^3\theta^3(t), \quad |\theta(t)\theta'(t)| \leq T\theta^3(t), \quad |\theta''(t)| \leq \frac{5}{2}T^2\theta^3(t).$$

Moreover, one has

$$\lim_{t\to 0^+} \theta(t) = \lim_{t\to T^-} \theta(t) = +\infty.$$

In the following lemma, we give some useful properties of the function z introduced in (2.83) which are obtained by direct computations applying Lemmas 2.6.6 and 2.7.2

Lemma 2.7.3 *Let $n \in \mathbb{N}^*$, then the function z introduced in (2.83) belongs at least in the class $C([0,T]; L^2(-\pi/2,\pi/2)) \cap C^2((0,T); D(\mathrm{M_n}))$ and satisfies*

$$\begin{cases} z(0,x) = z(T,x) = \partial_x z(0,x) = \partial_x z(T,x) = 0, & x \in [-\pi/2,\pi/2], \\ z(t,\pm\pi/2) = \partial_t z(t,\pm\pi/2) = \partial_x z(t,\pm\pi/2) = 0, & t \in (0,T). \end{cases} \tag{2.87}$$

Moreover, one has

$$\mathcal{P}_n^+ z + \mathcal{P}_n^- z = e^{-\varphi}\mathcal{P}_n g, \tag{2.88}$$

where $\mathcal{P}_n$ is the parabolic operator introduced in Proposition 2.6.4, and we let

$$\mathcal{P}_n^+ z = -\mathrm{M_n}\, z + (\partial_t\varphi - |\partial_x\varphi|^2)z \qquad \text{and} \qquad \mathcal{P}_n^- z = \partial_t z - 2\partial_x z\partial_x\varphi - (\partial_x^2\varphi)z. \tag{2.89}$$

Step 2: Integration by parts and weight exponential energy estimates satisfying the function $z(t,x)$

Let $Q = (0,T)\times(-\pi/2,\pi/2)$ and $dQ = dxdt$. Observe first that, $\mathcal{P}_n^+ z$ and $\mathcal{P}_n^- z$ defined in (2.89) belong to $L^2(Q)$ by the definition of $D(\mathrm{M_n})$ and Lemma 2.6.6. So, developing the $L^2(Q)$ squared norm in identity (2.88), leads to

$$\int_Q \mathcal{P}_n^+ z\mathcal{P}_n^- z dQ \le \frac{1}{2}\int_Q \left|e^{-\varphi}\mathcal{P}_n g\right|^2 dQ. \tag{2.90}$$

In the following, we compute the scalar product on the left-hand side of (2.90) using integration by parts and Fubini's Theorem.

Lemma 2.7.4 *Let $n \in \mathbb{N}^*$, then we have*

$$\begin{aligned}\int_Q \mathcal{P}_n^+ z\mathcal{P}_n^- z dQ = &-2\int_Q \partial_x^2\varphi|\partial_x z|^2 dQ + \frac{1}{2}\int_Q \partial_x^4\varphi|z|^2 dQ + \int_Q \partial_x\varphi q_n'(x)|z|^2 dQ \\ &- \frac{1}{2}\int_Q (\partial_t^2\varphi - 2\partial_x\varphi\partial_{tx}\varphi)|z|^2 dQ + \int_Q \partial_x\varphi\partial_x(\partial_t\varphi - |\partial_x\varphi|^2)|z|^2 dQ.\end{aligned} \tag{2.91}$$

We now bound from below the right-hand side of (2.91). Since $Q := (0,T)\times(-\pi/2,\pi/2) = (0,T)\times(\omega_{bdy}\cup\omega_{con}\cup\omega_{deg})$, we separate the integrals of the right hand side over $(0,T)\times J$, where $J \in \{\omega_{bdy},\omega_{con},\omega_{deg}\}$. Using Lemma 2.7.1 we immediately get

Lemma 2.7.5 *Let $n \in \mathbb{N}^*$ and assume (2.91). Then one has*

$$\int_Q \mathcal{P}_n^+ z\mathcal{P}_n^- z dQ = \int_0^T\int_{\omega_{bdy}} \mathrm{K_{bdy}}\, dQ + \int_0^T\int_{\omega_{con}} \mathrm{K_{con}}\, dQ + \int_0^T\int_{\omega_{deg}} \mathrm{K_{deg}}\, dQ, \tag{2.92}$$

where

$$\begin{aligned}
\mathrm{K}_{\mathrm{deg}} &= s\theta\left\{\left(\frac{2}{\cos^2 x}+2\right)|\partial_x z|^2+\left(\frac{\sin^2 x}{2\cos^4 x}+\frac{x\sin x}{2\cos^3 x}\right)|z|^2\right\}\\
&+\left\{\frac{2n^2 s\theta}{\cos^2 x}+2s^3\theta^3\left(\frac{1}{\cos^2 x}+1\right)(-\tan x-x+A_3)^2\right\}|z|^2\\
&+s\theta\left\{A_3\frac{(2n^2-1/2)}{\cos^4 x}+2s\theta'(-\tan x-x+A_3)^2-2n^2\frac{x\tan x}{\cos^2 x}\right\}|z|^2\\
&-\frac{s\theta''}{2}(\log\cos x-\frac{x^2}{2}+A_3(x+1))|z|^2, \qquad (2.93)
\end{aligned}$$

$$\begin{aligned}
\mathrm{K}_{\mathrm{bdy}} &= \frac{2s\theta}{\sin^2 x}\left\{|\partial_x z|^2+|z|^2\right\}+\frac{2s^3\theta^3}{\sin^2 x}\left(\frac{\cos x}{\sin x}+A_1\,\mathrm{sign}(x)\right)^2|z|^2\\
&+\left\{2s^2\theta\theta'\left(\frac{\cos x}{\sin x}+A_1\,\mathrm{sign}(x)\right)^2-\frac{s\theta''}{2}(\log|\sin x|+A_1|x|+A_2)\right\}|z|^2\\
&+\left\{-\frac{3s\theta}{\sin^4 x}+\underbrace{\frac{s\theta(2n^2-1/2)}{\cos^2 x}(1+A_1\,\mathrm{sign}(x)\tan x)}_{\textit{singular terms}}\right\}|z|^2, \qquad (2.94)
\end{aligned}$$

and

$$\begin{aligned}
\mathrm{K}_{\mathrm{con}} &= s\left\{\frac{\theta\beta^{(4)}}{2}+\theta\beta'\left(2n^2-\frac{1}{2}\right)\frac{\sin x}{\cos^3 x}-\frac{\theta''\beta}{2}+2s\theta\beta'^2(\theta'-s\theta^2\beta'')\right\}|z|^2\\
&-2s\theta\beta''|\partial_x z|^2. \qquad (2.95)
\end{aligned}$$

In the following lemmas, we bound from below (2.93) and (2.94) by positive terms.

Remark 2.7.3 *We stress that to get rid of singular terms in (2.94) (that in blue) that cannot be bounded at $\pm\pi/2$ we use the Hardy-Poincaré inequality given in Lemma 2.6.1.*

Lemma 2.7.6 *Let $n\in\mathbb{N}^*$. Then there exists a positive constant $s_1>0$ such that, for all*

$$s\geq s_1\max(T+T^2,T^2n), \qquad (2.96)$$

the following inequality holds

$$\int_0^T\int_{\omega_{deg}}\mathrm{K}_{\mathrm{deg}}\,dQ\geq\int_0^T\int_{\omega_{deg}}4s\theta|\partial_x z|^2+\eta_2^2 s^3\theta^3|z|^2 dQ, \qquad (2.97)$$

with η_2 as in (2.86) and $\mathrm{K}_{\mathrm{deg}}$ be given by (2.93).

Lemma 2.7.7 *There exists a positive constant $s_2>0$ such that, for all*

$$s\geq s_2(T+T^2), \qquad (2.98)$$

the following inequality holds

$$\int_0^T \int_{\omega_{bdy}} \mathrm{K}_{\mathrm{bdy}}\, dQ \geq \int_0^T \int_{\omega_{bdy}} 2s\theta|\partial_x z|^2 + 2s\theta|z|^2 + \frac{\eta_1^2}{2} s^3\theta^3|z|^2 dQ, \tag{2.99}$$

with η_1 *as in* (2.86) *and* $\mathrm{K}_{\mathrm{bdy}}$ *be given by* (2.94).

Remark 2.7.4 *Observe that the constant* s_1 *in Lemma 2.7.6 depends of* n *while the constant* s_2 *in Lemma 2.7.7 does not depend of* n.

The following lemma is a straightforward combination of Lemmas 2.7.6 and 2.7.7.

Lemma 2.7.8 *Let* $n \in \mathbb{N}$ *and* $R_0 = R_0(a', b') := \max(s_1, s_2)$. *Then for all*

$$s \geq R_0 \max(T + T^2, T^2 n), \tag{2.100}$$

it holds

$$\int_0^T \int_{\omega_{bdy}} \mathrm{K}_{\mathrm{bdy}}\, dQ + \int_0^T \int_{\omega_{deg}} \mathrm{K}_{\mathrm{deg}}\, dQ \geq \int_0^T \int_{I\setminus\omega_{con}} (2s\theta|\partial_x z|^2 + C_8 s^3\theta^3|z|^2) dQ. \tag{2.101}$$

We let $C_8 = C_8(a', b') := \min(\eta_1^2, \eta_2^2) > 0$ *and* $I\setminus\omega_{con} := (-\pi/2, \pi/2)\setminus\omega_{con} = \omega_{bdy} \cup \omega_{deg}$.

In the subcontrol region $\omega_{con} = (-b', -a') \cup (a', b')$, we have the following

Lemma 2.7.9 *Let* $n \in \mathbb{N}^*$ *and assuming* (2.95) *and* (2.100). *Then there exist positive constants* $C_9, C_{12} > 0$ *such that the following inequality holds*

$$|\,\mathrm{K}_{\mathrm{con}}\,| \leq C_9 s\theta|\partial_x z|^2 + C_{12} s^3\theta^3|z|^2. \tag{2.102}$$

Thanks to (2.90), (2.92), Lemmas 2.7.8 and 2.7.9, we immediately obtain the following.

Lemma 2.7.10 *Let* $n \in \mathbb{N}^*$. *Then for all* $s \geq R_0 \max(T + T^2, T^2 n)$, *one has*

$$\int_0^T \int_{I\setminus\omega_{con}} (2s\theta|\partial_x z|^2 + C_8 s^3\theta^3|z|^2) dQ \leq \int_0^T \int_{\omega_{con}} (C_9 s\theta|\partial_x z|^2 + C_{12} s^3\theta^3|z|^2) dQ + \frac{1}{2}\int_Q \left|e^{-\varphi}\mathcal{P}_n g\right|^2 dQ. \tag{2.103}$$

Step 3: Coming back to the function $g(t, x)$ and completion of the proof

In the following lemma, we come back to g.

Lemma 2.7.11 *Let* $n \in \mathbb{N}^*$ *and assume* (2.103). *Then there exist positive constants* C_{13}, C_{16} *and* C_{17} *such that for all* $s \geq R_0 \max(T + T^2, T^2 n)$, *it holds*

$$\int_Q (C_{13} s\theta|\partial_x g|^2 + (C_8/2) s^3\theta^3|g|^2) e^{-2\varphi} dQ \leq \int_0^T \int_{\omega_{con}} (C_{16} s\theta|\partial_x g|^2 + C_{17} s^3\theta^3|g|^2) e^{-2\varphi} dQ + \frac{1}{2}\int_Q \left|e^{-\varphi}\mathcal{P}_n g\right|^2 dQ. \tag{2.104}$$

In the following lemma we prove that terms similar to the second term of the right-hand side of (2.104) dominate the first one. We achieve this by the use of a smooth cut-off function.

Lemma 2.7.12 *Let $n \in \mathbb{N}^*$ and assume (2.104). Then there exists a positive constant $C_{19} > 0$ such that for all $s \geq R_0 \max(T + T^2, T^2 n)$, one has*

$$\int_Q (C_{13} s\theta |\partial_x g|^2 + (C_8/2) s^3\theta^3 |g|^2) e^{-2s\varphi} dQ \leq \int_0^T \int_{\omega_{a,b}} C_{19} s^3\theta^3 |g|^2 e^{-2s\varphi} dQ + \int_Q \left| e^{-s\varphi} \mathcal{P}_n g \right|^2 dQ. \tag{2.105}$$

We can now complete the proof of Carleman estimate (2.74).

Proof. (Proof of Proposition 2.6.4) It suffices to consider Lemma 2.7.12, and let

$$R_1 = R_1(\beta, \rho) := \frac{\min(C_{13}, C_8/2)}{\max(1, C_{19})}.$$

□

Part II

Control in Neurosciences

Contents

Introduction

1.1 . Purpose and motivation

The second part of the thesis explores a mathematically sound approach to understanding visual illusions in human perception using neuronal dynamics. Neuronal dynamics refers to the patterns of activity and interactions among neurons that give rise to our ability to see and understand the world. Our visual system processes information in different stages, with specialized neurons at each stage extracting specific details from what we see. The visual system shows dynamic and widespread activity patterns, from detecting basic features like edges and orientations to putting everything together and making sense of it.

The brain area which detects basic features such as spatial position, edges, local orientations and direction in visual stimuli from the retina is the primary visual cortex (hereafter referred to as V1), [HW59; HW62]. Evidence [EC79a; Bre+01; BC02; GST03; Tas95] suggests that regular geometrical patterns spontaneously emerge in V1 when its activity is due solely to the noisy internal fluctuation of its neurons, that is, in the absence of visual stimuli or sensory inputs. These patterns can be obtained using the Neural Fields (NF) equations modelling the cortical activity in V1.

In their pioneer work [EC79a], by using bifurcation techniques near a Turing-like instability, Ermentrout and Cowan found that the 2-dimensional two-layer NF equations derived by Wilson and Cowan in [WC73] is sufficient to theoretically describe the spontaneous formation (i.e., in the absence of external stimuli or visual sensory inputs) of some geometric patterns (horizontal, vertical and oblique stripes, square, hexagonal and rectangular patterns etc.) in V1. These patterns result from activity spreading over the field and correspond to states of highest cortical activities in V1. When they are transformed by the inverse of the retino-cortical map existing between the visual field and V1 [Too+82; Sch77] (refer to Section 2.4.2 of Chapter 2), what we obtain in the retina in terms of images are geometric visual hallucinations. They correspond to some of the form constants that Klüver had meticulously classified [Klü66], mainly those contrasting regions of white and black (funnel, tunnel, spiral, checkerboard, phosphenes), see Figs. 1.1 and 1.2 for visual illustration of funnel and tunnel patterns. The geometric forms of spontaneous and hallucinatory patterns are predicted by the neural dynamic equation used to model the cortical activity in V1 combined with the bijective non-linear retino-cortical mapping between the visual field and V1. Therefore, while spontaneous patterns that emerge in V1 give

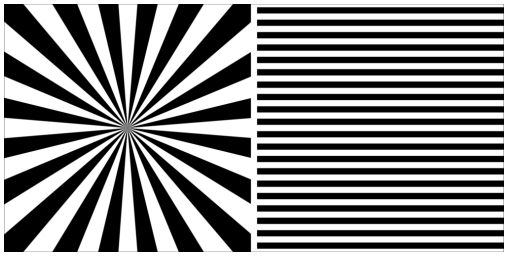

Figure 1.1: Funnel pattern in the retina (*left*). On the *right* the corresponding pattern in V1 after applying the retino-cortical map.

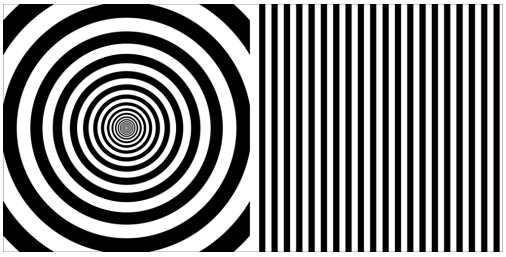

Figure 1.2: Tunnel pattern in the retina (*left*). On the *right* the corresponding pattern in V1 after applying the retino-cortical map.

us insight into the underlying architecture of the brain's neural network, little is known about how precisely the intrinsic circuitry of the primary visual cortex generates the patterns of activity that underlie the visual illusions induced by visual stimuli from de retina.

We study in this thesis the interaction between retinal stimulation by redundant geometrical patterns and the cortical response in the primary visual cortex focusing on the MacKay effect [Mac57] and Billock and Tsou's experiments [BT07]. We propose using the Amari-type equation combined with the retino-cortical map to reproduce these psychophysical experiments theoretically. The Amari-type equation (that we will derive in Section 2.3.2 of Chapter 2) is a mathematical model of neural activity that takes into account the interaction between excitatory and inhibitory neurons in a cortical tissue.

Roughly speaking, we utilize the Amari-type equation to describe the behaviour of neurons in V1 when the retina is exposed to visual stimuli. The model successfully replicates the MacKay effect and Billock and Tsou's visual illusions provided that the visual stimuli used in each of theses experiments are well-modelled.

Although our approach differs from that of Nicks *et al.* [Nic+21] in describing the MacKay-like effect, it agrees with the latter in emphasizing the role of inhibitory neurons in shaping the response of excitatory neurons to visual stimuli. This is consistent with the idea that inhibitory neurons play an important role in shaping the receptive fields of neurons in the visual cortex and that the interaction between excitatory and inhibitory neurons is crucial for visual processing.

Overall, we provide a novel perspective on the mechanisms underlying the MacKay-type effect, and highlights the importance of considering both excitatory and inhibitory neurons in models of visual processing.

1.2 . Strategy of study and presentation of our results

In Section 1.2.1, we present the strategy employed to provide a theoretical description of the MacKay effect [Mac57] and the psychophysical experiments conducted by Billock and Tsou [BT07]. Subsequently, in Section 1.2.2, we present and discuss our findings.

Our work originated in [TPC22], where we developed a novel approach to describe the MacKay effect (specifically, redundant stimulation) [Mac57] and Billock and Tsou's experiments [BT07]. Instead of relying on traditional mathematical tools such as bifurcation analysis,

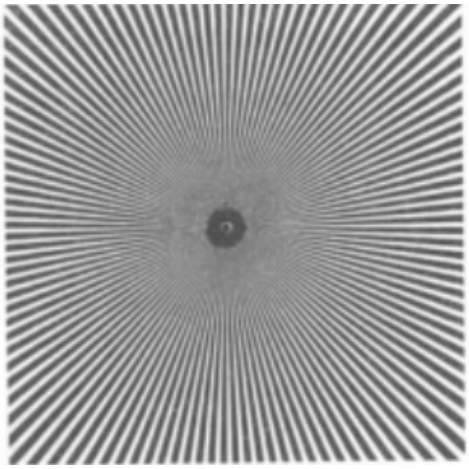

Figure 1.3: "MacKay-rays" [Mac57]: funnel pattern with hight redundant information in the fovea.

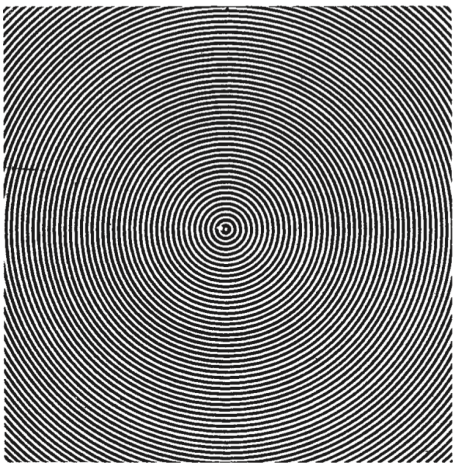

Figure 1.4: "MacKay-target" [Mac57]: tunnel pattern with hight redundant information.

perturbation theories, or multiscale analysis, commonly used to address neuroscience questions, we sought alternative methods via control of neural fields equations.

Indeed, these classical mathematical tools are highly suitable for describing phenomena like spontaneous geometric visual hallucinations that emerge in the visual field due to sudden qualitative changes in specific physiological parameters [Bre+01; EC79a; GST03; Tas95]. They also prove effective in understanding sensory-driven and self-organized cortical activity interactions when the visual stimulus exhibits regular shape and complete distribution across the visual field, with symmetry respecting a subgroup of the Euclidean group [Nic+21]. In simple terms, these tools are appropriate when dealing with equations that exhibit complete equivariance (commutation) with respect to a given group, typically the Euclidean group.

However, the original MacKay stimulus, known as the "MacKay rays" (refer to Figure 1.3), which plays a key role in the MacKay visual phenomena, consists of funnel patterns with high levels of redundant information in the fovea. As a result, the Euclidean symmetry of the funnel patterns is disrupted, rendering the "MacKay rays" visually irregular.

Similarly, the visual stimuli used in Billock and Tsou's experiments consist of funnel or tunnel patterns localized either in the fovea or periphery of the visual field (see, for instance, Figure 1.5 for a funnel pattern localized in the fovea). Consequently, Billock and Tsou's visual stimuli do not exhibit complete regularity or complete distribution across the visual field. Accordingly, neither the works of [Bre+01; EC79a] nor [Nic+21] can be directly employed to describe these complex visual phenomena.

Notice that even though the work made in [Nic+21] provides numerical simulations for replicating Billock and Tsou's experiments (including those for rotating solutions that are not considered in this thesis), it does not theoretically describe Billock and Tsou's experiments [BT07] but rather a variant of the MacKay effect where the visual stimulus is not the "MacKay rays" nor the "MacKay target" (see Figure 1.4) but a regular (symmetric with respect to some subgroups of the plane Euclidean group) funnel or tunnel patterns, which is fully distributed in the visual field as that of Figure 1.1 and 1.2.

Figure 1.5: Billock and Tsou's experiments: the presentation of funnel pattern stimulus in the fovea (centre of the visual field) induces an illusory perception of tunnel pattern in surround after a flickering of the empty region (the white region surrounding the stimulus pattern on the *left*). Adapted from [BT07, Fig. 3].

1.2.1 . Strategy of study

In our study, we begin by assuming that neurons in the primary visual cortex (V1) are interconnected in a homogeneous and isotropic manner.

Accordingly, we employ the following Amari-type equation [Ama77, Eq. (3)] to describe the cortical activity dynamics in V1, which corresponds to the two-dimensional space $\mathbb{R}^2$:

$$\partial_t a = -a + \mu\omega * f(a) + I. \tag{NF}$$

Here $a : \mathbb{R}_+ \times \mathbb{R}^2 \to \mathbb{R}$ is a function of time $t \in \mathbb{R}_+$ and the position $x \in \mathbb{R}^2$, the sensory input I represents the projection of the visual stimulus into V1 by the retino-cortical map. The connectivity kernel $\omega(x, y) = \omega(|x - y|)$ models the strength of connections between neurons located at positions $x \in \mathbb{R}^2$ and $y \in \mathbb{R}^2$. The function f captures the nonlinear response of neurons after activation, while the parameter $\mu > 0$ characterizes the intra-neural connectivity. The symbol $*$ denotes spatial convolution, as defined in (1.2) below.

Although the more plausible biological neuronal dynamics in V1 involve considering the orientation preferences of "simple cells", as done in [Bre+01, Eq. (1)] when describing contoured spontaneous cortical patterns, we initially neglect the orientation label entirely and focus on equation (NF) (which is identical to [Bre+01, Eq. (16)] when the sensory input is zero). This simplification is motivated by the fact that equation (NF) is sufficient for describing spontaneous funnel and tunnel patterns, and we expect it also to be suitable for describing psychophysical experiments involving these patterns. Additionally, our choice aligns with the advice of L. Nirenberg (Abel Prize 2015): "*If you want to study a high-dimensional phenomenon, start by considering the dimension* 2".

In these experiments, observers perceive an illusory afterimage in their visual field when viewing the visual stimulus, and this afterimage persists for a few seconds. Therefore, describing these intriguing visual phenomena in V1 using equation (NF) relies on explicitly studying the map Ψ, which associates the sensory input I with its corresponding stationary output $\Psi(I)$.

The stationary output represents the stationary solution of equation (NF) for a given I. Our goal is to prove that the cortical activity $a(t,\cdot)$, which is the solution of equation (NF), exponentially stabilizes towards $\Psi(I)$ as $t \to +\infty$. Then, perform qualitatively and quantitatively study of this stationary state in a convenient space.

This strategy can be thought of as a controllability approach, firstly because of the asymptotic study (qualitatively and quantitatively) of an input-output map and secondly since the sensory input in equation (NF) contains a control function which models the specificity of visual stimulus used in each experiment, for instance, the redundant information in the "MacKay rays" or the fact that funnel pattern in Billock and Tsou's experiments is localised in the visual field.

While sensory inputs in Billock and Tsou's experiments are time-varying, we found in our study that a temporal flicker of the complementary region where the stimulus is not localized is not necessary to reproduce these intriguing visual phenomena. Notice that this observation was already made in [Nic+21]. Our interpretation is that the phenomena of Billock and Tsou wholly result from the underlying non-local and nonlinear properties of neural activity in V1 rather than the temporal flickering of the complementary region where the stimulus is not localized.

1.2.2 . Presentation of results

To accurately model the visual stimuli used in these experiments, it is crucial to consider the redundant information present in the center of the funnel patterns known as the "MacKay rays". In our previous paper [TPC22], we established the following:

In order to reproduce the MacKay effect associated with this stimulus, equation (NF) needs to incorporate the redundant information present in the center of the funnel patterns. This observation arises from the underlying Euclidean symmetry of V1, which imposes restrictions on the geometric shapes of sensory inputs capable of inducing cortical illusions in V1. Interestingly, this mathematical evidence supports the observation previously made by MacKay in paragraph 2 of [Mac57]: "$[\cdots]$ *in investigations of the visual information system, it might be especially interesting to observe the effect of highly redundant information patterns since the nervous system might conceivably have its own ways of profiting from such redundancy* $[\cdots]$".

To model the redundant information in the center of the funnel pattern, we employed a control function equal to the characteristic function of a neighboring region of the fovea. Through numerical simulations, we demonstrated that equation (NF), together with an *odd* sigmoidal response function, successfully reproduces the MacKay effect associated with the "MacKay rays". We employed a similar approach to reproduce the MacKay effect associated with the "MacKay target", except that the control function was chosen as the characteristic function of two symmetric rays converging towards the fovea.

Simultaneously, we presented numerical results indicating that equation (NF), when combined with a non-symmetric (neither odd nor even) sigmoid response function, can accurately replicate Billock and Tsou's psychophysical experiments [BT07].

Having established that equation (NF), with an appropriate modeling of MacKay and Billock and Tsou's visual stimuli, reproduces these phenomena, our next objective was to provide a mathematical proof of the numerical results obtained in [TPC22].Therefore, in the paper [TPC23a], we addressed this question by heeding another crucial piece of advice from Nirenberg:

"*Have you tried to linearize?*" Surprisingly, we discovered that the linearized of (NF) is sufficient to describe and replicate the MacKay effect, indicating that the nonlinear nature of the response function does not play a role in its reproduction. Specifically, the saturation effect only serves to dampen high oscillations in the field. However, the linearized of (NF) fails to reproduce Billock and Tsou's phenomena. Intriguingly, equation (NF) produces either the "strong" (when the illusory contours in the afterimage does not extend through the physical stimulus) or "weak" (when the illusory contours in the afterimage extend through the physical stimulus) Billock and Tsou's phenomena depending on the shape of the nonlinearity used to model the neuronal response function.

In the paper [CPT23] (which will be available online soon), we provide a more detailed mathematical proof of the MacKay effect and the impossibility of reproducing Billock and Tsou's phenomena using the linearized version of (NF), employing complex and harmonic analysis tools and sharp inequality estimates. Specifically, we exploit the advantageous properties of the Fourier transform of Schwartz functions and tempered distributions. Additionally, by utilizing equation (NF) with a weak nonlinearity, we present the mathematical description of the "weak" Billock and Tsou's experiments, using tools from real and harmonic analysis. To the best of our knowledge, this is the first instance where such an approach has been employed to describe biological phenomena in neuroscience. This new approach offers the advantage of accommodating any geometrical visual stimulus, particularly those localized in the visual field. We hope that this perspective on the question can serve as a foundation for future investigations, such as describing other psychophysical phenomena including the apparent motion in quartet stimulus [GSH96], the flickering wheel illusion [SV13], the spin in the enigma stimulus of Isia Léviant [ZWF93; Lev96], or other psychophysical phenomena involving spontaneous cortical patterns such as the Barber pole, Café wall, Fraser spiral illusions, etc..

While much remains to be understood about the mechanisms underlying MacKay-type visual illusions, our study provides valuable insights into how the visual cortex processes contrast information from "simple" cortical patterns.

1.3 . Plan of this part

The structure of this thesis part is outlined as follows: Section 1.4 begins by introducing the general notations that will be utilized throughout the subsequent chapters.

In Chapter 2, we delve into the neural activity of spiking neurons. This chapter provides a comprehensive overview of the biophysics underlying neural communication in Section 2.2 and revisits the derivation of the Wilson-Cowan model [WC73] and the Amari model [Ama77] of cortical activity in Section 2.3. In Section 2.4, we present the retinotopic structure of the primary visual cortex as well as the analytical derivation of the retino-cortical map. We also overview the mathematical analysis leading to simple geometric visual hallucinations that spontaneously emerge in the retina, using bifurcation analysis of the Amari-type Equation (NF) near a Turing-like instability, in Section 2.5.

In Chapter 3, we investigate the mathematical description of MacKay-type visual illusion, focusing on the MacKay effect [Mac57] and Billock and Tsou's experiments [BT07]. Section 3.1.1

and 3.1.2 present the psychophysical experiments reported in these two papers. Section 3.1.3 discusses a preliminary result that describes the MacKay-like effect using neural fields equations via bifurcation theory and multiscale analysis. In Section 3.2, we highlight a motivation for using equation (NF) to describe these psychophysical experiments, and we present assumptions on model parameters used in this equation. In Section 3.3, we recall some preliminary results about the well-posedness of equation (NF) and define the binary pattern necessary to represent cortical activity in terms of white and black zones. Using equation (NF), in Sections 3.4 and 3.5, we investigate the description of the MacKay effect and Billock and Tsou experiments, respectively. In Section 3.4.4 and 3.5.2, we present numerical results to bolster our theoretical study.

Chapter 4 investigates the existence of equilibrium in a multi-layers neural fields population model of Wilson-Cowan when the sensory input is a proportional feedback that acts only on the system's state of population of excitatory neurons. There, we provide a mild condition on the response functions under which such an equilibrium exists. The interest of this work comes when we want to study how to disrupt pathological brain oscillations associated with Parkinson's disease by focusing on stimulation and measurements of the excitatory neural population.

In Appendix A, we provide additional mathematical complements that were essential in describing the MacKay effect visual illusions and the reproducibility of Billock and Tsou's experiments in Chapter 3.

Finally, in Appendix B, we provide a toolbox implemented with the Julia language to perform numerical implementation for the MacKay effect and Billock and Tsou's experiments.

1.4 . General notations

This section introduces general notations that we will use throughout the following.

Unless otherwise stated, p will denote any real number satisfying $1 \leq p \leq \infty$, and q will denote the conjugate to p given by $1/p+1/q = 1$. We adopt the convention that the conjugate of $p = 1$ is $q = \infty$ and vice-versa.

For $d \in \{1, 2\}$ and $\Omega \subset \mathbb{R}^d$ (with possibility that $\Omega = \mathbb{R}^d$) we denote by $L^p(\Omega)$ the Lebesgue space of class of real-valued measurable functions u on Ω such that $|u|$ is integrable over Ω if $p < \infty$, and $|u|$ is essentially bounded over Ω when $p = \infty$. We endow these spaces with their standard norms

$$\|u\|_p^p = \int_\Omega |u(x)|^p dx, \qquad \text{and} \qquad \|u\|_\infty = \operatorname*{ess\,sup}_{x\in\Omega} |u(x)|.$$

We let $\mathscr{X}_p := C([0,\infty); L^p(\mathbb{R}^d))$ be the space of all real-valued functions u on $\mathbb{R}^d \times [0,\infty)$ such that, $u(x,\cdot)$ is continuous on $[0,\infty)$ for a.e., $x \in \mathbb{R}^d$ and $u(\cdot,t) \in L^p(\mathbb{R}^d)$ for every $t \in [0,\infty)$. In $\mathscr{X}_p$, we will use the following norm $\|u\|_{L_t^\infty L_x^p} = \sup_{t\geq 0} \|u(\cdot,t)\|_p$.

For $x \in \mathbb{R}^2$, we denote by $|x|$ its Euclidean norm, and the scalar product with $\xi \in \mathbb{R}^2$ is defined by $\langle x, \xi\rangle = x_1\xi_1 + x_2\xi_2$.

We let $\mathcal{S}(\mathbb{R}^d)$ be the Schwartz space of rapidly-decreasing $C^\infty(\mathbb{R}^d)$ functions, and $\mathcal{S}'(\mathbb{R}^d)$ be its dual space, i.e., the space of tempered distributions. Then, $\mathcal{S}(\mathbb{R}^d) \subset L^p(\mathbb{R}^d)$ and

$L^p(\mathbb{R}^d) \subset \mathcal{S}'(\mathbb{R}^d)$ continuously. The Fourier transform of $u \in \mathcal{S}(\mathbb{R}^d)$ is defined by

$$\widehat{u}(\xi) := \mathcal{F}\{u\}(\xi) = \int_{\mathbb{R}^d} u(x) e^{-2\pi i \langle x, \xi \rangle} dx, \qquad \forall \xi \in \mathbb{R}^d. \tag{1.1}$$

We highlight that, for $1 \leq p \leq 2$, the above definition can be continuously extends to function $u \in L^p(\mathbb{R}^d)$ by density and Riesz-Thorin interpolation theorem. Whereas one can extend the above by duality to $\mathcal{S}'(\mathbb{R}^d)$. Therefore, apart from functions in $L^p(\mathbb{R}^d)$, $1 \leq p \leq 2$ whose Fourier transform may be directly computed by using the formula (1.1), we stress that the Fourier transform of functions belonging to the space $L^p(\mathbb{R}^d)$, $2 < p \leq \infty$ is usually computed by invoking this duality. We recall that $\mathcal{F}$ is a linear isomorphism from $\mathcal{S}(\mathbb{R}^d)$ to itself and from $\mathcal{S}'(\mathbb{R})$ to itself.

Finally, due to generalized Young-convolution inequality, the spatial convolution of two functions $u \in L^1(\mathbb{R}^d)$ and $v \in L^p(\mathbb{R}^d)$, $1 \leq p \leq \infty$ is defined by

$$(u * v)(x) = \int_{\mathbb{R}^d} u(x - y) v(y) dy, \qquad x \in \mathbb{R}^d. \tag{1.2}$$

CHAPTER 2

Dynamics of neuronal populations and visual hallucinations

2.1 . Introduction

The population formulation of neuronal activity is commonly used to elucidate the interactions between excitatory and inhibitory model neurons using neural fields (NF) equations. These equations provide a continuous description of the dynamics exhibited by a large population of synaptically coupled neurons. Consequently, NF equations serve as a valuable tool for studying and describing various neural processes, including but not limited to working memory [Lai+02], memory retrieval [Rec+15], motion perception [Gie12], pattern recognition [DR09] and visual hallucinations [EC79a; Bre+01].

Researchers can gain insights into neuronal populations' collective behaviour and dynamics using the neural fields equations. These equations facilitate the exploration of phenomena that emerge from the interactions and activities of many neurons, enabling a more comprehensive understanding of complex neural processes. The wide range of applications of NF equations demonstrates their utility in investigating diverse aspects of neural function and cognition.

Up to our knowledge the first attempt at developing a continuum approximation of neural activity is attributed to [Beu56]. He considered cells to have some properties similar to those of neurons. By assuming that those cells are randomly distributed in a given volume of model brain tissue and that they are only excitatory and sensitive (i.e., non-refractory), he was able to describe the activity of cells becoming activated per unit time at the instant t. Besides the inconsideration of refractoriness, Beurle's modelling of neural activity was over-simplified in the sense that many findings such as [RH59; HW63; HW65; Fre72; Fre68a; Fre68b] indicated that, the cells in the brain are both excitatory and inhibitory.

It was [WC72; WC73] who extended Beurles work to include excitatory and inhibitory neurons and refractoriness. Thus Wilson-Cowan model of neural (synaptic) activity is a two-layer network of a population of excitatory and inhibitory neurons.

Following the lines of such investigation, [Ama77] studied the dynamics of pattern formation

in one layer of neural activity, including excitatory and inhibitory neurons, with assumptions of short-range excitation and long-range inhibition. Moreover, it should be noted that the Amari model can also be obtained (see, [ET10]) from Wilson-Cowan's model by assuming that the inhibition is fast so that we may eliminate its dynamics.

NF equations can also be derived [Bre10; Dec+08; FTC09] from models of interconnected neural networks (NN). NN can be defined as an aggregate constituted of a large number of simple elements, neurons, organized in a strongly interconnected network. A first description of such NN goes up to the work of [MP43] in which they proposed formal neuron as binary threshold element. The study of NN gained renewed interest, especially among physicists, following an article by [Hop84] where he showed how specific networks have a structure similar to that of spin glasses and can be used as memory associative.

Besides the existence of Glia cells in the nervous system and non-spiking neurons in the mammalian retina [Lli03], throughout this thesis, we concentrate only on neural activity of spiking neurons, and we refer to [Bre11; Coo05; Coo10; Erm98] for a more detailed review on NF equations. For a recent advancement in neuronal population models, see [Coo23].

The plan of this chapter is the following: We provide a comprehensive overview of the biophysics underlying neural communication in Section 2.2 and revisit the derivation of the Wilson-Cowan model [WC73] and the Amari model [Ama77] of cortical activity in Section 2.3. In Section 2.4, we present the retinotopic structure of the primary visual cortex as well as the analytical derivation of the retino-cortical map. We also overview the mathematical analysis leading to simple geometric visual hallucinations perceived in the retina, associated with cortical patterns that spontaneously emerge in V1, using bifurcation analysis of the Amari-type Equation (NF) near a Turing-like instability, in Section 2.5.

2.2 . Biophysics of neuronal communication

In this section, we recall some elements of neural systems needed for deriving a spiking neuron's neuronal dynamics, such as action potential, spike trains, synaptic processing, and postsynaptic potential. For a comprehensive introduction to the biophysics of neurons in more detail, we suggest the books such as [Car12; Kan+00; Pur+04; DA01] primarily devoted to neuroscience, and [Izh07; ET10; Bre14; Ger+14; GK02] with emphasis on dynamical systems in neuroscience.

2.2.1 . A Spiking Neuron

A neuron is a fundamental cell that comprises the intricate neural circuits of the brain. Just like other cells (as observed by Ramón y Cajal in his groundbreaking work in neuroscience [Ram09]), a neuron consists of a cell body, also known as the *soma*. However, what sets neurons apart is their unique structure: they possess branching extensions that form a tree-like configuration. These extensions include receptive *dendrites* at one end and transmitting *axons* at the other end (refer to Figure 2.1).

The dendrites serve as the entry points for information coming from other neurons, functioning as input signals. Conversely, the axon carries the processed information and transmits it

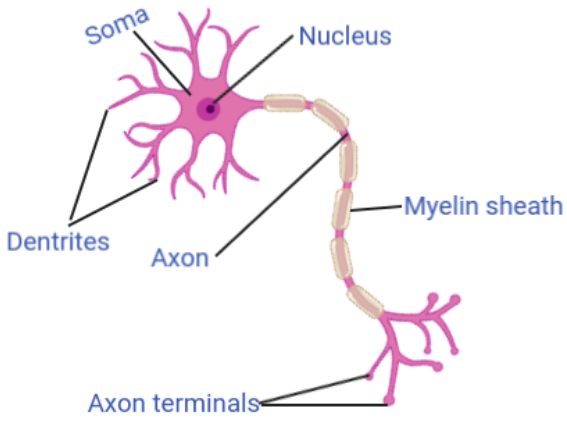

Figure 2.1: A basic neuron (created in BioRender.com)

to one or more downstream neurons, which then receive these output signals. This bidirectional flow of information distinguishes neurons as *functionally asymmetric* entities.

A neuron connects with numerous other nerve cells through specialized junctions known as *synapses*. On average, a single nerve cell can form approximately 10,000 connections. While electrical signals propagate within the nerve cell's branches, at the synapse, the communication between neurons primarily occurs through chemical messages called *neurotransmitters*, which are stored in specialized structures called *synaptic vesicles*. The neuron transmitting the message is commonly called the *presynaptic cell*, while the neuron receiving the message is known as the *postsynaptic cell*.

Input signals a neuron receives generate electrical transmembrane currents, causing changes in its membrane potential. These synaptic currents produce alterations known as postsynaptic potentials (PSPs). Small currents result in minor PSPs, while larger currents yield significant PSPs. The neural membrane contains voltage-sensitive channels that can amplify these PSPs. In some instances, when the PSPs reach a critical level, they trigger the generation of an *action potential* or *spike* at a specific region called the *axon hillock*. The action potential represents an abrupt and transient change in the membrane voltage, which propagates, without distortion, along the neuron's *axon* to the *axon terminals*. These axon terminals contain the synapses through which the neuron communicates with its target neurons.

2.2.2 . Synaptic signal transmission between two neurons

When a pulse, often referred to as a spike or action potential, travels along the presynaptic neuron, it eventually reaches the end of the membrane, known as the axon terminal. This arrival triggers the influx of calcium ions (Ca^{2+}) into the cell through specialized channels in the membrane. The increase in calcium concentration prompts the movement and fusion of vesicles containing neurotransmitters with the cell membrane [FZ85], see Figure 2.2. This process, known as exocytosis, releases the neurotransmitters into the synaptic cleft. Subsequently, the neurotransmitters diffuse across the synaptic cleft and bind to receptors situated on the

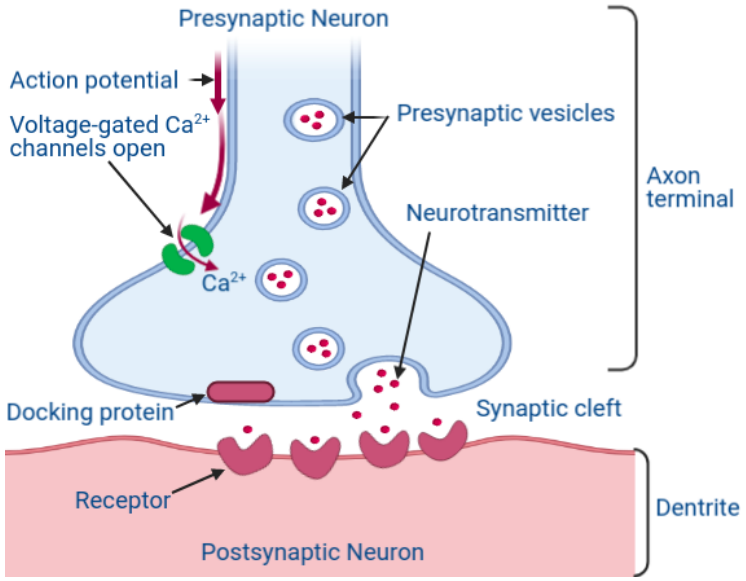

Figure 2.2: Process of synaptic signal transmission (Created in BioRender.com)

postsynaptic membrane of the receiving neuron.

The binding of neurotransmitters to their receptors initiates the opening of sodium ion (Na^+) channels on the postsynaptic membrane. This allows sodium ions to enter the cell, propagating the action potential towards the dendritic or somatic membranes of the postsynaptic neuron. As a result, currents flow through the dendrites, contributing to the overall electrical activity of the postsynaptic neuron.

It is important to note that the extent of sodium ion flow into the postsynaptic cell depends on the amount of neurotransmitter binding to the receptors. Insufficient neurotransmitter binding may fail to reach the threshold potential required to trigger an action potential. Hence, the response of the postsynaptic neuron follows an "all or nothing" principle. Sufficient neurotransmitter presence leads to initiating the action potential, resulting in impulse transmission and depolarization of the postsynaptic membrane potential. Conversely, if neurotransmitter release is inadequate, the neurotransmitters are degraded, and the sodium-potassium pumps work to restore the resting potential in the postsynaptic cell, causing hyperpolarization of the postsynaptic membrane potential.

A single synaptic event due to the arrival of an action potential at time T induces a synaptic current of the form [Erm98],

$$I_{\text{syn}}(t) = g_{\text{syn}}(t-T)(V_{\text{syn}} - V(t)). \tag{2.1}$$

Here V is the voltage of the postsynaptic neuron, V_{syn} is the synaptic reversal potential and $g_{\text{syn}}(t)$ is the change in synaptic conductance with $g_{\text{syn}}(t) = 0$ for $t < 0$. A typical form for $g_{\text{syn}}(t)$ is the difference of exponentials

$$g_{\text{syn}}(t) = \overline{g}\left(\frac{1}{\tau_d} - \frac{1}{\tau_r}\right)^{-1}(e^{-t/\tau_r} - e^{-t/\tau_d})H(t); \tag{2.2}$$

where $H(t)$ is the Heaviside step function, $\overline{g}$ is constant conductance, and $\tau_{d,r}$ are time constants determining the rise and fall of the synaptic response, respectively. There are two limits that are usually used:

$$g_{\text{syn}}(t) = \overline{g}\alpha^2 t e^{-\alpha t} H(t) \qquad \text{as} \qquad \tau_d \to \tau_r = \alpha^{-1}, \tag{2.3}$$

and

$$g_{\text{syn}}(t) = \overline{g} e^{-t/\tau_d} \qquad \text{as} \qquad \tau_r \ll \tau_d. \tag{2.4}$$

The sign of V_{syn} relative to the resting potential $V_{\text{rest}} \approx -65mV$ determines whether the synapse is excitatory ($V_{\text{syn}} > V_{\text{rest}}$) or inhibitory ($V_{\text{syn}} < V_{\text{rest}}$).

2.3 . Neuronal population models

In the preceding section, we briefly discussed several key properties related to the biophysics of individual spiking neurons and the synaptic interactions between pairs of such neurons. However, it is important to recognize that the brain comprises an extensive network of millions of neurons organized into distinct brain areas. Within each brain area, further subdivisions exist, forming different subregions, and within these subregions, multiple layers can be identified. Moreover, each layer consists of diverse cell types with unique characteristics.

Considering the complexity of the brain's structure, this section provides an overview of two prominent models that describe the activity of spiking neurons. These models have significantly influenced the field of neuronal dynamics based on our current understanding.

2.3.1 . Wilson-Cowan equations

Based on a statistical mechanical approach, Wilson-Cowan's equations are mean-field models, which describe the average behaviour of a large population of neurons rather than the behaviour of individual neuron. Despite its simplicity, these equations capture many essential features of cortical dynamics, such as the emergence of oscillations and the propagation of waves of activity [Coo05; EC79b]. Let us present the derivation of the model by simplifying the parameters appearing in the original one (we refer to [WC72; WC73] for more details).

Consider an interacting population of excitatory and inhibitory neurons which are homogeneously and isotropically distributed within a two-dimensional nervous tissue. Then, assume that all possible types of interaction are permitted (excitatory-excitatory, excitatory-inhibitory, inhibitory-excitatory and inhibitory-inhibitory) so that each type will be taken to be a function only of the distance between cells on the tissue.

We let $a_e(x,t)$ (resp. $a_i(x,t)$) denote the proportion of excitatory (resp. inhibitory) neurons becoming active per unit time at the instant t at the point x. Assume that an excitatory (resp. inhibitory) cell is only sensitive (i.e., able to trigger a spike after a supra stimulation) or in its absolutely refractory period with duration[1] r_e (resp. r_i) (the minimum duration between two spikes, i.e., the period in which it is incapable for the cell to generate an action potential no

[1]it is assumed that neuron is activated only if it receives a supra-threshold excitation. So, we may treat the relative refractory period of neurons as the moment it is sensitive.

matter how intense the stimulus). So neurons will become activated only if their postsynaptic potentials exceed a threshold and if they are the same time sensitive.

Let $\omega_{jj'}(x)$ *measure the probability* that a postsynaptic neuron of type j' is connected with a presynaptic neuron of type j at a distance x away. Here, j and j' belong to the set of excitatory and inhibitory neurons.

It is also assumed that excitatory (resp. inhibitory) cells are efferents neurons (resp. interneurons), so excitatory neurons' activity is transferred from one anatomical region to another. Then they receive different sensory (external) inputs $h_e(x,t)$ (resp. $h_i(x,t)$) at time t and position x from other regions of the brain (e.g. the thalamus etc.).

To average out rapid temporal variations taking place on a time scale shorter than the neural membrane time constant, it is assumed that the absolutely refractory period r_e (resp. r_i) of excitatory (resp. inhibitory) neurons is much less than the membrane time constant α_e (resp. α_i) of excitatory (resp. inhibitory) cells.

Finally, if the expected number of excitatory (resp. inhibitory) neurons receiving at least supra-threshold excitation during an interval δt at t is statistically independent of the sensitive proportion, then at the limiting case when $\delta t \to 0$, the dynamics of excitatory (resp. inhibitory) cells becoming active at time t at position x are governed by the following coupling nonlinear integrodifferential equations

$$\begin{cases} \alpha_e \dfrac{\partial a_e}{\partial t}(x,t) = -a_e(x,t) + \mu_e(x,t) S_e\left((\omega_{ee} * a_e(\cdot,t))(x) - (\omega_{ie} * a_i(\cdot,t))(x) + h_e(x,t)\right), \\ \alpha_i \dfrac{\partial a_i}{\partial t}(x,t) = -a_i(x,t) + \mu_i(x,t) S_i\left((\omega_{ei} * a_e(\cdot,t))(x) - (\omega_{ii} * a_i(\cdot,t))(x) + h_i(x,t)\right), \end{cases} \tag{2.5}$$

where

$$\mu_e(x,t) = 1 - r_e a_e(x,t) \qquad \text{and} \qquad \mu_i(x,t) = 1 - r_i a_i(x,t).$$

Equation (2.5) is a two-layer synaptic activity of interconnected excitatory and inhibitory neurons in nervous tissue. The functions S_e (resp. S_i) are the response functions for excitatory (resp. inhibitory) cells which are also usually called the firing rate functions. They give the expected proportion of the cells receiving as least threshold excitation per unit of time as a function of mean integrated excitation generated within excitatory (resp. inhibitory) neurons.

The numerical simulation done in [WC72] provides that a convenient approximation for S_j, $j = e, i$, can be a logistic function.

$$S_j(z) = \frac{1}{1 + \exp(-\gamma(z - \kappa))}. \tag{2.6}$$

The parameter $\gamma > 0$ determines the slope or sensitivity of the input-output characteristics of the population, and $\kappa > 0$ is the threshold beyond which a spiking neuron triggers a pulse.

2.3.2 . The Amari-type equation

The Amari-type equation describes the dynamics of the membrane potential of a neuron, which is the electrical potential difference across the cell membrane. This nonlinear integrodifferential equation considers the ion channels and synapses that contribute to the membrane potential and the neuron's firing rate.

The Amari-type equation is a mathematical model of neural activity that takes into account the interaction between excitatory and inhibitory neurons in cortical tissue and can be derived from the Wilson-Cowan equations (2.5) [ET10, Chapter 12, Section 12.4.1].

In Wilson-Cowan equations (2.5) , the terms $r_e a_e(x,t)$ and $r_i a_i(x,t)$ are the time-coarse grained approximations of

$$R_e(x,t) = \int_{t-r_e}^{t} a_e(x,t')dt' \qquad \text{and} \qquad R_i(x,t) = \int_{t-r_i}^{t} a_i(x,t')dt', \tag{2.7}$$

which represent respectively the excitatory and inhibitory cell proportions, which are absolutely refractory into time bins of size r_e and r_i at the location x.

The absolute refractory period determines the maximum frequency of action potentials that can be generated per unit of time at any point along the axon membrane, and the frequency of the spike train is directly related to the intensity of the stimulus. It follows that the proportion of absolutely refractory cells is associated with the intensity of the stimulus. Therefore, uniformly with respect to a location x on the tissue and a given time t, we substitute $r_e a_e$ and $r_i a_i$ by parameters that are constants with respect to x and t and which depend only on the intensity of the stimulus, namely

$$\nu_e := \nu_e(\text{stimulus intensity}) \qquad \text{and} \qquad \nu_i := \nu_i(\text{stimulus intensity}). \tag{2.8}$$

In other words, the parameters $0 \leq \nu_e, \nu_i \leq 1$ are rates that express how a substance acts respectively on excitatory and inhibitory activity. Then, Equation (2.5) can be recast as

$$\begin{cases} \alpha_e \dfrac{\partial a_e}{\partial t}(x,t) = -a_e(x,t) + \mu_e S_e\left((\omega_{ee} * a_e(\cdot,t))(x) - (\omega_{ie} * a_i(\cdot,t))(x) + h_e(x,t)\right), \\ \\ \alpha_i \dfrac{\partial a_i}{\partial t}(x,t) = -a_i(x,t) + \mu_i S_i\left((\omega_{ei} * a_e(\cdot,t))(x) - (\omega_{ii} * a_i(\cdot,t))(x) + h_i(x,t)\right), \end{cases} \tag{2.9}$$

where $\mu_e := 1 - \nu_e$ and $\mu_i := 1 - \nu_i$.

Further assumptions on inhibitory cells can contribute to reducing the two-layer equations (2.9) to single-layer neural activity's equation of Amari-type [Ama77, Eq. (3)]. Suppose that the neural membrane time constant of inhibition is much less than that of excitation, $\alpha_i \ll \alpha_e$, say $\alpha_i = 0$, for instantaneous inhibition.

Supported by experimental data comparing the firing properties of excitatory versus inhibitory neurons in the cortex [McC+85], we may assume that the firing rate function for the inhibitory cells is linear such that $S_i(x) = \gamma x$ for some positive constant $0 < \gamma \leq 1$ being the gain of the sigmoid function S_i. Finally, if we neglect the term describing the interaction

between inhibitory cells, $\omega_{ii} = 0$, to simplify the computations, then one obtains the following single-layer of synaptic activity of neurons in cortical tissue:

$$\alpha_e \frac{\partial a_e}{\partial t}(x,t) = -a_e(x,t) + \mu_e S_e \left(\int_{\mathbb{R}^2} \omega(x-y) a_e(y,t) dy + h(x,t) \right), \tag{2.10}$$

where,

$$h(x,t) := h_e(x,t) - \gamma \mu_i (\omega_{ie} * h_i(\cdot,t))(x), \tag{2.11}$$

$$\omega(x) := \omega_{ee}(x) - \gamma \mu_i (\omega_{ie} * \omega_{ei})(x). \tag{2.12}$$

If the response function S_e for excitatory cells is placed inside the integral in Equation (2.10) (can happen in case neuron activation rates are low [BC02]), then we obtain an equation similar to that analysed Amari [Ama77, Eq. (3)], which he studied the dynamics of pattern formation in a one-dimensional cortical tissue. Indeed, letting

$$a(x,t) = (\omega * a_e(\cdot,t))(x) + h(x,t), \tag{2.13}$$

one finds after differentiation with respect to t,

$$\frac{\partial a}{\partial t}(x,t) = -\alpha a(x,t) + \mu \int_{\mathbb{R}^2} \omega(x-y) f(a(y,t)) dy + I(x,t), \tag{2.14}$$

where $\alpha := \alpha_e^{-1}$, $\mu := \mu_e$, $f : s \mapsto \alpha S_e(s)$ and

$$I(x,t) = \alpha h(x,t) + \partial_t h(x,t). \tag{2.15}$$

The Amari-type Equation (2.14) has been used to model a wide range of neural phenomena, including the generation of action potentials, the propagation of signals along axons, and the control of waves like activities [ZME19]. It has also been used to study the effects of drugs induced geometric visual hallucinations [Bre+01, Section 2(c)] and other interventions on neural activity [CGP14].

Overall, the Amari-type equation is an essential tool for understanding the complex dynamics of neurons and their interactions in the brain, in particular, thanks to the fact that it is more amenable for mathematical analysis.

2.4 . The primary visual cortex

The primary visual cortex, also known as V1 or the striate cortex, is a key region in the occipital lobe at the back of the brain. Its role in analysing basic visual features forms the foundations of higher-level visual processing and our perception of the visual world. In this respect, understanding our cortical activity in V1 is modelled, and its implications for visual behaviour is a fascinating area of research.

By exploring the underlying V1 activity, we can gain valuable insights into visual phenomena, including hallucinations, illusions, and other aberrant visual behaviour.

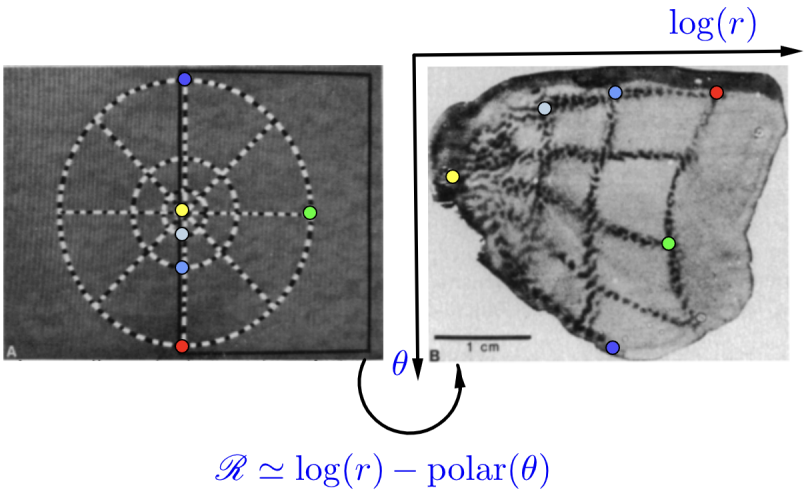

Figure 2.3: Coloured dots in the visual stimulus on the *left* is mapped into that on the *right* in V1, adapted from Tootell *et al.* [Too+82]. Focusing on the image on the *right*, one notices that following the horizontal direction from the left to right, coloured dots describe a log curve, while following the vertical path from the top to below, they represent the eccentricity.

2.4.1 . Retinotopic structure of V1

The functional architecture of V1 exhibits a remarkable characteristic known as retinotopic organization. The following key features can describe this organization:

(i) Neural organization: The neurons in the V1 area are arranged orderly, forming a topographic or retinotopic map (well-known as the retino-cortical map). This map represents a two-dimensional projection of the visual image formed on the retina. Notably, neighbouring regions of the visual field are represented by neighbouring regions of neurons in V1, establishing a bijective relationship;

(ii) Foveal representation: Near the fovea, which corresponds to the central region of the visual field, there is a larger representation of the image in the V1 area compared to the visual field. This means that the foveal region in V1 exhibits an enlarged representation, essentially resembling an expansion of the identity map;

(iii) Log-polar transformation: As we move away from the fovea, the retinotopic map in V1 undergoes a log-polar transformation. This transformation involves a mapping distortion, resulting in a logarithmic compression of the visual space. It means that regions of the visual field further away from the fovea are represented in a compressed manner in the V1 area.

These characteristics of retinotopic organization in the V1 striate cortex, as described by Sereno [Ser+95] and Tootell *et al.* [Too+82] (see, for instance Figure 2.3), highlight the systematic and structured nature of how visual information is processed and represented in the early visual system.

2.4.2 . Analytical derivation of the retino-cortical map

The retino-cortical map was first represented analytically as a complex logarithmic map in [Sch77]. In the following we review the representation made in [Bre+01, Section 1(b)].

A point in the visual field or the retina can be represented in polar coordinates by $(r, \theta) \in [0, +\infty) \times [0, 2\pi[$. From the physiological evidences of [HW59], a local region in V1 is a sheet of dimension 2 so that spatial position of any neuron in V1 can be represented in Cartesian coordinates by $(x_1, x_2) \in \mathbb{R}^2$.

Let ρ_R be the number of ganglion cells per solid degree within a given region A of the visual field and ρ the cortical magnification, i.e., the extent of striate cortex in millimetres corresponding to a degree of arc in visual space. Supported by the work of [HW74a; HW74b], ρ is sufficiently closed to unity to be replaced by it, whereas following [Dra77], ρ_R declines from the fovea with an inverse square law,

$$\rho_R = \frac{1}{(\omega_0 + \varepsilon r)^2}, \tag{2.16}$$

where ω_0 and ε are two physiological constant parameters.

The retino-cortical map $\mathscr{R} : (r, \theta) \in [0, +\infty) \times [0, 2\pi[\longmapsto (x_1, x_2) \in \mathbb{R}^2$ is then defined such that the following holds in a given region A of the visual field

$$\int_A \frac{r}{(\omega_0 + \varepsilon r)^2} dr d\theta = \int_A \rho_R r dr d\theta = \int_{\mathscr{R}(A)} \rho dx dy = \int_A |Jac(\mathscr{R})| dr d\theta. \tag{2.17}$$

Note that $\mathscr{R}$ is a bijective map which we assume to be bidifferentiable, since cortical magnification is a differential quantity [Sch77]. Then one deduces from (2.17) that

$$|Jac(\mathscr{R})| := \left| \frac{\partial x_1}{\partial r} \frac{\partial x_2}{\partial \theta} - \frac{\partial x_1}{\partial \theta} \frac{\partial x_2}{\partial r} \right| = \frac{r}{(\omega_0 + \varepsilon r)^2}.$$

Consistent with the physiological evidence of Tootell *et al.* [Too+82], we assume the existence of positive constant α such that

$$\frac{\partial x_1}{\partial r} = \frac{\alpha}{\omega_0 + \varepsilon r} \qquad \text{and} \qquad \frac{\partial x_2}{\partial \theta} = \frac{1}{\alpha} \frac{r}{\omega_0 + \varepsilon r}.$$

It follow that, for some $k_1 := k_1(\theta), k_2 := k_2(r) \in \mathbb{R}$, one has

$$x_1 = \frac{\alpha}{\varepsilon} \log\left(\frac{\omega_0 + \varepsilon r}{k_1}\right) \qquad \text{and} \qquad x_2 = \frac{1}{\alpha} \frac{r\theta}{\omega_0 + \varepsilon r} + k_2.$$

Recall that $(x_1, x_2) = (0, 0)$ when $r \to 0$ so that $k_1 \equiv \omega_0$ and $k_2 \equiv 0$. Therefore, one finds

$$x_1 = \frac{\alpha}{\varepsilon} \log\left(1 + \frac{\varepsilon}{\omega_0} r\right) \qquad \text{and} \qquad x_2 = \frac{1}{\alpha} \frac{r\theta}{\omega_0 + \varepsilon r}.$$

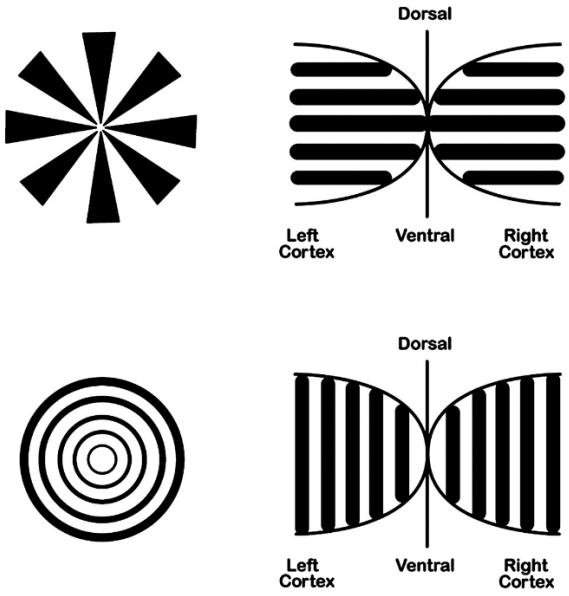

Figure 2.4: Visual illustration of the retino-cortical map, reproduced from [BT07]. Funnel pattern (*top-left*) in the retina is mapped through the retino-cortical map into pattern of horizontal stripes (*top-right*) in V1. Tunnel pattern (*bottom-left*) in the retina is mapped through the retino-cortical map into pattern of vertical stripes (*bottom-right*) in V1.

2.4.3 . Visual illustration of the retino-cortical map

In this section we will visually illustrate how simple patterns in the visual field are mapped into V1 via the retino-cortical map.

In what follows, consistent with the experiments we aim to describe, we will always accept that the log-polar transformation is an accurate approximation of the retino-cortical map. After rescaling physiological parameters, it simply takes the form

$$\begin{aligned} \mathscr{R}: \quad \mathbb{R}_{>0} \times \mathbb{S}^1 &\longrightarrow \mathbb{R}^2 \\ (r, e^{i\theta}) &\longmapsto \mathscr{R}(r,\theta) = (\log(r), \theta). \end{aligned} \tag{2.18}$$

Here $\mathbb{R}_{>0} \times \mathbb{S}^1$ models the retina or the visual field and $\mathbb{R}^2$ models V1 striate cortex when neglecting the orientation label. The following definition will be of interest. The notion of 2D manifolds and vector field was given in Section 1.2.1 in the first part.

Definition 2.4.1 (Pushforward of a vector field) *Let M and N be 2D manifolds, $\psi : M \to N$ a diffeomorphism and X be a vector field on M. The pushforward (or the "image") of X by ψ is the vector field $\psi_* X$ on N defined by*

$$(\psi_* X)(\psi(p)) = \frac{d}{dt}\bigg|_{t=0} \psi(\gamma(t)), \qquad \forall p \in M, \tag{2.19}$$

where γ is the integral curve of the vector field X satisfying $\gamma(0) = p$.

Assume that $M := \mathbb{R}_{>0} \times \mathbb{S}^1$ is endowed with the system of polar coordinates (r, θ) and $N := \mathbb{R}^2$ is endowed with the system of Cartesian coordinates (x_1, x_2).

Let X_1 be the vector field on M generating the counterclockwise rotation around the origin, $X_1 = \partial\theta$. Then the orbit of the flow of X_1 describes concentric circles centred at the origin in the manifold M.

The "image" of the vector field X_1 by the retino-cortical map $\mathscr{R}$ defined in (2.18) is the vector field X_2 on N obtained by pushing forward the vector field X_1 by $\mathscr{R}$. Letting $(x_1, x_2) = \mathscr{R}(r, \theta)$ for all $(r, \theta) \in M$, one has

$$X_2(x_1, x_2) := (\mathcal{R}_* X_1)(x_1, x_2) = \frac{d}{dt}\Big|_{t=0} (\log(r), \theta + t) = \frac{\partial}{\partial x_2}, \tag{2.20}$$

which is the vector field generating vertical translation in N.

The implication of this in visual system is that patterns consisting of concentric circles around the fovea in the human retina induce patterns of vertical stripes in the primary visual cortex via the retino-cortical map, see Figure 2.4 for visual illustration.

The above analysis also applies to the vector field $Y_1 := r\partial r$ on M generating the dilation that start at the origin. The orbit of the flow of Y_1 are rays that start from the origin. One therefore computes the vector field Y_2 on N image of Y_1 by the retino-cortical map $\mathscr{R}$ as

$$Y_2(x_1, x_2) := (\mathcal{R}_* Y_1)(x_1, x_2) = \frac{d}{dt}\Big|_{t=0} (t + \log(r), \theta) = \frac{\partial}{\partial x_1}, \tag{2.21}$$

which is the vector field generating horizontal translation in N. It follows that patterns consisting of rays that start from the fovea in the human retina induce patterns of horizontal stripes in the primary visual cortex via the retino-cortical map, see Figure 2.4 for visual illustration.

2.5 . On visual hallucinations

In this section, using the Amari-type equation, we briefly overview the mathematical exploration conducted to understand the underlying causes of the spontaneous formation of cortical patterns in the primary visual cortex.

2.5.1 . Geometric visual hallucinations

Hallucinations can arise in certain psychoses and various pathologies. They can also occur without any disease, often due to hyperactivation in specific brain regions that no longer receive sufficient sensory inputs from the retina. Visual hallucinations refer to the perception of objects or phenomena that do not exist or are not physically present before the individual experiences them [Ffy04].

When individuals are subjected to pressure on their eyeballs, they may experience a reaction in the retina after a brief delay of approximately 2 to 3 seconds. This can lead to the perception of phosphenes in the visual field, which manifests as small geometric shapes interconnected by curves such as circular arcs or logarithmic spirals. These fundamental geometric shapes are

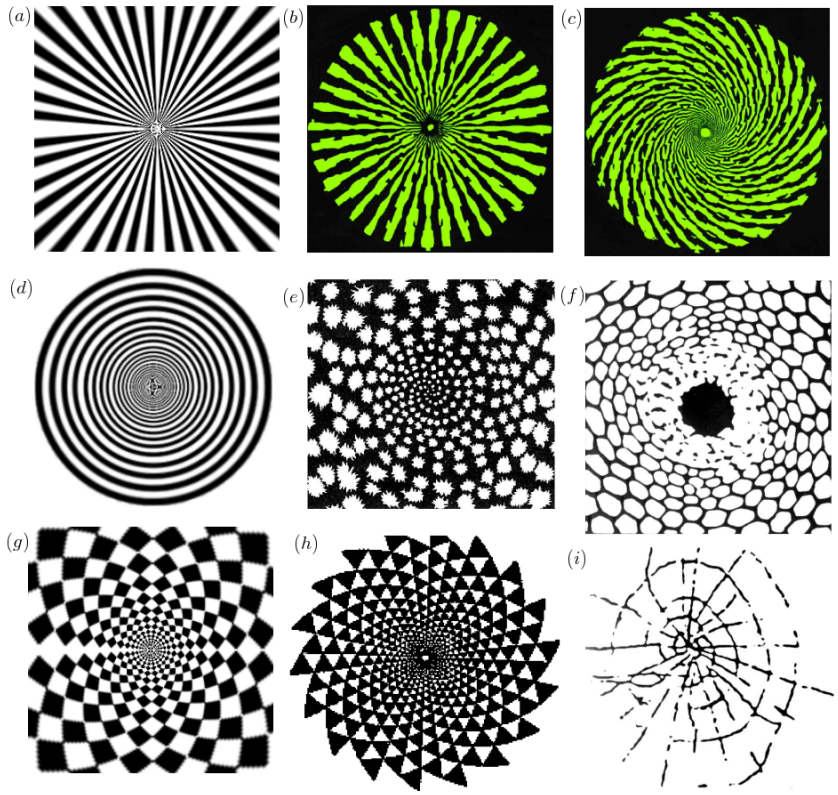

Figure 2.5: Artist's depictions of geometric visual hallucinations. Redrawn from Oster [Ost70], Siegel [Sie77], Patterson [Pat92], Clottes & Lewis-Williams [CL98].

commonly observed in phosphene experiences. Similarly, individuals (even those with blindness [KAO63]) influenced by hallucinogenic drugs like marijuana and LSD may encounter successive unreal visual perceptions such as honeycombs [CL98], funnels, and spirals [Ost70], which emerge in the visual field, see Figure 2.5.

In addition to these scenarios, spontaneous geometric visual hallucinations can manifest after exposure to flashing lights [Hel67] and in numerous other conditions documented by Klüver in [Klü66]. The exploration of these hallucinations from a mathematical standpoint aims to uncover the underlying mechanisms and shed light on the intricate relationship between neural activity and the resulting perceptual experiences. By delving into these mathematical investigations, we can deepen our understanding of the origins and manifestations of spontaneous geometric visual hallucinations across various contexts and conditions.

While simple cortical patterns can spontaneously emerge in V1 caused by epileptic activity due to the decrease of the influence of the inhibitory neurons on the excitatory neurons [Tas95], here, we are primarily concerned with the phenomenon accompanying the early stage of drug-induced (LSD, marijuana, etc.) simple cortical patterns in V1 [EC79a] due to an increase in the excitability of excitatory and inhibitory neurons beyond a certain threshold of neural activity. Then applying the inverse retino-cortical transformation to these patterns will yield simple geometric visual hallucinations that people experience daily.

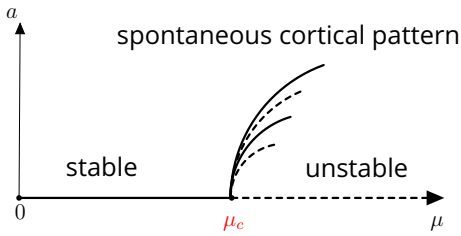

Figure 2.6: Bifurcation diagram. As the parameter μ increases and surpasses the critical value μ_c, a significant change occurs in the system's behaviour. The previously stable state, represented by the bold line, transitions into an unstable state, as indicated by the dashed lines. This transition causes the system to branch into other states (stable or unstable depending on model parameters) that we call *spontaneous cortical patterns*.

2.5.2 . Spontaneous cortical patterns formation in V1

We briefly discuss in this section the results on spontaneous cortical patterns (SCP), which refer to the bifurcating branches to the trivial stationary state of Equation (NF) in the absence of external input or sensory input. They can be considered as the paroxismic states of cortical activity in V1 or, in other words, the states of high cortical activity in V1.

In the absence of external input, that is, when $I \equiv 0$, one has that $a \equiv 0$ is a trivial stationary state to Equation (NF) since $f(0) = 0$. The linearised equation around it reads

$$\partial_t a = -a + \mu\omega * a.$$

Taking the Fourier transform of the above equation in the space $\mathcal{S}'(\mathbb{R}^2)$ of tempered distributions leads to

$$\widehat{a}(\xi, t) = e^{(-1+\mu\widehat{\omega}(\xi))t}\widehat{a}_0(\xi), \qquad \xi \in \mathbb{R}^2,\ t \geq 0, \tag{2.22}$$

where $\widehat{a}_0$ is the Fourier transform of the initial datum $a_0 \in \mathcal{S}'(\mathbb{R}^2)$. It follows that 0 is exponentially stable in the space of tempered distribution $\mathcal{S}'(\mathbb{R}^2)$ for small enough $\mu > 0$. It loses its stability the first time when μ grows beyond the critical value[2] μ_c given as follows,

$$\mu_c := \widehat{\omega}(q_c)^{-1}. \tag{2.23}$$

Here $q_c > 0$ is the wavenumber, the point at which $\widehat{\omega}(|\xi|)$ reaches its maximum for $|\xi| \geq 0$. Please, refer to Figure 2.6 for visual illustration.

We recall that the threshold parameter μ_c is called the *bifurcation point* in the dynamical system theory or the *control parameter* in complexity theory to refer to a parameter whose change can force a sudden qualitative change in pattern formation of the underlying system. In our context, It corresponds to the value of μ for which the intrinsic (that is, in the absence of external input) cortical activity in V1 is highest. Observe that for all $\mu < \mu_c$, the kernel of

$$L_\mu a = -a + \mu\omega * a, \tag{2.24}$$

[2]More precisely, $\mu_c := \alpha f'(0)^{-1}\widehat{\omega}(q_c)^{-1}$, where $\alpha > 0$ is the time constant of the membrane potential of cells in V1. Here we assumed that $\alpha = 1$ and $f'(0) = \max_{s\in\mathbb{R}} f'(s) = 1$.

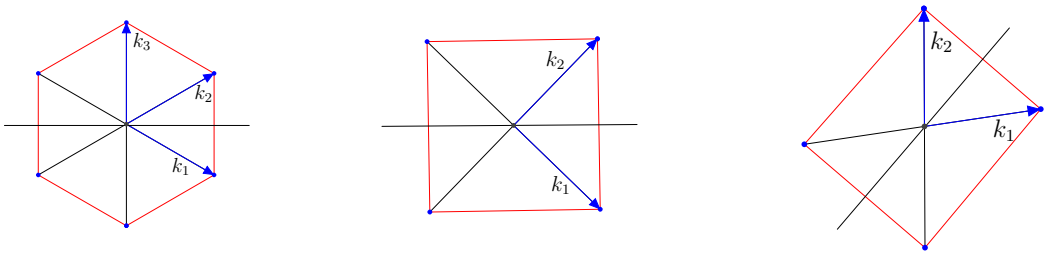

Figure 2.7: Hexagonal lattice (*left*), square lattice (*middle*) and rectangular lattice (*right*). The unit vectors $k_j \in \mathbb{R}^2$ are generator of these lattices satisfying $\widehat{(k_i, k_j)} = 60^\circ$ for the hexagonal lattice, $\widehat{(k_1, k_2)} = 90^\circ$ for square lattice and $\widehat{(k_1, k_2)} = \theta =$ any acute angle other than 90° and 60° for rectangular lattice.

viewed as a linear operator from $\mathcal{S}'(\mathbb{R}^2)$ to itself is trivial.

Since $I \equiv 0$, Equation NF is $\mathbf{E}(2)$-equivariant, that is, it commutes with the natural action of the Euclidean group $\mathbf{E}(2) = \mathbb{R}^2 \rtimes \mathcal{O}(2)$. Please, refer for instance to Section 3.3.2 of Chapter 3. Due to the $\mathcal{O}(2)$-equivariance and the fact that eigenfunctions of the convolution operator $\omega *$ in the space $\mathcal{S}'(\mathbb{R}^2)$ are of the form $e^{2i\pi\langle\xi,\cdot\rangle}$, $\xi \in \mathbb{R}^2$, at the bifurcation point $\mu = \mu_c$, the kernel of the linear operator L_{μ_c} is given by

$$\ker L_{\mu_c} = \operatorname{span}\left\{e^{2\pi i\langle r\xi_c,\cdot\rangle}\right\}_{r\in\mathcal{O}(2)},$$

where $\xi_c = q_c e^{i\phi_c}$ represents the critical wavevector with $q_c = |\xi_c|$ the wavenumber, $\phi_c = \arg\xi_c$, and $\mathcal{O}(2)$ is the orthogonal group of degree 2.

It is important to note that this kernel is infinite-dimensional, resulting in 0 being an eigenvalue of L_{μ_c} with infinite multiplicity, both geometrically and algebraically. Consequently, the classical local center manifold theory (see, [HI11, Chapter 2] or [CL00, Chapter 8] for instance) cannot be directly applied to compute the solutions bifurcating from the equilibrium zero. However, the translation equivariance of the system (NF) allows to address this issue by restricting the solution space to doubly-periodic functions, also known as planforms. Please, see for instance, [Sat78] for more details about "planform functions".

In summary, the stability analysis of the equilibrium $a = 0$ near the bifurcation point $\mu = \mu_c$ requires the utilization of local center manifold theory, taking into account the $\mathbf{E}(2)$-equivariance and the infinite-dimensional kernel of the linear operator. By considering the translation equivariance, we can study the solutions that bifurcate from the zero equilibrium within the space of planforms.

We will not address this question here since it is not our primary purpose in this thesis, and we refer the reader, for instance, in [Bre+01; BC02; EC79a] for more details. Nevertheless, notice that by restricting the plane $\mathbb{R}^2$ to hexagonal, square and rectangular lattices, at the bifurcation point, $\mu = \mu_c$, the kernel of the linear operator L_{μ_c} now consists of (finite number of) spontaneous cortical patterns of the form

$$SP(x) = \sum_{j=1}^{N} z_j \cos(\langle 2\pi k_j, x\rangle), \qquad k_j = (\cos\phi_j, \sin\phi_j), \tag{2.25}$$

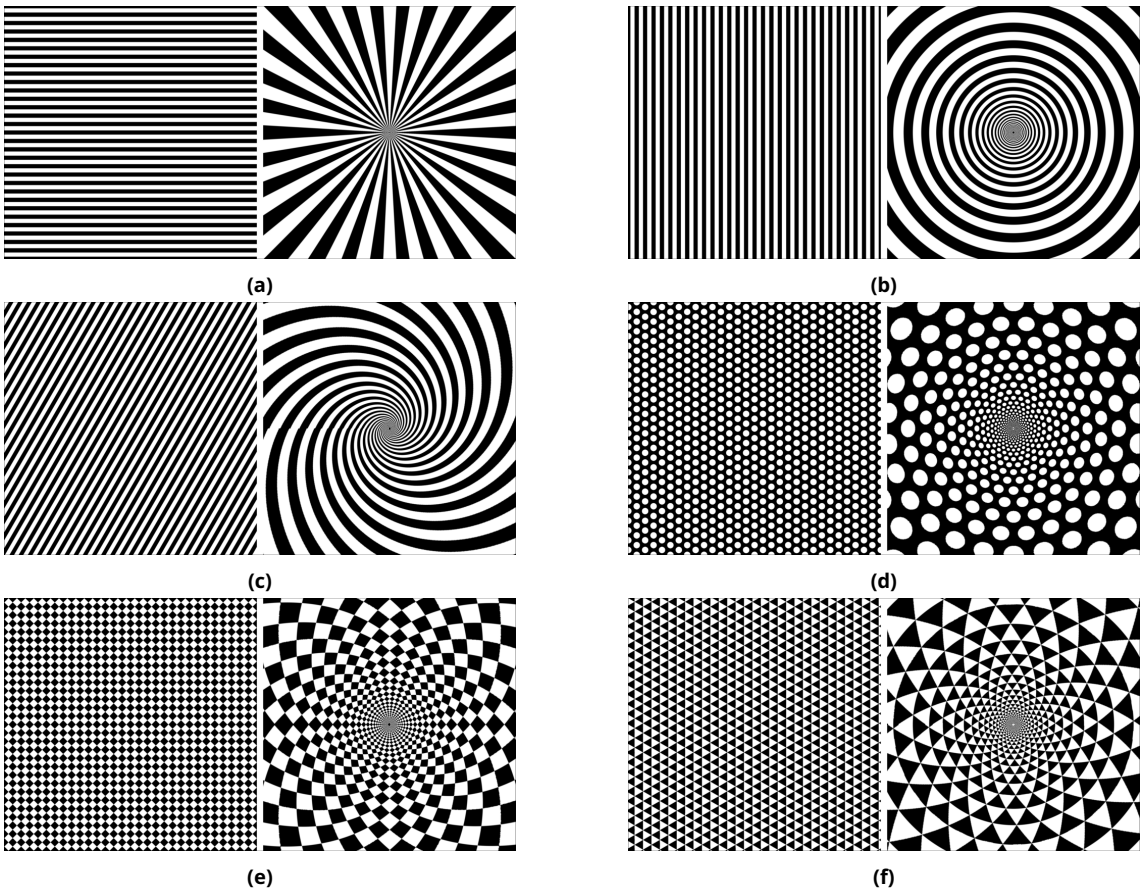

Figure 2.8: From *(a)* to *(f)*: Spontaneous cortical patterns on the *left* and corresponding Hallucinatory patterns on the *right* after applying the inverse retino-cortical map. They were initially obtained by Ermentrout & Cowan [EC79a]. See also Bressloff *et al.* [Bre+01, Figures 19, 20, 29 and 30].

where $(z_j, \phi_j) \in \mathbb{R}^2$ and $k_j \in \mathbb{R}^2$ satisfies $|k_j| = q_c$ for all $j \in \{1, \cdots, N\}$. For the hexagonal lattice, $N = 3$ while for the square and rectangular lattices $N = 2$, refer to Figure 2.7.

Following the convention adopted in [EC79a; Bre+01], we represent spontaneous cortical patterns (2.25) in cortical coordinates of V1 as binary images, where black corresponds to negative values of $SP(x)$ and white to positive ones. The retinal representation obtained from the cortical patterns via the inverse retino-cortical map leads to geometric visual hallucinations of form constants that Klüver had meticulously classified in his famous book [Klü66]. Please refer to Figure 2.8 for visual illustration.

The stability of these patterns can also be studied [EC79a; Bre+01], which depends strongly on the choice of physiological parameters involved in Equation (NF).

CHAPTER 3

On the description of MacKay-type visual illusions

3.1 . Introduction

Humans often perceive an illusory component not physically present in a visual stimulus. One of the earliest researchers to explore the visual effects induced by patterns comprising black-and-white zones was Helmholtz [Hel67]. He specifically associated the perception of rotating darker and brighter radial zones, following observing a pattern of black and white concentric rings, with the fluctuation of eye accommodation.

The plan of this chapter, which investigates the mathematical description of MacKay-type visual illusions, focusing on the MacKay effect [Mac57] and Billock and Tsou's experiments [BT07] is the following:

Section 3.1.1 and 3.1.2 present the psychophysical experiments reported in these two papers. Section 3.1.3 discusses the preliminary result [Nic+21] that describes the MacKay-like effect using neuronal fields equations via bifurcation theory and multiscale analysis.

In Section 3.2, we highlight a motivation for using equation (NF) to describe these psychophysical experiments, and we present assumptions on model parameters used in this equation.

In Section 3.3, we recall some preliminary results about the well-posedness of equation (NF) and define the binary pattern necessary to represent cortical activity in terms of white and black zones. Using equation (NF), in Sections 3.4 and 3.5, we investigate the description of the MacKay effect and Billock and Tsou experiments, respectively. In Section 3.4.4 and 3.5.2, we present numerical results to bolster our theoretical study.

3.1.1 . MacKay visual illusions from redundant stimulation

Around 1960, Donald MacKay made notable observations on the after-effects of visual stimulation using regular geometrical patterns containing highly redundant information. He associated

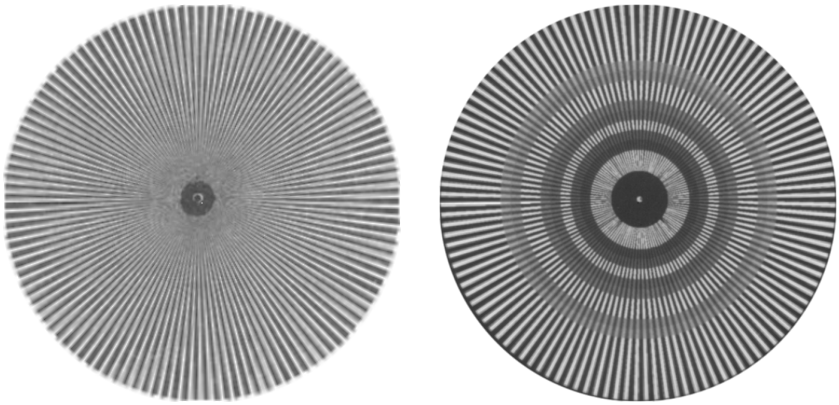

Figure 3.1: The MacKay effect results from redundant stimulation [Mac57], showcasing the illusion induced by the stimulus on the left, referred to as "MacKay rays". This stimulus leads to an illusory perception of concentric rings superimposed in its background, as illustrated on the right (artist's depiction by Isia Leviant [Lev96]). The adaptation of this figure is based on the original representation from [Mac57, Fig. 1] and [ZWF93, Fig. 1b].

this phenomenon, now known as the "MacKay effect", with a specific region of the visual cortex that potentially benefits from such redundancy [Mac57; Mac61].

The psychophysical experiments presented in this paper demonstrate that when a highly redundant visual stimulus, such as a funnel pattern (fan shapes), is presented at the fovea, an accompanying illusory tunnel pattern (concentric rings) emerges in the visual field, superimposed onto the stimulus pattern (see Fig. 3.1). Notably, the distance from the pattern to the retina or the illumination does not significantly affect these more intricate phenomena. Even a slight fluctuation in eye accommodation or a minor alteration in the distance from the pattern to the retina causes the positions of the brighter locations to vary. For most observers, the illusory contours in the background of the afterimage rotate rapidly at right angles to the stimulus pattern, either clockwise or counterclockwise.

Similarly, when viewing a tunnel pattern (concentric rings) as that of Figure 1.4, many observers perceive an illusory funnel pattern (fan shape) superimposed in the afterimage background. In both cases, observers often note rapidly fluctuating sectors, again rotating either clockwise or counterclockwise. Notably, the stimulus pattern does not need to fill the entire visual field; a portion of the stimulus is sufficient to generate a corresponding afterimage in the same portion. However, in both cases, the nervous system tends to prefer the direction perpendicular to the regular contours of the visual stimulus. This preference is attributed to the retino-cortical map, resulting in induced afterimages of superimposed patterns of horizontal and vertical stripes in V1.

The debate between Zeki [Zek94] and Gregory [Gre95] revolves around the attribution of illusory motion in the afterimages. Following MacKay's findings, Zeki attributes the illusory motion to the cerebral cortex, predominantly due to cortical activity in areas V5 and V1. On the other hand, Gregory relates the illusory motion to fluctuations in the accommodation of the eye's lens, as pointed out by Helmholtz [Hel67].

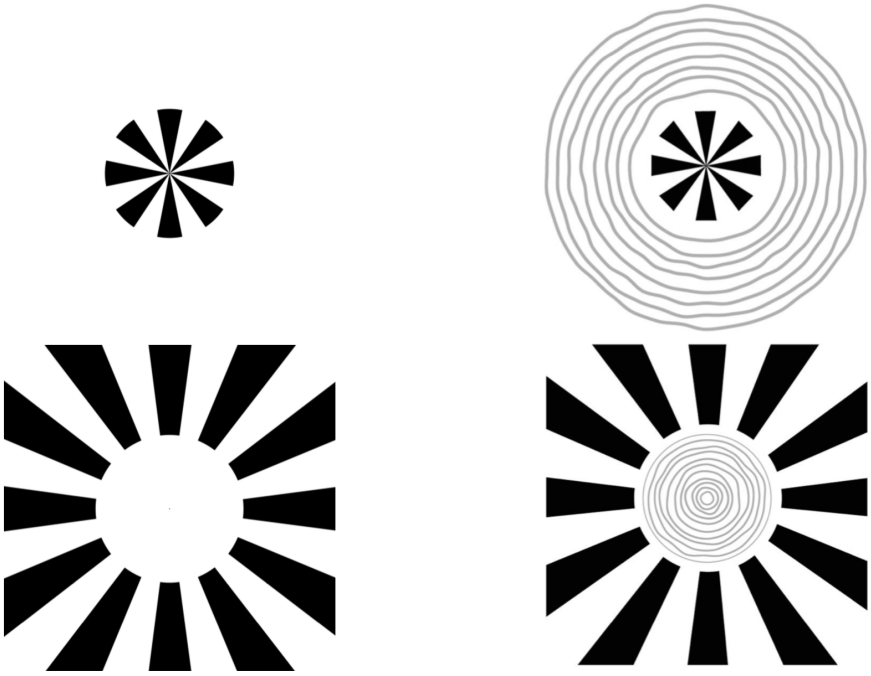

Figure 3.2: Billock and Tsou's experiments: the presentation of funnel pattern stimulus in the centre (image on the *top-left*) induces an illusory perception of tunnel pattern in surround (image on the *top-right*) after a flickering of the empty region (the white region surrounding the stimulus pattern on the *top-left*). We have a reverse effect on the *bottom*. Adapted from [BT07, Fig. 3].

3.1.2 . Billock and Tsou's psychophysical experiments

Significant visual effects associated with funnel and tunnel patterns have been observed in the psychophysical experiments conducted by Billock and Tsou [BT07]. Like the MacKay effects, the authors discovered that introducing biased stimuli elicits orthogonal responses in the visual field. When a physical stimulus is positioned at the fovea (the central region of the visual field), the resulting visual illusion appears in the flickering periphery. Conversely, the visual illusion emerges in the flickering centre if the physical stimulus is presented in the periphery.

Specifically, when a background flicker is combined with a funnel pattern centered on the fovea (or periphery), the observer experiences the illusory perception of a tunnel pattern in the periphery (or fovea, respectively). Similarly, when the periphery (or fovea) of a tunnel pattern located at the fovea (or periphery) is subjected to flickering, an illusory rotating funnel pattern is perceived in the periphery (or fovea).

In both cases, the illusory contours in the afterimage appear within the nonflickering region, depending on whether the flicker does not extend through the physical stimulus or if the empty region is flickered out of phase. Please refer to Figure 3.2 for a visual illustration. Moreover, we will refer to the experiments conducted by Billock and Tsou as "strong" (respectively "weak") when the illusory contours in the afterimage does not extend (respectively extend) through the physical stimulus.

3.1.3 . Preliminary work and comments

Up to our knowledge, the only attempt to theoretically replicate the MacKay-like phenomenon using neuronal fields equations has been undertaken by Nicks *et al.* [Nic+21]. They employed a model of cortical activity in V1, which included spike-frequency adaptation (SFA) of excitatory neurons, and utilized bifurcation and multi-scale analysis near a Turing-like instability to describe the MacKay-type effect associated with a fully distributed state-dependent external input representing cortical representations of funnel and tunnel patterns. By assuming a balanced condition[1] on the interaction kernel, they derived a dynamical equation for the amplitude of the stationary solution near the critical value of the parameter μ where spontaneous cortical patterns emerge in V1. Their theoretical results do not apply to localized inputs, such as those employed by MacKay and Billock and Tsou, although they provided numerical results demonstrating the capability of their model to replicate Billock and Tsou's experiments.

In the present study, to address the specificity of the external inputs utilized in these two psychophysical experiments (i.e., the redundant information in MacKay's stimuli and the localization of funnel and tunnel patterns used by Billock and Tsou within the visual field), we rely on a central assumption regarding the range of parameter μ. We assume that μ is smaller than the threshold μ_c, where cortical patterns spontaneously emerge in V1. From a neurophysiological standpoint, the corresponding stationary output of Equation (NF) remains unaltered in the presence of external input, and no spontaneous geometric hallucination occurs. Consequently, we cannot employ bifurcation techniques, perturbation theory, and multi-scale analysis. Nevertheless, we introduce a controllability approach that enables us to describe these phenomena in V1 and, therefore, in the retina due to the retino-cortical map.

We emphasize that under this assumption, we demonstrate that the resulting symmetry of the system (stemming from the Euclidean symmetry of the interaction kernel) restricts the geometric shape of visual stimuli capable of inducing illusory perceptions in the afterimage. By breaking the Euclidean symmetry of funnel and tunnel patterns using localized control functions, we provide both theoretical and numerical results showcasing the ability of Equation (NF) to replicate the illusory perceptions reported by MacKay. Similarly, we present numerical results indicating that Equation (NF) reproduces Billock and Tsou's experiments.

It should be noted that in the case of the MacKay effect, the localized control function models the redundant information present in the funnel and tunnel patterns. In contrast, the localized control function in Billock and Tsou's experiments models the localization of funnel and tunnel patterns either on the fovea or in the periphery of the visual field.

The main finding of this study demonstrates that the MacKay effect is essentially a linear phenomenon, where the nonlinear nature of the response function does not play a role in its replication. In contrast, Billock and Tsou's phenomena are entirely nonlinear and strongly dependent on the shape of the nonlinear function employed to model the neuronal response following activation. A "strong nonlinearity" replicates the "strong" Billock and Tsou's experiments, while a "weak nonlinearity" replicates the "weak" Billock and Tsou's experiments. We

[1] A kernel ω of "Mexican-hat" type distribution satisfies the balanced condition (between excitatory and inhibitory neurons) if its Fourier transform at zero equals 0.

achieve this through an asymptotic study of the map associating a sensory input with the corresponding stationary output.

Furthermore, the results presented herein imply that if apparent motion exists in the after-image reported by MacKay, it moves at a right angle to the stimulus pattern. This observation arises from the superimposition of static physical stimulus and afterimage in V1, which consist of horizontal and vertical stripes, combined with the fact that the inverse retino-cortical map preserves this opponency in the retina.

3.2 . Model and assumptions on parameters

3.2.1 . Neural fields model

In [Gie12], it was demonstrated that a variant of the Amari-type equation for neuronal activity in the retina could effectively describe the perceptual organization of the motion quartet, which is a stimulus consisting of two pairs of black and white dots flashing in an alternating sequence. The model proposed in the study employed a four-dimensional space variable, parameterized by the position of local motion in Cartesian coordinates (x_1, x_2) and the perceived motion vector (ρ, ϕ) in polar coordinates. By utilizing psychophysical data, the author identified the necessary parameters of the model to accurately capture the dynamic phenomena associated with the distributed representation of local motion information. Specifically, the model aimed to reproduce both the perceptual organization and the dynamic properties of the percept.

Moreover, it is well-established (see, for instance, [CE04; LSA11] and references therein) that neuronal field equations describing travelling waves and motion effects in the sensory cortex should incorporate the spike-frequency adaptation (SFA) of excitatory neurons to achieve greater biological realism.

However, this chapter focuses on providing a comprehensive mathematical description of *static* psychophysical phenomena related to irregular funnel and tunnel patterns such as the "MacKay rays" and "MacKay target" or regular funnel and tunnel patterns that do not fill all the visual field. Here, "static" refers to a physical visual stimulus that induces an afterimage on the retina, resulting in illusory contours that do not exhibit apparent motion. Considering the success of Ermentrout and Cowan's work [EC79a] in utilizing the original Wilson-Cowan model [WC73] to describe simple patterns such as funnel and tunnel patterns, we anticipate that a similar model (without incorporation of orientation label that models orientation preference of "simple cells" in V1 and without incorporating spike-frequency adaptation of excitatory neurons) will suffice to describe the visual illusions induced by these patterns. Consequently, we adopt the view that the neural activity in V1 evolves according to the Amari-type Equation (NF).

3.2.2 . Assumption on parameters

We make the following assumption on parameters involved in Equation (NF). The response function f belongs to the class $C^2(\mathbb{R})$, is non-decreasing , satisfying $f(0) = 0$ and $f'(0) = \max_{s\in\mathbb{R}} f'(s)$, please refer to Figure 3.3 (image on the left) for an example of response function. Unless otherwise stated, we consider f to be a nonlinear and sigmoid function, such that

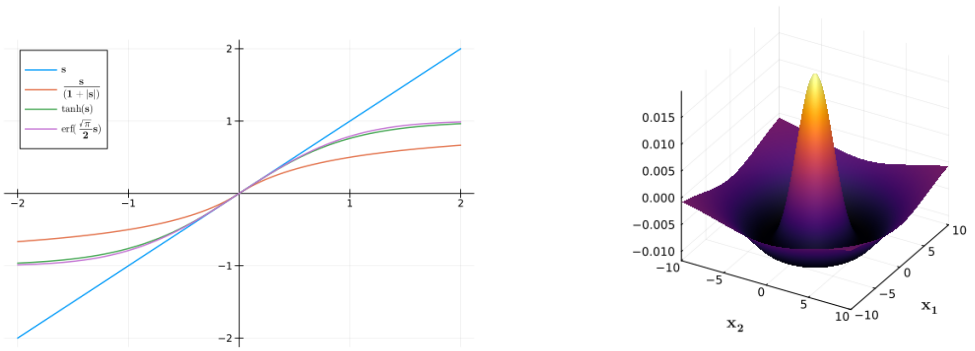

Figure 3.3: Possible response functions on the *left* where erf is the Gauss error function, and on the *right* a 2D DoG kernel ω. Here, $\kappa = 2$, $\sigma_1 = 2$, and $\sigma_2 = 4$.

$f'(0) = 1$ and $\|f\|_\infty = 1$. This assumption is permissible since, as long as $f'(0) \neq 0$, we can always define a sigmoid function $\widetilde{f}(s) = f(\lambda s)/\|f\|_\infty$ with $\lambda = \|f\|_\infty / f'(0)$ and $s \in \mathbb{R}$.

The interaction kernel ω used in this study is homogeneous and isotropic with respect to the spatial coordinates (x_1, x_2). It solely depends on the Euclidean distance between neurons and exhibits rotational symmetry. We adopt the well-known "Mexican-hat" distribution, which is a difference of Gaussians (DoG) characterized by two components. The first Gaussian describes short-range excitation interactions, while the second Gaussian represents long-range inhibition interactions between neurons in V1.

It is worth noting that these physiological considerations regarding the kernel ω align with the framework employing Equation (NF) to generate spontaneous cortical patterns in V1. To generate such patterns using a one-layer neural field Equation (NF), it follows from [EC80, Section 3] that the Fourier transform $\widehat{\omega}$ must reach its maximum at a non-zero wavenumber $q_c > 0$, known as the critical wavevector magnitude. As a critical wavevector, we refer to any vector $\xi_c \in \mathbb{R}^2$ satisfying $|\xi_c| = q_c$. Consequently, we define the connectivity function as

$$\omega(x) = [2\pi\sigma_1^2]^{-1} e^{-\frac{|x|^2}{2\sigma_1^2}} - \kappa[2\pi\sigma_2^2]^{-1} e^{-\frac{|x|^2}{2\sigma_2^2}}, \qquad x \in \mathbb{R}^2, \tag{3.1}$$

where $\kappa \geq 1$, $0 < \sigma_1 < \sigma_2$, and $\sigma_1\sqrt{\kappa} < \sigma_2$. The latter condition ensures the computation of the explicit value of the L^1-norm of ω; refer to Equation (3.4) below.

Remark 3.2.1 *The choice of centering ω at 0 is a matter of mathematical convenience. It is used to express the idea that the strength of interactions is maximized when the distance between interacting points is minimized. In mathematical terms, the point 0 in this context is just a notational convenience, representing the minimal distance between two interacting points in the field. When we say ω is "centered at 0", we mean that interactions are strongest between points that are closest together, and the strength diminishes as the distance between them increases. The "centre" could be translated to any other point in the neural field without changing the overall behaviour of the model, as the essential feature is the relative distance between interacting points.*

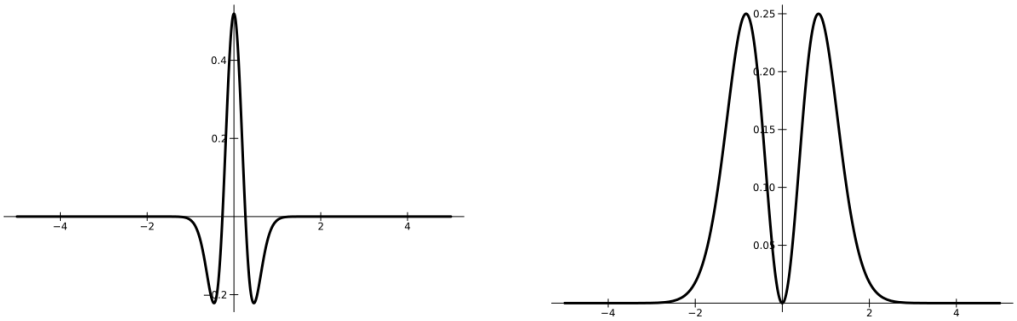

Figure 3.4: A kernel ω on the *left* and its Fourier transform $\widehat{\omega}$ on the *right* in one space dimension. Here, $\kappa = 1$, $2\pi^2\sigma_1^2 = 1$, and $2\pi^2\sigma_2^2 = 2$.

It is important to observe that $\omega(x) = \omega(|x|)$ and that ω belongs to the Schwartz space $\mathcal{S}(\mathbb{R}^2)$, implying that $\omega \in L^p(\mathbb{R}^2)$ for all real numbers $1 \leq p \leq \infty$. The Fourier transform of ω can be explicitly expressed as

$$\widehat{\omega}(\xi) = e^{-2\pi^2\sigma_1^2|\xi|^2} - \kappa e^{-2\pi^2\sigma_2^2|\xi|^2}, \qquad \forall \xi \in \mathbb{R}^2, \tag{3.2}$$

and $\widehat{\omega}$ reaches its maximum at every vector $\xi_c \in \mathbb{R}^2$ such that $|\xi_c| = q_c$. In other words, we have

$$q_c := \sqrt{\frac{\log\left(\frac{\kappa\sigma_2^2}{\sigma_1^2}\right)}{2\pi^2(\sigma_2^2 - \sigma_1^2)}} \qquad \text{and} \qquad \max_{r\geq 0}\widehat{\omega}(r) = \widehat{\omega}(q_c). \tag{3.3}$$

Additionally, the explicit expression for the L^1-norm of ω is given by

$$\|\omega\|_1 = (1-\kappa) + 2\left(\kappa e^{-\frac{\Theta^2}{2\sigma_2^2}} - e^{-\frac{\Theta^2}{2\sigma_1^2}}\right) \qquad \text{with} \qquad \Theta := \sigma_1\sigma_2\sqrt{\frac{2\log\left(\frac{\sigma_2^2}{\kappa\sigma_1^2}\right)}{\sigma_2^2 - \sigma_1^2}}. \tag{3.4}$$

It is important to emphasize that the kernel ω does not necessarily satisfy the *balanced*[2] condition $\widehat{\omega}(0) = 0$ between excitation and inhibition. However, this condition is met when $\kappa = 1$.

Please refer to Figure 3.3 (image on the right) for visual illustration of the kernel ω in 2D, and Figure 3.4 for a visual representation of the kernel ω (left) and its Fourier transform $\widehat{\omega}$ (right) in one space dimension. In this particular illustration, we have $\kappa = 1$, $2\pi^2\sigma_1^2 = 1$, and $2\pi^2\sigma_2^2 = 2$.

3.2.3 . Binary representation of patterns

Due to the retino-cortical map, funnel, and tunnel patterns are respectively given in Cartesian coordinates $x := (x_1, x_2) \in \mathbb{R}^2$ of V1 by

$$P_F(x) = \cos(2\pi\lambda x_2), \qquad P_T(x) = \cos(2\pi\lambda x_1), \quad \lambda > 0. \tag{3.5}$$

[2]For a homogeneous NF equation (i.e., when $I = 0$), this condition ensures the existence of a unique stationary state $a_0 = 0$ even if $f(0) \neq 0$. It was assumed, for instance, in [Nic+21] for deriving the amplitude equation of the stationary state near the bifurcation point μ_c.

This choice is motivated by analogy with the (spontaneous) geometric hallucinatory patterns described in [EC79a] and [Bre+01].

Given the above representation of funnel and tunnel patterns in cortical coordinates, to see how they look in terms of images, we represent them as contrasting white and black regions, see Figures 1.1 and 1.2. More precisely, define the binary pattern B_h of a function $h : \mathbb{R}^2 \to \mathbb{R}$ by

$$B_h(x) = \begin{cases} 0, & \text{if } h(x) > 0 \quad \text{(black)} \\ 1, & \text{if } h(x) \leq 0 \quad \text{(white)}. \end{cases} \tag{3.6}$$

It follows that B_h is essentially determined by the zero level-set of h. Since stimuli involved in the MacKay effect and Billock and Tsou experiments are binary patterns, our strategy in describing these phenomena consists in characterising the zero level-set of output patterns. That is, we are mainly devoted to studying the qualitative properties of patterns by viewing them as binary patterns.

3.3 . Preliminaries results on Amari-type equation

3.3.1 . Well-posedness of the Cauchy problem

We start this section by introducing the definition of stationary state to Equation (NF).

Definition 3.3.1 (Stationary state) *Let $a_0 \in L^p(\mathbb{R}^2)$. For every $I \in L^p(\mathbb{R}^2)$, a stationary state $a_I \in L^p(\mathbb{R}^2)$ to Equation (NF) is a time-invariant solution, viz.*

$$a_I = \mu\omega * f(a_I) + I. \tag{SS}$$

Many papers investigating biological phenomena using Amari-type equation usually deal with the homogeneous equation or posed on a bounded domain. In these cases, by standard assumptions on the kernel ω or on the response function f, it is straightforward to obtain the existence of at least one (even non-constant) stationary state to such equations, see for instance [Bre+01; EC79a; Nic+21; CE04]. In the case of an inhomogeneous equation posed on an unbounded domain as the case at hand, it can become a little bit more subtle to provide the existence of (non-constant) stationary state only with assumptions on ω and f. Nevertheless, in the case of an inhomogeneous equation posed on a bounded domain with a state-dependent external input, in [Bri+23], under a mild condition on the boundness of the response function, the existence of at least one stationary state is proved using Schaefer's fixed point Theorem.

In order to obtain a unique non-constant stationary state to the inhomogeneous Equation (NF), we will make a reasonable assumption on the parameter μ. As mentioned in the introduction, consistent with the phenomena that we aim to describe and the strategy used for that, we introduce the parameter[3]

$$\mu_0 := \|\omega\|_1^{-1} \leq \mu_c. \tag{3.7}$$

[3]More precisely, $\mu_0 := \alpha L_f^{-1} \|\omega\|_1^{-1}$, where $\alpha > 0$ and $L_f > 0$ are defined as in 2.

Here μ_c is the bifurcation point defined in (2.23), and $\|\omega\|_1$ is explicitly defined in (3.4). As we shall see below, given $I \in L^p(\mathbb{R}^2)$, μ_0 is the (natural) largest value of μ up to which we can provide a unique stationary state to Equation (NF) in the space $L^p(\mathbb{R}^2)$, that is, we will let $\mu < \mu_0$. In particular, when $p = 2$, and under the hypothesis that the kernel ω satisfies the balanced condition $\widehat{\omega}(0) = 0$, we can refine this hypothesis by assuming $\mu < \mu_c$.

The assumption $\mu < \mu_0$ implies that in the case $p = \infty$, if the external input $I \in L^\infty(\mathbb{R}^2)$ is strong compared with mutual excitation and inhibition, it will dominate the solutions (transient and stationary). It means that the contribution of the coupling term $\mu\omega * f(a)$ will not be quantitatively significant in the computation of the transient and stationary solutions as soon as $\|I\|_\infty \gg 1$ and for arbitrary $a_0 \in L^\infty(\mathbb{R}^2)$.

We collect in the following lemma some useful estimates that are immediate consequences of generalised Young-convolution inequality. We provide the proof for sake completeness.

Lemma 3.3.1 *Let $1 \leq p \leq \infty$. The nonlinear operator $\omega * f(\cdot)$ is well-defined and Lipschitz continuous from $\mathscr{X}_p$ into itself,*

$$\|\omega * f(a) - \omega * f(b)\|_{L^p_x L^\infty_t} \leq \|\omega\|_1 \|a - b\|_{L^p_x L^\infty_t}, \qquad \forall a, b \in \mathscr{X}_p. \tag{3.8}$$

Moreover,

1. *If $a \in \mathscr{X}_p$, then $\omega * f(a) \in \mathscr{X}_\infty$,*

$$\|\omega * f(a)\|_{L^\infty_x L^\infty_t} \leq \|\omega\|_q \|a\|_{L^p_x L^\infty_t}, \tag{3.9}$$

and

$$\|\omega * f(a)\|_{L^\infty_x L^\infty_t} \leq \|\omega\|_1; \tag{3.10}$$

2. *If $a \in \mathscr{X}_1$, then $\omega * f(a) \in \mathscr{X}_p$,*

$$\|\omega * f(a)\|_{L^p_x L^\infty_t} \leq \|\omega\|_p \|a\|_{L^1_x L^\infty_t}. \tag{3.11}$$

Proof. Let $1 \leq p \leq \infty$ and $a \in \mathscr{X}_p$. First, of all, by Lebesgue's Theorem of continuity under the integral sign, we have that $\omega * f(a)(\cdot, t)$ is measurable for any $t \in [0, \infty)$ and that $\omega * f(a)(x, \cdot)$ is continuous on $[0, \infty)$ for $\mathrm{a.e.}$, $x \in \mathbb{R}^2$. We then obtain by using Hölder inequality and the 1-Lipschitz continuity of f that

$$\begin{aligned} |\omega * f(a)(x,t)| &\leq \left\{\int_\Omega |\omega(x-y)|dy\right\}^{\frac{1}{q}} \left\{\int_\Omega |\omega(x-y)||a(y,t)|^p dy\right\}^{\frac{1}{p}} \\ &\leq \|\omega\|_1^{\frac{1}{q}} \left\{\int_{\mathbb{R}^2} |\omega(x-y)||a(y,t)|^p dy\right\}^{\frac{1}{p}}. \end{aligned}$$

Taking the $p-$th power on both sides of the above inequality and integrating it with variable x over $\mathbb{R}^2$, we find

$$\begin{aligned} \int_{\mathbb{R}^2} |\omega * f(a)(x,t)|^p dx &\leq \|\omega\|_1^{\frac{p}{q}} \int_{\mathbb{R}^2}\int_{\mathbb{R}^2} |\omega(x-y)||a(y,t)|^p dy dx \\ &\leq \|\omega\|_1^{\frac{p}{q}} \|\omega\|_1 \int_{\mathbb{R}^2} |a(y,t)|^p dy = \|\omega\|_1^p \int_{\mathbb{R}^2} |a(y,t)|^p dy. \end{aligned}$$

It follows that the operator $a \mapsto \omega * f(a)$ is well-defined from $\mathscr{X}_p$ to itself. So, the proof of (3.8) immediately follows by arguing as above. If $a \in \mathscr{X}_p$, then for a.e. $x \in \mathbb{R}^2$ and every $t \geq 0$, one obtains on the one hand

$$\begin{aligned} |\omega * f(a)(x,t)| &\leq \left\{ \int_{\mathbb{R}^2} |\omega(x-y)|^q dy \right\}^{\frac{1}{q}} \left\{ \int_{\mathbb{R}^2} |a(y,t)|^p dy \right\}^{\frac{1}{p}} \\ &\leq \|\omega\|_q \|a(\cdot,t)\|_p, \end{aligned}$$

which leads to the inequality (3.9). On the other hand, one has

$$|\omega * f(a)(x,t)| \leq \int_{\mathbb{R}^2} |\omega(x-y)||f(a(y,t))|dy \leq \|\omega\|_1,$$

leading to the inequality (3.10). Finally, if $a \in \mathscr{X}_1$ then one obtains

$$|\omega * f(a)(x,t)| \leq \left\{ \int_{\mathbb{R}^2} |\omega(x-y)|^p |a(y,t)|dy \right\}^{\frac{1}{p}} \left\{ \int_{\mathbb{R}^2} |a(y,t)|^q dy \right\}^{\frac{1}{q}}.$$

Taking the $p-$th power on both sides of the above inequality and integrating it with variable x over $\mathbb{R}^2$, we find

$$\begin{aligned} \int_{\mathbb{R}^2} |\omega * f(a)(x,t)|^p dx &\leq \|a(\cdot,t)\|_1^{\frac{p}{q}} \int_{\mathbb{R}^2} |\omega(x-y)|^p |a(y,t)| dy dx \\ &\leq \|\omega\|_p^p \|a(\cdot,t)\|_1^{\frac{p}{q}} \|a(\cdot,t)\|_1 = \|\omega\|_p^p \|a(\cdot,t)\|_1^p, \end{aligned}$$

so that (3.11) immediately follows and completes the proof of the lemma. □

In the following theorem, we prove the existence of a unique solution and a unique stationary state of the Cauchy problem associated with Equation (NF).

Theorem 3.3.1 *Let $1 \leq p \leq \infty$ and $I \in L^p(\mathbb{R}^2)$. For any initial datum $a_0 \in L^p(\mathbb{R}^2)$, there exists a unique $a \in \mathscr{X}_p$, solution of Equation (NF). Moreover, if $\mu < \mu_0$, there exists a unique stationary state $a_I \in L^p(\mathbb{R}^2)$ to (NF) satisfying (SS), and it holds*

$$\|a(\cdot,t) - a_I(\cdot)\|_p \leq e^{-(1-\mu\|\omega\|_1)t} \|a_0(\cdot) - a_I(\cdot)\|_p, \tag{3.12}$$

for every $t \geq 0$.

Proof. Let $1 \leq p \leq \infty$ and $I \in L^p(\mathbb{R}^2)$. The r.h.s. of Equation (NF) is a Lipschitz continuous map from $\mathscr{X}_p$ to itself by Lemma 3.3.1. It is then standard to obtain that for any initial datum $a_0 \in L^p(\mathbb{R}^2)$, Equation (NF) has a unique solution $a \in \mathscr{X}_p$ (see, for instance, [VF10]). Moreover, the map $\Phi_I : L^p(\mathbb{R}^2) \to L^p(\mathbb{R}^2)$ defined for all $u \in L^p(\mathbb{R}^2)$ by $\Phi_I(u) = I + \mu\omega * f(u)$ satisfies

$$\|\Phi_I(v) - \Phi_I(u)\|_p \leq \frac{\mu}{\mu_0} \|v - u\|_p, \qquad \forall u, v \in L^p(\mathbb{R}^2),$$

due to inequality (3.8). Since $\mu < \mu_0$, the existence of a unique stationary state $a_I \in L^p(\mathbb{R}^2)$ is obtained by invoking the contraction mapping principle.

We now set

$$b(x,t) = a(x,t) - a_I(x), \qquad (x,t) \in \mathbb{R}^2 \times [0,\infty), \tag{3.13}$$

where $a \in \mathscr{X}_p$ (resp. $a_I \in L^p(\mathbb{R}^2)$) is the unique solution (resp. the unique stationary state) of (NF). It follows that b is the solution of the following initial value Cauchy problem

$$\begin{cases} \partial_t b(x,t) = -b(x,t) + \mu \displaystyle\int_{\mathbb{R}^2} \omega(x-y)[f(b(y,t)+a_I(y)) - f(a_I(y))]dy, & (x,t) \in \mathbb{R}^2 \times [0,\infty), \\ b(x,0) = a_0(x) - a_I(x), & x \in \mathbb{R}^2, \end{cases} \tag{3.14}$$

which belongs to $b \in C([0,\infty); L^p(\mathbb{R}^2)) \cap C^1((0,\infty); L^p(\mathbb{R}^2))$. Moreover, b satisfies the following variations of the constants formula

$$b(x,t) = e^{-t}b(x,0) + \mu \int_0^t e^{-(t-s)} \int_{\mathbb{R}^2} \omega(x-y)[f(b(y,t)+a_I(y)) - f(a_I(y))]dy, \tag{3.15}$$

for all $(x,t) \in \mathbb{R}^2 \times [0,\infty)$.

Taking the $L^p(\mathbb{R}^2)$-norm of the above identity, we find for every $t \geq 0$,

$$\|b(\cdot,t)\|_p \leq e^{-t}\|b(\cdot,0)\|_p + \mu\|\omega\|_1 \int_0^t e^{-(t-s)}\|b(\cdot,s)\|_p ds. \tag{3.16}$$

Applying Gronwall's Lemma to inequality (3.16) one deduces for every $t \geq 0$,

$$\|b(\cdot,t)\|_p \leq e^{-(1-\mu\|\omega\|_1)t}\|b(\cdot,0)\|_p.$$

This proves the inequality (3.12) and completes the proof of the theorem. □

Remark 3.3.1 *Note that when $p = 2$ and the kernel ω satisfies the balanced condition $\widehat{\omega}(0) = 0$, Theorem 3.3.1 remains valid under the relaxed assumption $\mu < \mu_c$ applying Fourier transform and Plancherel formula.*

Proposition 3.3.1 *Let $I \in L^2(\mathbb{R}^2)$ and μ_c be defined in (2.23). For any initial datum $a_0 \in L^2(\mathbb{R}^2)$, there exists a unique $a \in \mathscr{X}_2$, solution of Equation (NF). Moreover, if $\mu < \mu_c$, and $\widehat{\omega}(0) = 0$, there exists a unique stationary state $a_I \in L^2(\mathbb{R}^2)$ to (NF) satisfying (SS), and*

$$\|a(\cdot,t) - a_I(\cdot)\|_2 \leq e^{-(1-\mu\widehat{\omega}(q_c))t}\|a_0(\cdot) - a_I(\cdot)\|_2, \tag{3.17}$$

for every $t \geq 0$.

Proof . Let $I \in L^2(\mathbb{R}^2)$ and $a_0 \in L^2(\mathbb{R}^2)$. The same argument as that in the proof of Theorem 3.3.1 ensures the existence an unicity of $a \in \mathscr{X}_2$, solution of Equation (NF). Recall that $\mu_c := \widehat{\omega}(q_c)^{-1}$, where $\widehat{\omega}(q_c) = \max_{r\geq 0}\widehat{\omega}(r)$. If $\widehat{\omega}(0) = 0$, then the kernel ω as defined in (3.1) satisfies $\widehat{\omega}(|\xi|) \geq 0$ for all $\xi \in \mathbb{R}^2$. In particular, $\widehat{\omega}(q_c) = \max_{r\geq 0}\widehat{\omega}(r) = \|\widehat{\omega}\|_\infty$. Define for

all $u \in L^2(\mathbb{R}^2)$ the map $\Phi_I : L^2(\mathbb{R}^2) \to L^2(\mathbb{R}^2)$ by $\Phi_I(u) = I + \mu\omega * f(u)$. Then for all $v \in L^2(\mathbb{R}^2)$, one gets by Plancherel identity the following,

$$\begin{aligned} \|\Phi_I(v) - \Phi_I(u)\|_2 = \|\widehat{\Phi_I(v)} - \widehat{\Phi_I(u)}\|_2 &= \mu\|\widehat{\omega}(\widehat{f(u)} - \widehat{f(v)})\|_2 \\ &\leq \mu\|\widehat{\omega}\|_\infty\|\widehat{f(u)} - \widehat{f(v)}\|_2 \\ &= \mu\widehat{\omega}(q_c)\|f(u) - f(v)\|_2 \\ &\leq \frac{\mu}{\mu_c}\|u - v\|_2, \end{aligned} \tag{3.18}$$

due to assumption that f is 1-Lipschitz continuous. Since $\mu < \mu_c$, the existence of a unique stationary state $a_I \in L^2(\mathbb{R}^2)$ is obtained by invoking the contraction mapping principle. We complete the proof by arguing as in that of Theorem 3.3.1 and using the trick to prove Inequality (3.18). □

Due to Theorem 3.3.1, we can introduce the following.

Definition 3.3.2 *Let $1 \leq p \leq \infty$, the nonlinear input-output map $\Psi : L^p(\mathbb{R}^2) \to L^p(\mathbb{R}^2)$ is defined by*

$$\Psi(I) = I + \mu\omega * f(\Psi(I)), \tag{3.19}$$

for all $I \in L^p(\mathbb{R}^2)$.

The proof of Part 2. of the following proposition is presented in Theorem A.1.3 in Appendix A.

Proposition 3.3.2 *Let $1 \leq p \leq \infty$, and μ_0 be defined by (3.7). If $\mu < \mu_0$, then,*

1. *The map Ψ is well-defined, bi-Lipschitz continuous, and it holds*

$$\|\Psi(I)\|_p \leq \frac{\mu_0}{\mu_0 - \mu}\|I\|_p, \qquad \text{for all} \qquad I \in L^p(\mathbb{R}^2); \tag{3.20}$$

2. *If $2 \leq p \leq \infty$, then Ψ and Ψ^{-1} belong to $C^1(L^p(\mathbb{R}^2); L^p(\mathbb{R}^2)$.*

Proof. We only provide the proof of Part 1. Let $I_1, I_2 \in L^p(\mathbb{R}^2)$. Then using inequality (3.8), we obtain

$$\|\Psi(I_1) - \Psi(I_2)\|_p \leq \frac{\mu}{\mu_0}\|\Psi(I_1) - \Psi(I_2)\|_p + \|I_1 - I_2\|_p.$$

It follows that

$$\|\Psi(I_1) - \Psi(I_2)\|_p \leq \frac{\mu_0}{\mu_0 - \mu}\|I_1 - I_2\|_p,$$

provided $\mu < \mu_0$. This implies that Ψ is Lipschitz continuous from $L^p(\mathbb{R}^2)$ to itself. On the other hand,

$$\Psi(I) = I + \mu\mathcal{Q}(\Psi(I)), \qquad \forall I \in L^p(\mathbb{R}^2),$$

where $\mathcal{Q} : L^p(\mathbb{R}^2) \to L^p(\mathbb{R}^2)$, $v \mapsto \mathcal{Q}(v) = \omega * f(v)$. One deduces from inequality (3.8),

$$\|\Psi(I_1) - \Psi(I_2)\|_p \geq |\|I_1 - I_2\|_p - \mu\|\mathcal{Q}(\Psi(I_1)) - \mathcal{Q}(\Psi(I_2))\|_p| \geq \|I_1 - I_2\|_p - \frac{\mu}{\mu_0}\|\Psi(I_1) - \Psi(I_2)\|_p.$$

It follows that

$$\|I_1 - I_2\|_p \leq \left(1 + \frac{\mu}{\mu_0}\right)\|\Psi(I_1) - \Psi(I_2)\|_p.$$

This shows that Ψ is bijective and Ψ^{-1} is Lipschitz continuous from $L^p(\mathbb{R}^2)$ to itself. □

3.3.2 . Equivariance of the input to stationary output map with respect to the plane Euclidean group

Let $\mathbf{E}(2)$ denote the Euclidean group, which is the symmetry group of $\mathbb{R}^2$. It is well known that (see, [Vil68, Chapter IV] for instance) $\mathbf{E}(2)$ is the cross product of two-dimensional real line space $\mathbb{R}^2$ and $\mathcal{O}(2)$ the group of Euclidean rotations and reflections of this space, the so-called orthogonal group :

$$\mathbf{E}(2) = \mathbb{R}^2 \rtimes \mathcal{O}(2).$$

For $g = (a, r) \in \mathbf{E}(2)$, one has $(a, r) \in \mathbb{R}^2 \times \mathcal{O}(2)$ and the group property is the following

$$\begin{cases} g_1 \cdot g_2 = (a_1, r_1) \cdot (a_2, r_2) = (r_1 a_2 + a_1, r_1 r_2), \\ g^{-1} = (-r^{-1}a, r^{-1}), \\ e = (0, \mathrm{Id}). \end{cases}$$

Here, g^{-1} is the inverse of $g = (a, r) \in \mathbf{E}(2)$, e is the identity in $\mathbf{E}(2)$ and Id is the identity in $\mathcal{O}(2)$.

Definition 3.3.3 (Action of $\mathbf{E}(2)$ on $\mathbb{R}^2$) *For $x \in \mathbb{R}^2$, the action of $g = (a, r) \in \mathbf{E}(2)$ on $\mathbb{R}^2$ is defined by*

$$gx = rx + a.$$

Definition 3.3.4 (Action of $\mathbf{E}(2)$ on $L^p(\mathbb{R}^2)$) *We define the action of $\mathbf{E}(2)$ on $L^p(\mathbb{R}^2)$ by the representation*

$$\begin{aligned} T : \quad \mathbf{E}(2) &\longrightarrow GL(L^p(\mathbb{R}^2)) \\ g &\longmapsto T_g, \end{aligned} \tag{3.21}$$

such that, for all $v \in L^p(\mathbb{R}^2)$ and for all $x \in \mathbb{R}^2$, it holds

$$(T_g v)(x) = v(g^{-1}x).$$

Here $GL(L^p(\mathbb{R}^2))$ is the group of automorphism from $L^p(\mathbb{R}^2)$ to itself.

We emphasise that the validity of the following proposition depends solely on the symmetry properties satisfied by the kernel ω rather than the nonlinear function f. It remains valid whatever the shape (even linear, etc.) of the response function f.

Proposition 3.3.3 *Let μ_0 be defined by (3.7). If $\mu < \mu_0$, then, the map Ψ defined in (3.19) and its inverse Ψ^{-1} are $\mathbf{E}(2)$-equivariant, that is Ψ and Ψ^{-1} commute with $\mathbf{E}(2)$.*

Remark 3.3.2 *As a consequence of Proposition 3.3.3 we have that a subgroup $\Gamma \subset \mathbf{E}(2)$ is a symmetry group of the sensory input $I \in L^p(\mathbb{R}^2)$ if and only if it is a symmetry group of the stationary output $\Psi(I)$. For example, if an external input depends solely on the x_1 variable, then the associated stationary state will also depend solely on the x_1 variable.*

Before starting the proof of Proposition 3.3.3, we need the following lemma.

Lemma 3.3.2 *Let $1 \leq p \leq \infty$. Then the operator $\mathcal{Q} : L^p(\mathbb{R}^2) \to L^p(\mathbb{R}^2)$, $v \mapsto \mathcal{Q}(v) = \omega * f(v)$ commutes with $\mathbf{E}(2)$.*

Proof. The fact that $\mathcal{Q}$ is well-defined is a consequence of Lemma 3.3.1. Let $g = (a, r) \in \mathbf{E}(2)$, we want to show that $T_g\mathcal{Q} = \mathcal{Q}T_g$, that is

$$(T_g(\mathcal{Q}(v)))(x) = (\mathcal{Q}(T_g v))(x), \qquad \forall v \in L^p(\mathbb{R}^2), \ \ \forall x \in \mathbb{R}^2.$$

On the one hand, one has

$$(T_g(\mathcal{Q}(v)))(x) = \mathcal{Q}(v)(g^{-1}x) = \int_{\mathbb{R}^2} \omega(|g^{-1}x - y|) f(v(y)) dy. \tag{3.22}$$

On the other hand, one has

$$(\mathcal{Q}(T_g v))(x) = \int_{\mathbb{R}^2} \omega(|x - y|)(f(T_g v))(y) dy = \int_{\mathbb{R}^2} \omega(|x - y|) f(v(r^{-1}(y - a))) dy.$$

Setting $z = r^{-1}(y - a)$, then $dy = |\det r| dz = dz$, since $r \in \mathcal{O}(2)$ and

$$|x - rz - a| = |r(r^{-1}(x - a) - z)| = |g^{-1}x - z|.$$

It follows that

$$(\mathcal{Q}(T_g v))(x) = \int_{\mathbb{R}^2} \omega(|g^{-1}x - z|) f(v(z)) dz, \tag{3.23}$$

which completes the proof by identifying (3.22) and (3.23). □

Proof. (of Proposition 3.3.3) We want to prove that $T_g\Psi = \Psi T_g$ and $T_g\Psi^{-1} = \Psi^{-1}T_g$ for all $g \in \mathbf{E}(2)$. This is equivalent to prove that for all $I \in L^p(\mathbb{R}^2)$, $T_g\Psi(I) = \Psi(T_g I)$ and $T_g\Psi^{-1}(I) = \Psi^{-1}(T_g I)$. It follows from Lemma 3.3.2 that

$$T_g\Psi(I) = T_g I + \mu T_g \mathcal{Q}(\Psi(I)) = T_g I + \mu \mathcal{Q}(T_g\Psi(I)).$$

On the other hand, one has

$$\Psi(T_g I) = T_g I + \mu \mathcal{Q}(\Psi(T_g I)).$$

So, by unicity of stationary state provided by Theorem 3.3.1, we obtain $T_g\Psi(I) = \Psi(T_g I)$. Arguing similarly, we prove that Ψ^{-1} is also $\mathbf{E}(2)$-equivariant. □

3.4 . On the MacKay effect

As mentioned in the introduction, we reiterate that the physical visual stimuli employed in MacKay's experiments consist of funnel and tunnel patterns with highly localized redundant information. Taking into account Equation (3.5) and the retino-cortical map, we incorporate these patterns as external inputs in Equation (NF), such that $I \in \{P_F, P_T\} + \varepsilon v$, where $\varepsilon > 0$ and v represents a localized function in the cortical domain intended to model the redundant

information present in the funnel and tunnel patterns. In this context, the function v can also be regarded as a localized distributed control, aiming to disrupt the *global* plane Euclidean symmetry of the funnel or tunnel pattern.

In Section 3.4.1, assuming that the response function f is linear, we provide a more general result showing that spontaneous cortical patterns defined in (2.25) cannot induce illusory contours in the output pattern. In particular, we deduce that $I \in \{P_F, P_T\}$ cannot induce the MacKay effect using Equation (NF) . Then using MacKay's stimuli $I \in \{P_F, P_T\} + \varepsilon v$, we prove in Section 3.4.2 that the linearised of (NF) is sufficient to theoretically describes the MacKay effect. Thus the phenomenon starts in the linear regime, so the effect of saturating f should only dampen out high oscillations occurring in the system. In Section 3.4.3, we provide theoretical proof of all these results when the response function f is a nonlinear sigmoid function satisfying assumptions given in Section 3.2.2.

3.4.1 . A priori analysis

In this section, we prove that it is necessary to break the Euclidean symmetry of funnel and tunnel pattern by localized control function for replicating the MacKay effect with Equation (NF), both with a linear and nonlinear response function.

Our first result is the following.

Theorem 3.4.1 *Let $a_0 \in L^\infty(\mathbb{R}^2)$ and $I \in L^\infty(\mathbb{R}^2)$ given by $I(\cdot) = \cos(2\pi\langle\xi_0, \cdot\rangle)$, for some $\xi_0 \in \mathbb{R}^2$. Assume that the response function f is linear. If $\mu < \mu_0$, it holds*

$$a(\cdot, t) \xrightarrow[t\to\infty]{} \frac{I(\cdot)}{1 - \mu\widehat{\omega}(\xi_0)}, \qquad \text{exponentially in} \qquad L^\infty(\mathbb{R}^2), \tag{3.24}$$

where $a \in \mathscr{X}_\infty$ is the solution of (NF) with initial datum a_0.

Proof. The stationary state associated with $I(\cdot) = \cos(2\pi\langle\xi_0, \cdot\rangle)$ is given by $a_I(\cdot) = I(\cdot)/(1 - \mu\widehat{\omega}(\xi_0))$. Indeed, one has for $x \in \mathbb{R}^2$,

$$I(x) + \mu(\omega * a_I)(x) = I(x) + \frac{\mu}{1 - \mu\widehat{\omega}(\xi_0)}(\omega * I)(x) = \frac{I(x)}{1 - \mu\widehat{\omega}(\xi_0)} = a_I(x), \tag{3.25}$$

since $\omega * I = \widehat{\omega}(\xi_0)I$. Therefore, if $\mu < \mu_0$, the result follows by the unicity of stationary state and exponential convergence of a to a_I in the space $L^\infty(\mathbb{R}^2)$ provided by Theorem 3.3.1. □

Corollary 3.4.1 *Assume that the response function f is linear. If $\mu < \mu_0$, then a_F (resp. a_P) is a funnel (resp. tunnel) pattern in shape as P_F (resp. P_T). In particular, Equation (NF) with a linear response function cannot reproduce the MacKay effect starting with an external input equal to P_F or P_T.*

Proof. Due to Theorem 3.4.1, the stationary states associated with P_F and P_T are respectively proportional to P_F and P_T so that they have the same binary pattern respectively (see, Section 3.2.3), and then the same geometrical shape in terms of images. □

The following notation is needed: if F is a real-valued function defined on $\mathbb{R}^2$, we use $F^{-1}(\{0\})$ to denote the zero level-set of F.

We provide a similar result as that of Theorem 3.4.1 with the presence of the nonlinear function f in Equation (SS). This result shows, in particular, that even in the presence of the nonlinearity, Equation (NF) cannot describe the MacKay effect when the external input is chosen equal to P_F or P_T. Since P_F and P_T play symmetry roles, we focus only on P_F. We recall that they are analytically given in Cartesian cortical coordinates in V1 by (3.5).

Theorem 3.4.2 *Assume that the external input in Equation (SS) is given by $I = P_F \in L^\infty(\mathbb{R}^2)$. If $\mu < \mu_0$, then the stationary state $a_F := \Psi(P_F) \in L^\infty(\mathbb{R}^2)$ associated with P_F explicitly depends solely upon x_2. Moreover, one has the following.*

1. *The function a_F is even and $1/\lambda$-periodic with respect to x_2;*
2. *The function a_F is infinitely differentiable, and Lipshitz continuous;*
3. *If in addition $\mu < \mu_0/2$ and the function f is odd, then a_F has a discrete and countable number of zeroes with respect to x_2, identical with that of $x_2 \mapsto \cos(2\pi\lambda x_2)$ on $\mathbb{R}$.*

Remark 3.4.1 *Notice the assumption $\mu < \mu_0/2$ in part 3. of Theorem 3.4.2 instead of $\mu < \mu_0$. We think this is a technical assumption because of the strategy used in our proof since numerical results suggest that part 3. remains valid for all $\mu < \mu_0$. Moreover, the assumption on the parity of f is also technical, and we conjecture that if f is not odd, then a_F will still have a discrete and countable number of zeroes with respect to x_2, such that*

$$a_F^{-1}(\{0\}) = \mathbb{R} \times \left\{ z_k \in \left] \frac{k}{2\lambda}, \frac{k+1}{2\lambda} \right[\mid k \in \mathbb{Z} \right\}, \tag{3.26}$$

and, for all $k \in \mathbb{Z}$,

$$|z_k - \tau_k| \leq \frac{\arcsin(\mu\mu_0^{-1})}{2\pi\lambda}, \qquad \text{where} \qquad \tau_k := \frac{2k+1}{4\lambda}. \tag{3.27}$$

The gap between the zeroes of a_F and those of P_F provided by (3.27) shows that on each interval, z_k and τ_k become arbitrarily closed depending on whether μ is not closed to μ_0. Nevertheless, if λ is taken sufficiently large, z_k and τ_k become arbitrarily close independently of $\mu_0 - \mu$.

Proof. (of Parts 1. and 2. of Theorem 3.4.2) For ease of notation, we assume in the sequel that $\lambda = 1$. We know by Part 3. of Proposition 3.3.3 that if P_F or a_F has a subgroup of $\mathbf{E}(2)$ as a group of symmetry, the other has the same subgroup as a group of symmetry and conversely. Since $P_F(x_1, x_2)$ is independent on x_1, it follows that $a_F(x_1, x_2)$ is also independent on x_1 for all $(x_1, x_2) \in \mathbb{R}^2$. Similarly, since P_F is invariant under the action of the reflection with respect to the straight $x_1 = 0$, that is, $P_F(x_1, -x_2) = P_F(x_1, x_2)$ for all $(x_1, x_2) \in \mathbb{R}^2$, one deduces that $a_F(x_1, -x_2) = a_F(x_1, x_2)$. Thus, a_F is an even function with respect to x_2. Similarly, since P_F is invariant under the translation by vector $(0, -1) \in \mathbb{R}^2$, it follows that a_F is also invariant under this translation so that a_F is 1-periodic with respect to x_2.

The fact that a_F is infinitely differentiable on $\mathbb{R}^2$ follows immediately from that $P_F \in C^\infty(\mathbb{R}^2)$, the kernel $\omega \in \mathcal{S}(\mathbb{R}^2) \subset C^\infty(\mathbb{R}^2) \cap L^1(\mathbb{R}^2)$ and that f is bounded. Writing now $a_F(x_2) := a_F(x_1, x_2)$ for notational ease, we obtain that a_F is also given by

$$a_F(x_2) = \cos(2\pi x_2) + \mu[\omega_1 * f(a_F)](x_2), \qquad x_2 \in \mathbb{R}, \tag{3.28}$$

where ω_1 is a 1D difference of Gaussian kernel . Let $a'_F := \partial_{x_2} a_F$, then due to (3.28), one obtains

$$a'_F(x_2) = -2\pi \sin(2\pi x_2) + \mu[\omega'_1 * f(a_F)](x_2), \qquad x_2 \in \mathbb{R}. \tag{3.29}$$

Since $\|f\|_\infty \leq 1$ by assumption, it follows that $\|a'_F\|_\infty \leq 2\pi + \mu\|\omega'_1\|_1 < \infty$. Therefore a_F is Lipschitz continuous. □

We now present an argument to prove Part 3. of Theorem 3.4.2.

Proof. (of Part 3. of Theorem 3.4.2) Notice that $a_F = \Psi(P_F)$ satisfies

$$a_F = P_F + \mu\omega * f(a_F). \tag{3.30}$$

In particular, thanks to Parts 1., one has $a_F^{-1}(\{0\}) \supset \mathbb{R} \times \{\pm 1/4 + k \mid k \in \mathbb{Z}\}$.

To show the converse inclusion, let $x_* := (x_1^*, x_2^*)$ verifying $a_F(x_*) = 0$. From (3.30), it follows

$$\cos(2\pi x_1^*) = -\mu \int_{\mathbb{R}^2} \omega(y) f(a_F(x_* - y)) dy. \tag{3.31}$$

On the one hand, by exploiting trigonometric formulae for the cosine, one has for $\mathrm{a.\,e.}, y \in \mathbb{R}^2$,

$$a_F(x_* - y) = \sin(2\pi x_1^*)\sin(2\pi y_1) + \mu \int_{\mathbb{R}^2} k(y, z) f(a_F(x_* - z)) dz, \tag{3.32}$$

where $k(x, y) := \omega(x - y) - \cos(2\pi x_1)\omega(y)$, satisfies

$$K := \sup_{x \in \mathbb{R}^2} \int_{\mathbb{R}^2} |k(x, y)| dy = 2\|\omega\|_1. \tag{3.33}$$

Since $\mu < \mu_0/2$, the contracting mapping principle shows that for every $I \in L^\infty(\mathbb{R}^2)$ there exists a unique solution $b \in L^\infty(\mathbb{R}^2)$ to

$$b(x) = I(x) + \mu \int_{\mathbb{R}^2} k(x, y) f(b(y)) dy. \tag{3.34}$$

By (3.32), function $b(y) := a_F(x_* - y)$ is the unique solution of the above equation associated with $I(y) = \sin(2\pi x_1^*)\sin(2\pi y_1)$.

On the other hand, since ω is symmetric and the sigmoid f is an odd function, we have also for $\mathrm{a.\,e.}, y \in \mathbb{R}^2$,

$$-a_F(x_* + y) = \sin(2\pi x_1^*)\sin(2\pi y_1) + \mu \int_{\mathbb{R}^2} k(y, z) f(-a_F(x_* + z)) dz, \tag{3.35}$$

so that, the function $\tilde{b}(y) = -b(-y)$ is also solution of Equation (3.34) associated with the input $I(y) = \sin(2\pi x_1^*)\sin(2\pi y_1)$. By unicity of solution, one then has $b(-y) = -b(y)$ for $\mathrm{a.\,e.}, y \in \mathbb{R}^2$. This shows that $y \mapsto \omega(y) f(a_F(x_* - y))$ is an odd function on $\mathbb{R}^2$, since ω is symmetric and f is an odd function, which implies that the r.h.s. of (3.31) is equal to 0 and thus that $x^* \in P_F^{-1}(\{0\})$. □

The proof of the following corollary follows the same lines as that of Corollary 3.4.1.

Corollary 3.4.2 *Under assumption $\mu < \mu_0$, a_F (resp. a_T) is a funnel (resp. tunnel) pattern in shape. In particular, Equation (NF) with a sigmoid activation function cannot reproduce the MacKay effect starting with an external input equal to P_F or P_T.*

3.4.2 . The MacKay effect with a linear response function

The results we provide in this section aim to replicate the MacKay effect using Equation (NF) when the response function f is linear. The Corollary 3.4.1 shows that, for our model of cortical activity in V1, one cannot obtain the MacKay effect in the linear regime without breaking the Euclidean plane symmetry of the external input when chosen equal to P_F or P_T.

Our purpose now is to show that Equation (NF) with the linear response function and external input $I \in \{P_F, P_T\} + \varepsilon v$ reproduces the MacKay effect. Here v is a suitable control function which should model the redundant information in MacKay's stimuli.

Remark 3.4.2 *We notice that only the description of the MacKay effect related to the funnel pattern will be shown for ease of presentation and reader convenience. Then, in the rest of this section, we focus on describing the MacKay effect related to the "MacKay rays"; see the image on the left of Fig 3.1.*

One of the fundamental properties of the retinotopic projection of the visual field into V1 is that small objects centred on the fovea (centre of the visual field) have a much larger representation in V1 than do similar objects in the peripheral visual field. Consistent with that, a more realistic cortical representation of the "MacKay rays" visual stimulus consists of taking the external input in Equation (NF) as $I(x) = P_F(x) + \varepsilon H(\theta - x_1)$, where $\varepsilon > 0$, $\theta \geq 0$ (typically, $\theta \gg 1$) and H is the Heaviside step function, modelling the redundant information in the centre of the funnel pattern. Note that this corresponds to redundant information in horizontal stripes in the left area of the cortex.

To keep the presentation more clear as possible for reader convenience, we let $\theta = 0$, and we assume that the cortical representation of the "MacKay rays" visual stimulus is given by

$$I(x) = \cos(2\pi\lambda x_2) + \varepsilon H(-x_1), \qquad \lambda,\ \varepsilon > 0,\ x := (x_1, x_2) \in \mathbb{R}^2. \tag{3.36}$$

Theorem 3.4.3 *Assume that the response function f is linear and the input I is given by (3.36). If $\mu < \mu_0$, then, the unique stationary state to Equation (NF) is given for all $(x_1, x_2) \in \mathbb{R}^2$ by*

$$a_I(x_1, x_2) = \frac{\cos(2\pi\lambda x_2)}{1 - \mu\widehat{\omega}(\xi_0)} + \varepsilon g(x_1), \qquad \xi_0 := (0, \lambda), \tag{3.37}$$

where $g : \mathbb{R} \to \mathbb{R}$ has a discrete and countable set of zeroes on $(0, +\infty)$.

Observe that under the assumption that the response function f is linear, Equation (NF) becomes linear. It follows that the first term in the r.h.s. of (3.37) is the stationary output associated with the input P_F by using Theorem 3.4.1, and b is the stationary output associated with the external input $v(x_1, x_2) = H(-x_1)$.

Since the external input v explicitly depends only upon the variable x_1, the associated stationary output b also depends solely on that variable (a consequence of Remark 3.3.2). Thus, we are now devoted to computing the solution b of the following equation

$$b(x) = I(x) + \mu(\omega_1 * b)(x), \qquad x \in \mathbb{R}, \tag{3.38}$$

where $I(x) = H(-x)$ and the 1-D kernel ω_1 is given by

$$\omega_1(x) = [\sigma_1\sqrt{2\pi}]^{-1} e^{-\frac{x^2}{2\sigma_1^2}} - \kappa[\sigma_2\sqrt{2\pi}]^{-1} e^{-\frac{x^2}{2\sigma_2^2}}, \qquad x \in \mathbb{R}. \tag{3.39}$$

$$\widehat{\omega_1}(\xi) = e^{-2\pi^2\sigma_1^2\xi^2} - \kappa e^{-2\pi^2\sigma_2^2\xi^2}. \tag{3.40}$$

Lemma 3.4.1 *Let $I \in \mathcal{S}'(\mathbb{R})$ and the kernel $\omega_1 \in \mathcal{S}(\mathbb{R})$ be defined by (3.39). Under the assumption $\mu < \mu_c$, there is a unique solution $b \in \mathcal{S}'(\mathbb{R})$ to Equation (3.38), which is given by*

$$b = I + \mu K * I. \tag{3.41}$$

Here the kernel $K \in \mathcal{S}(\mathbb{R})$ is defined of all $x \in \mathbb{R}$ by

$$K(x) = \int_{-\infty}^{+\infty} e^{2i\pi\xi x}\widehat{K}(\xi)d\xi, \qquad \text{where} \qquad \widehat{K}(\xi) = \frac{\widehat{\omega_1}(\xi)}{1 - \mu\widehat{\omega_1}(\xi)}, \qquad \forall \xi \in \mathbb{R}. \tag{3.42}$$

Proof. First of all, under assumptions on I and ω_1, we have that Equation (3.38) is well-posed in $\mathcal{S}'(\mathbb{R})$. Then taking respectively the Fourier transform of (3.38) and the inverse Fourier transform in the space $\mathcal{S}'(\mathbb{R})$, we find that $b \in \mathcal{S}'(\mathbb{R})$ is given by (3.41) with $K \in \mathcal{S}(\mathbb{R})$ defined as in (3.42). Indeed, observe that $\widehat{K}$ is well-defined on $\mathbb{R}$ due to hypothesis $\mu < \mu_c$, with μ_c being defined in (2.23), and it belongs to the Schwartz space $\mathcal{S}(\mathbb{R})$ as the product of a $C^\infty(\mathbb{R})$ function and an element of $\mathcal{S}(\mathbb{R})$. □

Due to Lemma 3.4.1, inverting the kernel K defined in (3.42) and providing an asymptotic behaviour of its zeroes on $\mathbb{R}$ will helpful to complete the proof of Theorem 3.4.3. To achieve this, we use tools from complex and harmonic analysis. Let us consider the extension of $\widehat{K}$ in the set $\mathbb{C}$ of complex numbers,

$$\widehat{K}(z) = \frac{\widehat{\omega_1}(z)}{1 - \mu\widehat{\omega_1}(z)}, \qquad z \in \mathbb{C}. \tag{3.43}$$

Then $\widehat{K}$ is a meromorphic function on $\mathbb{C}$, and its poles are zeroes of the entire function

$$h(z) := 1 - \mu e^{-2\pi^2\sigma_1^2 z^2} + \kappa\mu e^{-2\pi^2\sigma_2^2 z^2}, \qquad z \in \mathbb{C}. \tag{3.44}$$

Remark 3.4.3 *The holomorphic function h is an exponential polynomial [BG12, Chapter 3] in $-z^2$ with frequencies $\alpha_0 = 0$, $\alpha_1 = 2\pi^2\sigma_1^2$ and $\alpha_2 = 2\pi^2\sigma_2^2$ satisfying $\alpha_0 < \alpha_1 < \alpha_2$ due to assumptions on σ_1 and σ_2. It is normalized since the coefficient of 0-frequency equals 1. A necessary condition for h for being factorizable [BG12, Remarks 3.1.5, p. 201] is that parameters σ_1 and σ_2 are taken so that it is simple, we refer to [BG12, Definition 3.1.4, p. 201] for the definition. For h to be simple, α_1 and α_2 need to be commensurable, i.e., $\alpha_1/\alpha_2 \in \mathbb{Q}$, which is equivalent to $\sigma_1^2/\sigma_2^2 \in \mathbb{Q}$. Here $\mathbb{Q}$ denote the set of rational numbers.*

Remark 3.4.4 *For ease in computation and pedagogical presentation, we assume in the rest of this section that parameters in the kernel ω defined in (3.1) and then in the 1-D kernel ω_1 defined in (3.39) are given by $\kappa = 1$, $2\pi^2\sigma_1^2 = 1$ and $2\pi^2\sigma_2^2 = 2$. In this case, one has $\mu_0 := \|\omega\|_1^{-1} = 2$ and $\mu_c := \widehat{\omega}(\xi_c)^{-1} = 4$. In particular ω satisfies the balanced condition $\widehat{\omega}(0) = 0$. Then, assuming in this particular consideration that $\mu := 1 < \mu_0 = 2$ is not a loss of generality.*

Consequently, Theorem 3.4.3 follows from the following proposition. The proof is an immediate consequence of Lemma 3.4.1 and Theorem A.1.1, and Proposition A.1.1 given in Section A.1.1.

Proposition 3.4.1 *Let $I(x) = H(-x)$, $x \in \mathbb{R}$, H being the Heaviside step function. Under the considerations of Remark 3.4.4, the solution $b \in L^\infty(\mathbb{R})$ of (3.38) is given, for $x > 0$, by*

$$e^{\pi x\sqrt{\frac{2\pi}{3}}}b(x) = \frac{\sqrt{3}}{\pi}\cos\left(\frac{\pi}{3} + \pi x\sqrt{\frac{2\pi}{3}}\right) + O\left(\frac{1}{x}\right). \tag{3.45}$$

Moreover, letting $(\theta_k)_{k\in\mathbb{N}^*}$ and $(\tau_k)_{k\in\mathbb{N}^*}$ be respectively zeroes and extrema of $x \mapsto \cos(\pi/3 + \pi x\sqrt{2\pi/3})$ for $x > 0$, the zeroes of b in $(0, +\infty)$ are a countable sequence $(\rho_k)_{k\in\mathbb{N}^*}$ such that ρ_k is unique in the interval $J_k :=]\tau_k, \tau_{k+1}[$ for all $k \in \mathbb{N}^*$ and it holds

$$|\theta_{k+1} - \rho_k| \leq \frac{\sqrt{6}}{2\pi^2}\arcsin\left(\frac{2\sqrt{5}}{5\pi(3k-1)}\right), \qquad \forall k \in \mathbb{N}^*. \tag{3.46}$$

Proof. If $I(x) = H(-x)$, $x \in \mathbb{R}$, is the input in Equation (3.38), then by Lemma 3.4.1 and Theorem A.1.1, the solution $b \in L^\infty(\mathbb{R})$ of (3.38) is given for all $x > 0$ by

$$\begin{aligned}\frac{b(x)}{2\sqrt{\pi}} &= \int_x^{+\infty} e^{-\pi y\sqrt{\frac{2\pi}{3}}}\cos\left(\frac{\pi}{12} + \pi y\sqrt{\frac{2\pi}{3}}\right)dy \\ &\quad + \int_x^{+\infty}\sum_{k=1}^{+\infty}\frac{e^{-\pi c_k y\sqrt{\frac{2\pi}{3}}}}{c_k}\cos\left(\frac{\pi}{12} + \pi c_k y\sqrt{\frac{2\pi}{3}}\right)dy \\ &\quad + \int_x^{+\infty}\sum_{k=1}^{+\infty}\frac{e^{-\pi d_k y\sqrt{\frac{2\pi}{3}}}}{d_k}\sin\left(\frac{\pi}{12} - \pi d_k y\sqrt{\frac{2\pi}{3}}\right)dy,\end{aligned} \tag{3.47}$$

where the sequences $(c_k)_k$ and $(d_k)_k$ are defined in (A.2). Since these two sequences are positives and tend to $+\infty$ as $k \to +\infty$, we can commute the integrals and the sums in the r.h.s of (3.47) for all $x > 0$. One finds,

$$\begin{aligned}b(x) &= \frac{\sqrt{3}}{\pi}\cos\left(\frac{\pi}{3} + \pi x\sqrt{\frac{2\pi}{3}}\right)e^{-\pi x\sqrt{\frac{2\pi}{3}}} + \frac{\sqrt{3}}{\pi}\sum_{k=1}^{+\infty}\frac{e^{-\pi c_k x\sqrt{\frac{2\pi}{3}}}}{c_k^2}\cos\left(\frac{\pi}{3} + \pi c_k x\sqrt{\frac{2\pi}{3}}\right) \\ &\quad - \frac{\sqrt{3}}{\pi}\sum_{k=1}^{+\infty}\frac{e^{-\pi d_k x\sqrt{\frac{2\pi}{3}}}}{d_k^2}\cos\left(\frac{\pi}{3} + \pi d_k x\sqrt{\frac{2\pi}{3}}\right),\end{aligned} \tag{3.48}$$

and (3.45) immediately follows. Finally, to prove (3.46), it suffices to repeat the proof of Lemma A.1.1 and Proposition A.1.1 given in Section A.1.1. □

The Proposition 3.4.1 implies that if the external input is the V1 representation of the "MacKay rays" as defined by (3.36), then the associated stationary state corresponds to the V1 representation of the afterimage reported by MacKay [Mac57]. Moreover, Theorem 3.3.1 ensures that the average membrane potential $a(x,t)$ of neurons in V1 located at $x \in \mathbb{R}^2$ at time $t \geq 0$ exponentially stabilises on the stationary state when $t \to \infty$. It follows that Equation (NF) theoretically replicates the MacKay effect associated with the "MacKay rays" at the cortical level. Due to the retino-cortical map between the visual field and V1, we deduce the theoretical description of the MacKay effect for the "MacKay rays" at the retinal level.

Remark 3.4.5 *We emphasise that a linear combination of the Heaviside step function in the x_2-variable as a perturbation of the V1 representation of the tunnel pattern (called "MacKay target") gives rise to the MacKay effect description related to this pattern.*

3.4.3 . The MacKay effect with a nonlinear response function

This section aims to show that Equation (NF) with a nonlinear response function f still replicates the MacKay effect associated with the "MacKay rays" and the "MacKay target", see Figures 1.3 and 1.4.

Remark 3.4.1 and Corollary 3.4.2 shows that, for our model of cortical activity in V1 modelled by Equation (NF), one cannot replicate the MacKay effect even with a nonlinear response function (having standard properties in most neural fields model, namely, a sigmoid) without breaking the Euclidean plane symmetry of the external input when chosen equal to P_F or P_T.

In the following, in order to see why a response function with sigmoid shape replicates the MacKay effect, we assume the following hypothesis.

Hypothesis 3.4.1 *The response function f satisfies: $f \in C^2(\mathbb{R})$, f is odd and $f(s) = s$ for all $|s| \leq 1$. We also assume that $\max_{s\in\mathbb{R}} f'(s) = 1$.*

Let us model the cortical representation of the "MacKay rays" input by the following

$$I(x) = \gamma P_F(x) + \varepsilon H(-x_1), \qquad x := (x_1, x_2) \in \mathbb{R}^2, \tag{3.49}$$

where $\gamma \geq 0$ is a control parameter, $\varepsilon > 0$ and $P_F(x) = \cos(2\pi\langle \xi_0, x\rangle)$ is an analytical representation of the funnel pattern in cortical coordinates, where $\xi_0 = (0, \lambda)$ with $\lambda > 0$.

The first result of this section is then the following

Proposition 3.4.2 *Let the input I be defined by (3.49) with $\varepsilon > 0$ small and $\gamma \leq 1 - \mu\widehat{\omega}(\xi_0)$. Under the assumption, $\mu < \mu_0$, equation (NF) with a response function satisfying Hypothesis 3.4.1 replicates the MacKay effect associated with the "MacKay rays".*

Proof . On one hand, the stationary solution associated with $I(x) = \gamma P_F(x) + \varepsilon v(x_1, x_2)$, where $v(x_1, x_2) = H(-x_1)$ satisfies (3.19) in $L^\infty(\mathbb{R}^2)$, i.e.,

$$\Psi(\gamma P_F + \varepsilon v) = \gamma P_F + \varepsilon v + \mu\omega * f(\Psi(\gamma P_F + \varepsilon v)). \tag{3.50}$$

On the other hand, since $\|P_F\|_\infty = 1 = \|v\|_\infty$, $0 < \gamma \leq 1 - \mu\widehat{\omega}(\xi_0) \leq 1$ and $\varepsilon \ll 1$, we can apply Theorem A.1.3 and obtain

$$\Psi(\gamma P_F + \varepsilon v) = \Psi(\gamma P_F) + \varepsilon D\Psi(\gamma P_F)v + o(\varepsilon), \tag{3.51}$$

where $D\Psi(\gamma P_F)v$ is the differential of Ψ at γP_F in the direction of v. It also follows from Theorems 3.3.1 and A.1.2 that for some $g_1 \geq 0$, it holds $\|\Psi(\gamma P_F)\|_\infty \leq g_1 = \gamma\|P_F\|_\infty + (\mu/\mu_0)f(g_1) < 3/2$. Thus, injecting (3.51) into (3.50) and Taylor expansion of f in the first order leads to

$$\Psi(\gamma P_F) = \gamma P_F + \mu\omega * f(\Psi(\gamma P_F)), \quad D\Psi(\gamma P_F)v = v + \mu\omega * [f'(\Psi(\gamma P_F))D\Psi(P_F)v.] \tag{3.52}$$

Thanks to Hypothesis 3.4.1 and the assumption $\gamma \leq 1 - \mu\widehat{\omega}(\xi_0)$, one has $\Psi(\gamma P_F) = \gamma P_F/(1 - \mu\widehat{\omega}(\xi_0))$. Indeed, since $|\gamma P_F/(1 - \mu\widehat{\omega}(\xi_0)| \leq 1$ and $\omega * P_F = \widehat{\omega}(\xi_0)P_F$, one has that

$$\gamma P_F + \mu\omega * f\left(\frac{\gamma P_F}{1 - \mu\widehat{\omega}(\xi_0)}\right) = \gamma P_F + \frac{\mu\gamma\omega * P_F}{1 - \mu\widehat{\omega}(\xi_0)} = \frac{\gamma P_F}{1 - \mu\widehat{\omega}(\xi_0)}. \tag{3.53}$$

Therefore, $\Psi(\gamma P_F)$ is also a funnel pattern when represented in term of binary image. Moreover, since $|\Psi(\gamma P_F)| \leq 1$, one has $f'(\Psi(\gamma P_F)) = 1$, and $D\Psi(\gamma P_F)v = v + \mu\omega * D\Psi(P_F)v$ has a discrete and countable set of zeroes by Proposition 3.4.1. The result then follows at once. □

Proposition 3.4.3 *Let $v \in L^\infty(\mathbb{R}^2)$. Under the assumption $\mu < \mu_0$, the map $\Pi : \gamma \in \mathbb{R}_{\geq 0} \mapsto \Pi(\gamma) = u_\gamma \in L^\infty(\mathbb{R}^2)$, where u_γ is the solution of $u_\gamma = v + \mu\omega * [f'(\Psi(\gamma P_F))u_\gamma]$ is Lipschitz continuous.*

Proof. Let $v \in L^\infty(\mathbb{R}^2)$ be fixed and $\gamma \in \mathbb{R}_{\geq 0}$. If $u_\gamma \in L^\infty(\mathbb{R}^2)$ is the solution of $u_\gamma = v + \mu\omega * [f'(\Psi(\gamma P_F))u_\gamma]$, then, under the assumption $\mu < \mu_0$ and Hypothesis 3.4.1, one has $\|u_\gamma\|_\infty \leq \|v\|_\infty\mu_0/(\mu - \mu_0)$. Let now $\gamma_1, \gamma_2 \in \mathbb{R}_{\geq 0}$, then using Inequality (3.20), one finds

$$\begin{aligned} \|\Pi(\gamma_1) - \Pi(\gamma_2)\|_\infty &\leq \mu\|\omega\|_1\|f'(\Psi(\gamma_1 P_F))u_{\gamma_1} - f'(\Psi(\gamma_2 P_F))u_{\gamma_2}\|_\infty \\ &\leq \frac{\mu}{\mu_0}\|\Pi(\gamma_1) - \Pi(\gamma_2)\|_\infty + \frac{\mu\mu_0\|v\|_\infty f''_\infty}{(\mu_0 - \mu)^2}|\gamma_1 - \gamma_2|, \end{aligned} \tag{3.54}$$

where f''_∞ is the L^∞-norm of the second derivative f''. The result then follows at once. □

Let us define the positive quantity

$$\gamma_0 := \sup\{\gamma \geq 0 \mid \|\Psi(\gamma' P_F)\|_\infty \leq 1, \text{for all } \gamma' \in [0, \gamma]\}. \tag{3.55}$$

Observe that γ_0 is not necessary finite and that if $0 \leq \gamma \leq \gamma_0$, then $f'(\Psi(\gamma P_F)) = 1$. It follows that if $\gamma_0 = +\infty$, then $\|\Psi(\gamma P_F)\|_\infty \leq 1$ for all $\gamma \geq 0$ and therefore, under Assumption $\mu < \mu_0$, Equation (NF) with a response function satisfying Hypothesis 3.4.1 and with the input I defined by (3.49) with $\varepsilon > 0$ will always reproduce the MacKay effect associated with "MacKay rays" thanks to Proposition 3.4.3.

In the case where γ_0 is finite, one has the following.

Theorem 3.4.4 *Let $L > 0$. If γ_0 defined by (3.55) is finite, there exists $\delta > 0$ such that the stationary solution to Equation (NF) with a response function satisfying Hypothesis 3.4.1 and with the input I defined by (3.49) with $\varepsilon > 0$ small and $|\gamma - \gamma_0| \leq \delta$ has the same zeroes structure as in the linear case in $[0, L] \times \mathbb{R}$, under Assumption $\mu < \mu_0$. In particular, it replicates the MacKay effect associated with the "MacKay rays".*

Proof. Let $\varepsilon > 0$ be small and γ_0 defined by (3.55) be finite. On the one hand, by definition of γ_0 and Proposition 3.4.2, the stationary solution $a_I(x_1, x_2)$ to Equation (NF) with a response function satisfying Hypothesis 3.4.1 and with the input I defined by (3.49) with $\gamma = \gamma_0$ has a discrete and countable zero-level set with respect to each of its variables $x_1 > 0$ and $x_2 \in \mathbb{R}$. On the other hand, one has for all $\gamma \geq 0$, $\Psi(\gamma P_F + \varepsilon v) = \Psi(\gamma P_F) + \varepsilon u_\gamma + o(\varepsilon)$ where $u_\gamma \in L^\infty(\mathbb{R}^2)$ is the solution of $u_\gamma = v + \mu\omega * [f'(\Psi(\gamma P_F))u_\gamma]$. We known from Theorems 3.4.1 and 3.4.2 that $\Psi(\gamma P_F)$ has a discrete set of zeroes with respect to x_2 as P_F, and from Proposition 3.4.3 that for all $\eta > 0$, there exists $\delta > 0$ such that, if $|\gamma - \gamma_0| \leq \delta$ it holds $\|u_\gamma - u_{\gamma_0}\|_\infty \leq \eta$. Therefore, since u_{γ_0} has a discrete set of zeroes with respect to $x_1 > 0$, then the zeroes of the function u_γ cannot accumulate at any of those zeroes in a finite interval, that is, the zeroes of both functions are distributed similarly in $[0, L] \times \mathbb{R}$ for all finite $L > 0$. □

Remark 3.4.6 *Although a sigmoid nonlinearity such as $f(s) = \tanh(s)$ or $f(s) = \operatorname{erf}(s\sqrt{\pi}/2)$ does not satisfies the assumption $f(s) = s$ for $|s| \leq 1$, it is almost linear in a small interval of the form $(-\varepsilon, \varepsilon)$, $\varepsilon > 0$ in such a way that Theorem 3.4.4 should be a theoretical explanation of why Equation (NF) with this nonlinearity replicates the MacKay effect.*

3.4.4 . Numerical results for the MacKay effect

The numerical implementation is performed with Julia, where we coded retino-cortical map for visualising each experiment, see Section B.1 of Appendix B. Moreover, given a sensory input I, the associated stationary output a_I is numerically implemented via an iterative fixed-point method, see Section B.3 of Appendix B.

Also, following the convention adopted in [EC79a; Bre+01] for geometric visual hallucinations, we present binary versions of these images, where black corresponds to positive values and white to negative ones, see Section 3.2.3.

The cortical data is defined on a square $(x_1, x_2) \in [-L, L]^2$, $L = 10$ with steps $\Delta x_1 = \Delta x_2 = 0.01$. For the reproduction of the MacKay effect (see Section B.4 of Appendix B), parameters in the kernel ω given by (3.1) are $\kappa = 1$, $2\pi^2\sigma_1^2 = 1$, and $2\pi^2\sigma_2^2 = 2$. We also choose $\mu := 1$. We collected some representative results in Figures 3.5, 3.6, 3.7 and 3.8. Here, we visualize in the retinal representation obtained from the cortical patterns via the inverse retino-cortical map. In Figure 3.5, we exhibit the MacKay effect associated with the "MacKay rays". In this case, the sensory input is chosen as $I(x) = \cos(5\pi x_2) + \varepsilon H(2 - x_1)$, where $\varepsilon = 0.025$ and H being the Heaviside step function.

Similarly, we exhibit in Figure 3.6 the MacKay effect associated with the "MacKay target". In this case, the sensory input is $I(x) = \cos(5\pi x_1) + \varepsilon(H(-x_2 - 9.75) + H(x_2 - 9.75) + H(0.25 - |x_2|))$, where $\varepsilon = 0.025$ and H being the Heaviside step function.

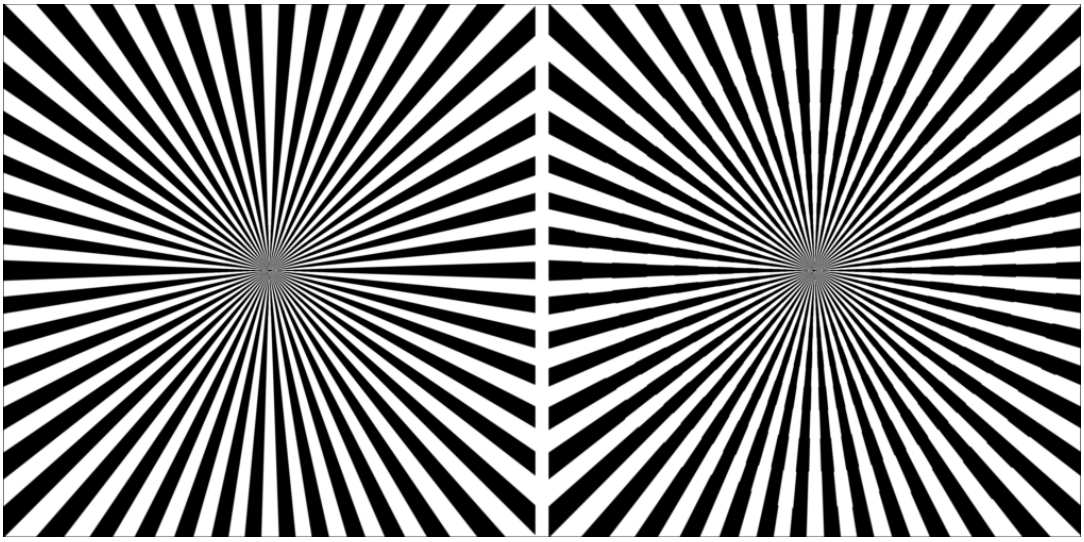

Figure 3.5: MacKay effect (*right*) on the "MacKay rays" (*left*). We use the linear response function $f(s) = s$. The sensory input is chosen as $I(x) = \cos(5\pi x_2) + \varepsilon H(2 - x_1)$, $\varepsilon = 0.025$, where H is the Heaviside step function.

We use a linear response function ($f(s) = s$) for the two figures. However, the phenomenon can be reproduced with any sigmoid function, see for instance, Figure 3.7 and Figure 3.8.

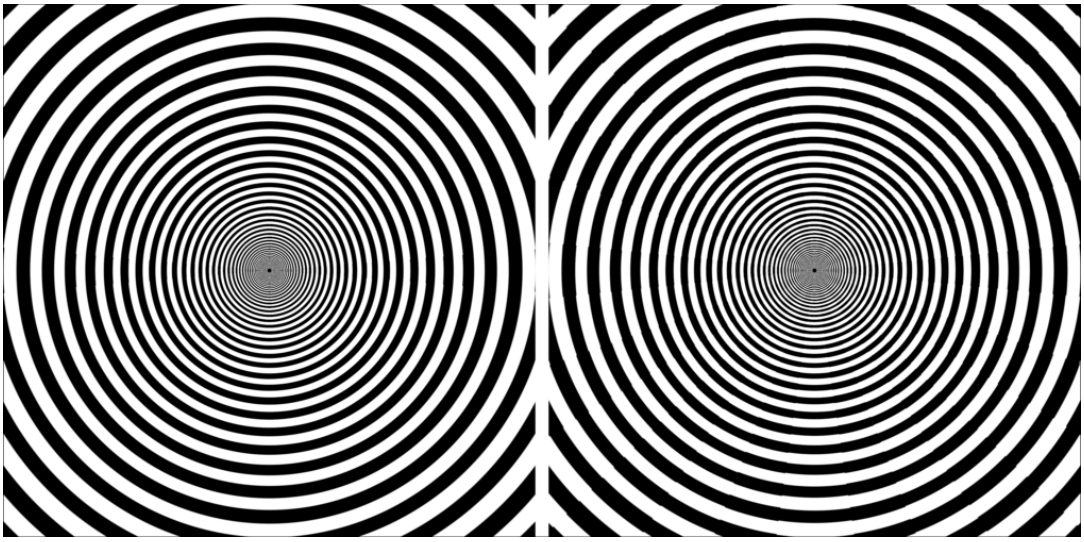

Figure 3.6: MacKay effect (*right*) on the "MacKay target" (*left*).We use the linear response function $f(s) = s$. The sensory input is $I(x) = \cos(5\pi x_1) + \varepsilon(H(-x_2 - 9.75) + H(x_2 - 9.75) + H(0.25 - |x_2|))$, $\varepsilon = 0.025$, where H is the Heaviside step function.

Remark 3.4.7 *Although the Gaussian kernel is usually used in image processing and computer vision tasks due to its proximity to the visual system, it cannot replicate the MacKay effect if*

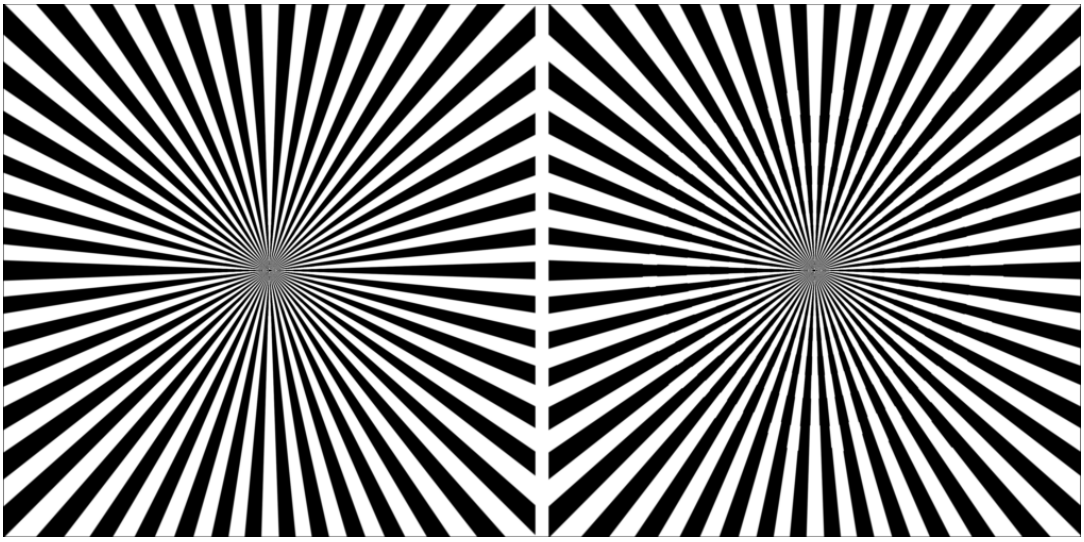

Figure 3.7: MacKay effect (*right*) on the "MacKay rays" (*left*). We use the nonlinear response function $f(s) = s/(1+|s|)$. The sensory input is chosen as $I(x) = \cos(5\pi x_2) + \varepsilon H(2 - x_1)$, $\varepsilon = 0.025$, where H is the Heaviside step function.

we use it as the kernel in Equation (NF)*. A physiological reason for this is that we used a one-layer model of NF equations. It is not then biologically realistic to model synaptic interactions with a Gaussian, which would model only excitatory-type interactions between neurons, see also Remark A.1.2 in Appendix A.1.1 for a theoretical explanation.*

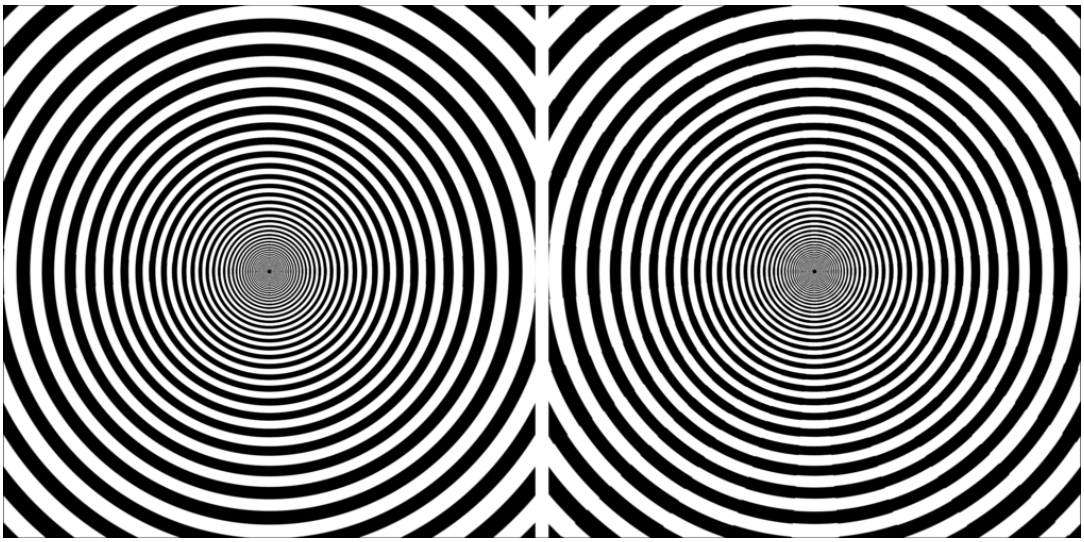

Figure 3.8: MacKay effect (*right*) on the "MacKay target" (*left*).We use the nonlinear response function $f(s) = s/(1+|s|)$. The sensory input is $I(x) = \cos(5\pi x_1) + \varepsilon(H(-x_2 - 9.75) + H(x_2 - 9.75) + H(0.25 - |x_2|))$, $\varepsilon = 0.025$, where H is the Heaviside step function.

3.5 . On Billock and Tsou's experiments

In this section, we investigate the description of Billock and Tsou's phenomena using Equation (NF). We begin by proving that these phenomena are wholly nonlinear in contrast to the MacKay effect. That is, equation (NF) with a linear response function f cannot reproduce these psychophysical experiments.

3.5.1 . Unreproducibility of Billock and Tsou experiments: linear response function

In this section, we consider the assumption that the response function f is linear. To simplify our analysis, we specifically focus on the funnel pattern centered on the fovea within the visual field. As a result, the corresponding sensory input I consists of a localized pattern of horizontal stripes in the left area of the V1 cortex by the retino-cortical map.

Previously, in [TPC23a, Proposition 5.], we proved that (NF) with a linear response function is incapable of reproducing Billock and Tsou's experiments, as verified through direct Fourier transform computations. While this finding sufficed to establish our desired outcome, it failed to offer deeper insights into the qualitative properties of the stationary state associated with the sensory input utilized in these experiments. Specifically, it did not precisely characterise the zero-level set of this stationary state. To address this gap, we draw upon the qualitative properties of the sensory input I and utilize tools from Complex and harmonic analysis. Consequently, we present the following key result in this section.

Theorem 3.5.1 *Let $f(s) = s$, for all $s \in \mathbb{R}$ and the sensory input I in (NF) be given for all $(x_1, x_2) \in \mathbb{R}^2$ by $I(x_1, x_2) = \cos(2\pi\lambda x_2)H(-x_1)$, $\lambda > 0$ and H being the Heaviside step function. Then, under assumption $\mu < \mu_0$, the zero-level set $\mathcal{Z}_a$ of the stationary state $a \in L^\infty(\mathbb{R}^2)$ satisfies*

$$\mathcal{Z}_a \cap [(0, +\infty) \times \mathbb{R}] = [\mathcal{X}_1 \times \mathbb{R}] \cup [(0, +\infty) \times \mathcal{X}_2], \tag{3.56}$$

where $\mathcal{X}_1$ and $\mathcal{X}_2$ are discrete sets, respectively in $(0, +\infty)$ and $\mathbb{R}$.

To prove Theorem 3.5.1, we proceed pedagogically in two steps. We also assume without loss of generality that $\lambda = 1$ to keep the presentation clear for reader convenience. Recall that, under hypotheses of Theorem 3.5.1, the stationary state $a \in L^\infty(\mathbb{R}^2)$ is given by

$$a(x_1, x_2) = \cos(2\pi x_2)H(-x_1) + \mu \int_{\mathbb{R}^2} \omega(x - y)a(y)dy, \qquad (x_1, x_2) \in \mathbb{R}^2, \tag{3.57}$$

where the kernel ω is defined in (3.1).

Lemma 3.5.1 *Under hypotheses of Theorem 3.5.1, the stationary state $a \in L^\infty(\mathbb{R}^2)$ is 1-periodic, even, Lipschitz continuous and infinitely derivable with respect to its second variable.*

Proof. Using that the convolution operator commutes with translation, that the input $I(x_1, x_2) = \cos(2\pi x_2)H(-x_1)$ and ω are even with respect to x_2, one deduces that a is 1-periodic and

even with respect to x_2. The fact that $a \in L^\infty(\mathbb{R}^2)$ is infinitely derivable with respect to x_2 follows from that for a.e. $x_1 \in \mathbb{R}$, $I(x_1,\cdot) \in C^\infty(\mathbb{R})$ and $\omega \in \mathcal{S}(\mathbb{R}^2) \subset C^\infty(\mathbb{R}^2) \cap L^1(\mathbb{R}^2)$. Let us turn to an argument to show that a is Lipschitz continuous with respect to x_2. Taking the derivative of (3.57) with respect to x_2, one finds

$$a'(x_1,x_2) := \partial_{x_2} a(x_1,x_2) = -2\pi \sin(2\pi x_2) H(-x_1) + \mu \int_{\mathbb{R}^2} \omega(x-y) a'(y) dy, \qquad (x_1,x_2) \in \mathbb{R}^2. \tag{3.58}$$

It follows that for a.e. $x_1 \in \mathbb{R}$,

$$\|a'(x_1,\cdot)\|_{L^\infty(\mathbb{R})} \leq \frac{2\pi}{1-\frac{\mu}{\mu_0}},$$

showing that $a(x_1,\cdot)$ is Lipschitz continuous for a.e. $x_1 \in \mathbb{R}$. □

Lemma 3.5.2 *Under hypotheses of Theorem 3.5.1, the stationary state $a \in L^\infty(\mathbb{R}^2)$ is given by*

$$a(x_1,x_2) = a_1(x_1)\cos(2\pi x_2), \qquad (x_1,x_2) \in \mathbb{R}^2. \tag{3.59}$$

Here $a_1 \in L^\infty(\mathbb{R})$ is given by

$$a_1(x_1) = H(-x_1) + \mu (W_1 * H(-\cdot))(x_1), \qquad x_1 \in \mathbb{R}. \tag{3.60}$$

where $W_1 \in \mathcal{S}(\mathbb{R})$ is defined for all $x_1 \in \mathbb{R}$ by

$$W_1(x_1) = \int_{-\infty}^{+\infty} e^{2i\pi x_1 \xi} \frac{\widehat{\psi_1}(\xi)}{1-\mu\widehat{\psi_1}(\xi)} d\xi, \quad \widehat{\psi_1}(\xi) = e^{-2\pi^2\sigma_1^2(1+\xi^2)} - \kappa e^{-2\pi^2\sigma_2^2(1+\xi^2)}, \quad \xi \in \mathbb{R}. \tag{3.61}$$

Proof. We fix $x_1 \in \mathbb{R}$. Since $x_2 \mapsto a(x_1,x_2)$ is 1-periodic and even on $\mathbb{R}$, we expand $a(x_1,\cdot)$ in term of Fourier series as

$$a(x_1,x_2) = \sum_{n=0}^{\infty} a_n(x_1)\cos(2\pi n x_2), \qquad x_2 \in \mathbb{R}, \tag{3.62}$$

$$a_0(x_1) = \int_0^1 a(x_1,t)dt, \qquad \text{and} \qquad a_n(x_1) = 2\int_0^1 a(x_1,t)\cos(2\pi n t)dt, \qquad x_1 \in \mathbb{R}. \tag{3.63}$$

Due to Lemma 3.5.1, one has that the derivative $a'(x_1,\cdot)$ of a with respect to x_2 is continuous and bounded on $\mathbb{R}$. Thus $a'(x_1,\cdot)$ belongs to $L^2([-1,1])$, the space of real-valued measurable and square-integrable functions over $[-1,1]$. Since $a(x_1,\cdot)$ is absolutely continuous (Lipschtiz continuous by Lemma 3.5.1) on $\mathbb{R}$, it follows from [FK74, Théorème 2.] that its Fourier series converges uniformly to $a(x_1,\cdot)$ on $\mathbb{R}$. Observe also that (3.63) defines functions $a_n \in L^\infty(\mathbb{R})$ for all $n \in \mathbb{N}$, so that one gets obviously for all $x_1 \in \mathbb{R}$ and for all $\sigma > 0$,

$$\sum_{n=0}^{+\infty} \int_{-\infty}^{\infty} \left| \frac{1}{\sigma\sqrt{2\pi}} e^{-\frac{(x_1-y_1)^2}{2\sigma^2}} e^{-2\pi^2\sigma^2 n^2} a_n(y_1)\cos(2\pi n x_2) \right| dy_1 \lesssim [4] \frac{1}{1-e^{-2\pi^2\sigma^2}}. \tag{3.64}$$

[4] Let $\gamma_1, \gamma_2 \geq 0$, then $\gamma_1 \lesssim \gamma_2$ if there exists $M > 0$ such that $\gamma_1 \leq M\gamma_2$.

By substituting (3.62) into (3.57), one finds that the latter is equivalent to the following family of one-dimensional linear integral equation indexed by $n \in \mathbb{N}$.

$$a_n(x_1) = \delta_{1,n} H(-x_1) + \mu\alpha(\psi_n * a_n)(x_1), \qquad x_1 \in \mathbb{R}, \tag{3.65}$$

where $\delta_{1,n}$ is the usual Kronecker symbol and the kernel ψ_n is given for every $n \in \mathbb{N}$, by

$$\psi_n(s) = e^{-2\pi^2 n^2 \sigma_1^2} \frac{e^{-\frac{s^2}{2\sigma_1^2}}}{\sigma_1\sqrt{2\pi}} - \kappa e^{-2\pi^2 n^2 \sigma_2^2} \frac{e^{-\frac{s^2}{2\sigma_2^2}}}{\sigma_2\sqrt{2\pi}}, \qquad s \in \mathbb{R}. \tag{3.66}$$

For $n \neq 1$, equations (3.65) yields to

$$(\delta - \mu\alpha\psi_n) * a_n = 0, \qquad \text{in} \qquad \mathcal{S}'(\mathbb{R}), \tag{3.67}$$

where δ is the Dirac distribution at 0. Taking the Fourier transform of (3.67) in the space $\mathcal{S}'(\mathbb{R})$, one obtains for all $\xi \in \mathbb{R}$,

$$(1 - \mu\widehat{\psi_n}(\xi))\mathcal{F}\{a_n\}(\xi) = 0, \qquad n \neq 1. \tag{3.68}$$

It is not difficult to see that $\max\{\widehat{\psi_n}(\xi) \mid \xi \in \mathbb{R}\} \leq \max\{\widehat{\omega}(\xi) \mid \xi \in \mathbb{R}^2\} \leq \|\omega\|_1$. Since $\mu\|\omega\|_1 < 1$ by assumption, one deduces $1 - \mu\widehat{\psi_n}(\xi) > 0$ for all $\xi \in \mathbb{R}$, and therefore $\mathcal{F}\{a_n\} \equiv 0$. It follows that

$$a_n \equiv 0, \qquad \text{for all} \qquad n \neq 1. \tag{3.69}$$

In the case $n = 1$, one has

$$a_1(x_1) = H(-x_1) + \mu(\psi_1 * a_1)(x_1), \qquad x_1 \in \mathbb{R}. \tag{3.70}$$

Finally, arguing as in the proof of Lemma 3.4.1, we find (3.60) and (3.61). □

Remark 3.5.1 *To make the presentation more understandable, in the rest of this section, we let parameters in the kernel ω in (3.1) are such that $\kappa = 1$, $\sigma_1 = 1/\pi\sqrt{2}$ and $\sigma_2 = \sigma_1\sqrt{2}$. The motivation for this choice is explained in Remark 3.4.3. We also let $\mu = 1$, see Remark 3.4.4.*

Remark 3.5.2 *Using Theorem (A.2.1), and arguing similarly as in the case of MacKay effect description in linear case, we can prove that a_1 has a discrete and countable set of zeroes in $(0, +\infty)$, refer to Section A.1.1 and Proposition 3.4.1.*

Proof . (of Theorem 3.5.1) To complete the proof of Theorem 3.5.1 it suffices to consider Lemma 3.5.2, Remark 3.5.2 and observe that a given by (3.59) satisfies (3.56). □
A consequence of Theorem 3.5.1 is the following.

Corollary 3.5.1 *Assume the neurones' response function is linear. Under the assumption $\mu < \mu_0$, equation (NF) does not reproduce Billock and Tsou's experiments associated with a sensory input consisting of a pattern of horizontal stripes localised in the left area in the cortex V1.*

Proof . Given that the sensory input in equation (NF) is a pattern consisting of horizontal stripes localised in the left area in the cortex V1, Theorem 3.5.1 shows that the corresponding stationary state consists of a mixture of patterns of horizontal and vertical stripes in the right area in V1 instead of vertical stripes only, as Billock and Tsou reported. □

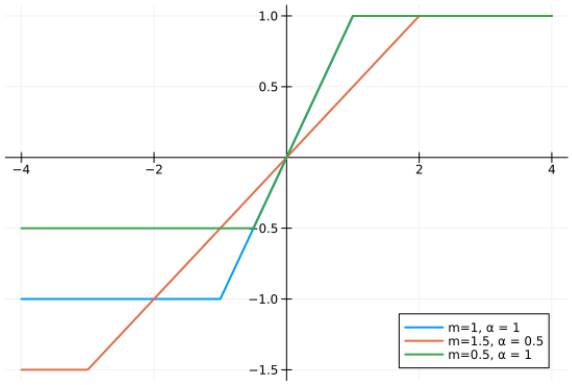

Figure 3.9: Nonlinear response functions $f_{m,\alpha}(s) = \max(-m, \min(1, \alpha s))$ for different values of m and α.

3.5.2 . Reproducibility of Billock and Tsou's experiments with a sigmoid response function and numerical results

In Section 3.5.1, we proved that Equation (NF) with a linear response function does not reproduce Billock and Tsou's experiments.

To see how the shape of the nonlinearity f is involved in the reproducibility, we first consider the family of nonlinear sigmoid functions

$$f_{m,\alpha}(s) = \max(-m, \min(1, \alpha s)) = \begin{cases} 1, & \text{if} \quad s \geq \frac{1}{\alpha}, \\ \alpha s, & \text{if} \quad -\frac{m}{\alpha} \leq s \leq \frac{1}{\alpha}, \\ -m, & \text{if} \quad s \leq -\frac{m}{\alpha}, \end{cases} \quad , \qquad s \in \mathbb{R}, \tag{3.71}$$

with $m \geq 0$ and $\alpha > 0$. Please, refer to Figure 3.9 for visual illustration. The goal is to figure out ranges on parameters m and α where $f_{m,\alpha}$ replicate these phenomena or not. Since the maximal slope α of $f_{m,\alpha}$ is no longer equal to 1, we let

$$\mu_\alpha := \alpha^{-1} \|\omega\|_1^{-1}, \tag{3.72}$$

which will play the role of μ_0 in the rest of this section.

Remark 3.5.3 *Let $I \in L^p(\mathbb{R}^2)$ and $a_0 \in L^p(\mathbb{R}^2)$ be respectively the sensory input and the initial datum in Equation (NF). Using the contraction mapping principle as soon as $\mu < \mu_\alpha$, it is straightforward to prove for fixed $m \geq 0$ and $\alpha > 0$ the existence of unique stationary solution $a_{m,\alpha} \in L^p(\mathbb{R}^2)$ to Equation (NF) where f is replaced by $f_{m,\alpha}$.*

It is a straightforward consequence of Theorem A.1.2 in the Appendix A.1.2 that if $I \in L^\infty(\mathbb{R}^2)$, the solution $a_{m,\alpha} \in L^\infty(\mathbb{R}^2)$ satisfies

$$\|a_{m,\alpha}\|_\infty \leq C_{m,\alpha}, \tag{3.73}$$

where $C_{m,\alpha} > 0$ is the smaller fixed point of the function $x \mapsto \|I\|_\infty + \frac{\mu}{\mu_\alpha} f_{m,\alpha}(x)$ on $(0, +\infty)$. Moreover, thanks to expression of $f_{m,\alpha}$ given by (3.71) it is immediate that $C_{m,\alpha} = C_\alpha$, that is $C_{m,\alpha}$ does not depend on m.

We therefore has the following.

Proposition 3.5.1 *Let $I \in L^\infty(\mathbb{R}^2)$ and $\alpha > 0$ be given. Under the hypothesis $\mu < \mu_\alpha$, the unique solution $a_{m_1,\alpha} \in L^\infty(\mathbb{R}^2)$ of Equation (NF) with $f_{m_1,\alpha}$ coincides with the unique solution $a_{m_2,\alpha} \in L^\infty(\mathbb{R}^2)$ of Equation (NF) with $f_{m_2,\alpha}$ as soon as $m_1, m_2 \geq m_\alpha$, where*

$$m_\alpha := \alpha C_\alpha. \tag{3.74}$$

Applied to Billock and Tsou's experiments, Proposition 3.5.1 implies the following helpful result.

Corollary 3.5.2 *Let $I \in L^\infty(\mathbb{R}^2)$, $\alpha > 0$ and $m_1 \geq m_\alpha$ be given where m_α is defined by (3.74). Under the hypothesis $\mu < \mu_\alpha$, if the sigmoid $f_{m_1,\alpha}$ reproduces BT, then any sigmoid $f_{m,\alpha}$ reproduces BT as soon as $m \geq m_1$.*

In [TPC22, Figs. 5 and 6], we illustrated the capability of Equation (NF) to reproduce Billock and Tsou experiments with the nonlinear response function

$$f(s) = (1 + \exp(-s + 0.25))^{-1} - (1 + \exp(0.25))^{-1}.$$

In Section 3.5.1, we proved that a linear response function does not reproduce these phenomena.

In what follows, for a real function u, the translation $\tau_{x_0}u$ of u by $x_0 \in \mathbb{R}$ is the real function defined by $(\tau_{x_0}u)(x) = u(x - x_0)$.

We recall that one of the fundamental properties of the retinotopic projection of the visual field into V1 is that small objects centred on the fovea (centre of the visual field) have a much larger representation in V1 than do similar objects in the peripheral visual field. Consistent with that, a more realistic cortical representation of the BT visual stimulus associated, e.g., with the funnel pattern localised in the peripheral visual field consists of taking the sensory input as $I(x_1, x_2) = \cos(2\pi x_2)(\tau_{x_0}H)(x_1)$. Here $x_0 \gg 1$, and H is the Heaviside step function, modelling that the funnel pattern is localised in the peripheral visual field. Note that this corresponds to sensory input consisting of horizontal stripes in the right area of the cortex V1.

For numerical implementation performed with Julia, we assume that the cortical data is defined on a square $(x_1, x_2) \in [-L, L]^2$, $L = 10$ with steps $\Delta x_1 = \Delta x_2 = 0.01$, see Sections B.1, B.3 and B.5 of Appendix B. We exhibit in Figures. 3.10 and 3.11 Billock and Tsou's experiments for a funnel-like stimulus localised at the periphery and fovea, respectively. As images, we have a fan shape pattern at the periphery (resp. fovea) and white in the fovea (respectively periphery). We use the kernel ω defined in (3.1) with $\sigma_1 = 0.1$, $\sigma_2 = 0.5$ and $\kappa = 4.56$.

In Figure. 3.10, the stimulus is $I(x) = \cos(4\pi x_2)H(x_1 - 6)$, and the nonlinearity is $f(s) = \max(-0.2, \min(1, 1.7s))$. In Fig. 3.11, the stimulus is $I(x) = \cos(4\pi x_2)H(6 - x_1)$ and the nonlinearity is $f(s) = \max(-0.2, \min(1, 1.2s))$. In Figure. 3.12, the stimulus is $I(x) = \cos(4\pi x_2)H(6 - x_1)$: On the left, the nonlinearity used is $f(s) = \max(-0.2, \min(1, 1.2s))$, and on the right, we use $f(s) = \max(-1.2, \min(1, s))$. In the afterimage on the left of Fig. 3.12, the fan shape does not extend to the periphery, whereas on the right, the fan shape extends through the periphery.

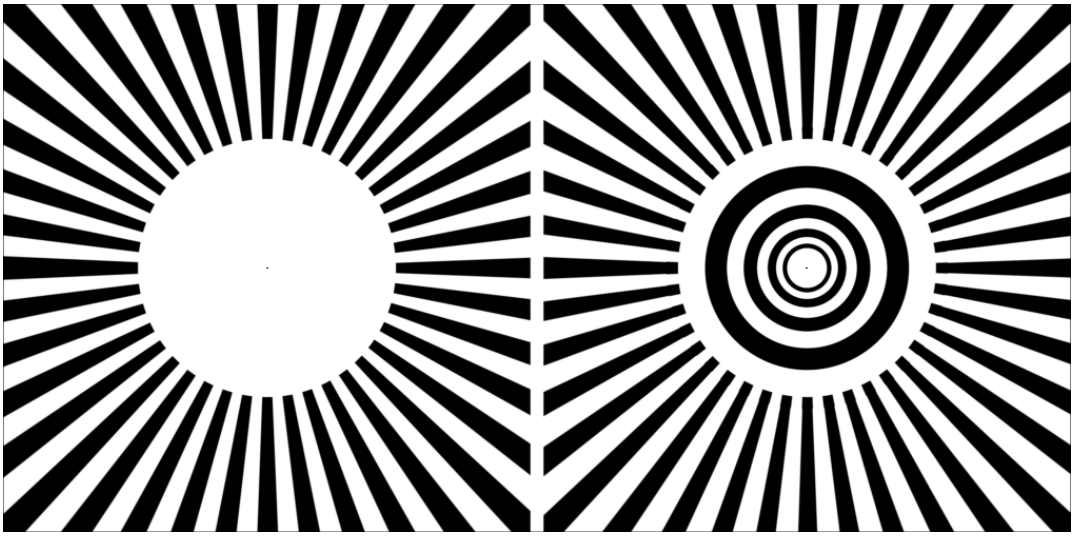

Figure 3.10: Billock and Tsou's experiments: funnel stimulus localised at the periphery (*left*) and afterimage (*right*).

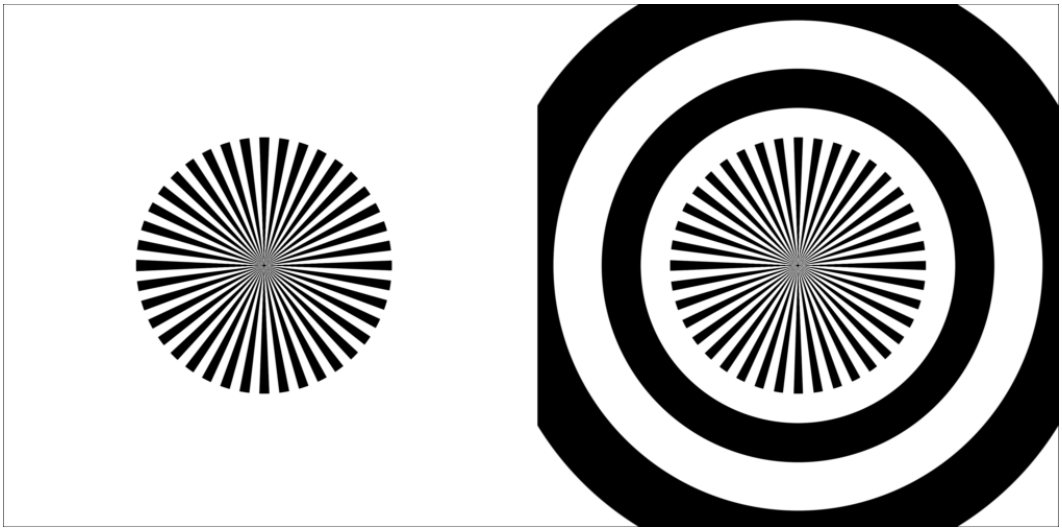

Figure 3.11: Billock and Tsou's experiments: funnel stimulus localised at the fovea (*left*) and afterimage (*right*).

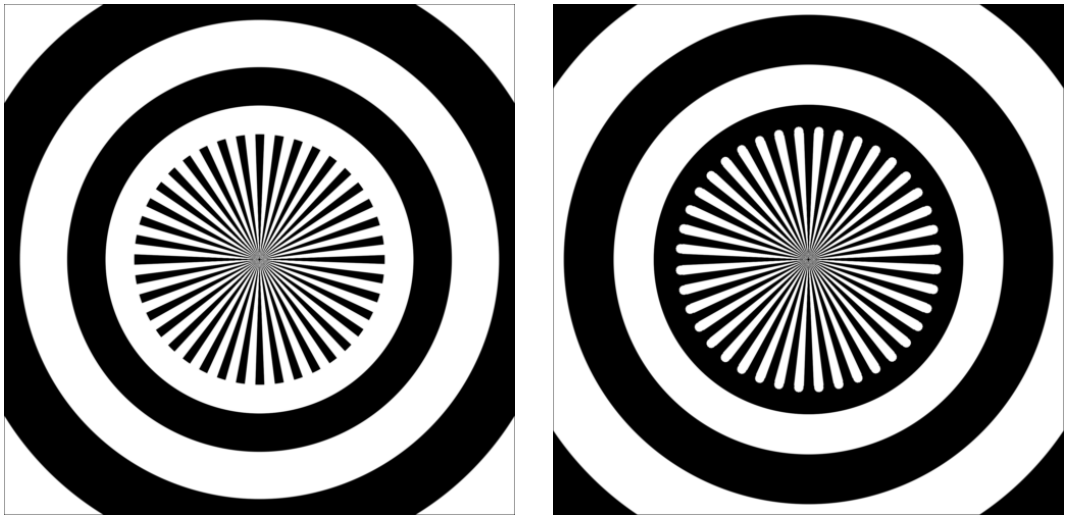

Figure 3.12: After-images in Billock and Tsou's experiments: funnel stimulus localised at the fovea as in Figure 3.11 (left). On the *right* (respectively *left*) illusory contours extend (resp. does not) to the periphery.

In order to see how $f_{m,\alpha}$ is involved on the reproducibility of Billock and Tsou's experiments related to the localised funnel pattern on the fovea of the visual field

$$I(x_1, x_2) = \cos(2\pi x_2)(\tau_{-6}H)(-x_1) = \cos(2\pi x_2)H(6 - x_1), \qquad (x_1, x_2) \in \mathbb{R}^2, \tag{3.75}$$

we assume that

$$(m, \alpha) \in \{(k/10, \ell/10) \mid k = 0, \dots, 30,\ \ell = 1, \dots, 30\}, \tag{3.76}$$

due to Corollary 3.5.2. In the Figure 3.13, we depicted regions where $f_{m,\alpha}$ reproduces Billock and Tsou's experiments associated with a funnel pattern localised in the fovea of the visual field or not, depending on the values of parameters m and α. Please, refer to Section B.5.2 in Appendix B if you want to see how Figure 3.13 is numerically obtained.

Remark 3.5.4 *While currently engaged in theoretical justifications for the replication of Billock and Tsou phenomena using Equation* (NF) *with a "good" nonlinearity, as it is ongoing in [CPT23], it is essential to note that the positive outcomes obtained through numerical simulations in Figure 3.13 should sufficiently substantiate this. Indeed, the code works via a fixed point arguments. Let a be the exact stationary solution given by the contraction mapping principle and v_h^N be the corresponding N-th iteration approximate solution with respect to the spatial discretisation step h. It should be possible to prove that*

$$\|a - v_h^N\|_\infty \leq O(1/N) + O(h), \tag{3.77}$$

where $N \gg 1$ and $h \ll 1$. The same argument used in the proof of Theorem 3.4.4 then guaranteed that v_h^N captures correctly the structure of zeroes of a.

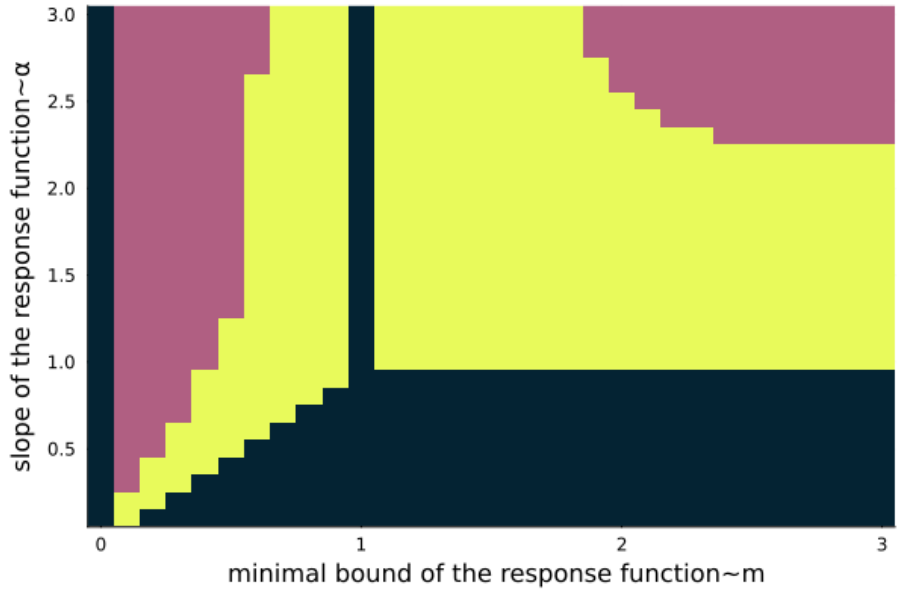

Figure 3.13: Range of (m, α) where $f_{m,\alpha}$ reproduce or not Billock and Tsou's experiments associated with a funnel pattern localised in the fovea of the visual field. The *magenta region* corresponds to the values of m and α where $f_{m,\alpha}$ reproduces the "strong" Billock and Tsou's experiments (the illusory contours does not extend through the physical stimulus in the afterimage). The *yellow region* corresponds to the values of m and α where $f_{m,\alpha}$ reproduces the "weak" Billock and Tsou's experiments (the illusory contours extend through the physical stimulus in the afterimage) and the *black region* corresponds to the values of m and α where $f_{m,\alpha}$ does not reproduce Billock and Tsou's experiments, neither "strong" nor "weak".

3.5.3 . Ongoing works

As mentioned in Remark 3.5.4, we are currently engaged in [CPT23], to

1. understanding theoretically why the well-used non-linearities $f_{1,\alpha}(s) = \max(-1, \min(1, \alpha s))$ and $f_{0,\alpha}(s) = \max(0, \min(1, \alpha s))$ do not replicate Billock and Tsou's experiments. At this stage of our work, it seems that $f_{1,\alpha}$ does not replicate these intriguing visual phenomena due to some *compensation effect* related to that $f_{1,\alpha}$ is asymmetric (odd function).

2. theoretically replicate the "weak" Billock and Tsou's experiments with the non-linear response function

$$f_{\infty,\alpha}(s) = \begin{cases} 1, & \text{if} \quad s \geq \frac{1}{\alpha}, \\ \alpha s, & \text{if} \quad s \leq \frac{1}{\alpha}, \end{cases} \qquad = 1 - \max(0, 1 - \alpha s),$$

which essentially corresponds to the limiting case $m \to \infty$. Observe that restricting to this case is consistent with Corollary 3.5.2. In particular, it will be also a great achievement if we clearly understand why it is necessary required that the slope $\alpha \geq 1$ for $f_{\infty,\alpha}$ to replicate these phenomena as suggest the numerical results in Figure 3.13.

Even though Figure 3.13 does not provide information about the unreporducibility of Billock and Tsou's experiments using the non-linearity

$$f_{m,\infty}(s) = \begin{cases} 1, & \text{if} \quad s > 0, \\ 0, & \text{if} \quad s = 0, \\ -m, & \text{if} \quad s < 0, \end{cases}$$

corresponding to the sign function when $m = 1$, it does not actually reproduce the phenomenon. It is also our interest to understand theoretically why this non-linearity does not work.

CHAPTER 4

Existence of an equilibrium for neural fields under output proportional feedback

4.1 . Introduction

Investigating the dynamical mechanisms that underlie spatially structured activity states in cortical tissue is of fundamental importance for understanding a diverse array of neurobiological phenomena, encompassing both natural processes and pathological conditions.

Beyond using neuronal dynamics to comprehend the interplay between sensory-driven and self-organizing cortical activity in the primary visual cortex [CPT23; Nic+21; TPC22; TPC23a; TPC23b], neural field equations offer a valuable tool for advancing our understanding of cerebral functions characterized by propagating waves, such as the oscillatory instability observed in the mechanism of epileptic seizures and the generation of pathological oscillations in Parkinson's disease [MJ03; Cha+17].

The use of spatiotemporal models to describe the activity of neuronal populations is considerably increasing [Bre11; Tas97]. A fundamental inquiry in the analytical study of neural fields revolves around the stability of stationary solutions. This inquiry is essential for understanding the functioning of the brain as modelled by the equilibrium pattern and its implications for overall brain function.

In the purpose to disrupt pathological brain oscillations associated with Parkinson's disease, the authors of [Cha+17] proved that the closed-loop system resulting from the output proportional feedback stabilization of a class of delayed neural fields equation of Wilson-Cowan type [WC73] is input-to-state stable (ISS) for sufficiently high gain, subject to the existence of an equilibrium point for the closed-loop system.

This chapter then follows the lines of [Bri+23] providing mild conditions under which such an equilibrium exists. We show, in particular, that the boundedness of the nonlinear response functions is enough to guarantee the existence of an equilibrium.

4.2 . Presentation of the main result

In [Cha+17, Section 4], the following delayed neural fields equations are considered.

$$\tau_1(r)\frac{\partial z_1}{\partial t}(r,t) = -z_1(r,t) + S_1\left(I_1^\star(r) + \alpha(r)u(r,t) + \sum_{j=1}^{2}\int_\Omega w_{1j}(r,r')z_j(r',t-d_j(r,r'))\mathrm{d}r'\right), \tag{4.1a}$$

$$\tau_2(r)\frac{\partial z_2}{\partial t}(r,t) = -z_2(r,t) + S_2\left(I_2^\star(r) + \sum_{j=1}^{2}\int_\Omega w_{2j}(r,r')z_j(r',t-d_j(r,r'))\mathrm{d}r'\right). \tag{4.1b}$$

Here $\Omega \subset \mathbb{R}^q$ is a compact set, $z_i(r,t)$ is the neural activity at position $r \in \Omega$ and time $t \in \mathbb{R}_+$ of population $i \in \{1,2\}$, $\tau_i : \Omega \to \mathbb{R}_{>0}$ is a time constant distribution, $S_i : \mathbb{R} \to \mathbb{R}$ is a non-decreasing continuous function, $w_{ij} \in L^2(\Omega^2;\mathbb{R})$ represents the synaptic coupling distribution for $i,j \in \{1,2\}$, $d_j : \Omega^2 \to [0,\bar{d}]$ for some $\bar{d} \geq 0$, $u : \Omega \times \mathbb{R}_+ \to \mathbb{R}$ is the controlled input, $\alpha : \Omega \to \mathbb{R}_+$ is a bounded function reflecting the in-homogeneity of the received input, and $I_i^\star \in L^2(\Omega;\mathbb{R})$ is a constant uncontrolled input.

The aim of [Cha+17] is to disrupt pathological brain oscillations related to Parkinson's disease by relying on stimulation and measurements of the first neuronal population only. To that aim, the system is controlled in closed loop with a partial proportional feedback:

$$u(r,t) = -k(z_1(r,t) - z_{ref}(r)). \tag{4.2}$$

where $k \in \mathbb{R}_+$ denotes the proportional gain and $z_{ref} : \Omega \to \mathbb{R}$ is a target distribution.

In order to investigate the robust stability of the closed-loop system, the authors assume[1] *a priori* the existence of an equilibrium point $(z_1^\star, z_2^\star) \in L^2(\Omega;\mathbb{R})^2$ for (4.1a)-(4.1b), at which they aim to stabilize the system. A similar assumption was made in [Det+15], which investigates the same closed-loop.

The existence of such an equilibrium in the absence of proportional control can be established by invoking [FVG09, Theorem 3.6], which exploits compactness arguments. As stressed in [Cha+17], this result cannot readily be invoked for (4.1a)-(4.1b). As a matter of fact, the control law (4.2) does not define a compact operator, thus making the use of Schaefer's fixed point theorem more delicate.

Our main result is then the following.

Theorem 4.2.1 *Let Ω be a compact set of $\mathbb{R}^q$, $q \in \mathbb{N}$. Given any $i,j \in \{1,2\}$, let $I_i^\star \in L^2(\Omega,\mathbb{R})$, $\tau_i : \Omega \to \mathbb{R}_{>0}$, $d_i : \Omega^2 \to [0,\bar{d}]$ for some $\bar{d} \geq 0$, $w_{ij} \in L^2(\Omega^2,\mathbb{R})$, $\alpha : \Omega \to \mathbb{R}_+$ be a bounded function, and $z_{ref} \in L^2(\Omega,\mathbb{R})$. If $k \geq 0$ and $S_i : \mathbb{R} \to \mathbb{R}$ is a continuous bounded function for each $i \in \{1,2\}$, then the closed-loop system (4.1a)-(4.1b) admits at least one equilibrium in $L^2(\Omega;\mathbb{R})^2$.*

[1] More precisely, on page 266 of [Cha+17]: " For now on, we simply assumed that such an equilibrium exists. "

4.3 . Proof of the main result

In order to establish the result in Theorem 4.2.1, we first observe that $(z_1^\star, z_2^\star)$ is an equilibrium point of (4.1a)-(4.1b) if and only if it is a fixed point of the nonlinear map $T : L^2(\Omega;\mathbb{R})^2 \to L^2(\Omega;\mathbb{R})^2$ defined by $T(z_1, z_2) := (T_1(z_1, z_2), T_2(z_1, z_2))$, where

$$T_1(z_1, z_2)(r) := S_1\left(I_1^\star(r) - k\alpha(r)(z_1(r) - z_{ref}(r)) + \sum_{j=1}^{2}\int_\Omega w_{1j}(r, r')z_j(r')\mathrm{d}r'\right),$$

$$T_2(z_1, z_2)(r) := S_2\left(I_2^\star(r) + \sum_{j=1}^{2}\int_\Omega w_{2j}(r, r')z_j(r')\mathrm{d}r'\right).$$

Consider the map $\mathcal{T} : L^2(\Omega;\mathbb{R})^2 \to L^2(\Omega;\mathbb{R})^2$ defined by

$$\mathcal{T}(x_1, x_2) := (\mathcal{T}_1(x_1, x_2), \mathcal{T}_2(x_1, x_2)),$$

where

$$\mathcal{T}_1(x_1, x_2)(r) := I_1^\star(r) - k\alpha(r)(S_1(x_1(r)) - z_{ref}(r)) + \sum_{j=1}^{2}\int_\Omega w_{1j}(r, r')S_1(x_j(r'))\mathrm{d}r',$$

$$\mathcal{T}_2(x_1, x_2)(r) := I_2^\star(r) + \sum_{j=1}^{2}\int_\Omega w_{2j}(r, r')S_2(x_j(r'))\mathrm{d}r'.$$

Then $(z_1^\star, z_2^\star)$ is a fixed point of T if and only if there exists a fixed point $(x_1^\star, x_2^\star)$ of $\mathcal{T}$ such that $(z_1^\star, z_2^\star) = (S_1(x_1^\star), S_2(x_2^\star))$. Indeed, if $(z_1^\star, z_2^\star)$ is a fixed point of T, then $(z_1^\star, z_2^\star) = (S_1(x_1^\star), S_2(x_2^\star))$ for some $(x_1^\star, x_2^\star) \in L^2(\Omega, \mathbb{R})^2$ and direct computations yield that $(x_1^\star, x_2^\star)$ is a fixed point of $\mathcal{T}$. Conversely, it also follows from the definitions of T and $\mathcal{T}$ that if $(x_1^\star, x_2^\star)$ is a fixed point of $\mathcal{T}$, then $(S_1(x_1^\star), S_2(x_2^\star))$ is a fixed point of T.

Hence, it is sufficient to find a fixed point of $\mathcal{T}$ in $L^2(\Omega, \mathbb{R})^2$ in order to prove Theorem 4.2.1. This is ensured by the following lemma.

Lemma 4.3.1 *Let X be a Hilbert space, $f \in X$, $W : X \to X$ be a continuous nonlinear compact operator, $\rho : X \to X$ be a continuous nonlinear uniformly bounded operator and $\sigma : X \to X$ be a continuous nonlinear monotone operator that maps bounded sets to bounded sets. Then the map $G : X \to X$ defined by*

$$G(x) := W(\rho(x)) - \sigma(x) + f$$

admits at least one fixed point in X.

Proof. The proof is an adaptation of [FVG09, Theorem 3.6], that dealt with the uncontrolled case (*i.e.*, $k = 0$). It is based on Schaefer's fixed point theorem. Since σ is continuous, monotone, and maps bounded sets to bounded sets, the map $x \mapsto x/2 + \sigma(x)$ is a maximal

monotone operator on X according to [Bar76, Chapter 2, Corollary 1.1]. Hence the nonlinear map $H : X \to X$ defined by $H(x) := x + \sigma(x)$ has a continuous inverse H^{-1} on X. Consider the map $\pi : X \to X$ defined by $\pi(x) := H^{-1}(W(\rho(x)) + f)$. Then π is continuous and compact, since H^{-1}, ρ and W are continuous and W is compact. Set $E := \{x \in X \mid \exists \lambda \in (0,1),\, x = \lambda\pi(x)\}$. Since ρ is uniformly bounded, there exists a bounded set $B \subset X$ such that $\rho(E) \subset B$. Since W is compact and H^{-1} is continuous, $H^{-1}(W(B) + f)$ is a relatively compact set, hence $\pi(E)$ is bounded and so is E. Thus, according to Schaefer's fixed point theorem, π admits at least one fixed point $x^\star$ in X. Then $H(x^\star) = W(\rho(x^\star)) + f$, *i.e.* $x^\star$ is a fixed point of G. □

We now can present the proof of Theorem 4.2.1.

Proof. (of Theorem 4.2.1) To prove Theorem 4.2.1 from Lemma 4.3.1, we set $X = L^2(\Omega;\mathbb{R})^2$, $f = (I_1^\star + k\alpha z_{ref}, I_2^\star)$, $W(x_1,x_2)(r) = \sum_{j=1}^2(\langle w_{1j}(r,\cdot), x_j\rangle_{L^2}, \langle w_{2j}(r,\cdot), x_j\rangle)$, $\rho(x_1,x_2) = (S_1(x_1), S_2(x_2))$, $\sigma(x_1,x_2) = (k\alpha S_1(x_1), 0)$. Then $\mathcal{T} = G$. The operator W is compact as a Hilbert–Schmidt integral operator (since the maps w_{ij} are in $L^2(\Omega^2,\mathbb{R})$). Moreover, ρ is continuous and uniformly bounded since each S_i is continuous and bounded by assumption. Finally, σ is continuous, monotone and maps bounded sets to bounded sets since S_1 is continuous, non-decreasing, and bounded, and $k\alpha \geq 0$. Therefore, all the assumptions of Lemma 4.3.1 are satisfied, which ends the proof of Theorem 4.2.1. □

4.4 . Discussion and further works

In [Cha+17], the maps S_i are not assumed to be bounded. However, in most neural fields models, these activation functions are supposed to be bounded (as in [FVG09] for example). This boundedness reflects the fact that the activity of a given neuronal population cannot exceed a certain value due to biological considerations. Consequently, the boundedness of the activation functions does not induce a too demanding additional requirement in practice. In particular, this boundedness requirement holds naturally for the modeling of the neuronal populations involved in the generation of pathological oscillations related to Parkinson's disease, which is the main scope of [Cha+17; Det+15].

Nevertheless, neural fields are sometimes used with unbounded activation functions S_i, such as Rectified Linear Units (ReLU). Then, Theorem 4.2.1 does not apply but two additional results can be given. Firstly, if they are linear, then σ, W and ρ in Lemma 4.3.1 are also linear. Hence the closed-loop (4.1a)-(4.1b) admits an equilibrium if and only if f lies in the range of the linear operator $x \mapsto x + \sigma(x) - W(\rho(x))$, and it is unique if and only if the operator is injective. Secondly, if the map π is a contraction, then the existence of a unique fixed point of π (hence of G) follows from the Banach fixed-point theorem (instead of Schaefer's) with no boundedness assumption on the maps S_i.

Note that Lemma 4.3.1 allows to take into account more general neural fields than (4.1) and more general feedback laws than (4.2). In particular, higher dimensional models (with state $(z_i)_{1\leq i\leq N}$, $N \in \mathbb{N}$) as well as nonlinear feedback laws can be considered. The only assumption to check is that σ remains a continuous monotone operator, mapping bounded sets to bounded sets, or more generally that $H : x \mapsto x + \sigma(x)$ has a continuous inverse.

Instead of the partial proportional feedback (4.2), a partial proportional-integral feedback of the form

$$\begin{aligned} \dot{y}_1(r,t) &= z_1(r,t) - z_{ref}(r), \\ u(r,t) &= -k_P(z_1(r,t) - z_{ref}(r)) - k_I y_1(r,t), \end{aligned} \tag{4.3}$$

where k_P and k_I denote non-negative gains, can also be considered. In that case, if z_{ref} lies in the image of $L^2(\Omega;R)$ by S_1 and under the conditions of Theorem 4.2.1, the closed-loop system (4.1)-(4.3) admits at least one equilibrium $(z_1^\star, z_2^\star, y_1^\star) \in L^2(\Omega;\mathbb{R})^3$. Moreover, $z_1^\star = z_{ref}$.

The proof follows directly from applying Theorem 4.2.1 (or [FVG09, Theorem 3.6]) to the z_2-subsystem to find $z_2^\star$ satisfying

$$z_2^\star(r) = S_2(I_2^\star(r) + \int_\Omega w_{21}(r,r')z_{ref}(r')\mathrm{d}r' + \int_\Omega w_{22}(r,r')z_2^\star(r')\mathrm{d}r'),$$

and then setting $y_1^\star$ such that

$$z_{ref}(r) = S_1(I_1^\star(r) - k_I\alpha(r)y_1^\star(r) + \int_\Omega w_{11}(r,r')z_{ref}(r')\mathrm{d}r' + \int_\Omega w_{12}(r,r')z_2^\star(r')\mathrm{d}r').$$

Note that the asymptotic behaviour of the closed-loop system (4.1)-(4.3) has not been investigated, contrarily to (4.1a)-(4.1b), which is considered in [Cha+17].

Sufficient conditions are given in [Cha+17] for the input-to-state stability (ISS) of (4.1a)-(4.1b) at some equilibrium point under the assumption of the existence of an equilibrium. Naturally, this implies the uniqueness of the equilibrium point, hence of the fixed point of T.

Under the additional assumption that I_i, S_i, α and z_{ref} are continuous maps, it can be proved that T defines a mapping from $C(\Omega;\mathbb{R})^2$ into itself, and admits a fixed point in $C(\Omega;\mathbb{R})^2$. Indeed, following the proof of Lemma 4.3.1, the only missing assumptions are that $X = C(\Omega;\mathbb{R})^2$ is not a Hilbert space but a Banach space, and σ is not monotone. However, the map $H : C(\Omega;\mathbb{R})^2 \to C(\Omega;\mathbb{R})^2$ defined by $H(x) := x + \sigma(x)$ still admits a continuous inverse. Therefore, the conclusion of Lemma 4.3.1 remains valid. In particular, if the fixed point given in Theorem 4.2.1 (*a priori* lying in $L^2(\Omega;\mathbb{R})^2$) is unique due to the ISS property shown in [Cha+17], then it actually lies $C(\Omega;\mathbb{R})^2$.

Despite the generality of the fixed-point approach developed in Lemma 4.3.1, our result does not solve the question of existence of an equilibrium in cases where the maps S_i are unbounded. In particular, ReLU activation functions such as $S_i : x \mapsto \max(0,x)$ (used to model neurons of the visual cortex for example, see [Hee92]) do not fall within our framework. This question could be investigated in future works.

APPENDIX A

Miscellaneous Complements

A.1 . Complement results for the MacKay effect

A.1.1 . Complement results for the MacKay effect description in the linear regime

This section contains various complements used in Section 3.4.2 to describe the MacKay effect when the response function in Equation (NF) is linear.

The first result is the following.

Theorem A.1.1 *Under the considerations of Remark 3.4.4, the kernel K defined in (3.42) can be recast for all $x \in \mathbb{R}^*$ as*

$$\begin{aligned}\frac{K(x)}{2\sqrt{\pi}} &= e^{-\pi|x|\sqrt{\frac{2\pi}{3}}}\cos\left(\frac{\pi}{12}+\pi|x|\sqrt{\frac{2\pi}{3}}\right)+\sum_{k=1}^{\infty}\frac{e^{-\pi c_k|x|\sqrt{\frac{2\pi}{3}}}}{c_k}\cos\left(\frac{\pi}{12}+\pi c_k|x|\sqrt{\frac{2\pi}{3}}\right)\\ &\quad+\sum_{k=1}^{\infty}\frac{e^{-\pi d_k|x|\sqrt{\frac{2\pi}{3}}}}{d_k}\sin\left(\frac{\pi}{12}-\pi d_k|x|\sqrt{\frac{2\pi}{3}}\right),\end{aligned} \tag{A.1}$$

where

$$c_k=\sqrt{1+6k}\qquad k\in\mathbb{N}\qquad \textit{and}\qquad d_k=\sqrt{-1+6k},\qquad k\in\mathbb{N}^*. \tag{A.2}$$

Proof. We start by introducing for a fixed $x\in\mathbb{R}$, the function

$$g: z\in\mathbb{C}\mapsto g(z)=e^{2i\pi zx}\frac{\widehat{\omega_1}(z)}{1-\widehat{\omega_1}(z)}=e^{2i\pi zx}\widehat{K}(z),\qquad \widehat{\omega_1}(z)=e^{-z^2}-e^{-2z^2}. \tag{A.3}$$

We have that g is a meromorphic function with simple poles (zeroes of the exponential polynomial h defined in (3.44)) distributed as in Figure A.1 that we enumerate as $p_{k,\ell}$ and $q_{k,\ell}$ where $\ell\in\{0,\cdots,3\}$, by

$$p_{k,\ell}=c_k e^{i\frac{\pi}{4}}i^{\ell}\sqrt{\frac{\pi}{3}},\qquad k\in\mathbb{N}\qquad\text{and}\qquad q_{k,\ell}=d_k e^{i\frac{\pi}{4}}i^{\ell}\sqrt{\frac{\pi}{3}},\qquad k\in\mathbb{N}^*, \tag{A.4}$$

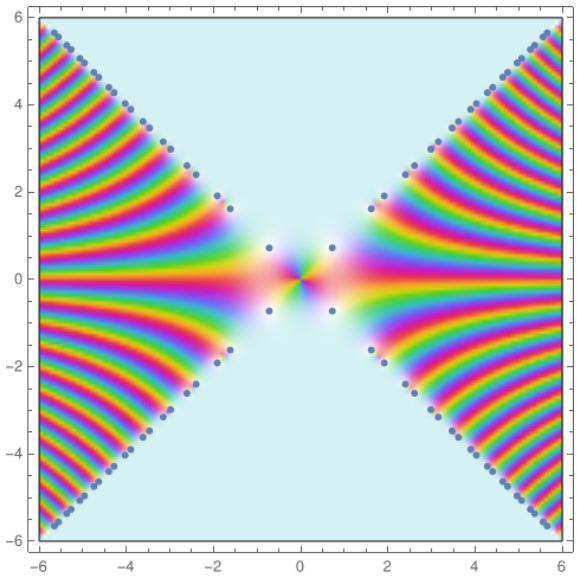

Figure A.1: Zeroes in the complex plane of the exponential polynomial h defined in (3.44). Here $\kappa = \mu = 1$, $2\pi^2\sigma_1^2 = 1$ and $2\pi^2\sigma_2^2 = 2$.

where c_k and d_k are defined as in (A.2). Since $\widehat{\omega}(p_{k,\ell}) = 1 = \widehat{\omega}(q_{k,\ell})$, we find the residues of g to be given by

$$\mathrm{Res}(g, p_{k,\ell}) = -\frac{e^{i\frac{\pi}{4}} i^\ell e^{i(-1)^\ell \frac{\pi}{3}}}{2c_k\sqrt{\pi}} e^{2i\pi x p_{k,\ell}}, \qquad k \in \mathbb{N}, \tag{A.5}$$

$$\mathrm{Res}(g, q_{k,\ell}) = \frac{e^{i\frac{\pi}{4}} i^\ell e^{-i(-1)^\ell \frac{\pi}{3}}}{2d_k\sqrt{\pi}} e^{2i\pi x q_{k,\ell}}, \qquad k \in \mathbb{N}^*. \tag{A.6}$$

We now fix $x > 0$, and we let

$$R_n := \sqrt{n\pi}, \qquad n \in \mathbb{N}^*.$$

We consider the path Γ_n straight along the real line axis from $-R_n$ to R_n and then counterclockwise along a semicircle centred at $z = 0$ in the upper half of the complex plane, $\Gamma_n = [-R_n, R_n] \cup C_n^+$, where $C_n^+ = \{R_n e^{i\phi} \mid \phi \in [0, \pi]\}$. Then, by the residue Theorem, one has for all $n \in \mathbb{N}^*$,

$$\begin{aligned}
\int_{-R_n}^{R_n} g(\xi)d\xi + \int_{C_n^+} g(z)dz &= 2\pi i \sum_{\ell=0}^{\ell=1}\sum_{k=0}^{n-1} \mathrm{Res}(g, p_{k,\ell}) + 2\pi i \sum_{\ell=0}^{\ell=1}\sum_{k=1}^{n-1} \mathrm{Res}(g, q_{k,\ell}) \\
&= 2\sqrt{\pi} e^{-\pi x\sqrt{\frac{2\pi}{3}}} \cos\left(\frac{\pi}{12} + \pi x\sqrt{\frac{2\pi}{3}}\right) + \\
&\quad 2\sqrt{\pi}\sum_{k=1}^{n-1} \frac{e^{-\pi c_k x\sqrt{\frac{2\pi}{3}}}}{c_k} \cos\left(\frac{\pi}{12} + \pi c_k x\sqrt{\frac{2\pi}{3}}\right) + \\
&\quad 2\sqrt{\pi}\sum_{k=1}^{n-1} \frac{e^{-\pi d_k x\sqrt{\frac{2\pi}{3}}}}{d_k} \sin\left(\frac{\pi}{12} - \pi d_k x\sqrt{\frac{2\pi}{3}}\right).
\end{aligned} \tag{A.7}$$

We set

$$A_n(x) := \int_{C_n^+} g(z)dz.$$

Then, one obtains,

$$\begin{aligned} |A_n(x)| &\leq R_n \int_0^{\pi} e^{-2R_n\pi x\sin(\phi)}|\widehat{K}(R_ne^{i\phi})|d\phi \\ &= \underbrace{R_n \int_0^{\frac{\pi}{4}} e^{-2R_n\pi x\sin(\phi)}|\widehat{K}(R_ne^{i\phi})|d\phi}_{J_1} + \underbrace{R_n \int_{\frac{\pi}{4}}^{\frac{3\pi}{4}} e^{-2R_n\pi x\sin(\phi)}|\widehat{K}(R_ne^{i\phi})|d\phi}_{J_2} \\ &\quad + \underbrace{R_n \int_{\frac{3\pi}{4}}^{\pi} e^{-2R_n\pi x\sin(\phi)}|\widehat{K}(R_ne^{i\phi})|d\phi}_{J_3}. \end{aligned} \tag{A.8}$$

Since $|\widehat{K}(R_ne^{i\phi})| \leq 1$ for all $\phi \in [0,\pi]$, uniformly w.r.t. $n \in \mathbb{N}^*$, one has for all $x > 0$,

$$\begin{aligned} J_2 := R_n \int_{\frac{\pi}{4}}^{\frac{3\pi}{4}} e^{-2R_n\pi x\sin(\phi)}|\widehat{K}(R_ne^{i\phi})|d\phi &\leq R_n \int_{\frac{\pi}{4}}^{\frac{3\pi}{4}} e^{-2R_n\pi x\sin(\phi)}d\phi \\ &\leq \frac{\pi R_n}{2} e^{-R_n\pi x\sqrt{2}} \xrightarrow[n\to+\infty]{} 0. \end{aligned} \tag{A.9}$$

On the other hand, there exist a positive constant $C > 0$ independent of $n \in \mathbb{N}^*$ ($C := 3/2$ is valid) such that for all $\phi \in [0,\pi]$, it holds

$$|\widehat{K}(R_ne^{i\phi})| = \left|\frac{\widehat{\omega_1}(R_ne^{i\phi})}{1-\widehat{\omega_1}(R_ne^{i\phi})}\right| \leq C|\widehat{\omega_1}(R_ne^{i\phi})| \leq C\left(e^{-R_n^2\cos(2\phi)} + e^{-2R_n^2\cos(2\phi)}\right), \qquad \forall n \in \mathbb{N}^*.$$

Since $\cos(2\phi) \geq -\frac{4}{\pi}\phi + 1$ for all $\phi \in [0,\pi/4]$, one deduces

$$\begin{aligned} J_1 + J_3 &\leq 2R_n \int_0^{\frac{\pi}{4}} e^{-2R_n\pi x\sin(\phi)}|\widehat{K}(R_ne^{i\phi})|d\phi \leq 2CR_n \int_0^{\frac{\pi}{4}} e^{-R_n^2\cos(2\phi)}d\phi \\ &\leq 4CR_ne^{-R_n^2} \int_0^{\frac{\pi}{4}} e^{\frac{4}{\pi}R_n^2\phi}d\phi = \frac{C\pi}{R_n}\left[1-e^{-R_n^2}\right] \xrightarrow[n\to+\infty]{} 0. \end{aligned} \tag{A.10}$$

To summarise, one has for all $x > 0$,

$$\int_{C_n^+} g(z)dz \xrightarrow[n\to+\infty]{} 0.$$

By taking the limit as $n \to +\infty$ in (A.7) we find for all $x > 0$,

$$\begin{aligned} \frac{K(x)}{2\sqrt{\pi}} &= e^{-\pi x\sqrt{\frac{2\pi}{3}}}\cos\left(\frac{\pi}{12} + \pi x\sqrt{\frac{2\pi}{3}}\right) + \sum_{k=1}^{+\infty} \frac{e^{-\pi c_k x\sqrt{\frac{2\pi}{3}}}}{c_k}\cos\left(\frac{\pi}{12} + \pi c_k x\sqrt{\frac{2\pi}{3}}\right) \\ &\quad + \sum_{k=1}^{+\infty} \frac{e^{-\pi d_k x\sqrt{\frac{2\pi}{3}}}}{d_k}\sin\left(\frac{\pi}{12} - \pi d_k x\sqrt{\frac{2\pi}{3}}\right). \end{aligned} \tag{A.11}$$

Finally, the result follows at once since K is an even function. □

Remark A.1.1 *Since the kernel K is even on $\mathbb{R}$, throughout the following, we restrict its study to $\mathbb{R}_+$.*

In the following lines, we aim to prove that K admits a discrete and countable set of zeroes on $\mathbb{R}_+^*$. It is a consequence of the following.

Lemma A.1.1 *For all $x \in \mathbb{R}_+^*$, it holds that*

$$\frac{e^{\pi x\sqrt{\frac{2\pi}{3}}}K(x)}{2\sqrt{\pi}} = \cos\left(\frac{\pi}{12} + \pi x\sqrt{\frac{2\pi}{3}}\right) + \frac{S(x)}{x}, \tag{A.12}$$

where

$$|S(x)| \leq \frac{\sqrt{6}}{3\pi^2}. \tag{A.13}$$

Moreover, the derivative of K satisfies

$$\frac{\sqrt{3}e^{\pi x\sqrt{\frac{2\pi}{3}}}K'(x)}{4\pi^2} = -\sin\left(\frac{\pi}{3} + \pi x\sqrt{\frac{2\pi}{3}}\right) + T(x), \tag{A.14}$$

where

$$|T(x)| \leq \frac{1 + \pi x\sqrt{\frac{2\pi}{3}}}{\pi^3 x^2}. \tag{A.15}$$

Proof. Let $x > 0$, one starts with the equation

$$\frac{K(x)}{2\sqrt{\pi}} = e^{-\pi x\sqrt{\frac{2\pi}{3}}}\cos\left(\frac{\pi}{12} + \pi x\sqrt{\frac{2\pi}{3}}\right) + R_1(x) + R_2(x),$$

where $R_1(x) = \sum_{k=1}^{+\infty} r_1(k)\cos\left(\frac{\pi}{12} + \pi c_k x\sqrt{\frac{2\pi}{3}}\right)$ and $R_2(x) = \sum_{k=1}^{+\infty} r_2(k)\sin\left(\frac{\pi}{12} - \pi d_k x\sqrt{\frac{2\pi}{3}}\right)$. The functions r_1 and r_2 are defined on $\mathbb{R}_+$ and $[1/3, +\infty)$ respectively by

$$r_1(t) = \frac{e^{-A\sqrt{1+6t}}}{\sqrt{1+6t}}, \qquad r_2(t) = \frac{e^{-A\sqrt{-1+6t}}}{\sqrt{-1+6t}} \qquad \text{with} \quad A = \pi x\sqrt{\frac{2\pi}{3}}.$$

Since r_1 is decreasing on $\mathbb{R}_+$ one deduces that

$$|R_1(x)| \leq \sum_{k=1}^{+\infty} r_1(k) \leq \sum_{k=1}^{+\infty}\int_{k-1}^{k} r_1(t)\,dt = \int_0^{\infty} r_1(t)\,dt = \int_0^{\infty} e^{-A\sqrt{1+6t}}\frac{dt}{\sqrt{1+6t}} = \frac{e^{-A}}{3A}.$$

The same argument gives the same inequality for $|R_2(x)|$ and inequality (A.13) follows at once. On the other hand, it is straightforward to observe that the sum $S(x)$ in (A.12) is uniformly

(normally in fact) convergent on $(-\infty,-B]\cup[B,+\infty)$ for all $B>0$. Thus, after derivation under the sum, one finds for all $x>0$,

$$\begin{aligned}\frac{\sqrt{3}e^{\pi x\sqrt{\frac{2\pi}{3}}}K'(x)}{4\pi^2} &= -\sin\left(\frac{\pi}{3}+\pi x\sqrt{\frac{2\pi}{3}}\right)-e^{\pi x\sqrt{\frac{2\pi}{3}}}\sum_{k=1}^{\infty}e^{-\pi c_k x\sqrt{\frac{2\pi}{3}}}\sin\left(\frac{\pi}{3}+\pi c_k x\sqrt{\frac{2\pi}{3}}\right)\\ &\quad -e^{\pi x\sqrt{\frac{2\pi}{3}}}\sum_{k=1}^{\infty}e^{-\pi d_k x\sqrt{\frac{2\pi}{3}}}\sin\left(\frac{\pi}{3}-\pi d_k x\sqrt{\frac{2\pi}{3}}\right)\\ &= -\sin\left(\frac{\pi}{3}+\pi x\sqrt{\frac{2\pi}{3}}\right)+T(x),\end{aligned}$$

where

$$|T(x)|\le e^{\pi x\sqrt{\frac{2\pi}{3}}}\sum_{k=1}^{\infty}\left(e^{-\pi c_k x\sqrt{\frac{2\pi}{3}}}+e^{-\pi d_k x\sqrt{\frac{2\pi}{3}}}\right)\le 2e^{\pi x\sqrt{\frac{2\pi}{3}}}\sum_{k=1}^{\infty}e^{-\pi d_k x\sqrt{\frac{2\pi}{3}}},$$

since $c_k\ge d_k$ for all $k\ge 1$. But one has

$$\sum_{k=1}^{\infty}e^{-\pi d_k x\sqrt{\frac{2\pi}{3}}}\le\sum_{k=1}^{\infty}\int_{k-\frac{2}{3}}^{k}e^{-\pi x\sqrt{-1+6t}\sqrt{\frac{2\pi}{3}}}dt=\int_{\frac{1}{3}}^{\infty}e^{-\pi x\sqrt{-1+6t}\sqrt{\frac{2\pi}{3}}}dt=\frac{1+\pi x\sqrt{\frac{2\pi}{3}}}{2\pi^3x^2}e^{-\pi x\sqrt{\frac{2\pi}{3}}},$$

so that inequality (A.15) follows at once and completes the proof of the lemma. □

Proposition A.1.1 *Let $(x_k)_{k\in\mathbb{N}^*}$ and $(y_k)_{k\in\mathbb{N}^*}$ denote the sequences of zeroes and extrema of the function $x\mapsto\cos(\pi/12+\pi x\sqrt{2\pi/3})$ on $\mathbb{R}_+^*$ respectively. There exists $(z_k)_{k\in\mathbb{N}^*}$, sequence of zeroes of K in $\mathbb{R}_+^*$ such that z_k is the unique zero of K in the interval $I_k:=]y_k,y_{k+1}[$ for all $k\in\mathbb{N}^*$ and*

$$|x_{k+1}-z_k|\le\frac{\sqrt{3}}{\pi\sqrt{2\pi}}\arcsin\left(\frac{8}{\pi(12k-1)}\right),\qquad\forall k\in\mathbb{N}^*.\tag{A.16}$$

Proof. We fix $k\in\mathbb{N}^*$, then one has

$$|S(y_k)|\le\frac{2}{\pi\sqrt{6\pi}y_k}=\frac{8}{\pi(12k-1)}\le\frac{8}{11\pi}<1,$$

by Lemma A.1.1. One deduces that

$$e^{\pi y_k\sqrt{\frac{2\pi}{3}}}\frac{K(y_k)}{2\sqrt{\pi}}=(-1)^k+S(y_k)\begin{cases}<0, & \text{if } k \text{ is odd,}\\ >0, & \text{if } k \text{ is even.}\end{cases}$$

It follows that K admits at least one zero z_k in the interval I_k by the intermediate value theorem. Let us prove that z_k is the unique zero in this interval. We let $\widetilde{z}$ be an arbitrary zero of K in the interval I_k and set $e_k:=\widetilde{z}-x_{k+1}$. Then one has by Lemma A.1.1

$$S(\widetilde{z})=-\cos\left(\frac{\pi}{12}+\pi\widetilde{z}\sqrt{\frac{2\pi}{3}}\right)=(-1)^k\sin\left(\pi e_k\sqrt{\frac{2\pi}{3}}\right),\tag{A.17}$$

and

$$\left|\sin\left(\pi e_k\sqrt{\frac{2\pi}{3}}\right)\right| \leq \frac{2}{\pi\sqrt{6\pi}\widetilde{z}} \leq \frac{2}{\pi\sqrt{6\pi}y_k} \leq \frac{2}{\pi\sqrt{6\pi}y_1} = \frac{8}{11\pi}. \tag{A.18}$$

On the other hand, using (A.17) and trigonometric identity for sine, one obtains

$$\begin{aligned}\frac{\sqrt{3}e^{\pi\widetilde{z}\sqrt{\frac{2\pi}{3}}}K'(\widetilde{z})}{4\pi^2} &= -\sin\left(\frac{\pi}{12}+\pi\widetilde{z}\sqrt{\frac{2\pi}{3}}+\frac{\pi}{4}\right)+T(\widetilde{z})\\ &= \frac{(-1)^{k+1}}{\sqrt{2}}\cos\left(\pi e_k\sqrt{\frac{2\pi}{3}}\right)+\frac{1}{\sqrt{2}}S(\widetilde{z})+T(\widetilde{z}).\end{aligned} \tag{A.19}$$

By using (A.17), (A.18) and (A.15) one finds

$$\cos\left(\pi e_k\sqrt{\frac{2\pi}{3}}\right) \geq \sqrt{1-\frac{8}{11\pi}} > \sqrt{1-\frac{1}{2}} = \frac{1}{\sqrt{2}},$$

and

$$\left|\frac{1}{\sqrt{2}}S(\widetilde{z})+T(\widetilde{z})\right| \leq \frac{1}{\sqrt{2}}\frac{8}{11\pi}+\frac{1+\pi y_1\sqrt{\frac{2\pi}{3}}}{\pi^3 y_1^2} < \frac{1}{2}.$$

It follows that

$$K'(\widetilde{z})\begin{cases}>0, & \text{if} \quad k \quad \text{is odd},\\ <0, & \text{if} \quad k \quad \text{is even}.\end{cases}$$

Let $\widetilde{z}$ and $\widetilde{z}'$ be successive zeroes of K in I_k and assume that k is odd to be fixed. Then $K'(\widetilde{z})>0$ and $K'(\widetilde{z}')>0$. By Rolle's theorem, there exists $\widetilde{z}''\in(\widetilde{z},\widetilde{z}')$ such that $K(\widetilde{z}'')=0$ and $K'(\widetilde{z}'')<0$, which is a contradiction of the fact that any zero $\widetilde{z}$ in I_k satisfies $K'(\widetilde{z})>0$. Thus z_k is the unique zero of K in the interval I_k. Finally, inequality (A.18) applied with $\widetilde{z}=z_k$ leads to inequality (A.16), and this completes the proof of the proposition. □

Remark A.1.2 *Suppose we model the interaction of V1 neurons in Equation (NF) with a Gaussian kernel ω. In that case, we will obtain that the associated kernel $\widehat{K}$ defined in (A.3) has two isolated poles located on the imaginary axis of the complex plane. The zero-order terms which dominate the expansion of K given by (A.1) are only an exponential decreasing function without a cosine multiplicative factor. Therefore, the kernel K will never have infinitely many discrete distributed zeroes.*

A.1.2 . Complements for the MacKay effect description in the nonlinear regime

The results provided in this section were used in Section 3.4.3 to describe the MacKay effect when the response function in Equation (NF) is nonlinear.

We recall from Theorem 3.3.1 that, given $1\leq p\leq\infty$ and $I\in L^p(\mathbb{R}^2)$, then for any $a_0\in L^p(\mathbb{R}^2)$, the initial value Cauchy problem associated with Equation (NF) has a unique solution $a\in\mathscr{X}_p$. It is implicitly given for all $x\in\mathbb{R}^2$, and $t\geq 0$ by

$$a(x,t)=e^{-t}a_0(x)+\left(1-e^{-t}\right)I(x)+\mu\int_0^t e^{-(t-s)}(\omega*f(a))(x,s)ds. \tag{A.20}$$

Given $I \in L^\infty(\mathbb{R}^2)$, the following theorem improves the upper bound of the L^∞-norm of the stationary state $a_I \in L^\infty(\mathbb{R}^2)$ provided in (3.20).

Theorem A.1.2 *Let $a_0 \in L^\infty(\mathbb{R}^2)$, $I \in L^\infty(\mathbb{R}^2)$ with $\|I\|_\infty = 1$ and $a \in \mathscr{X}_\infty$ be the solution of (NF). It holds*

$$\limsup_{t\to+\infty} \|a(\cdot,t)\|_\infty \leq g_1, \tag{A.21}$$

where $g_1 > 0$ is the smaller fixed point of the following function

$$g : x \in \mathbb{R} \longmapsto 1 + \frac{\mu}{\mu_0} f(x) \in \mathbb{R}_+^*. \tag{A.22}$$

Proof. We start by using (A.20) (3.10) and Minkowski's inequality to obtain for a.e. $x \in \mathbb{R}^2$ and every $t \geq 0$,

$$|a(x,t)| \leq e^{-t}\|a_0\|_{L^\infty} + (1 - e^{-t}) + \frac{\mu}{\mu_0}(1 - e^{-t}). \tag{A.23}$$

Letting $t \to \infty$ in the last inequality, we find $V_\infty := \limsup_{t\to+\infty} \|a(\cdot,t)\|_\infty \leq 1 + \mu/\mu_0$, showing in particular that $V_\infty < \infty$. It follows that

$$\forall \varepsilon > 0,\ \exists T_\varepsilon > 0 \text{ s.t., } \forall t \geq T_\varepsilon,\ \ \|a(\cdot,t)\|_\infty \leq V_\infty + \varepsilon. \tag{A.24}$$

Applying the variation of constants formula (A.20), starting at $T_\varepsilon > 0$, one deduces for every $t > T_\varepsilon$ that

$$\begin{aligned} \|a(\cdot,t)\|_\infty &\leq e^{-(t-T_\varepsilon)}\|a(\cdot,T_\varepsilon)\|_\infty + \left(1 - e^{-(t-T_\varepsilon)}\right) + \mu\|\omega\|_1 \int_{T_\varepsilon}^t e^{-(t-s)} f(\|a(\cdot,s)\|_\infty) ds \\ &\leq e^{-(t-T_\varepsilon)}(V_\infty + \varepsilon) + 1 + \frac{\mu}{\mu_0} f(V_\infty + \varepsilon). \end{aligned} \tag{A.25}$$

Letting respectively $t \to \infty$ and $\varepsilon \to 0$ in the preceding inequality we find

$$V_\infty \leq 1 + \frac{\mu}{\mu_0} f(V_\infty). \tag{A.26}$$

Let $(u_n)_n$ be the real sequence defined by

$$u_0 = V_\infty, \qquad u_{n+1} = g(u_n), \qquad \forall n \geq 1. \tag{A.27}$$

Then $(u_n)_n$ is a bounded and non-decreasing sequence.

The boundedness of $(u_n)_n$ follows from the boundedness[1] of the sigmoid function f. Let us prove by induction that the sequence $(u_n)_n$ is increasing. Due to the inequality (A.26), one has

$$u_1 = g(u_0) = 1 + \frac{\mu}{\mu_0} f(u_0) = 1 + \frac{\mu}{\mu_0} f(V_\infty) \geq V_\infty = u_0.$$

[1]Notice that in the case where the response function f is only Lipschitz continuous (with the Lipschitz constant equal to $f'(0) = 1$) but not bounded, the sequence $(u_n)_n$ is still bounded, via

$$|u_n| \leq V_\infty + \frac{\mu_0}{\mu_0 - \mu}, \qquad \forall n \in \mathbb{N}.$$

If $u_n \geq u_{n-1}$ then, since f is non-decreasing, one obtains

$$u_{n+1} = g(u_n) = 1 + \frac{\mu}{\mu_0} f(u_n) \geq 1 + \frac{\mu}{\mu_0} f(u_{n-1}) = g(u_{n-1}) = u_n,$$

showing that $(u_n)_n$ is a non-decreasing sequence. The monotone convergence and fixed point Theorems, we have that $(u_n)_n$ converges to the smaller fixed point $g_1 > 0$ of the function g, and (A.21) follows. □

Let $1 \leq p \leq \infty$, we introduce for every $I \in L^p(\mathbb{R}^2)$, the map $\Phi_I : L^p(\mathbb{R}^2) \mapsto L^p(\mathbb{R}^2)$ defined for all $v \in L^p(\mathbb{R}^2)$ by

$$\Phi_I(v) = I + \mu\omega * f(v). \tag{A.28}$$

Theorem A.1.3 *Let $2 \leq p \leq \infty$. If $\mu < \mu_0$, then Ψ belongs to $C^1(L^p(\mathbb{R}^2); L^p(\mathbb{R}^2))$ and the differential at $I \in L^p(\mathbb{R}^2)$ is given by*

$$D\Psi(I)h = (\mathrm{Id} - D\Psi(I))^{-1}h, \qquad \forall h \in L^p(\mathbb{R}^2). \tag{A.29}$$

The proof of Theorem A.1.3 is a consequence of the following two lemmas.

Lemma A.1.2 *Let $2 \leq p \leq \infty$ and $I \in L^p(\mathbb{R}^2)$. If $\mu < \mu_0$, then Φ_I belongs to the space $C^1(L^p(\mathbb{R}^2); L^p(\mathbb{R}^2))$ and the differential at $v \in L^p(\mathbb{R}^2)$ is given by*

$$(D\Phi_I(v)h)(x) = \mu \int_{\mathbb{R}^2} \omega(x-y) f'(v(y))h(y)dy, \qquad \forall h \in L^p(\mathbb{R}^2),\ x \in \mathbb{R}^2, \tag{A.30}$$

and the following holds

$$\|D\Phi_I(v)\|_{\mathscr{L}(L^p(\mathbb{R}^2))} < 1. \tag{A.31}$$

Proof. It is straightforward to show that for all $1 \leq p \leq \infty$, and $I \in L^p(\mathbb{R}^2)$, the map Φ_I is Gateau-differentiable at every $v \in L^p(\mathbb{R}^2)$, the Gateau-differential is given for every $h \in L^p(\mathbb{R}^2)$ by (A.30) and

$$\|D\Phi_I(v)h\|_p \leq \frac{\mu}{\mu_0}\|h\|_p. \tag{A.32}$$

Let us now show that for all $2 \leq p \leq \infty$, the Gateau-differential

$$\begin{aligned} D\Phi_I : \quad L^p(\mathbb{R}^2) &\longrightarrow \mathscr{L}(L^p(\mathbb{R}^2)) \\ v &\longmapsto D\Phi_I(v), \end{aligned} \tag{A.33}$$

is continuous. To this end, we will prove that $D\Phi_I$ is Lipschitz continuous. Let $v_1, v_2 \in L^p(\mathbb{R}^2)$ and $h \in L^p(\mathbb{R}^2)$, we set

$$R_h : x \in \mathbb{R}^2 \longmapsto R_h(x) = \int_{\mathbb{R}^2} \omega(x-y)[f'(v_1(y)) - f'(v_2(y))]h(y)dy. \tag{A.34}$$

Using Hölder inequality, we find

$$|R_h(x)|^p \leq \|\omega\|_q \left(\int_{\mathbb{R}^2} |f'(v_1(y)) - f'(v_2(y))|^q \frac{|\omega(x-y)|^q}{\|\omega\|_q^q} dy \right)^{\frac{p}{q}} \|h\|_p^p.$$

It follows by Jensen inequality' and f''_∞-Lipschitz continuity of f' (f is at least $C^2(\mathbb{R})$ by assumption), that,

$$|R_h(x)|^p \leq \|\omega\|_q^{1-q}(f''_\infty)^p \left(\int_{\mathbb{R}^2} |v_1(y)-v_2(y)|^p|\omega(x-y)|^q dy\right)\|h\|_p^p,$$

provided $p/q \geq 1$, i.e., $2 \leq p \leq \infty$. Therefore,

$$\|D\Phi_I(v_1)h - D\Phi_I(v_2)h\|_p \leq \mu f''_\infty \|\omega\|_q \|v_1-v_2\|_p \|h\|_p,$$

and then

$$\begin{aligned}\|D\Phi_I(v_1)-D\Phi_I(v_2)\|_{\mathscr{L}(L^p(\mathbb{R}^2))} &= \sup_{\substack{h\in L^p(\mathbb{R}^2)\\ \|h\|_p=1}} \|D\Phi_I(v_1)h - D\Phi_I(v_2)h\|_p \\ &\leq \mu f''_\infty \|\omega\|_q \|v_1-v_2\|_p.\end{aligned}$$

Finally, using (A.32) we find for all $v \in L^p(\mathbb{R}^2)$,

$$\|D\Phi_I(v)\|_{\mathscr{L}(L^p(\mathbb{R}^2))} = \sup_{\substack{h\in L^p(\mathbb{R}^2)\\ \|h\|_p=1}} \|D\Phi_I(v)h\|_p \leq \frac{\mu}{\mu_0} < 1.$$

□

Lemma A.1.3 *Let $2 \leq p \leq \infty$. Under assumption $\mu < \mu_0$, the map*

$$\begin{aligned}\mathcal{G}: \quad L^p(\mathbb{R}^2)\times L^p(\mathbb{R}^2) &\longrightarrow L^p(\mathbb{R}^2)\\ (I,a) &\longmapsto \mathcal{G}(I,\Psi(I)) = a - \Phi_I(a),\end{aligned} \tag{A.35}$$

belongs to $C^1(L^p(\mathbb{R}^2)\times L^p(\mathbb{R}^2); L^p(\mathbb{R}^2))$ and the partial derivative $D_a\mathcal{G}(I,a)$ is invertible in $\mathscr{L}(L^p(\mathbb{R}^2))$.

Proof. Since Φ_I is differentiable at $a \in L^p(\mathbb{R}^2)$ for all $I \in L^p(\mathbb{R}^2)$, one has for all $(J,b) \in L^p(\mathbb{R}^2)\times L^p(\mathbb{R}^2)$,

$$\begin{aligned}\mathcal{G}(I+J,a+b) &= a+b-\Phi_{I+J}(a) - D\Phi_{I+J}(a)b + o(\|b\|_p)\\ &= \mathcal{G}(I,a) + (\mathrm{Id} - D\Phi_I(a))b - J + o(\|b\|_p).\end{aligned}$$

The map $L_{(I,a)} : L^p(\mathbb{R}^2)\times L^p(\mathbb{R}^2) \longrightarrow L^p(\mathbb{R}^2)$, $L_{(I,a)}(J,b) = (\mathrm{Id} - D\Phi_I(a))b - J$, is linear and bounded,

$$\|L_{(I,a)}(J,b)\|_{L^p(\mathbb{R}^2)} \leq \left(1+\frac{\mu}{\mu_0}\right)\|(J,b)\|_{L^p(\mathbb{R}^2)\times L^p(\mathbb{R}^2)}.$$

It follows that $\mathcal{G}$ is differentiable at $(I,a) \in L^p(\mathbb{R}^2)\times L^p(\mathbb{R}^2)$ and

$$D\mathcal{G}(I,a)(J,b) = (\mathrm{Id} - D\Phi_I(a))b - J, \qquad \forall (J,b) \in L^p(\mathbb{R}^2)\times L^p(\mathbb{R}^2).$$

We now show that the map $(I,a)\in L^p(\mathbb{R}^2)^2\mapsto D\mathcal{G}(I,a)\in\mathscr{L}(L^p(\mathbb{R}^2)^2,L^p(\mathbb{R}^2))$ is continuous. Let $(I_1,a_1),(I_2,a_2)\in L^p(\mathbb{R}^2)\times L^p(\mathbb{R}^2)$. One has for all $(J,b)\in L^p(\mathbb{R}^2)\times L^p(\mathbb{R}^2)$,

$$\begin{aligned}\|D\mathcal{G}(I_1,a_1)(J,b)-D\mathcal{G}(I_2,a_2)(J,b)\|_p &= \|D\Phi_{I_1}(a_1)b-D\Phi_{I_2}(a_2)b\|_p\\ &\leq \|D\Phi_{I_1}(a_1)-D\Phi_{I_1}(a_2)\|_{\mathscr{L}(L^p(\mathbb{R}^2))}\|(b,J)\|_{L^p(\mathbb{R}^2)^2}.\end{aligned}$$

It follows by Lemma A.1.2 that

$$\begin{aligned}\|D\mathcal{G}(I_1,a_1)-D\mathcal{G}(I_2,a_2)\|_{\mathscr{L}(L^p(\mathbb{R}^2)^2,L^p(\mathbb{R}^2))} &\leq \|D\Phi_{I_1}(a_1)-D\Phi_{I_2}(a_2)\|_{\mathscr{L}(L^p(\mathbb{R}^2))}\\ &\leq \mu f''_\infty\|\omega\|_q\|(I_1,a_1)-(I_2,a_2)\|_{L^p(\mathbb{R}^2)^2},\end{aligned}$$

showing that $\mathcal{G}$ belongs to $C^1(L^p(\mathbb{R}^2)\times L^p(\mathbb{R}^2);L^p(\mathbb{R}^2))$. Finally, if $I\in L^p(\mathbb{R}^2)$, $a_I:=\Psi(I)\in L^p(\mathbb{R}^2)$ then $D_a\mathcal{G}(I,a_I)=\mathrm{Id}-D\Phi_I(a_I)$, is invertible in $\mathscr{L}(L^p(\mathbb{R}^2))$ by Neumann expansion lemma. □

We now can present the proof of Theorem A.1.3.

Proof. (of Theorem A.1.3) Let $2\leq p\leq\infty$. For fixed $I\in L^p(\mathbb{R}^2)$, $a_I:=\Psi(I)\in L^p(\mathbb{R}^2)$, we have $\mathcal{G}(I,a_I)=0$, and $D_a\mathcal{G}(I,a_I)$ is invertible in $\mathscr{L}(L^p(\mathbb{R}^2))$ by Lemma A.1.3. It follows by the implicit function Theorem that there is an open neighbourhood $\mathcal{V}$ of I in $L^p(\mathbb{R}^2)$, an open neighbourhood $\mathcal{W}$ of a_I in $L^p(\mathbb{R}^2)$ and a map $\Sigma:\mathcal{V}\to\mathcal{W}$ of class C^1 such that the following holds

$$(\mathrm{I}\in\mathcal{V},\ a\in\mathcal{W}\text{ and }\ \mathcal{G}(\mathrm{I},a)=0)\Longleftrightarrow(\mathrm{I}\in\mathcal{V}\text{ and }\ a=\Sigma(\mathrm{I})).$$

Thereby, $\Psi(\cdot)|_{\mathcal{V}}=\Sigma(\cdot)$ and then Ψ is C^1 at I. Since $I\in L^p(\mathbb{R}^2)$ is arbitrary, it follows that Ψ belongs to $C^1(L^p(\mathbb{R}^2);L^p(\mathbb{R}^2))$. Moreover, taking the derivative of $\mathcal{G}(I,\Psi(I))=0$ at I, we deduce that

$$(\mathrm{Id}-D\Phi_I(\Psi(I)))\,(D\Psi(I)h)=h,\qquad\forall h\in L^p(\mathbb{R}^2).\tag{A.36}$$

Thus, (A.29) is an immediate consequence of (A.31), (A.36) and Neumann expansion lemma. □

A.2 . Complement result for Billock and Tsou's

This section contains a result used in Section 3.5.1 to prove that Equation (NF) with linear response function does not reproduce Billock and Tsou's experiments.

Theorem A.2.1 *Under the considerations of Remark 3.5.1, the kernel W_1 defined in (3.61) can be recast for all $x\in\mathbb{R}^*$ and some $\phi_k:=\phi_k(m_k,n_k)\in\mathbb{R}$ and $\theta_k:=\theta_k(m_k,n_k)\in\mathbb{R}$, as*

$$\begin{aligned}\frac{\sqrt{3}}{2\pi}W_1(x) &= \frac{e^{-2\pi m_0|x|}}{\sqrt{n_0^2+m_0^2}}\cos\left(2\pi n_0|x|+\frac{4\pi}{3}-\phi_0\right)+\\ &\sum_{k=1}^{n-1}\frac{e^{-2\pi m_k|x|}}{\sqrt{n_k^2+m_k^2}}\cos\left(2\pi n_k|x|+\frac{4\pi}{3}-\phi_k\right)+\\ &\sum_{k=1}^{n-1}\frac{e^{-2\pi e_k|x|}}{\sqrt{f_k^2+e_k^2}}\cos\left(2\pi e_k|x|+\frac{4\pi}{3}-\theta_k\right).\end{aligned}\tag{A.37}$$

Here

$$m_k^2 = \frac{1+\sqrt{1+\frac{\pi^2}{9}c_k^4}}{2}, \qquad n_k^2 = \frac{-1+\sqrt{1+\frac{\pi^2}{9}c_k^4}}{2}, \qquad k \in \mathbb{N}, \tag{A.38}$$

$$e_k^2 = \frac{1+\sqrt{1+\frac{\pi^2}{9}d_k^4}}{2}, \qquad f_k^2 = \frac{-1+\sqrt{1+\frac{\pi^2}{9}d_k^4}}{2}, \qquad k \in \mathbb{N}, \tag{A.39}$$

and c_k and d_k are given by (A.2).

Proof. We recall that for $x_1 \in \mathbb{R}$, one has

$$W_1(x_1) = \int_{-\infty}^{+\infty} e^{2i\pi x_1 \xi} \frac{\widehat{\psi_1}(\xi)}{1-\widehat{\psi_1}(\xi)} d\xi, \qquad \widehat{\psi_1}(\xi) = e^{-2(1+\xi^2)} - e^{-2(1+\xi^2)}, \qquad \xi \in \mathbb{R}.$$

We are looking for poles of the following meromorphic function

$$h(z) = \frac{\widehat{\psi_1}(z)}{1-\widehat{\psi_1}(z)} e^{2i\pi x_1 \xi}, \qquad \widehat{\psi_1}(z) = e^{-(1+z^2)} - e^{-2(1+z^2)}, \qquad z \in \mathbb{C}. \tag{A.40}$$

Since $\widehat{\psi_1}(z) = \widehat{\omega_1}(\sqrt{1+z^2})$, where $\widehat{\omega_1}$ is given as in (A.3), it follows by careful computations that the poles of h in $\mathbb{C}$ are given by $F_{k,\ell}$, $\overline{F_{k,\ell}}$, $G_{k,\ell}$ and $\overline{G_{k,\ell}}$, where for $\ell \in \{0,1\}$, one has

$$F_{k,\ell} = (-1)^\ell n_k + i m_k, \qquad k \in \mathbb{N}, \qquad \text{and} \qquad G_{k,\ell} = (-1)^\ell f_k + i e_k, \qquad k \in \mathbb{N}^*,$$

where m_k and n_k are given by (A.38), and e_k and f_k are given by (A.39).. Then the residue of h are given for $\ell \in \{0,1\}$ by

$$\mathrm{Res}(h, F_{k,\ell}) = \frac{(-1)^\ell i \overline{F_{k,\ell}} e^{(-1)^\ell i \frac{\pi}{3}}}{2\sqrt{3+\frac{\pi^2}{3}c_k^4}} e^{2i\pi x_1 F_{k,\ell}}, \qquad \mathrm{Res}(h, F_{k,\ell}) = \overline{\mathrm{Res}(h, \overline{F_{k,\ell}})}, \qquad k \in \mathbb{N}, \tag{A.41}$$

$$\mathrm{Res}(h, G_{k,\ell}) = \frac{-(-1)^\ell i \overline{G_{k,\ell}} e^{-(-1)^\ell i \frac{\pi}{3}}}{2\sqrt{3+\frac{\pi^2}{3}d_k^4}} e^{2i\pi x_1 G_{k,\ell}}, \qquad \mathrm{Res}(h, G_{k,\ell}) = \overline{\mathrm{Res}(h, \overline{G_{k,\ell}})}, \qquad k \in \mathbb{N}^*. \tag{A.42}$$

We now fix $x_1 > 0$, and we let

$$R_n := \frac{\sqrt{\sqrt{1+\frac{\pi^2}{9}c_n^4} + \sqrt{\sqrt{1+\frac{\pi^2}{9}d_n^4}}}}{2}, \qquad n \in \mathbb{N}^*.$$

We consider the path Γ_n straight along the real line axis from $-R_n$ to R_n and then counterclockwise along a semicircle centred at $z = 0$ in the upper half of the complex plane, $\Gamma_n = [-R_n, R_n] \cup C_n^+$, where $C_n^+ = \{R_n e^{i\theta} \mid \theta \in [0,\theta]\}$. Then, by the residue Theorem, one

has for all $n \in \mathbb{N}^*$,

$$\begin{aligned}\int_{-R_n}^{R_n} h(\xi)d\xi + \int_{C_n^+} h(z)dz &= 2\pi i \sum_{\ell=0}^{\ell=1}\sum_{k=0}^{n-1} \mathrm{Res}(h, F_{k,\ell}) + 2\pi i \sum_{\ell=0}^{\ell=1}\sum_{k=1}^{n-1} \mathrm{Res}(h, G_{k,\ell}) \\ &= \frac{2\pi}{\sqrt{3}} \frac{e^{-2\pi m_0|x|}}{\sqrt{n_0^2+m_0^2}} \cos\left(2\pi n_0|x| + \frac{4\pi}{3} - \phi_0\right) + \\ &\quad \frac{2\pi}{\sqrt{3}} \sum_{k=1}^{n-1} \frac{e^{-2\pi m_k|x|}}{\sqrt{n_k^2+m_k^2}} \cos\left(2\pi n_k|x| + \frac{4\pi}{3} - \phi_k\right) + \\ &\quad \frac{2\pi}{\sqrt{3}} \sum_{k=1}^{n-1} \frac{e^{-2\pi f_k|x|}}{\sqrt{f_k^2+e_k^2}} \cos\left(2\pi e_k|x| + \frac{4\pi}{3} - \theta_k\right), \qquad \text{(A.43)}\end{aligned}$$

where $\phi_k := \phi_k(m_k, n_k) \in \mathbb{R}$ and $\theta_k := \theta_k(e_k, f_k) \in \mathbb{R}$ are such that

$$\cos\phi_k = \frac{n_k}{\sqrt{m_k^2+n_k^2}}, \qquad \sin\phi_k = \frac{m_k}{\sqrt{m_k^2+n_k^2}}, \qquad k \in \mathbb{N},$$

$$\cos\theta_k = -\frac{f_k}{\sqrt{e_k^2+f_k^2}}, \qquad \sin\theta_k = \frac{e_k}{\sqrt{e_k^2+f_k^2}}, \qquad k \in \mathbb{N}^*.$$

Arguing similarly as in the proof of Theorem A.1.1, we can prove that

$$\int_{C_n^+} h(z)dz \xrightarrow[n\to+\infty]{} 0.$$

Finally passing in the limit as $n \to +\infty$ in Equation (A.43) completes the proof. □

Same-type analysis can be made to prove that the kernel W_1 has a countable and discrete set of zeroes in $(0, +\infty)$, as in the case of the kernel K studied in Section A.1.1, refer in particular to Proposition A.1.1.

APPENDIX B

A toolbox that replicates the MacKay effect and Billock and Tsou's experiments numerically

In this appendix, we provide a toolbox implemented with the Julia [Bez+17] language to perform numerical implementation for the MacKay effect [Mac57] and Billock and Tsou's experiments [BT07].

B.1 . Numerical implementation of the retino-cortical map

We need to define the retino-cortical map (see, Section 2.4.2) that maps retinal coordinates to the primary visual cortex V1.

B.1.1 . Point types

We start by defining the type of points we will use. Remembering that coordinates on the visual field (or in the retina) are polar coordinates $(r, \theta) \in [0, \infty) \times [0, 2\pi)$ from the fovea and that coordinates on V1 are standard Cartesian coordinates $(x, y) \in \mathbb{R}^2$.

```
# Standard cartesian coordinates in the retinal plane
struct CartesianPoint{T<:Real}
   x::T
   y::T
end

CartesianPoint(x::Real, y::Real) = CartesianPoint(promote(x,y)...)

  x(p::CartesianPoint) = p.x
  y(p::CartesianPoint) = p.y
```

```
# Polar coordinates in the retinal plane

struct RetinalPoint{T<:Real}
   r::T
   θ::T
end

RetinalPoint(r::Real, θ::Real) = RetinalPoint(promote(r,θ)...)

  r(p::RetinalPoint) = p.r
  θ(p::RetinalPoint) = p.θ

# Conversions cartesian <-> polar

Base.convert(::Type{RetinalPoint}, p::CartesianPoint; args...) =
           RetinalPoint( sqrt( x(p)^2 + y(p)^2 ), atan(y(p), x(p)) )
Base.convert(::Type{CartesianPoint}, p::RetinalPoint; args...) =
             CartesianPoint( r(p)*cos(θ(p)) , r(p)*sin(θ(p)) )

# Coordinates in the cortical plane
struct CorticalPoint{T<:Real}
     x::T
     y::T
end

CorticalPoint(x::Real, y::Real) = CorticalPoint(promote(x,y)...)
x(p::CorticalPoint) = p.x
y(p::CorticalPoint) = p.y
```

B.1.2 . Conversion formulas

Recall from Section 2.4.2 that the retino-cortical map is given by

$$(r,\theta) \mapsto (x,y) := (\log(1+r), \theta r/(1+r)),$$

where we set $\alpha = \varepsilon = \omega_0 = 1$.

```
# retinal to cortical
Base.convert(::Type{CorticalPoint}, p::RetinalPoint; far_from_fovea = false
) =
far_from_fovea ?  CorticalPoint(log(1+ r(p)) , (r(p)*θ(p))/(1+r(p))) :
CorticalPoint(log(r(p)) , θ(p))

# cortical to retinal
```

```
function Base.convert(::Type{RetinalPoint}, p::CorticalPoint{T};
far_from_fovea = false) where T<:Real
   if iszero( x(p) )
       return RetinalPoint{T}(0,0)
   end
   r = far_from_fovea ?  exp(x(p))-1 : exp(x(p))
   far_from_fovea ? RetinalPoint( r , y(p)*( 1 + 1/r) ) : RetinalPoint( r ,
 y(p))
end

# cartesian <-> cortical conversions

Base.convert(::Type{CorticalPoint}, p::CartesianPoint; args...) =
      convert(CorticalPoint, convert(RetinalPoint, p; args...); args...)
Base.convert(::Type{CartesianPoint}, p::CorticalPoint; args...) =
      convert(CartesianPoint, convert(RetinalPoint, p; args...))
```

B.2 . Converting an image from retinal to cortical and conversely

We will represent an image in the retinal plane as a function in the square $[-10, 10] \times [-10, 10]$. Let's find out to what part of the cortical plane this square corresponds.

```
a = zeros(200,200)

mesh(img) = [ CartesianPoint(x,y) for x in range(-10,10, length = size(img,
 1)), y in range(-10,10, length = size(img, 2))]

x.(convert.(CorticalPoint, mesh(a))) |> extrema |> display
y.(convert.(CorticalPoint, mesh(a))) |> extrema |> display


# We should adjust the intervals for the inverse map (cort2res)
x.(convert.(CorticalPoint, mesh(a), far_from_fovea = true)) |> extrema |>
display
y.(convert.(CorticalPoint, mesh(a), far_from_fovea = true)) |> extrema |>
display
```

We then define the functions to convert images from their retinal to their cortical representations.

```
using Images, ImageShow
using Interpolations

function fovea(img)
  xs = range(-1,1, length = size(img, 1))
  ys = range(-1,1, length = size(img, 2))
```

```
  eltype(img)[ xs[i]^2+ys[j]^2 < 1 ? img[i,j] : 1. for i in 1:length(xs), j
 in 1:length(ys)  ]
end

function res2cort(img; far_from_fovea = false)
# Linear interpolation of starting image
  xs = range(-10,10, length = size(img, 1))
  ys = range(-10,10, length = size(img, 2))
  interp_linear = LinearInterpolation((xs, ys), transpose(convert.(Float64,
 img)), extrapolation_bc = Line())

  res = similar(img, Gray)
  xs = far_from_fovea ?  range(0.068, 2.717, length = size(img,1)) : range(
-2.644, 2.649, length = size(img,1))
  ys = far_from_fovea ?  range(-2.851, 2.851, length = size(img,2)) : range
(-3.136, 3.136, length = size(img,2))
  for i in 1:size(img,2), j in 1:size(img,1)
    p = convert(CartesianPoint, CorticalPoint(xs[i], ys[j]), far_from_fovea
 = far_from_fovea)
    res[j,i] =  convert(Gray, interp_linear(x(p), y(p)))
  end

  res
end

function cort2res(img; far_from_fovea = false)
# Linear interpolation of starting image
  xs = far_from_fovea ?  range(0.068, 2.717, length = size(img,1)) : range(
-2.644, 2.649, length = size(img,1))
  ys = far_from_fovea ?  range(-2.851, 2.851, length = size(img,2)) : range
(-3.136, 3.136, length = size(img,2))
  interp_linear = LinearInterpolation((xs, ys), transpose(convert.(Float64,
 img)), extrapolation_bc = Line())

  res = similar(img, Gray)
  xs = range(-10,10, length = size(img, 1))
  ys = range(-10,10, length = size(img, 2))
  for i in 1:size(img,2), j in 1:size(img,1)
    p = convert(CorticalPoint, CartesianPoint(xs[i], ys[j]), far_from_fovea
 = far_from_fovea)
    res[j,i] =  convert(Gray, interp_linear(x(p), y(p)))
  end

  res
end
```

B.3 . Finding the stationary state to Amari-type equation

The theory tells us that, given an input I, the corresponding stationary state is $\Psi(I)$ that solves the following equation:

$$\Psi(I)(x) = \mu \int \omega(x-y) f(\Psi(I)(y))\, dy + I(x), \qquad x \in \mathbb{R}^2.$$

We then code an iterative procedure (which converges thanks to contraction mapping principle) to derive $\Psi(I)$.

Definition of the convolution operator $K(a) = \omega * a$.

```
using OffsetArrays, ImageFiltering
# define a generic kernel ω
(x,y) -> ω(x,y)

As(Δx; L=10) = centered([Δx^2*ω(x,y) for x in -L:Δx:L, y in -L:Δx:L])

function K(a, As)
  imfilter(a,reflect(As),"reflect")
end
```

Fixed point routine.

```
using Distances, ForwardDiff
function Ψ(I; Δx = .01, max_iter = 100, threshold = 1e-11)
  # define a generic response function and its derivative
  s -> σ(s)
  g(s) = ForwardDiff.derivative(s -> σ(s), s)
  # As first step we take I
  prec = I
  ΨI = I
  # to keep track of final iteration
  final_iter = max_iter
  for i in 1:max_iter
    ΨI = (μ/g(0))*K(σ.(ΨI), As(Δx)) + I
    evaluate(Chebyshev(), prec, ΨI)
    if Chebyshev()(prec, ΨI) <= threshold
      final_iter = i
      break
    else
      prec = ΨI
    end
  end
  println("Extrema of I: ", extrema(I), ", extrema of ΨI: ", extrema(ΨI))
  a        = [I[i,j]>0 ? 0. : 1. for i in 1:size(I,1), j in 1:size(I,1)]
  b        = [ΨI[i,j]>0 ? 0. : 1. for i in 1:size(ΨI,1), j in 1:size(ΨI,1
)]
```

```
  A         = Gray.(rotl90(a))
  B         = Gray.(rotl90(b))
  A_1       = cort2res(A)
  B_1       = cort2res(B)
  hcat(A_1, ones(Gray, (size(A_1,1),50)), B_1)
end
```

B.4 . Toolbox for the MacKay effect

We now replicate the MacKay effect. We first start by setting model parameters.

```
##################
# MacKay effect #
##################

#interaction kernel ω
ω(x,y)    = π*exp(-π^2*(x^2+y^2))-π*exp(-π^2*(x^2+y^2)/2)/2

#Fourier transform of ω
ω_1(r)    = exp(-r^2)-exp(-2*r^2)

#wavenumber
q_c       = sqrt(log(2))

#parameter μ_0
μ_0       = 2

#bifurcation point
μ_c       = 1/ω_1(q_c)

#parameter μ
μ         = 1
```

In the following, we show that the MacKay effect can be reproduced with a linear response function $\sigma(s) = s$. On the left we have the external input in the retina and on the right the illusory after-image perceived.

```
# MacKay effect for funnel pattern (``MacKay rays'')
Δx            = .01
L             = 10
λ             = 5π
H(r;γ=0.025)  = r ≥ 0 ? γ : 0.        # Heaviside step function
f(x,y)        = cos(λ*y)
χ(x,y)        = H(2-x)                # localized function
v(x,y)        = f(x,y)+χ(x,y)
I             = [v(x,y) for x in -L:Δx:L, y in -L:Δx:L]
```

```
#the response function is linear
σ(s)      = s
Ψ(I, Δx=Δx,threshold = 1e-15)
```

Executing the above code gives images B.1.

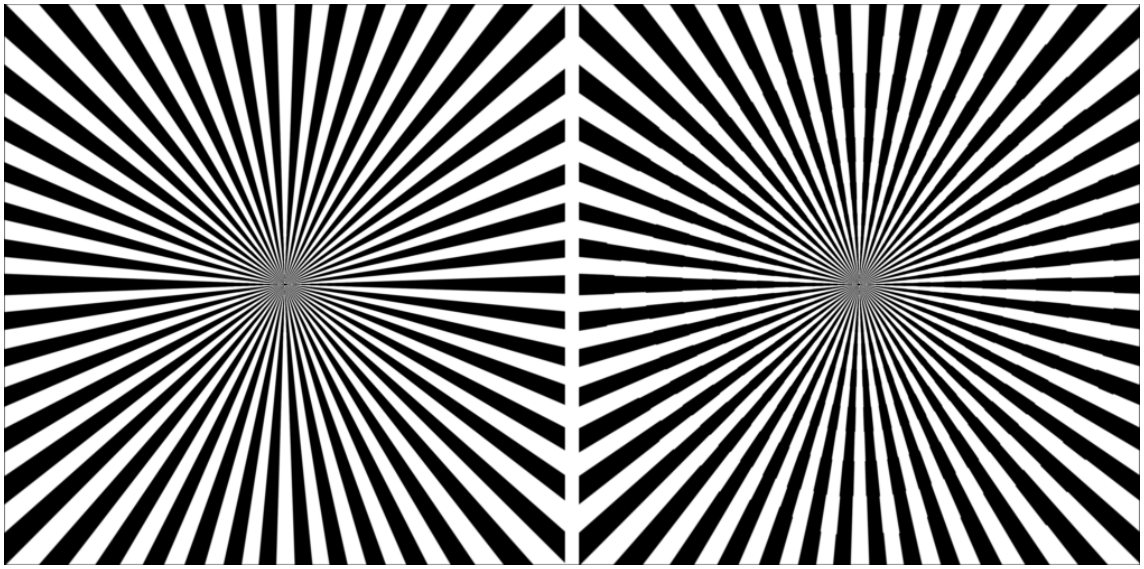

Figure B.1: MacKay effect (*right*) on the "MacKay rays" (*left*). We use the linear response function $f(s) = s$. The sensory input is chosen as $I(x) = \cos(5\pi x_2) + \varepsilon H(2 - x_1)$, $\varepsilon = 0.025$, where H is the Heaviside step function.

B.5 . Toolbox for Billock and Tsou experiments

B.5.1 . Reproducing Billock and Tsou experiments

We now replicate Billock and Tsou experiments. We first start by setting model parameters.

```
###################################
# Billock and Tsou's experiments #
###################################

σ₁      = 0.1
σ₂       = 0.5
κ         = (σ₁/σ₂)^2*exp(2*pi^2*(σ₂^2-σ₁^2))

#kernel ω
ω(x,y)    = (1/(2π*σ₁^2))*exp(-(x^2+y^2)/(2*σ₁^2))-κ*(1/(2π*σ₂^2))*exp(-(x^
2+y^2)/(2*σ₂^2))
```

```
#Fourier transform of ω
ω_1(r)    = exp(-2*pi^2*σ_1^2*r^2)-κ*exp(-2*pi^2*σ_2^2*r^2)

#wavenumber
q_c       = sqrt(log(κ*σ_2^2/σ_1^2)/(2π^2*(σ_2^2-σ_1^2)))

#L^1-norm of ω
Θ         = σ_1*σ_2*sqrt(2*log(σ_2^2/(κ*σ_1^2))/(σ_2^2-σ_1^2))
C_1       = (1-κ)+2*(κ*exp(-0.5*Θ^2/σ_2^2)-exp(-0.5*Θ^2/σ_1^2))

#parameter μ_0
μ_0       = 1/C_1

#bifurcation point
μ_c       = 1/ω_1(q_c)

#parameter μ
μ         = 0.99*μ_0
```

In the following, we show that Billock and Tsou's experiments can be reproduced with a nonlinear response function $\sigma(s) = \max(-m, \min(1, \alpha * s))$. On the left we have the external input in the retina and on the right the illusory after-image perceived.

```
# Billock and Tsou's experiments for funnel pattern localised in the
periphery
Δx        = .01
L         = 10
λ         = 4π

# funnel pattern
f(x,y)    = cos(λ*y)

#localised function
χ(x,y)    = (6 ≤ x ≤ L) && (-L ≤ y ≤ L) ? 1 : 0.
v(x,y)    = f(x,y)*χ(x,y)

#external input for funnel pattern localised in the periphery
I    = [v(x,y) for x in -L:Δx:L, y in -L:Δx:L]

# response function (m = 0.2, α = 0.8)
σ(r)      = max(-0.2,min(1,0.8*r))

Ψ(I, Δx=Δx,threshold = 1e-11)
```

Executing the above code gives images B.2.

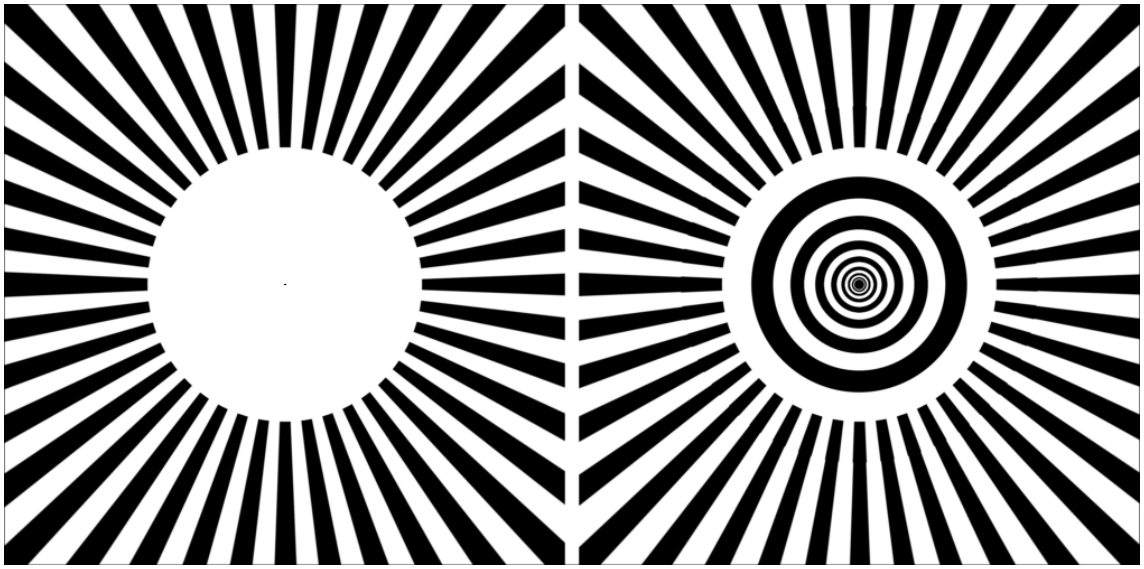

Figure B.2: Billock and Tsou's experiments: funnel stimulus localised at the periphery (*left*) and afterimage (*right*).

B.5.2 . Relation between response function parameters and reproducibility of Billock and Tsou phenomena

Theorem 3.5.1 tells us that phenomena reported by Billock and Tsou [BT07] are wholly nonlinear. It means, Equation (NF) with a linear response function f do not reproduce the phenomena.

Let us consider the family of "sigmoid" functions

$$f_{m\alpha}(s) = \max(-m, \min(1, \alpha * s)), \qquad s \in \mathbb{R},$$

where $m \geq 0$ and $\alpha > 0$. We want to provide a range of parameters (m, α) where the sigmoid $f_{m\alpha}$ reproduces the phenomena or not:

1) In the region in *magenta* the couple (m, α) reproduces the phenomenon;

2) In the region in *yellow* the couple (m, α) reproduces the phenomenon and the illusory contours extend through the surround;

3) In the region in *black*, the couple (m, α) does not reproduce the phenomenon.

To code these results, we have to slightly modify the procedure $\Psi(I, ...)$ output performed in Section B.3, which gives the stationary state associated with an input I. Indeed, we only need the matrix form of the stationary state. Moreover, we consider that the maximal slope α of $f_{m\alpha}$ is no longer equal to 1.

```
using Distances
using ForwardDiff
function Ψ(I, m::Model; max_iter = 100, threshold = 1e-15)
  @unpack Δx, σ, μ = m
  # derivative of the response function σ
  g(s) = ForwardDiff.derivative(s -> σ(s), s)
```

```
  # As first step we take I
  prec = I
  ΨI = I
  # to keep track of final iteration
  final_iter = max_iter
  for i in 1:max_iter
    ΨI = (μ/g(0))*K(σ.(ΨI), m) + I
    evaluate(Chebyshev(), prec, ΨI)
    if Chebyshev()(prec, ΨI) <= threshold
      final_iter = i
    break
    else
      prec = ΨI
    end
  end
  binary.(ΨI) |> rotl90
end
```

The code which provides the range of (m, α) where $f_{m\alpha}$ reproduces Billock and Tsou's experiments or not is then the following.

```
using ProgressMeter

function BT_reproduction(I, ms, ns, m::Model; max_iter = 100, threshold = 1
e-11, verbose = false)
  S  = zeros(Int,length(ms), length(ns))     # Storage matrix
  @showprogress for k in 1:(length(ms) * length(ns))
  i, j = fldmod1(k, length(ns))
  cur_model = Model(m; σ = Σ(m = ms[i], α = ns[j]))
  mat  = Ψ(I, cur_model,threshold = threshold);
  a1  = mat[1:size(mat,1),1602:size(mat,2)]
  if (a1 == zeros(size(a1)...)) || (a1 == ones(size(a1)...))
    S[i,j] = 0
    verbose && println("(", ms[i], ";", ns[j], ") does not reproduce the
phenomenon")
  else
    compteur = 0
    for l in 1:size(a1,2)-1
      if (a1[:,l] != zeros(size(a1,1))) && (a1[:,l] != ones(size(a1,1)))
        compteur += 1
      else
      break
      end
    end
    verbose && println("compteur = ", compteur)
    for l in compteur+1:size(a1,2)
```

```
      if (a1[:,l] != zeros(size(a1,1))) && (a1[:,l] != ones(size(a1,1)))
        S[i,j] = 0
        verbose && println("(", ms[i], ";", ns[j], ") does not reproduce
the phenomenon")
        break
      elseif (l+1 ≤ size(a1,2))
        continue
      else
        for k in compteur+1:size(a1,2)-1
          if (a1[:,k+1:size(a1,2)] == ones(size(a1,1),size(a1,2)-k)) || (a1
[:,k+1:size(a1,2)] == zeros(size(a1,1),size(a1,2)-k))
            S[i,j] = 0
            verbose && println("(", ms[i], ";", ns[j], ") does not
reproduce the phenomenon")
            break
          elseif (a1[:,k] != a1[:,k+1]) && ((a1[:,k+1:size(a1,2)] == ones(
size(a1,1),size(a1,2)-k)) || (a1[:,k+1:size(a1,2)] == zeros(size(a1,1),size
(a1,2)-k)))
            S[i,j] = 0
            verbose && println("(", ms[i], ";", ns[j], ") does not
reproduce the phenomenon")
            break
          elseif (compteur == 0) && (a1[:,k] != a1[:,k+1]) && (a1[:,k+1:
size(a1,2)] != ones(size(a1,1),size(a1,2)-k)) && (a1[:,k+1:size(a1,2)] !=
zeros(size(a1,1),size(a1,2)-k))
            S[i,j] = 1
            verbose && println("(", ms[i], ";", ns[j], ") reproduces the
phenomenon")
            break
          elseif (compteur != 0) && (a1[:,k] != a1[:,k+1]) && (a1[:,k+1:
size(a1,2)] != ones(size(a1,1),size(a1,2)-k)) && (a1[:,k+1:size(a1,2)] !=
zeros(size(a1,1),size(a1,2)-k))
            S[i,j] = 2
            verbose && println("(", ms[i], ";", ns[j], ") reproduces the
phenomenon but the illusory contours extend through the complementary
region")
            break
            end
          end
        end
      end
    end
  end
S
end
```

Bibliography

[ABB19] A. Agrachev, D. Barilari, and U. Boscain. *A comprehensive introduction to sub-Riemannian geometry*. Vol. 181. Cambridge University Press, 2019 (cit. on pp. 18, 26).

[ABS08] A. Agrachev, U. Boscain, and M. Sigalotti. "A Gauss-Bonnet-like Formula on Two-Dimensional Almost-Riemannian Manifolds". In: *Discrete & Continuous Dynamical Systems - A* 20.4 (2008), pp. 801–822 (cit. on p. 19).

[All18] D. Allonsius. "Etude spectrale d'opérateurs de Sturm-Liouville et applications à la contrôlabilité de problèmes paraboliques discrets et continus". PhD thesis. Aix Marseille Université, 2018 (cit. on pp. 22, 28).

[Ama77] S.-i. Amari. "Dynamics of Pattern Formation in Lateral-Inhibition Type Neural Fields". In: *Biological cybernetics* 27.2 (1977), pp. 77–87 (cit. on pp. 58, 60, 63, 64, 69, 70).

[Bao67] M. S. Baouendi. "Sur Une Classe d'opérateurs Elliptiques Dégénérés". In: *Bul. Soc. Math. France* 79 (1967), pp. 45–87 (cit. on p. 26).

[Bar76] V. Barbu. *Nonlinear semigroups and differential equations in Banach spaces*. Springer, 1976 (cit. on p. 116).

[BCG14] K. Beauchard, P. Cannarsa, and R. Guglielmi. "Null Controllability of Grushin-type Operators in Dimension Two". In: *J. Eur. Math. Soc.* 16.1 (2014), pp. 67–101 (cit. on pp. 10, 22, 26, 27, 32, 40, 46).

[BDE20] K. Beauchard, J. Dardé, and S. Ervedoza. "Minimal Time Issues for the Observability of Grushin-type Equations". In: *Annales de l'Institut Fourier* 70.1 (2020), pp. 247–312 (cit. on pp. 10, 22, 28, 40, 46).

[Bea+15] K. Beauchard, B. Helffer, R. Henry, and L. Robbiano. "Degenerate Parabolic Operators of Kolmogorov Type with a Geometric Control Condition". In: *ESAIM: COCV* 21.2 (Apr. 2015), pp. 487–512 (cit. on pp. 22, 46).

[BMM15] K. Beauchard, L. Miller, and M. Morancey. "2d Grushin-type Equations: Minimal Time and Null Controllable Data". In: *Journal of Differential Equations* 259.11 (Dec. 2015), pp. 5813–5845 (cit. on pp. 10, 21, 22, 27, 28, 40).

[BG12] C. A. Berenstein and R. Gay. *Complex analysis and special topics in harmonic analysis*. Springer Science & Business Media, 2012 (cit. on p. 97).

[BG88] M. Berger and B. Gostiaux. *Differential geometry: manifolds, curves, and surfaces*. Graduate texts in mathematics 115. Translation of: Géométrie différentielle Includes indexes. New York: Springer-Verlag, 1988 (cit. on pp. 18, 30).

[Beu56] R. L. Beurle. "Properties of a Mass of Cells Capable of Regenerating Pulses". In: *Philosophical Transactions of the Royal Society of London. Series B, Biological Sciences* (1956), pp. 55–94 (cit. on p. 63).

[Bez+17] J. Bezanson, A. Edelman, S. Karpinski, and V. B. Shah. "Julia: A fresh approach to numerical computing". In: *SIAM review* 59.1 (2017), pp. 65–98 (cit. on p. 130).

[BZ16] U. Biccari and E. Zuazua. "Null Controllability for a Heat Equation with a Singular Inverse-Square Potential Involving the Distance to the Boundary Function". In: *Journal of Differential Equations* 261.5 (Sept. 2016), pp. 2809–2853 (cit. on p. 46).

[BT10] V. A. Billock and B. H. Tsou. "A Special Case of the MacKay Effect Generates Geometric Hallucinations: Stochastic Resonance in Pattern Formation Driven by Fractal (1/f) Noise". In: *Journal of Vision* 3.9 (Mar. 2010), pp. 350–350 (cit. on p. 10).

[BT07] V. A. Billock and B. H. Tsou. "Neural Interactions between Flicker-Induced Self-Organized Visual Hallucinations and Physical Stimuli". In: *Proceedings of the National Academy of Sciences* 104.20 (May 2007), pp. 8490–8495 (cit. on pp. 10, 56–60, 73, 79, 81, 130, 138).

[BT12] V. A. Billock and B. H. Tsou. "Elementary Visual Hallucinations and Their Relationships to Neural Pattern-Forming Mechanisms." In: *Psychological Bulletin* 138.4 (2012), pp. 744–774 (cit. on p. 10).

[BPS16] U. Boscain, D. Prandi, and M. Seri. "Spectral Analysis and the Aharonov-Bohm Effect on Certain Almost-Riemannian Manifolds". In: *Communications in Partial Differential Equations* 41.1 (Jan. 2016), pp. 32–50 (cit. on p. 19).

[BL13] U. Boscain and C. Laurent. "The Laplace-Beltrami Operator in Almost-Riemannian Geometry". In: *Ann. inst. Fourier* 63.5 (2013), pp. 1739–1770 (cit. on pp. 19, 24).

[BC02] P. C. Bressloff and J. D. Cowan. "Spontaneous Pattern Formation in Primary Visual Cortex". In: *Institute of Physics: Bristol, 2002. In: Nonlinear dynamics: where do we go from here? Chap 11* (2002), p. 53 (cit. on pp. 55, 70, 77).

[Bre11] P. C. Bressloff. "Spatiotemporal Dynamics of Continuum Neural Fields". In: *Journal of Physics A: Mathematical and Theoretical* 45.3 (2011), p. 033001 (cit. on pp. 64, 113).

[Bre10] P. C. Bressloff. "Stochastic Neural Field Theory and the System-Size Expansion". In: *SIAM Journal on Applied Mathematics* 70.5 (2010), pp. 1488–1521 (cit. on p. 64).

[Bre14] P. C. Bressloff. *Waves in Neural Media: From Single Neurons to Neural Fields*. Lecture Notes on Mathematical Modelling in the Life Sciences. New York: Springer-Verlag, 2014 (cit. on p. 64).

[Bre+01] P. C. Bressloff, J. D. Cowan, M. Golubitsky, P. J. Thomas, and M. C. Wiener. "Geometric Visual Hallucinations, Euclidean Symmetry and the Functional Architecture of Striate Cortex". In: *Philosophical Transactions of the Royal Society of London. Series B: Biological Sciences* 356.1407 (2001), pp. 299–330 (cit. on pp. 55, 57, 58, 63, 70, 72, 77, 78, 86, 101).

[BM97] H. Brezis and M. Marcus. "Hardy's inequalities revisited". In: *Annali della Scuola Normale Superiore di Pisa-Classe di Scienze* 25.1-2 (1997), pp. 217–237 (cit. on p. 40).

[Bri+23] L. Brivadis, C. Tamekue, A. Chaillet, and J. Auriol. "Existence of an equilibrium for delayed neural fields under output proportional feedback". In: *Automatica* 151 (2023), p. 110909 (cit. on pp. 10, 86, 113).

[CG14] P. Cannarsa and R. Guglielmi. "Null Controllability in Large Time for the Parabolic Grushin Operator with Singular Potential". In: *Geometric Control Theory and Sub-Riemannian Geometry*. Vol. 5. Cham: Springer International Publishing, 2014, pp. 87–102 (cit. on pp. 10, 40, 46).

[Car39] T. Carleman. *Sur un problème d'unicité pour les systèmes d'équations aux dérivées partielles à deux variables indépendantes*. Almqvist & Wiksell, 1939 (cit. on p. 32).

[Car12] N. R. Carlson. *Physiology of Behavior*. 11th edition. Boston: Pearson, Jan. 2012 (cit. on p. 64).

[CCM19] V. Casarino, P. Ciatti, and A. Martini. "From refined estimates for spherical harmonics to a sharp multiplier theorem on the Grushin sphere". In: *Advances in Mathematics* 350 (2019), pp. 816–859 (cit. on p. 34).

[Caz14] C. Cazacu. "Controllability of the Heat Equation with an Inverse-Square Potential Localized on the Boundary". In: *SIAM J. Control Optim.* 52.4 (Jan. 2014), pp. 2055–2089 (cit. on p. 45).

[Cha+17] A. Chaillet, G. I. Detorakis, S. Palfi, and S. Senova. "Robust Stabilization of Delayed Neural Fields with Partial Measurement and Actuation". In: *Automatica* 83 (Sept. 2017), pp. 262–274 (cit. on pp. 10, 113, 114, 116, 117).

[CPT23] Y. Chitour, D. Prandi, and C. Tamekue. “A mathematical replication of MacKay-type visual illusions”. In: *to appear* (2023) (cit. on pp. 60, 110, 111, 113).

[CL00] P. Chossat and R. Lauterbach. *Methods in Equivariant Bifurcations and Dynamical Systems*. Advanced Series in Nonlinear Dynamics v. 15. World Scientific Publishing Company, 2000 (cit. on p. 77).

[CL98] J. Clottes and D. Lewis-Williams. *Shamans of Prehistory*. Harry N Abrams Incorporated, 1998 (cit. on p. 75).

[Coo10] S. Coombes. “Large-scale neural dynamics: simple and complex”. In: *NeuroImage* 52.3 (2010), pp. 731–739 (cit. on p. 64).

[Coo23] S. Coombes. “Next generation neural population models”. In: *Frontiers in Applied Mathematics and Statitics* (2023), 9::1128224 (cit. on p. 64).

[Coo05] S. Coombes. “Waves, Bumps, and Patterns in Neural Field Theories”. In: *Biological cybernetics* 93.2 (2005), pp. 91–108 (cit. on pp. 64, 67).

[CGP14] S. Coombes, P. beim Graben, and R. Potthast. “Tutorial on neural field theory”. In: *Neural fields: theory and applications* (2014), pp. 1–43 (cit. on p. 70).

[Cor07] J.-M. Coron. *Control and Nonlinearity*. Mathematical Surveys and Monographs v. 136. Providence, R.I: American Mathematical Society, 2007 (cit. on pp. 10, 17, 46).

[CH53] R. Courant and D. Hilbert. *Methods of Mathematical Physics. Vol.1: ...* Literaturverz. S. 546 - 549. Weinheim: Wiley-VCH, 1953 (cit. on pp. 34, 39).

[CE04] R. Curtu and B. Ermentrout. “Pattern formation in a network of excitatory and inhibitory cells with adaptation”. In: *SIAM Journal on Applied Dynamical Systems* 3.3 (2004), pp. 191–231 (cit. on pp. 83, 86).

[DR09] V. K. David and S. Rajasekaran. *Pattern Recognition Using Neural and Functional Networks*. Studies in Computational Intelligence vol. 160. Berlin: Springer, 2009 (cit. on p. 63).

[DA01] P. Dayan and L. F. Abbott. *Theoretical Neuroscience: Computational and Mathematical Modeling of Neural Systems*. The MIT Press, 2001 (cit. on p. 64).

[Dec+08] G. Deco, V. K. Jirsa, P. A. Robinson, M. Breakspear, and K. Friston. “The Dynamic Brain: From Spiking Neurons to Neural Masses and Cortical Fields”. In: *PLoS Comput Biol* 4.8 (2008), e1000092 (cit. on p. 64).

[Det+15] G. I. Detorakis, A. Chaillet, S. Palfi, and S. Senova. “Closed-loop stimulation of a delayed neural fields model of parkinsonian STN-GPe network: a theoretical and computational study”. In: *Frontiers in neuroscience* 9 (2015), p. 237 (cit. on pp. 10, 114, 116).

[DR77] S. Dolecki and D. L. Russell. “A general theory of observation and control”. In: *SIAM Journal on Control and Optimization* 15.2 (1977), pp. 185–220 (cit. on p. 31).

[Dra77] N. Drasdo. “The Neural Representation of Visual Space”. In: *Nature* 266.5602 (Apr. 1977), pp. 554–556 (cit. on p. 72).

[DK20] M. Duprez and A. Koenig. “Control of the Grushin equation: non-rectangular control region and minimal time”. In: *ESAIM: Control, Optimisation and Calculus of Variations* 26 (2020), p. 3 (cit. on pp. 10, 22, 23, 28).

[Erm98] G. B. Ermentrout. “Neural Networks as Spatio-Temporal Pattern-Forming Systems”. In: *Reports on progress in physics* 61.4 (1998), p. 353 (cit. on pp. 64, 66).

[EC79a] G. B. Ermentrout and J. D. Cowan. “A Mathematical Theory of Visual Hallucination Patterns”. In: *Biol. Cybernetics* 34.3 (Oct. 1979), pp. 137–150 (cit. on pp. 55, 57, 63, 75, 77, 78, 83, 86, 101).

[EC80] G. B. Ermentrout and J. D. Cowan. “Large Scale Spatially Organized Activity in Neural Nets”. In: *SIAM J. Appl. Math.* 38.1 (Feb. 1980), pp. 1–21 (cit. on p. 84).

[ET10] G. B. Ermentrout and D. H. Terman. *Mathematical Foundations of Neuroscience*. Interdisciplinary Applied Mathematics. New York: Springer-Verlag, 2010 (cit. on pp. 64, 69).

[EC79b] G. Ermentrout and J. D. Cowan. “Temporal oscillations in neuronal nets”. In: *Journal of mathematical biology* 7 (1979), pp. 265–280 (cit. on p. 67).

[Erv08] S. Ervedoza. “Control and Stabilization Properties for a Singular Heat Equation with an Inverse-Square Potential”. In: *Communications in Partial Differential Equations* 33.11 (Oct. 2008), pp. 1996–2019 (cit. on pp. 40, 45).

[FR71] H. O. Fattorini and D. L. Russell. “Exact controllability theorems for linear parabolic equations in one space dimension”. In: *Archive for Rational Mechanics and Analysis* 43.4 (1971), pp. 272–292 (cit. on pp. 16, 17).

[FVG09] O. Faugeras, R. Veltz, and F. Grimbert. “Persistent neural states: stationary localized activity patterns in nonlinear continuous n-population, q-dimensional neural networks”. In: *Neural computation* 21.1 (2009), pp. 147–187 (cit. on pp. 114–117).

[FTC09] O. D. Faugeras, J. D. Touboul, and B. Cessac. “A Constructive Mean-Field Analysis of Multi Population Neural Networks with Random Synaptic Weights and Stochastic Inputs”. In: *Frontiers in computational neuroscience* 3 (2009), p. 1 (cit. on p. 64).

[Ffy04] D. Ffytche. "Visual hallucination and illusion disorders: a clinical guide". In: *Advances in Clinical Neuroscience and Rehabilitation* 4.2 (2004), pp. 16–18 (cit. on p. 74).

[FZ85] A. L. Fogelson and R. S. Zucker. "Presynaptic Calcium Diffusion from Various Arrays of Single Channels. Implications for Transmitter Release and Synaptic Facilitation". In: *Biophysical journal* 48.6 (1985), pp. 1003–1017 (cit. on p. 65).

[FK74] S. Fomine and A. N. Kolmogorov. *Eléments de la théorie des fonctions et de l'analyse fonctionnelle*. Editions Mir, 1974 (cit. on p. 105).

[Fou22] J. B. J. Fourier. *Théorie analytique de la chaleur*. Firmin Didot, 1822 (cit. on p. 15).

[Fre68a] W. J. Freeman. "Analog Simulation of Prepyriform Cortex in the Cat". In: *Mathematical Biosciences* 2.1-2 (1968), pp. 181–190 (cit. on p. 63).

[Fre68b] W. J. Freeman. "Effects of Surgical Isolation and Tetanization on Prepyriform Cortex in Cats." In: *Journal of neurophysiology* 31.3 (1968), pp. 349–357 (cit. on p. 63).

[Fre72] W. J. Freeman. "Waves, Pulses, and the Theory of Neural Masses". In: *Progress in Theoretical Biology* 2.1 (1972), pp. 1–10 (cit. on p. 63).

[FI96] A. Fursikov and O. Y. Imanuvilov. "Controllability of Evolution Equations. In vol. 34, Lect. Notes Ser. Seoul National University, Seoul". In: *Korea* (1996) (cit. on pp. 17, 45, 46).

[FIK12] K. Furutani, C. Iwasaki, and T. Kagawa. "An action function for a higher step Grushin operator". In: *Journal of Geometry and Physics* 62.9 (2012), pp. 1949–1976 (cit. on p. 15).

[GK02] W. Gerstner and W. M. Kistler. *Spiking Neuron Models: Single Neurons, Populations, Plasticity*. Cambridge, U.K. ; New York: Cambridge University Press, 2002 (cit. on p. 64).

[Ger+14] W. Gerstner, W. M. Kistler, R. Naud, and L. Paninski. *Neuronal Dynamics: From Single Neurons to Networks and Models of Cognition*. Cambridge University Press, 2014 (cit. on p. 64).

[GSH96] M. A. Giese, G. Schöner, and H. S. Hock. "Neural field dynamics for motion perception". In: *International Conference on Artificial Neural Networks*. Springer. 1996, pp. 335–340 (cit. on p. 60).

[Gie12] M. A. Giese. *Dynamic Neural Field Theory for Motion Perception*. Vol. 469. Springer Science & Business Media, 2012 (cit. on pp. 63, 83).

[GST03] M. Golubitsky, L. J. Shiau, and A. Török. "Bifurcation on the Visual Cortex with Weakly Anisotropic Lateral Coupling". In: *SIAM J. Appl. Dyn. Syst.* 2.2 (Jan. 2003), pp. 97–143 (cit. on pp. 55, 57).

[Gre95] R. L. Gregory. “Brain-created visual motion: an illusion?” In: *Proceedings of the Royal Society of London. Series B: Biological Sciences* 260.1358 (1995), pp. 167–168 (cit. on p. 80).

[Gru70] V. Grušin. “On a class of hypoelliptic operators”. In: *Mathematics of the USSR-Sbornik* 12.3 (1970), p. 458 (cit. on p. 26).

[Hl11] M. Haragus and G. Iooss. *Local Bifurcations, Center Manifolds, and Normal Forms in Infinite-Dimensional Dynamical Systems*. London: Springer London, 2011 (cit. on p. 77).

[Hee92] D. J. Heeger. “Half-squaring in responses of cat striate cells”. In: *Visual neuroscience* 9.5 (1992), pp. 427–443 (cit. on p. 117).

[Hel67] H. L. F. Helmholtz. *Optic physiologique*. Masson, 1867 (cit. on pp. 75, 79, 80).

[Hop84] J. J. Hopfield. “Neurons with Graded Response Have Collective Computational Properties like Those of Two-State Neurons”. In: *Proceedings of the national academy of sciences* 81.10 (1984), pp. 3088–3092 (cit. on p. 64).

[Hör67] L. Hörmander. “Hypoelliptic Second Order Differential Equations”. In: *Acta Math.* 119.0 (1967), pp. 147–171 (cit. on pp. 26, 33).

[HW59] D. H. Hubel and T. N. Wiesel. “Receptive Fields of Single Neurones in the Cat’s Striate Cortex”. In: *The Journal of Physiology* 148.3 (Oct. 1959), pp. 574–591 (cit. on pp. 55, 72).

[HW62] D. H. Hubel and T. N. Wiesel. “Receptive Fields, Binocular Interaction and Functional Architecture in the Cat’s Visual Cortex”. In: *The Journal of Physiology* 160.1 (Jan. 1962), pp. 106–154 (cit. on p. 55).

[HW65] D. H. Hubel and T. N. Wiesel. “Receptive Fields and Functional Architecture in Two Nonstriate Visual Areas (18 and 19) of the Cat”. In: *Journal of neurophysiology* 28.2 (1965), pp. 229–289 (cit. on p. 63).

[HW63] D. H. Hubel and T. N. Wiesel. “Receptive Fields of Cells in Striate Cortex of Very Young, Visually Inexperienced Kittens”. In: *Journal of Neurophysiology* 26.6 (Nov. 1963), pp. 994–1002 (cit. on p. 63).

[HW74a] D. H. Hubel and T. N. Wiesel. “Sequence Regularity and Geometry of Orientation Columns in the Monkey Striate Cortex”. In: *J. Comp. Neurol.* 158.3 (Dec. 1974), pp. 267–293 (cit. on p. 72).

[HW74b] D. H. Hubel and T. N. Wiesel. “Uniformity of Monkey Striate Cortex: A Parallel Relationship between Field Size, Scatter, and Magnification Factor”. In: *J. Comp. Neurol.* 158.3 (Dec. 1974), pp. 295–305 (cit. on p. 72).

[Ima95] O. Y. Imanuilov. “Controllability of Parabolic Equations”. In: *Sb. Math.* 186.6 (June 1995), pp. 879–900 (cit. on pp. 17, 45).

[Izh07] E. M. Izhikevich. *Dynamical Systems in Neuroscience: The Geometry of Excitability and Bursting*. Computational Neuroscience. Cambridge, Mass: MIT Press, 2007 (cit. on p. 64).

[Kan+00] E. R. Kandel, J. H. Schwartz, T. M. Jessell, S. Siegelbaum, A. J. Hudspeth, and S. Mack. *Principles of Neural Science*. Vol. 4. McGraw-hill New York, 2000 (cit. on p. 64).

[Klü66] H. Klüver. *Mescal and Mechanisms of Hallucinations*. Chicago: Univ. of Chicago Press, 1966 (cit. on pp. 55, 75, 78).

[Koe17] A. Koenig. "Non-null-controllability of the Grushin operator in 2D". In: *Comptes Rendus Mathematique* 355.12 (2017), pp. 1215–1235 (cit. on pp. 10, 22, 23, 28, 46).

[KAO63] A. E. Krill, H. J. Alpert, and A. M. Ostfeld. "Effects of a Hallucinogenic Agent in Totally Blind Subjects". In: *Archives of Ophthalmology* 69.2 (Feb. 1963), pp. 180–185 (cit. on p. 75).

[Lai+02] C. R. Laing, W. C. Troy, B. Gutkin, and G. B. Ermentrout. "Multiple Bumps in a Neuronal Model of Working Memory". In: *SIAM Journal on Applied Mathematics* 63.1 (2002), pp. 62–97 (cit. on p. 63).

[LR95] G. Lebeau and L. Robbiano. "Contrôle Exact De L'équation De La Chaleur". In: *Communications in Partial Differential Equations* 20.1-2 (Jan. 1995), pp. 335–356 (cit. on p. 17).

[Lev96] I. Leviant. "Does 'brain-power' make Enigma spin?" In: *Proceedings of the Royal Society of London. Series B: Biological Sciences* 263.1373 (1996), pp. 997–1001 (cit. on pp. 60, 80).

[Lio88] J.-L. Lions. *Contrôlabilité exacte, perturbations et stabilisation de systemes distribues. Tome 1*. Vol. 8. Masson, Paris, 1988 (cit. on p. 31).

[Lli03] R. R. Llinás. "The contribution of Santiago Ramon y Cajal to functional neuroscience". In: *Nature Reviews Neuroscience* 4.1 (2003), pp. 77–80 (cit. on p. 64).

[LSA11] Y. Lu, Y. Sato, and S.-i. Amari. "Traveling Bumps and Their Collisions in a Two-Dimensional Neural Field". In: *Neural Computation* 23.5 (May 2011). In this paper, author use external inputs to control stationary solutions to Neural field equation., pp. 1248–1260 (cit. on p. 83).

[Mac57] D. M. MacKay. "Moving Visual Images Produced by Regular Stationary Patterns". In: *Nature* 180.4591 (Oct. 1957), pp. 849–850 (cit. on pp. 10, 56, 57, 59, 60, 79, 80, 99, 130).

[Mac61] D. M. MacKay. "Visual Effects of Non-redundant Stimulation". In: *Nature* 192.4804 (Nov. 1961), pp. 739–740 (cit. on pp. 10, 80).

[MV06] P. Martinez and J. Vancostenoble. “Carleman estimates for one-dimensional degenerate heat equations”. In: *Journal Of Evolution Equations* 6 (2006), pp. 325–362 (cit. on pp. 41, 42).

[McC+85] D. A. McCormick, B. W. Connors, J. W. Lighthall, and D. A. Prince. “Comparative Electrophysiology of Pyramidal and Sparsely Spiny Stellate Neurons of the Neocortex”. In: *Journal of Neurophysiology* 54.4 (Oct. 1985), pp. 782–806 (cit. on p. 69).

[MP43] W. S. McCulloch and W. Pitts. “A Logical Calculus of the Ideas Immanent in Nervous Activity”. In: *The bulletin of mathematical biophysics* 5.4 (1943), pp. 115–133 (cit. on p. 64).

[MJ03] J. Milton and P. Jung. *Epilepsy as a dynamic disease*. Springer Science & Business Media, 2003 (cit. on p. 113).

[Mor15] M. Morancey. “Approximate Controllability for a 2D Grushin Equation with Potential Having an Internal Singularity”. In: *Annales de l’Institut Fourier* 65.4 (2015), pp. 1525–1556 (cit. on pp. 10, 40, 46).

[Nai68] M. A. Naimark. *Linear differential operators. Part II: Linear differential operators in Hilbert space*. Frederick Ungar Publishing Company, 1968 (cit. on p. 38).

[Nic+21] R. Nicks, A. Cocks, D. Avitabile, A. Johnston, and S. Coombes. “Understanding Sensory Induced Hallucinations: From Neural Fields to Amplitude Equations”. In: *SIAM J. Appl. Dyn. Syst.* 20.4 (2021), pp. 1683–1714 (cit. on pp. 10, 56, 57, 59, 79, 82, 85, 86, 113).

[Ost70] G. Oster. “Phosphenes”. In: *Sci Am* 222.2 (Feb. 1970), pp. 82–87 (cit. on p. 75).

[Pat92] A. Patterson. *A field guide to rock art symbols of the greater Southwest*. Big Earth Publishing, 1992 (cit. on p. 75).

[Paz12] A. Pazy. *Semigroups of linear operators and applications to partial differential equations*. Vol. 44. Springer Science & Business Media, 2012 (cit. on pp. 33, 34).

[Pur+04] D. Purves, G. J. Augustine, D. Fitzpatrick, W. Hall, A.-S. LaMantia, and L. White, eds. *Neuroscience*. 3rd ed. Sunderland, Mass: Sinauer Associates, Publishers, 2004 (cit. on p. 64).

[Ram09] S. Ramón y Cajal. *Histologie Du Système Nerveux de l’homme et Des Vertébrés.* Ed. française rev. & mise à jour par l’auteur, tr. de l’espagnol par L. Azoulay. Vol. 1. Paris : Maloine, 1909, pp. 1–1012 (cit. on p. 64).

[RH59] F. Ratliff and H. K. Hartline. “The Responses of Limulus Optic Nerve Fibers to Patterns of Illumination on the Receptor Mosaic”. In: *The Journal of general physiology* 42.6 (1959), pp. 1241–1255 (cit. on p. 63).

[Rec+15] S. Recanatesi, M. Katkov, S. Romani, and M. Tsodyks. “Neural Network Model of Memory Retrieval”. In: *Frontiers in computational neuroscience* 9 (2015), p. 149 (cit. on p. 63).

[Sat78] D. Sattinger. “Group Representation Theory, Bifurcation Theory and Pattern Formation”. In: *Journal of Functional Analysis* 28.1 (Apr. 1978), pp. 58–101 (cit. on p. 77).

[Sch77] E. L. Schwartz. “Spatial Mapping in the Primate Sensory Projection: Analytic Structure and Relevance to Perception”. In: *Biol. Cybern.* 25.4 (Dec. 1977), pp. 181–194 (cit. on pp. 55, 72).

[Ser+95] M. Sereno, A. Dale, J. Reppas, K. Kwong, J. Belliveau, T. Brady, B. Rosen, and R. Tootell. “Borders of Multiple Visual Areas in Humans Revealed by Functional Magnetic Resonance Imaging”. In: *Science* 268.5212 (May 1995), pp. 889–893 (cit. on p. 71).

[Sie77] R. K. Siegel. “Hallucinations”. In: *Sci Am* 237.4 (Oct. 1977), pp. 132–139 (cit. on p. 75).

[SV13] R. Sokoliuk and R. VanRullen. “The Flickering Wheel Illusion: When α Rhythms Make a Static Wheel Flicker”. In: *Journal of Neuroscience* 33.33 (2013) (cit. on p. 60).

[Str83] R. S. Strichartz. “Analysis of the Laplacian on the complete Riemannian manifold”. In: *Journal of functional analysis* 52.1 (1983), pp. 48–79 (cit. on p. 33).

[Str86] R. S. Strichartz. “Sub-Riemannian Geometry”. In: *J. Differential Geom.* 24.2 (Jan. 1986) (cit. on p. 33).

[Tam22] C. Tamekue. “Null controllability of the parabolic spherical Grushin equation”. In: *ESAIM: Control, Optimisation and Calculus of Variations* 28 (2022), p. 70 (cit. on pp. 10, 21, 25, 31, 36, 44, 46).

[Tam23] C. Tamekue. “Parabolic spherical Baouendi-Grushin equation: Minimal time for null controllability”. In: *to appear* (2023) (cit. on p. 23).

[TPC23a] C. Tamekue, D. Prandi, and Y. Chitour. “Cortical origins of MacKay-type visual illusions: A case for the non-linearity”. In: *2023 IFAC*. 2023 (cit. on pp. 59, 104, 113).

[TPC23b] C. Tamekue, D. Prandi, and Y. Chitour. “MacKay-Type Visual Illusions via Neural Fields”. In: *International Conference on Geometric Science of Information*. Springer. 2023, pp. 501–508 (cit. on p. 113).

[TPC22] C. Tamekue, D. Prandi, and Y. Chitour. “Reproducing sensory induced hallucinations via neural fields”. In: *2022 IEEE-ICIP*. 2022, pp. 3326–3330 (cit. on pp. 56, 59, 108, 113).

[Tas95] P. Tass. “Cortical Pattern Formation during Visual Hallucinations”. In: *J Biol Phys* 21.3 (1995), pp. 177–210 (cit. on pp. 55, 57, 75).

[Tas97] P. Tass. “Sscillatory Cortical Activity during Visual Hallucinations”. In: *Journal of biological physics* 23 (1997), pp. 21–66 (cit. on p. 113).

[Too+82] R. Tootell, M. Silverman, E. Switkes, and R. De Valois. “Deoxyglucose Analysis of Retinotopic Organization in Primate Striate Cortex”. In: *Science* 218.4575 (Nov. 1982), pp. 902–904 (cit. on pp. 55, 71, 72).

[VF10] R. Veltz and O. Faugeras. “Local/global analysis of the stationary solutions of some neural field equations”. In: *SIAM Journal on Applied Dynamical Systems* 9.3 (2010), pp. 954–998 (cit. on p. 88).

[Vil68] N. Vilenkin. *Special Functions and the Theory of Group Representations*. Trans. by V. Singh. Vol. 22. Translations of Mathematical Monographs. Providence, Rhode Island: American Mathematical Society, Dec. 1968 (cit. on p. 91).

[Wey50] H. Weyl. *The theory of groups and quantum mechanics*. Courier Corporation, 1950 (cit. on p. 15).

[WC73] H. R. Wilson and J. D. Cowan. “A Mathematical Theory of the Functional Dynamics of Cortical and Thalamic Nervous Tissue”. In: *Kybernetik* 13.2 (1973), pp. 55–80 (cit. on pp. 55, 60, 63, 64, 67, 83, 113).

[WC72] H. R. Wilson and J. D. Cowan. “Excitatory and Inhibitory Interactions in Localized Populations of Model Neurons”. In: *Biophysical journal* 12.1 (1972), pp. 1–24 (cit. on pp. 63, 67, 68).

[ZWF93] S. Zeki, J. D. G. Watson, and R. S. J. Frackowiak. “Going beyond the Information given: The Relation of Illusory Visual Motion to Brain Activity”. In: *Proc. R. Soc. Lond. B* 252.1335 (June 1993), pp. 215–222 (cit. on pp. 60, 80).

[Zek94] S. Zeki. “The cortical Enigma: a reply to Professor Gregory”. In: *Proceedings of the Royal Society of London. Series B: Biological Sciences* 257.1350 (1994), pp. 243–245 (cit. on p. 80).

[ZME19] A. Ziepke, S. Martens, and H. Engel. “Control of Nonlinear Wave Solutions to Neural Field Equations”. In: *SIAM J. Appl. Dyn. Syst.* 18.2 (Jan. 2019), pp. 1015–1036 (cit. on pp. 10, 70).